12-2007

Fabrication and Analysis of Polymeric Nanocomposites from Cellulose Fibrils

Qingzheng Cheng
University of Tennessee - Knoxville

To the Graduate Council:

I am submitting herewith a dissertation written by Qingzheng Cheng entitled "Fabrication and Analysis of Polymeric Nanocomposites from Cellulose Fibrils." I have examined the final electronic copy of this dissertation for form and content and recommend that it be accepted in partial fulfillment of the requirements for the degree of Doctor of Philosophy, with a major in Natural Resources.

Siqun Wang, Timothy G. Rials, Major Professor

We have read this dissertation and recommend its acceptance:

David P. Harper, Kevin M. Kit

Accepted for the Council:

Carolyn R. Hodges

Vice Provost and Dean of the Graduate School

(Original signatures are on file with official student records.)

To the Graduate Council:

We are submitting herewith a dissertation written by Qingzheng Cheng entitled "Fabrication and Analysis of Polymeric Nanocomposites from Cellulose Fibrils." We have examined the final electronic copy of this dissertation for form and content and recommend that it be accepted in partial fulfillment of the requirements for the degree of Doctor of Philosophy, with a major in Natural Resources.

Siqun Wang
Major Professor

Timothy G. Rials
Co-Major Professor

We have read this dissertation
and recommend its acceptance:

David P. Harper

Kevin M. Kit

Accepted for the Council:

Carolyn R. Hodges
Vice Provost and Dean of the
Graduate School

(Original signatures are on file with official student records.)

FABRICATION AND ANALYSIS OF POLYMERIC NANOCOMPOSITES FROM CELLULOSE FIBRILS

A Dissertation

Presented for the

Doctor of Philosophy Degree

The University of Tennessee, Knoxville

Qingzheng Cheng

December 2007

DEDICATION

This dissertation is dedicated to my wife and my son, since I could not be successful without their support, love, patience, encouragement and sacrifices.

This dissertation is also dedicated to my father Mr. Diangong Cheng and my mother Mrs. Yanfang Tan for their support, understanding, love and encouragement, which have made all my endeavors possible. I pray for my dad and beg his forgiveness because I did not accompany him during his last years in this world before May 2007.

ACKNOWLEDGEMENTS

There are many people who deserve my sincerest thanks for supporting me to finish this dissertation. First of all, I am most thankful to my advisor, Dr. Siqun Wang and co-advisor Dr. Timothy G. Rials for providing me an important opportunity to work in this project, supporting me financially, and for their inspiration, advice and guidance in obtaining my degree.

I would also prefer to thank my committee members, Dr. David P. Harper, and Dr. Kevin M. Kit, not only for being my committee member, but also for their valuable suggestions throughout my course of study and experiment of this dissertation in the University of Tennessee. Many thanks to Dr. Qingyou Han, who was my committee member and gave me a lot of advice about ultrasonic treatment. It's a pity that he cannot be my committee anymore because he became a professor at Mechanical Engineering Technology Department, Purdue University and moved from Oak Ridge National Lab to West Lafayette, Indiana.

Many thanks to my family members, especially my sisters and brothers for providing me in the values of a higher education, for supporting and understanding me in the ways that I would love to do, and for taking care of my parents instead of me.

Special thanks to Mr. Chris Helton and Miss Amanda Silk for helping me to finish my project in the past years. I would prefer to thank the professors, colleagues and lab mates who also deserve my truthful thanks. I could not name all of them here. If you are one of many anonymous friends, you will know that I have appreciated your help and

friendship during my time in Knoxville, Tennessee Forest Products Center, University of Tennessee. Thanks to Dr. Cheng Xing, Seung-Hwan Lee, Dr. Suzhou Yin, Dr. William Tze, Mr. William Moschler, Dr. Nicole Labbé, Dr. Nicolas André, Dr. Adam Taylor, Mr. Timothy M. Young, Trairat Numswan, Sundeep Nair, Yan Wu and Xinan Zhang for helping me with school related works and for providing ample opportunities to have fun.

Thank Dr. Shirley Spears and Mr. Steve Skirius of Buckeye Technologies Inc., Memphis, TN, for their valuable assistances in the dimension analyses of fibers and fibrils measured by Kajaani FiberLab 3. Thank Dr. Joseph Spruiell of Department of Material Science and Engineering, University of Tennessee, for his help of WAXD; Dr. John R. Dunlap of the Division of Biology, University of Tennessee, for his valuable assistances in SEM experiments; Dr. Svetlana Zivanovic, Dr. Federico Harte, Dr. Tao Wu of Food Science and Technology, University of Tennessee, for their valuable assistances in homogenizer and freeze dry experiments; Lenzing company for their supply of Lyocell fibers; Creafill Fiber Corp. for their providing pure cellulose; Kimberly-Clark Worldwide, Inc. for their providing pulp fiber; FiberVisions, Georgia for their supply of PP fibers; FMC BioPolymer, for their donation of microcrystalline cellulose (MCC).

Finally, special thanks to USDA Wood Utilization Research Program, USDA McIntire-Stennis Forestry Program, Cherokee National Forest, and Tennessee Agricultural Experiment Station project # 96 and #83 for funding.

ABSTRACT

A novel process using high-intensity ultrasonication (HIUS) was developed to isolate fibrils from cellulose fibers. The geometrical characteristics of the fibrils were investigated using polarized light microscopy (PLM), scanning electron microscopy (SEM) and atomic force microscopy (AFM). Results show that small fibrils with diameter ranging from about thirty nanometers to several micrometers were peeled from the fibers. The degree of fibrillation of the fibers was significantly increased. The crystallinities or molecular structures of most of the cellulose materials were changed by HIUS treatment.

To evaluate the fibrils degradation by HIUS, a method using AFM was modified and developed to measure the elastic modulus of single cellulose fibrils. The results indicated that it was necessary to consider the penetration of AFM tips to the cellulose fibril surfaces. In the diameter range of 150 to 300 nm, the elastic moduli of Lyocell fibrils did not have significant differences between the HIUS treatment time of 30 min and 60 min. The modulus of Lyocell fibrils with diameters from 150 to 180 nm was evaluated about 98 GPa and it decreased dramatically when the diameter was more than 180 nm. The elastic moduli of cellulose fibrils were not significantly different between isolation methods of HIUS and high-pressure homogenizer for pure cellulose fiber, between different cellulose sources of pulp fibers treated by homogenizer. The elastic modulus of fibrils from regenerated cellulose fibers was higher than that of natural fibers.

The treated fiber and separated fibrils were used to reinforce poly(vinyl alcohol), poly(lactic acid), and polypropylene by film casting or compression molding. Both of the tensile modulus and strength of nano-biocomposites reinforced with treated fiber and separated fibrils were higher than those of the untreated fiber reinforced composites. The morphological characteristics of the nanocomposites were investigated with SEM, AFM, and PLM. The dispersion of fibrils was not perfect, and the adhesions between the polymer and fibrils were not good without further modification of the fibrils. The fibrils on the fibers and isolated from the fibers may be the role that the tensile modulus and strength of the treated fiber and separated fibril reinforced composites were higher than those of the untreated fiber.

TABLE OF CONTENTS

LIST OF FIGURES

Chapter 2

Chapter 3

Chapter 4

Chapter 5

Chapter 6

Chapter 7

Appendix B

LIST OF TABLES

Chapter 2

Chapter 3

Chapter 4

Chapter 5

Chapter 6

CHAPTER 1. INTRODUCTION

1.1. Brief Background

Cellulose fibers are renewable, biodegradable, and the most abundant natural biopolymers in the world, which are synthesized mainly in plants such as woods, crop stalks, grasses, and vegetables. In order to save our natural materials and reduce the dependence on petroleum, it is becoming more and more important to investigate the utilization of the biomass effectively, non-costly, environmentally friendly in recent years. So that high value products as bio-oils, biodegradable composites and polymeric nanocomposites may be made from natural biomass.

In the past two decades, a lot of interests having been focused on by many researchers and manufactures to use natural fibers to replace artificial fibers such as glass fibers as reinforcement material and fillers to make environmentally safe products because they have many advantages such as renewable, low cost, low density, low energy consumption, high specific strength and modulus, high sound attenuation, nonabrasive nature, relatively reactive surface. Furthermore, fibrils in micro and nano scales isolated from natural fibers may have much higher mechanical properties, so that much attention have been paid in the past two decades to study how to generate fibrils and how to combine them with polymers to make nanocomposites, which are expected to be have improved strength and stiffness and other performances than the composites that reinforced with fibers. As one of the next generation materials, the research of bio-based nanocomposites has grown very fast because of its environmental friend, which might include completely biodegradable composites (both the fibril and polymer matrix are biodegradable) and partly biodegradable composites (at least the fibril is biodegradable).

It is still challengeable to isolate fibrils (include micro and nano scales) with reasonable cost and low degradation, and how to disperse them evenly and effectively in polymer matrixes, although many methods have been developed to generate fibrils (e.g., chemical and mechanical) and to produce bio-nanocomposites (e.g., film casting and freeze dry followed by compressive molding and/or extrusion).

Problems and challenges in polymeric nanocomposites reinforced with cellulose fibrils in micro and nano scales:

1. Disintegration of cellulose to fibrils without severe degradation, with low cost and environmental friend;

2. Characterizations of the fibrils and nanocomposites, especially the mechanical properties of individual fibrils to check the effects of isolation process;

3. Dispersion of cellulose fibrils in polymer matrixes;

4. Characterization and improvement of the adhesion between fibrils and polymer matrixes;

5. Applications and biodegradability of bio-based polymeric nanocomposites in the ecological system.

1.2. Research Objectives

Three objectives were focused in this project. The first was to isolate cellulose fibrils from Lyocell fiber (a regenerated cellulose fiber), pure cellulose fiber, pulp fiber, and microcrystalline cellulose by high intensity ultrasonic treatment and to characterize the physical properties of the fibrils. The second was to fundamentally measure the

elastic moduli of individual cellulose fibrils to check the fibril degradation. The third was to reinforce several polymers, especially some biodegradable polymers, to make polymeric nanocomposites, and to characterize their properties.

Based on the three objectives, this dissertation includes five main Chapters besides this one for introduction, Chapter 2 for literature review, and Chapter 8 for conclusions and recommendations.

Chapter 3 described the novel process to isolate fibrils from cellulose fibers by high intensity ultrasonication (HIUS), discussed its possibility and energy consumption, and characterized the fibrils. As comparison and reference, high-pressure homogenizer (HPH) and alkali pretreatment were also tried to optimize the fibril isolation parameters from cellulose fibers.

In Chapter 4, a method to measure the elastic moduli of individual cellulose fibrils using AFM by nano-scale three-point bending test and nanoindentation was modified and developed in order to evaluate the fibril degradation by HIUS treatment.

Based on Chapter 4, Chapter 5 was focused on the measurements and comparisons of elastic moduli of single fibrils isolated by mechanical treatments including HIUS and HPH from different cellulose resources to check the effects of process and source on elastic modulus of individual cellulose fibrils.

To evaluate the reinforcements of the fibrils isolated in Chapter 3, the physical and mechanical properties of polymeric nanocomposites including poly(vinyl alcohol), poly(lactic acid), and polypropylene, reinforced with treated Lyocell fibers by HIUS were investigated and discussed in Chapter 6.

To compare the reinforcement of treated cellulose fibers (mixture of fiber and fibril) described in Chapter 6, Chapter 7 focused on the physical and mechanical properties of poly(vinyl alcohol) nanocomposites reinforced with the separated cellulose fibrils by centrifuge from several treated cellulose fibers by HIUS treatment obtained in Chapter 3.

1.3. Rational and Significance

The world market for composites has been growing very fast since 90s. Bio-based nanocomposites, one of the green materials for the next generation, have a great market potential for dramatic growth in recent years. By nanotechnology, many new properties, such as mechanical properties e.g. strength, modulus and dimensional stability, decreased permeability to gases, water and hydrocarbons, thermal stability and heat distortion temperature, flame retardancy and reduced smoke emissions, chemical resistance, surface appearance, electrical conductivity, optical clarity in comparison to conventionally filled polymers, can be obtained from old and recognized materials by just reducing their particle size. Current methods including chemical and mechanical treatments to produce cellulose-based fibrils in micro and nano scales are low yield, not environmental friendly and/or not energy efficient. The goals of this research were to investigate the fundamentals of the isolation of cellulose fibrils from biomass by using high-intensity ultrasound as an approach without any chemical treatment, the characterization of the produced and by-products, especially the measurement of the mechanical properties of single cellulose fibrils by AFM for the first time, and the fabrication of bio-based

nanocomposites reinforced polymers with the cellulose fibrils. This high-intensity ultrasound technique is an environmentally benign method and a simplified process that may make fiber isolation and chemical modification simultaneously.

This work will develop a novel method to generate fibrils from natural cellulose fibers for polymer reinforcement to make bio-based nanocomposites, which may have great growth potential for renewable resource in automotive and building industries, especially in the applications where biocompatibility and environmentally responsible design and construction are required. Bio-based nanocomposites can replace conventional petroleum-based composites at least partly as a new, high performance, lightweight green nanocomposite materials because they possess the improved strength and stiffness, reduced gas/water vapor permeability, a lower coefficient of thermal expansion, and an increase heat deflection temperature. At the same time, as a new method, the measurement of the mechanical properties of single fibrils by AFM may evaluate the degradation of cellulose fibrils during the isolation and may be as one fundamental bridge to connect the properties of the fibrils as reinforcing material and the properties of the reinforced nanocomposites.

CHAPTER 2. LITERATURE REVIEW

2.1. Abstract

Cellulose is the world's most abundant natural, renewable, biodegradable polymer. It is a high-performance skeletal biocomposite consisting of a matrix of lignin and hemicellulose reinforced by microfibrils, which include crystalline with almost defect-free and the consequence of axial physical properties approaching those of perfect crystals. During the past two decades, many researchers have been devoted to isolate fibrils in micro and nano scales from natural cellulose by ether chemical or mechanical method and use them to reinforce polymers to process nanocomposites. This Chapter reviews the isolation and characterization methods of cellulose fibrils, the fabrication and characterization of nanocomposites made by blending cellulose fibrils with polymer matrixes. The ultrasonic technology and its treatment on cellulose were briefly introduced as well.

Keywords: Cellulose, characterization, fibrils, isolation, micro, microfibrils, nano, nanocomposites, ultrasonic technology.

2.2. Introduction

Cellulose is a renewable, biodegradable and the most abundant natural biopolymer in the world. Natural cellulose fibers are synthesized mainly in plants such as grasses, reeds, stalks, and woody vegetation. And the main structural component of plants is cellulose, which constitutes 40 to 50% of wood, 80% of flax and 90% of cotton fiber. Green algae, some bacteria and animals have cellulose chains in their cell walls (Lima

and Borsali, 2004). Abundant wastes are potential raw materials for biobased products in the United States. The estimated waste biomass was about 280 million metric tons per year (Table 2.1), and much of this is crop residues, predominantly from corn—about 100 million metric tons of corn residues are produced annually (Gallagher and Johnson, 1995).

In recent years, interest has grown to focus on how to use natural fibers to replace synthetics such as glass fibers as reinforcement material and fillers to make environmentally safe products (George et al., 2001). The fibrils isolated from natural fibers may have much higher mechanical properties because fibrils include higher cellulose crystal regions that have very high elastic modulus than fibers (Sakurada et al., 1962). Thus attention has been paid in the past two decades to study how to make fibrils and how to combine them with polymers to make nanocomposites (Berglund, 2005; Cheng et al., 2007a; Cheng et al., 2007b; Herrick et al., 1983; Turbak et al., 1983). Microfibers are defined as fibers of cellulose of 0.1-1 μm in diameter, with a corresponding minimum length of 5-50 μm (Chakraborty et al., 2006). The definition of nanotechnology developed by Franks was: "the technology where dimensions or tolerances in the range 0.1 to 100 nm (from the size of an atom to the wavelength of light) play a critical role" (Franks, 1987). The definition of nano-size material has broadened significantly to a large variety of systems that include at least one-dimension at the nanometer scale (1-100 nm) (Jordan et al., 2005).

Cellulose fibrils isolated from natural fibers normally have a wide range of diameters depending on the cellulose source and the process methods. Cellulose whisker,

Table 2.1 Estimated available waste biomass in the United States

Feedstock	Quantity (1000 dry metric tons)
Recycled primary paper pulp sludge	3,400
Urban tree residue	38,000
Mixed office paper	4,600
Sugarcane bagasse	700
Newsprint	11,200
Rice	2,700
Corn gluten feed	5,700
Spent brewers grains	1,100
Distillers' dried grains	1,800
Corn gluten meal	1,100
Small grain straw	0
Wood mill residue	5,600
Corn stover	100,000
Cotton gin waste	15,000
Sulfite waste liquor	61,000
Cheese whey from dairy	28,000
Total	279,900

Source: Rooney (1998).

nanofibrils, and nanocrystals were used to describe the single microfibrils with diameter from several nm to tens nm. While fibrils generated by mechanical methods have much bigger diameters that range from tens nm to several μm. In this paper, a term of cellulose fibril or fibril aggregate is used to describe the needle-like or thread-like material generated from cellulose fibers including single and bundles of microfibrils with diameters of tens nm to several μm.

Cellulose fibers and fibrils have good mechanical properties with low density, thus they have attracted great attention as an alternative to glass, carbon, and other polymeric fibers. Table 2.2 shows the tensile mechanical properties of various fibers (Lilaseca and Peijs, 2005). The nanofibrils are the smallest structural units of plant fiber, which are a bundle of stretched cellulose chain molecules with Young's modulus of about 137 GPa (Sakurada et al., 1962). Although fibrils have the high Young's modulus and tensile strength, they have not been used in structural materials commercially and successfully. The two major barriers are how to isolate fibrils from the natural fiber cell wall at reasonable cost and low degradation and how to disperse them evenly and effectively in polymer matrix (Zimmermann et al., 2004). The research of nanocomposites reinforced by fibrils, especially bio-based nanocomposites as one of the next generation materials, has grown very fast because of its environmental friendly in recent years, which are expected to be have improved strength and stiffness (Samir et al., 2004; Zimmermann et al., 2004).

Table 2.2 Mechanical properties of various fibers

Material	Young's Modulus (GPa)	Tensile Strength (GPa)
Jute	26-65	0.39-0.77
Flax	27-100	0.34-1.03
Ramie	60-128	0.40-0.94
Cotton	5-13	0.28-0.60
Wood	10-40	1
Regenerated cellulose	36	1.4
Cellulose nanofibrils	130-150	10
Glass	70-85	2-3.5
Aramid	60-200	3-3.6

Source: Lilaseca and Peijs (2005)

2.3. Cellulose

Cellulose is a classical extracellular high-performance skeletal biocomposite consisting of a matrix reinforced by fibrous biopolymer. The whisker like microfibrils, which are crystalline with almost defect-free and the consequence of axial physical properties approaching those of perfect crystals, are biosynthesized and deposited in a continuous fashion by plants or animals. Wood, one of the most important plants for human being, is not only a good building material, but also an abundant cellulose source.

2.3.1. Chemical components of the wood cell wall

Wood tissue is composed of a group of polymeric components, which make up the bulk of the wood cell walls. All the polymeric components are mixed in the wall and determined the physical and mechanical properties of wood. A typical wood cell include

primary wall, secondary wall (S1, S2, S3), and Lumen. (Panshin and Zeeuw, 1980; Fengel and Wegener, 1984).

There are two chemical components in wood cell wall. The primary components, which establish the chemical and physical nature of the cell wall and constitute the bulk of material of the wood cell wall, include cellulose (40-50%), hemicellulose (20-35%) and lignin (15-35%). The cellulose is the most important single component in the cell wall and has primary relationship to the wood physical behavior. The hemicellulose and lignin are also important in the wall because they act as matrix in the natural polymer composites. The secondary components in the wall include ash (<1%) and extractives, such as tannins, volatile oils and resins, gums, latex, alkaloids, and other compounds. The secondary components may not significantly affect the structure of the cell, but may give the bulk of wood many specific characteristics, such as resistance to natural degradation, color, and odor (Fengel and Wegener, 1984; Panshin and Zeeuw, 1980).

Several models have been built for polymeric wood components in the internal wood cell wall, mainly focused on the primary components: cellulose, hemicellulose and lignin. Preston (1962) and Marchessault (1964) models only considered the association of cellulose and hemicellulose. In 1970, Fengel made a model that takes account of the presence of lignin, which enclose the largest units (25 nm in diameter) combined with cellulose and hemicellulose. The smallest units, which are the single crystalfibrils in the cell wall, are separated by monomolecular hemicellulose layers. Kerr and Goring made a new one in 1975, which consists of layers of cellulose-hemicellulose blocks interrupted in the radial and tangential direction by lignin-hemicellulose blocks.

Another proposed model for the difference of the arrangement of elementary fibrils in softwood and hardwood assumed that the microfibril may include crystal, semi-crystal, and amorphous regions, and the elementary fibrils have a diameter of 3.5 nm, while the microfibril may be composed of four elementary fibrils (Tsuchikawa and Siesler, 2006).

2.3.3. Chemical and crystalline structure of cellulose

Figure 2.1 shows the structure of a wood cell wall from big fiber to crystal structure (Pohler et al., online). Wood combines high strength and elasticity, which are from the composite structure of its cell walls: cellulose fibrils embed in lignin and hemicellulose matrix.

The structure of cellulose was clearly established by Staudinger until 1926, although the first investigations on cellulose by Braconnot in 1819 and Payen in 1839 (Lima and Borsali, 2004). Cellulose is a high-molecular-weight linear homopolymer, consisting of repeating β-D-glucopyranosyl units joined by (1-4) glycosidic linkages in a

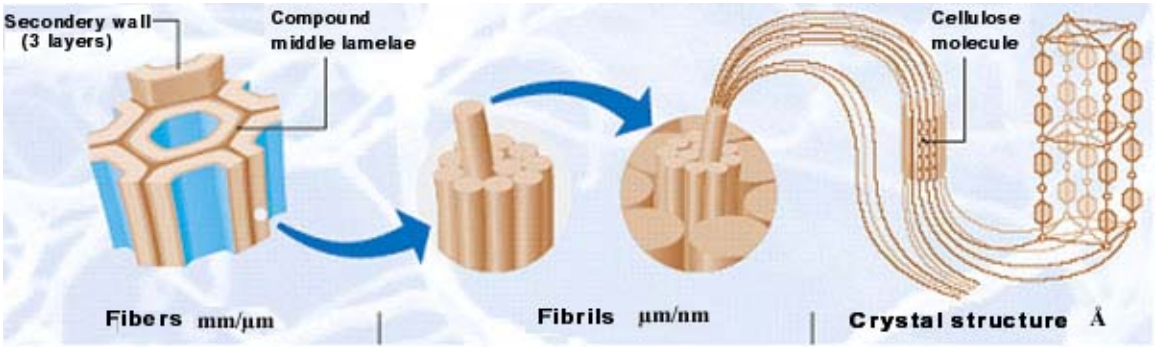

Figure 2.1 Structure of a wood cell wall: from fiber to crystal structure (Source: Zimmermann et al., 2004)

variety of arrangements. Cellulose is a (1-4)-link β-D-glucoglycan, β-D-glupynanose unit, which is joined to form a linear-molecular chain (Figure 2.2) (Chaplin, online). The hydrogen bonds formed between the ring oxygen atom of one glycosyl unit and the hydrogen atom of the C-3 hydroxyl group of the preceding ring hinder the free rotation of the rings on their linking glycosidic bonds resulting in the stiffening of the chain. The adjacent cellulose chains fit closely together in an ordered crystalline region, so that high strength can be observed in plants and some cellulose-constituted animals and cellulose is insoluble in common solvents. In nature, cellulose chains have a DP of approximately 10000 glucopyranose units in wood cellulose and 15000 in native cellulose cotton (Chaplin, online; Sjostrom, 1993).

Microfibrils are constituted by amorphous and crystalline domains, are biosynthesized and self-assembled from cellulose chains. The degree of crystallinity (ratio of the mass of crystalline domains to the total mass of the cellulose) and typical dimensions are dependent on their origin (Sarko and Muggli, 1974; Woodcock and Sarko, 1980). Cellulose exists basically in four different forms, the cellulose I (I_α and I_β), II, III, IV, which can be interconverted by chemical and thermal processes (Lima and Borsali, 2004; Woodcock and Sarko, 1980). Or Cellulose was described displaying six

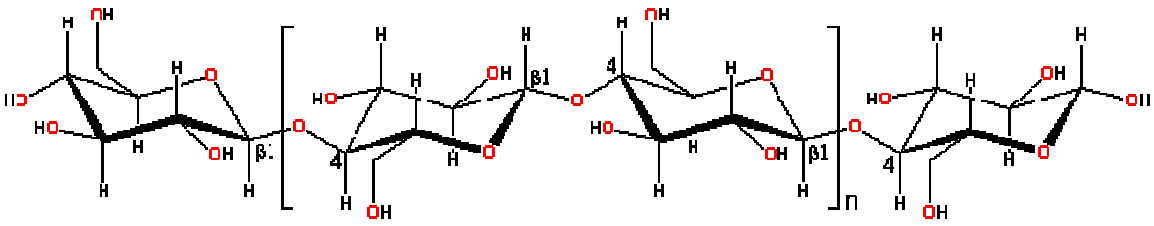

Figure 2.2 Basic chemical structure of cellulose biopolymer (Source: Chaplin, online).

different polymorphs, namely I, II, III_I, III_{II}, IV_I, and IV_{II} with the possibility of conversion from one form to another (O'Sullivan, 1997; Samir et al., 2005).

Most research was focused on elucidating the crystal structure of native cellulose (cellulose I) since 1934 (Meyer and Misch, 1937). Crystalline structure of ramie native cellulose was proposed with a monoclinic unit cell constituted of two anti-parallel polysaccharide chains with dimensions a=0.835 nm, b=0.79 nm, c=1.03 nm being the fiber axis, and γ=84. While for alga *Vilonia*, the proposed model was a triclinic unit cell with more important dimensions a and b, which was confirmed by X-ray fiber diffraction analysis (Finkenstadt and Millane, 1998). The differences between the monoclinic and triclinic structures are illustrated in Figure 2.3 (Lima and Borsali, 2004).

2.4. Isolation Methods of Fibrils

How to generate fibrils in nano and micro scales from cellulose fibers is still challengeable. Two common methods have been developed to obtain fibrils. One is the chemical way mainly by strong acid hydrolysis, which removed the amorphous regions

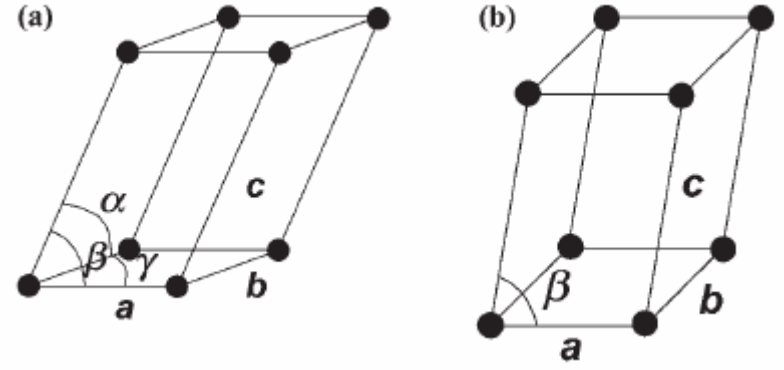

Figure 2.3 (a) Lattice in monoclinic structure. (b) Lattice in triclinic structure (Source: Li ma and Borsali, 2004).

of cellulose fiber. This method can be used to generate cellulose crystal or nanofibril, commonly called cellulose whisker or nanocrystal. The other method is the mechanical way mainly by strong shear force such as using homogenizer to separate cellulose fiber to fibrils. This method can be used to generate cellulose microfibril or its bundles, commonly called microfibrillated cellulose (MFC).

2.4.1. Chemical treatments

The cellulose nanocrystal can be generated by chemical treatment, especially acid hydrolysis, from various biomass resources. A typical procedure to prepare cellulose nanocrystal (CNXL) was described in five steps: hydrolysis by acid, centrifugation and neutralization, rinse with deionized water by centrifuge, dispersion by ultrasonic irradiation, ultrafiltration to remove any remaining ions (Choi and Simonsen, 2006).

Cellulose whisker or nanocrystal have been obtained from wood fibers (Beck-Candanedo et al., 2005; Bondeson et al., 2006; Chakraborty et al., 2005; Chakraborty et al., 2006; Kvien et al., 2005; Marcovich et al., 2006; Orts et al., 2005; Pu et al., 2007; Zimmermann et al., 2004), cotton (Choi and Simonsen, 2006; Gindl and Keckes, 2005; Lu et al., 2005; Orts et al., 2005; Podsiadlo et al., 2005; Wang et al., 2006), ramie (Lu et al., 2006), tunicate mantles (Ljungberg et al., 2005; Samir et al., 2006; Sturcova et al., 2005; Yuan et al., 2006), shrimp shell (Sriupayo et al., 2005), sugar beet pulp (Dufresne et al., 1997b), potato tuber cells (Dufresne et al., 2000), swede root (Hepworth and Bruce, 2000), starch (Thielemans et al., 2006), and bacterial cellulose (Dufresne and Vignon, 1998; Edgar and Gray, 2002). The amorphous regions of cellulose fiber act as structural

defects and are responsible for the transverse cleavage of the microfibrils into short mono-crystals under acid hydrolysis. Table 2.3 shows the dimensions of cellulose nanocrystals from various sources (Beck-Candanedo et al., 2005).

2.4.2. Mechanical treatments

Several mechanical methods were used to isolate cellulose fibrils. The high pressure refiner or a supergrinder was used to treat certain concentration (3WT%) of cellulose fiber slurries with up to 30 times passes through small gap (0.1 mm) (Chakraborty et al., 2005; Iwamoto et al., 2005; Nakagaito et al., 2005; Nakagaito and Yano, 2005; Taniguchi, 1996; Taniguchi and Okamura, 1998; Wang and Sain, 2007; Yano and Nakahara, 2004; Yano et al., 2005). Sulphite pulp suspension was treated with an ultra-turrax (24000 rpm, 8 h) and then a microfluidizer (1000 bar, 60 min) was used to disperse and homogenize the cellulose fibrils (Zimmermann et al., 2004). High-pressure homogenizer treatment is another commonly used method. A certain concentration (3wt%) of pulp fiber slurry or cellulose slurry treated by other mechanical methods was pumped at high pressure through a spring-loaded valve assembly. The valve was opened and closed to subject the slurry to a large pressure drop and high shear and impact forces generated in the narrow slit of the valve opening. This process could be repeated up to 30 times to make uniform fibrils and good fibril suspensions (Dufresne et al., 1997b; Herrick et al., 1983; Nakagaito and Yano, 2005; Turbak et al., 1983; Yano and Nakahara, 2004; Yano et al., 2005; Zimmermann et al., 2004). Most of these fibrils are not commercially used yet, except one called mcirofibrillated cellulose (MFC), which is used in some

Table 2.3 Dimensions of cellulose nanocrystals from various sources

Cellulose type	Length	Cross Section
Tunicate	100 nm - several μm	10-20 nm
Bacterial	100 nm - several μm	5-10 nm by 30-50 nm
Algal (Valonia)	>1000 nm	10 to 20 nm
Cotton	200-350 nm	5 nm
Wood	100-300 nm	3-5 nm diameter

industrial applications, such as food, cosmetic, and medicinal products (Lima and Borsali, 2004; Turbak et al., 1983). Current commercial products are too expensive for reinforcing filler, as its price is around $10 per pound. Mechanical treated cellulose fibrils from wood fiber are shown in Figure 2.4 (Zimmermann et al., 2004).

Although various means of generating cellulose fibrils have been attempted in recent years, there are still some disadvantages; such as the chemical method is low yield,

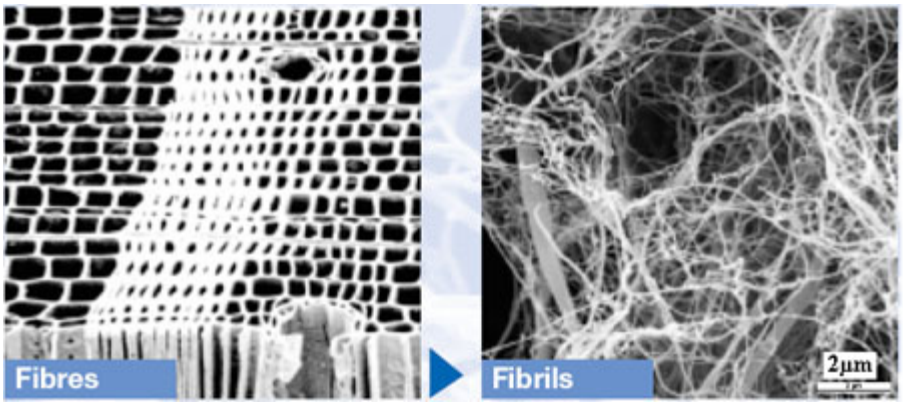

Figure 2.4 Cellulose fibrils isolated by mechanical treatment from wood fiber (Source: Zimmermann et al., 2004)

not environmentally friendly, while mechanical treatment degrades cellulose and is not energy efficient. There is not a well-established method of producing these fibrils on a mass scale.

2.5. Characterizations of Fibrils

Many methods have been used for fibril characterization, including physical and chemical analyses, as well as mechanical characterization.

2.5.1. Physical analysis

Several tools can be used for morphological observation, such as Scanning electron microscope (SEM) (Bhatnagar and Sain, 2005; Bondeson et al., 2006; Chakraborty et al., 2005; Chakraborty et al., 2006; Choi and Simonsen, 2006), atomic force microscope (AFM) (Beck-Candanedo et al., 2005; Bhatnagar and Sain, 2005; Chakraborty et al., 2005; Chakraborty et al., 2006; Choi and Simonsen, 2006; Kvien et al., 2005; Zimmermann et al., 2004), and transmission electron microscopy (TEM) (Bhatnagar and Sain, 2005; Bondeson et al., 2006; Chakraborty et al., 2005; Choi and Simonsen, 2006; Kvien et al., 2005; Zimmermann et al., 2004). Some TEM images of nanofibrils from different resources are shown in Figure 2.5 (Samir et al., 2005).

The degree of fibrillation of the fibers may be evaluated by water retention value (WRV). This test is used in paper pulp characterization, which is based on subjecting a sample of water slurry or water-saturated pulp to a standard centrifuged force with standard conditions of time, temperature, and apparatus. After centrifuged, the sample is

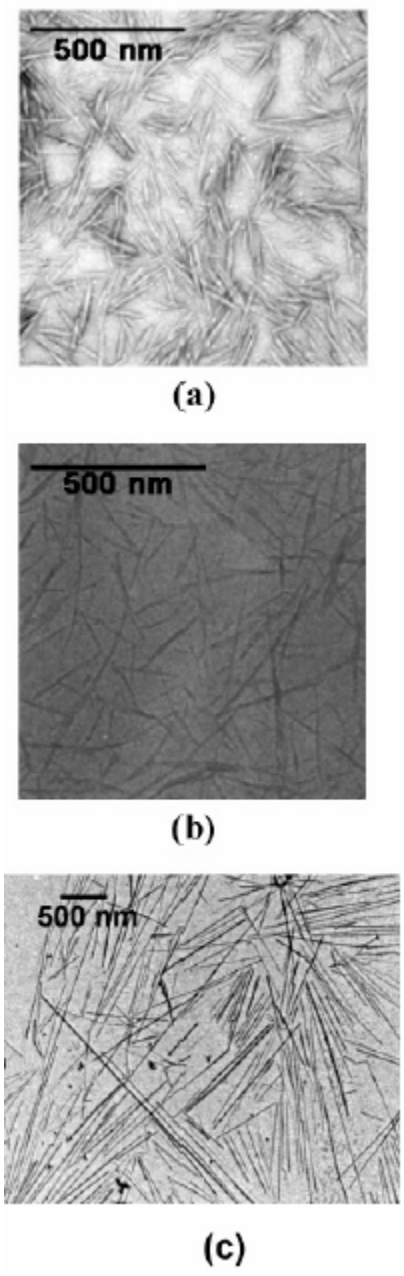

Figure 2.5 Transmission electron micrograph from a dilute suspension of hydrolyzed (a) cotton, (b) sugar-beet pulp and (c) tunicin (Source: Samir et al., 2005)

then weighted and dried at 105˚C to calculate the WRV. Addition of a fluted filter of tea bag paper as a liner for the filtration thimble was used for microfibrillated cellulose (MFC) samples in the setup of WRV measurement of paper pulp. The centrifuge was operated at 3600 rpm for 10 min for MFC. The centrifuged samples were weighted and then dried at 105˚C to constant weight (Herrick et al., 1983; Laka et al., 2000; Turbak et al., 1983; Yano and Nakahara, 2004).

2.5.2. Chemical analysis

The Wide angle X-ray diffraction (WAXD) is used to study the crystallinity of the Fibrils. The estimated crystallinity of nanofibers from wood kraft pulp was 54%, while crystallinity of flax and rutabaga nanofibers was estimated as 59% and 64%, respectively (Bhatnagar and Sain, 2005). The crystallinity of bleached kraft pulp, microfiber, and microcrystalline cellulose was estimated as 45%, 54%, and 64%, respectively (Chakraborty et al., 2006).

The chemical properties of chemical treated cellulose fibers may be studied by FTIR. Infrared measurements showed the removal of pectins due to vanishing of characteristic bands at approximately 1740 cm^{-1} (carboxylate groups) and at approximately 1590 and 1240 cm^{-1} (acetyl and methyl ester groups, respectively) (Bhatnagar and Sain, 2005). The surface charge of fibrils may be measured by conductometric titrations with sodium hydroxide. Surface charge density calculation may be made using the dimensions determined by AFM, assuming a cylindrical shape and a density of 1.6 g/cm^3 for the cellulose nanofibrils (Beck-Candanedo et al., 2005).

2.5.3. Mechanical properties

Mechanical properties of a single cellulose fibril are very important, especially when the ultimate aim of the fibrils is for reinforcement in composite materials, but mechanical properties of individual cellulose fibrils are rarely studied, and no literatures about measurement of mechanical properties of cellulose fibrils isolated from cellulose cell wall were found. The mechanical properties of single wood fiber have been studied by several researchers (Page et al. 1972; Mott et al. 1996; Xing et al., 2007). For smaller fibrils, it is difficult to measure the mechanical properties directly due to the difficulty in isolating individual cellulose fibrils without severe degradation, measuring the tiny forces and deformations involved, as well as characterizing the complex and uneven diameters or widths.

The elastic modulus of the crystalline region of cellulose was determines either experimentally or theoretically. Experimental deformation micromechanics of natural cellulose fibers were studied using Raman spectroscopy (Blackwel et al., 1970a; Blackwel et al., 1970b; Wiley and Atalla, 1987). The Young's modulus of microcrystalline cellulose (flax and hemp) was estimated to be 25±4 GPa from the values of the shift rate of the 1095cm^{-1} band using Raman spectroscopy (Eichhorn and Young, 2001). X-ray diffraction was also used to evaluate the elastic modulus of the crystalline region of cellulose and the obtained elastic modulus of the crystalline region of ramie fiber was 137 GPa (Matsuo, 1990; Matsuo et al., 1990; Sakurada et al., 1962).

Tan and Lim (2006) reviewed the experimental techniques for the mechanical characterization of nanofibers, namely tensile test, bend test and indentation done at the

nanoscale (Table 2.4). As a relative new method to obtain the elastic modulus of nano scale fibers using atomic force microscope (AFM), a nanoscale three-point bending test has been used in several fields, especially for carbon nanotubes. An AFM cantilever tip is used to apply a small load at the midpoint along the suspended length of a single nanofiber, which is suspended over a small groove. This method has been used to obtain the elastic modulus of nanosized beams, such as silicon carbide nanorods and multiwall carbon nanotubes (Wong et al. 1997; Salvetat et al. 1999a; Salvetat, et al. 1999b; Salvetat-Delmotte and Rubio 2002), β-chitin fibers (Xu et al. 1994), and PLLA nanofibers (Figure 2.6) (Tan and Lim 2004). A model was used to calculate the elastic modulus of the fiber after a force and deflection curve is obtained. The bending deflection of a nanofiber was determined by measuring the difference between the cantilever deflections over the *Z*-piezo displacement on a silicon wafer substrate and on the nanofiber as shown in Figure 2.7 (Tombler et al. 2000; Tan and Lim 2004).

Elastic modulus of bacterial cellulose nanofibers was measured by a atomic force microscope (AFM) (Wan et al., 2006).Nanoindentation study of a single poly(L-lactic acid) nanofiber was performed using an atomic force microscope (AFM) cantilever tip. The Hertz theory of contact mechanics was used to analyze the indentation data (Tan and Lim, 2005).

Table 2.4 Mechanical characterization of nanofibers

Test methods	Instruments and techniques	Materials
Tensile test	(a) Atomic force microscope cantilevers	Carbon nanotubes (CNTs) Polyethylene oxide
	(b) Commercial nano tensile tester	Polycaprolactone Poly(L-lactic acid) (PLLA)
	(c) Custom made in situ TEM tester	CNTs
	(d) AFM-based nanoindentation system	Poly(L-lactic-co-glycolic acid)
Bend test	(a) Three-point bend test using AFM	Silicon & silicon dioxide CNTs Conductive polymers (polypyrrole) Biological materials (b-chitin) PLLA
	(b) Lateral displacement of free-end of fiber using AFM tip	CNTs & silicon carbide nanorods
	(c) Buckling of fiber using AFM	WS2 nanotubes
Nano-indentation	(a) Elastic–plastic indention using AFM-based nanoindentation system	Silver nanowires
	(b) Elastic–plastic indention using AFM	Silk
	(c) Elastic indention using AFM	Polyacrylonitrile (PAN) & PAN-CNT/graphite composite fibers Polypyrrole PLLA
Others	(a) Electrically induced deflections in TEM	CNTs
	(b) Resonating wire bridged across prongs of microfabricated tuning fork	Nitrocellulose/toluene sulfonamide formaldehyde resin
	(c) Resonant contact AFM	Polypyrrole Silver & lead nanowires

Source: Tan and Lim, 2005

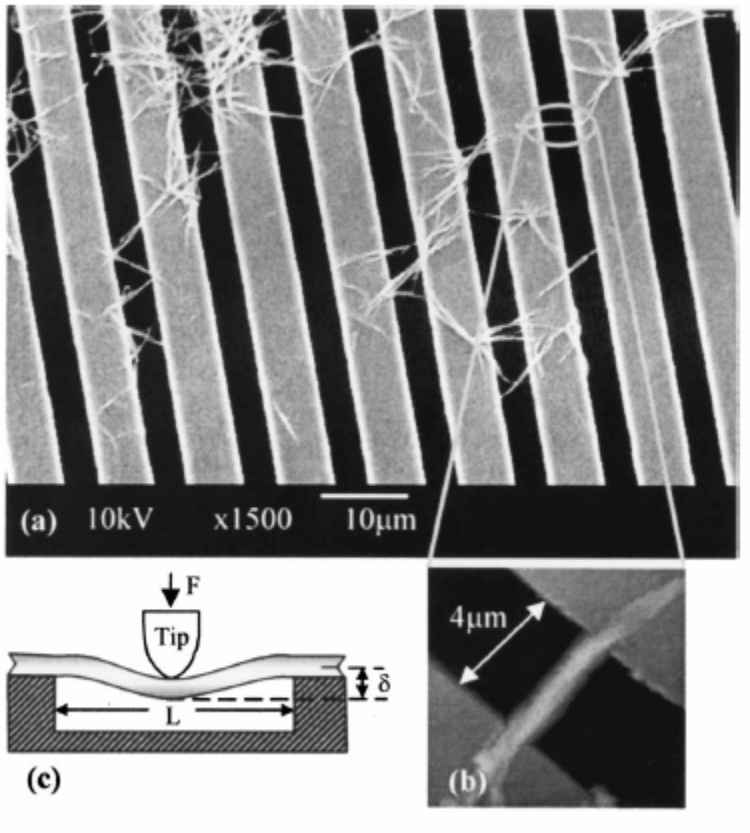

Figure 2.6 Nanofibers suspended over etched grooves of silicon wafer: (a) Electron micrograph of PLLA nanofibers deposited onto the silicon wafer; (b) AFM contact mode image of a single nanofiber (300 nm diameter) suspended over an etched groove; (c) schematic diagram of a nanofiber with mid-span deflected by an AFM tip (Source: Tan and Lim, 2004)

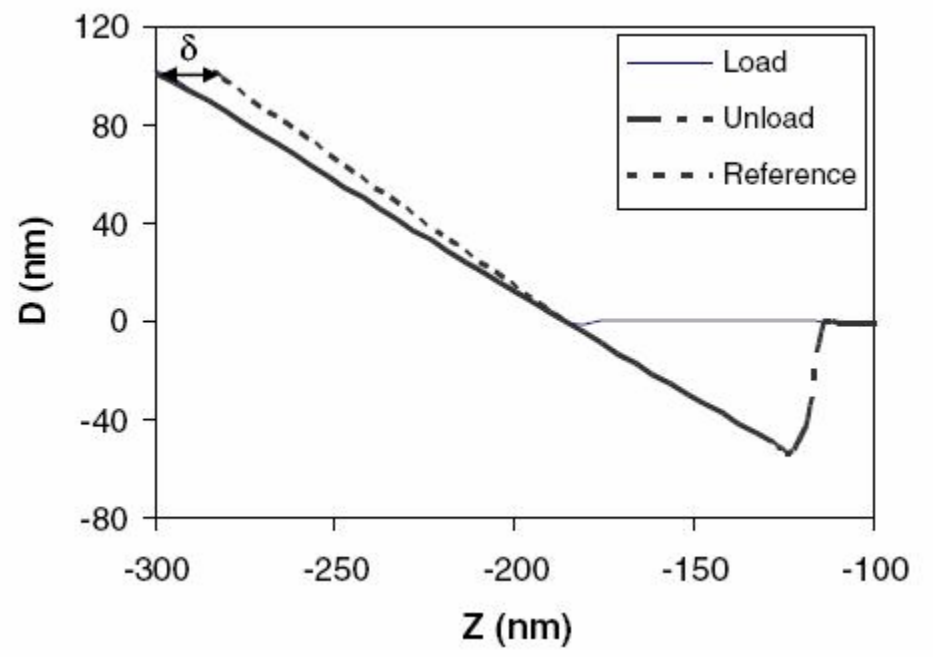

Figure 2.7 Plot of cantilever deflection (D) vs vertical displacement of the *z*-piezo (Z). A reference curve is obtained by measuring the cantilever deflection over the Z piezo displacement on a silicon wafer. The loading and unloading curves are obtained by using the AFM tip to deflect the midspan of the nanofiber. The deflection of the fiber, δ, is the difference between the loading and the reference curve (Source: Tan and Lim, 2004)

2.6. Fabrications and Characterization of Nanocomposites

2.6.1. Fabrication

The production of nanocomposites with cellulose fibrils of a high aspect ratio for load-bearing applications is relatively new. A wide range of nanocomposites has been studied to investigate the reinforcements of the fibrils, but there are still some problems, such as the dispersion of cellulose fibrils in polymer matrices, especially when they are hydrophobic. The most frequently used method is solvent evaporation casting, including water soluble and water non-soluble (use organic solvents). Nanocomposite films can be made by solvent casting method in Teflon or propylene dishes (Bhatnagar and Sain, 2005; Choi and Simonsen, 2006; Favier et al., 1995; Gindl and Keckes, 2005; Kvien et al., 2005; Taniguchi and Okamura, 1998). Fibrils freeze-drying followed by hot-pressing method can be used too (Dufresne et al., 1997a). Iwamoto et al. (2005) reported on optically transparent composites reinforced with cellulose nanofibers isolated by a high-pressure homogenizer treatment and a grinder treatment from wood pulp fiber. The method was to make mats by vacuum filtered using membrane filter. After dried, the mats were immersed in neat acrylic resin and then the resin was cured by UV light. They have also demonstrated on a web-like network of bacterial microfibrils from *Acetobacter xylinum* as a reinforcement material for optically functional composites (Yano et al., 2005). Another mat method was used to make PF resin composite using hot pressed at 160˚C for 30 min at high pressures of 30, 50, and 100 MPa (Nakagaito and Yano, 2005). Additional method of filtration mats followed by a compressive molding was used in this study (Cheng et al., 2007a).

2.6.2. Characterization

Various analysis instruments can be used to investigate the characterization of the obtained composites, e.g., mechanical properties, morphological characteristics, and thermal properties. Tensile tests (Bhatnagar and Sain, 2005; Chakraborty et al., 2006; Choi and Simonsen, 2006; Hepworth and Bruce, 2000; Marcovich et al., 2006; Orts et al., 2005; Taniguchi and Okamura, 1998; Zimmermann et al., 2004; Zimmermann et al., 2005), bending test (Nakagaito and Yano, 2005), and dynamic mechanical analysis (DMA) (Choi and Simonsen, 2006; Favier et al., 1995; Ljungberg et al., 2006; Svagan et al., 2007) were conducted to test the mechanical properties. Because DMA is strongly sensitive to the morphology of the composite, it will allow one to determine the mechanical behavior of nanocomposites in a broad temperature/frequency range. For morphological characterizations of nanocomposite, atomic force microscopy (AFM)(Kvien et al., 2005; Pu et al., 2007; Zimmermann et al., 2005), scanning electron microscope (SEM) (Marcovich et al., 2006; Svagan et al., 2007; Taniguchi and Okamura, 1998; Zimmermann et al., 2004), and transmission electron microscopy (TEM) (Kvien et al., 2005; Zimmermann et al., 2005) were commonly used. These techniques will be helpful to investigate the homogeneity of the composite, presence of voids, dispersion level of the fibrils within the continuous matrix, presence of aggregates, sedimentation, the interface between the fibril and the polymer matrix, and possible orientation of the fibrils. Thermal properties are also very important for nanocomposites. Differential scanning calorimetry (DSC), DMA, and thermogravimetric analyzer (TGA) (Ljungberg et al., 2006; Lu et al., 2006; Marcovich et al., 2006; Orts et al., 2005; Samir et al., 2006;

Sriupayo et al., 2005) were used to evaluate of the thermal transition property, enthalpy relaxation, crystallization and melting behavior of the nanocomposites. X-ray diffractograms was used to identify the crystal morphology of nanocomposites (Gindl and Keckes, 2005; Ljungberg et al., 2006; Sriupayo et al., 2005).

2.7. Ultrasonic Technology

High intensity ultrasonication (HIUS) can produce very strong mechanical oscillating power, so the separation of cellulose fibrils from biomass will be possible by the action of hydrodynamic forces of ultrasound. High-intensity ultrasounds are high frequency and low-amplitude oscillations as compared with sound oscillations and mechanical vibrations. They are widely used in many processes, especially in emulsification, catalysis, homogenization, disaggregation, scission, and dispersion. The first relevant works date back to 1927 (Wood and Loomis, 1927). Ultrasound is a cyclic sound pressure with a frequency greater than the upper limit of human hearing that is approximately 20 kHz (Figure 2.8) (Abramov, 1998).

2.7.1 Components of an ultrasonic processor

An ultrasonic processor consists of three major components: an ultrasonic power supply (generator), a converter (transducer) and a probe (horn). And a variety of accessories may be used to expand the capabilities of Ultrasonic Processors (Figure 2.9) (Anonymous, 2002).

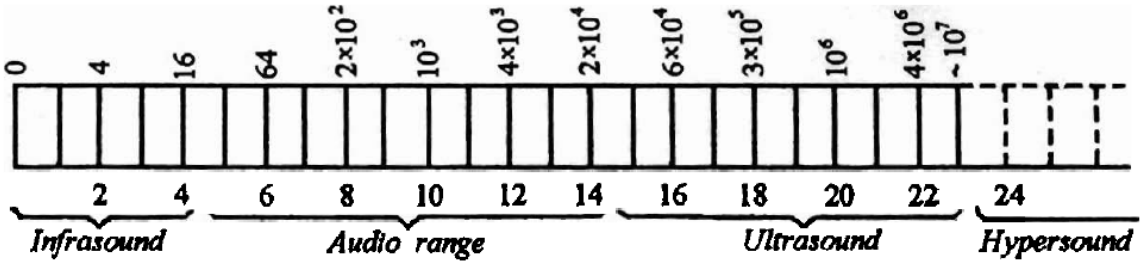

Figure 2.8 Logarithmic frequency scale for elastic vibrations (Source: Abramov, 1998)

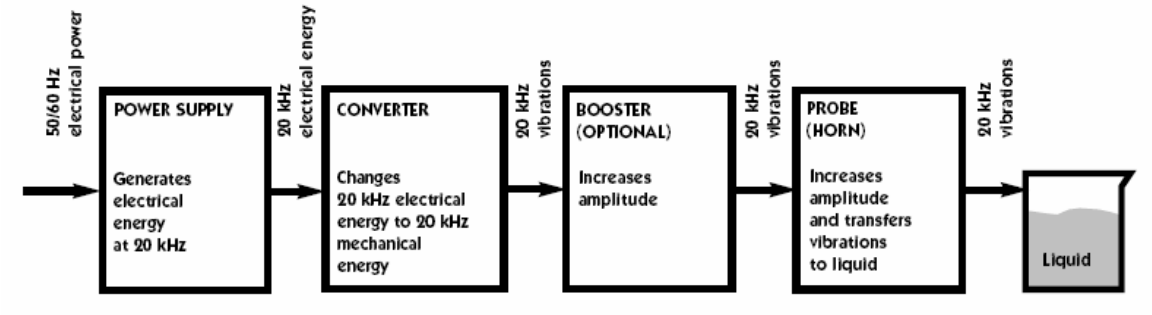

Figure 2.9 Major components of an ultrasonic processors (Source: Anonymous, 2002)

Three types of converters can be used to produce high-intensity ultrasonic waves in liquid media: piezoelectric, magnetostrictive, and mechanical converters. For the first two types, the transducer converts electrical energy to ultrasonic energy. The mechanical generators include two groups: whistles and sirens. The piezoelectric transducers are commonly used. After the generator converts 50/60 Hz voltage to high-frequency (e.g. 20 kHz) electrical energy, the piezoelectric crystals in the converter change electrical energy to small mechanical vibrations. The probe can amplify the longitudinal vibrations generated by the converter and transmit to the water as ultrasonic waves, which consist of alternate compressions and rarefactions. Because of the negative pressures in the rarefaction period, water is fractured or torn to create millions of microscopic bubbles or

called cavities. This is how the ultrasonic processor induces cavitation (Figure 2.10). When the bubbles are subjected to positive pressures in the compression stage, they oscillate and grow to an unstable size. Finally the bubbles implode and creating millions of shock waves, which generate high temperature of more than 5000ºC and high pressure of more than 500 atm at the implosion sites (Suslick, 1990). The mechanism of ultrasonically induced cavitation will be described in the following sections.

2.7.2 Length determination of waveguides (probes)

In ultrasonic technology, piezoelectric transducers are commonly used. Piezoceramics (ferroelectric ceramics) is one of the piezoelectric materials and Pb zirconate-titanate (PZT) is most frequently used to make piezoelectric transducer. Figure 2.11 shows a cross-section of a compound s piezoelectric transducer (Abramov, 1998).

The transducer is very important for an ultrasonic processor, but the dimensions of probes are also important because it transmits the ultrasonic vibrations to the processed media. A technological ultrasonic vibratory system consists of transducer, horn, waveguide/radiator and fixture as shown in Figure 2.12. The part 5 and 6 in the figure can be considered waveguide/radiator or called probe, also called sonotrode, which transmits vibrations of a certain type, such as longitudinal, bending, torsional, etc., from their source to a load. In this case for processing a liquid at room temperatures, the main vibration is longitudinal. The waveguide must satisfy certain equipments in order to operate as a guide of certain waves. For example, a uniform-section rod will be excited, when (Abramov, 1998):

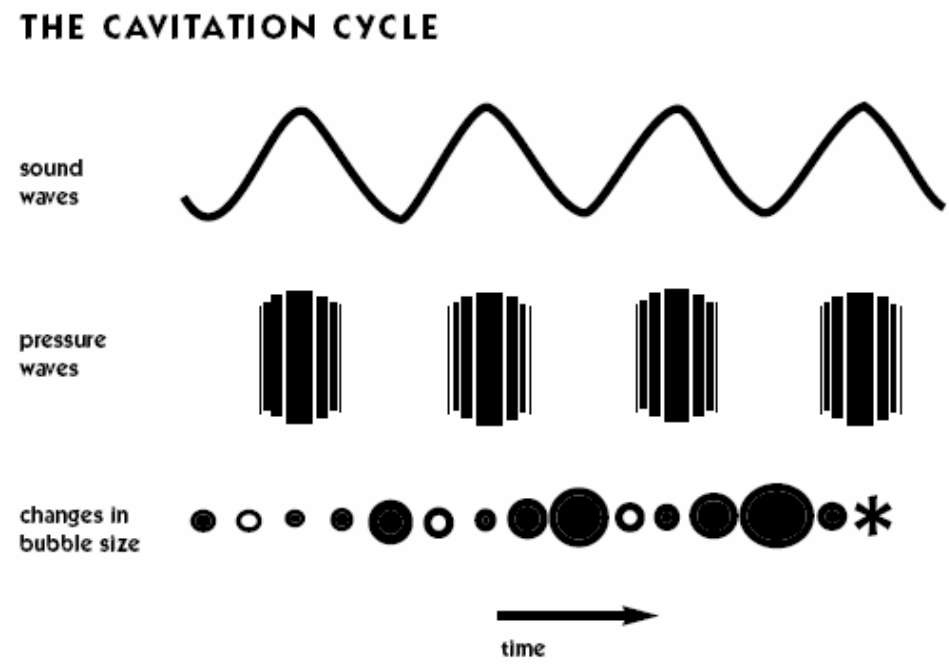

Figure 2.10 A schematic of cavitation cycle (Source: Anonymous, 2002)

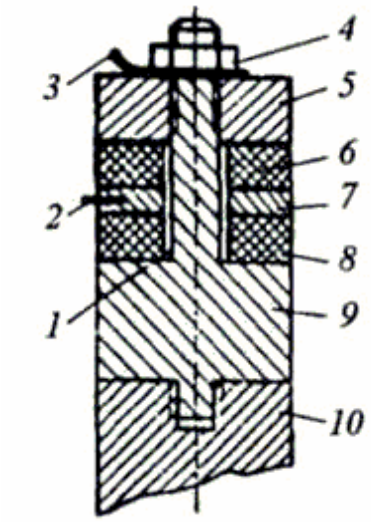

Figure 2.11 Cross-sectional view of a compound piezoelectric transducer: (1) insulating bush, (2) electrode, (3) grounding electrode, (4) nut, (5) upper metal plating, (6, 8) piezoceramic elements, (7) metal washer, (9) lower plating, (10) waveguide (Source: Abramov, 1998)

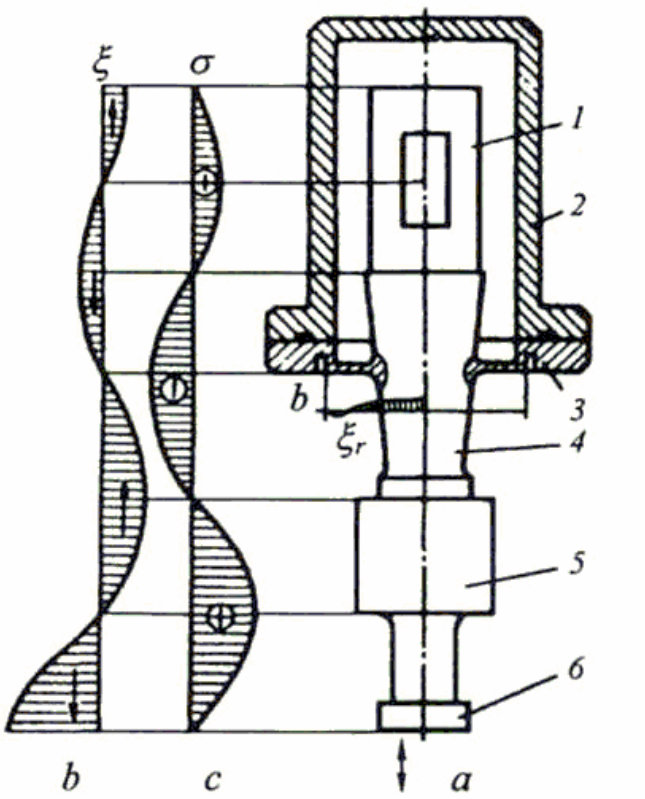

Figure 2.12 Cross-sectional view of an ultrasonic stack and the longitudinal distribution patterns of (b) displacement and (c) stress: (1) magnetostrictive transducer; (2) housing; (3) fixture; (4) horn; (5) sonotrode; (6) radiator. Arrows indicate the direction of wave propagation (Source: Abramov, 1998)

$$0.05 < \frac{d}{\lambda} < 0.5 \tag{2.1}$$

where d is the maximum linear dimension across a waveguide and λ is the wavelength in the waveguide material.

In this case, assume the shape of the waveguide is a uniform, circular cylinder. For a free end of waveguide, the resonant frequency f_0 of the waveguide and its length should follow the equation:

$$f_0 = \frac{c_l}{2l} n \tag{2.2}$$

where n = 1, 2, 3; and c_l is the sound velocity in the waveguide material.

For a fix frequency, the length waveguide can be calculated using:

$$l = \frac{c_l}{2 f_0} n \tag{2.3}$$

For example, if the material is Titanium VT-1, its c_l = 5072 m/s, assume the fixed frequency is 20kHz, and then the length of the waveguide will be 4.99 in (when n=1, half wavelength), and 9.98 in (n=2, whole wavelength).

2.7.3. Mechanism of ultrasonically induced cavitation in water.

The "cavitation" phenomenon, which generates bubbles in liquid, is the working principle of an ultrasonic processor in water. It lasts only a few microseconds, and the amount of energy released by each individual bubble is very tiny, but the cumulative energy generated by huge amount of bubbles is extremely high, so ultrasonic processors can be used to treat many kinds of materials in water or other liquids. Cavitation implies

nucleation, growth, pulsation, and subsequent collapse of bubbles or cavities. Bubble nucleation in liquids was reviewed by Blander, which was about the theoretical and experimental aspects of bubble nucleation and explosive boiling. It requires the creation of a new interface as we1l as the transfer of molecules from the liquid into the bubble to create a bubble in a liquid (Blander, 1979).

An acoustic wave in the rarefaction phase produces tensile stress, which results in the forming of bubbles or discontinuities and cavities appear. Once being formed, the bubble can pulse, or increase to the maximum size (2.65 mm in water) and then collapse. This cavitation behavior has been investigated theoretically and experimentally by many researchers. The behavior and motion of cavities depend on both properties of the liquid and ultrasonic field. In estimating the cavitational strength of a liquid containing vapor or gas nuclei (tiny bubbles), the peak sound pressure P_m should be below a critical value P_c^v, known as the vapor cavitation threshold, to keep the bubble stable. Above this value, the bobble will grow and collapse finally (Abramov, 1998; Kornfeld, 1951).

$$P_c^v = P_0 - P_v + \frac{2}{3\sqrt{3}}\sqrt{\frac{(2\sigma_L / R_0)^3}{P_0 - P_v + 2\sigma_L / R_0}} \tag{2.4}$$

where P_0 is the initial air pressure, P_v is the saturation vapor pressure, R_0 is the initial radius.

The pulsating bubble in an acoustic field can increase in size through a rectified diffusion due to gas diffusion from liquid even it is not saturated with gas and the sound pressure threshold becomes (Hsieh and Plesset, 1961; Strasberg, 1961):

$$P_c^g = \sqrt{\frac{2}{3}} P_0 \sqrt{1 + \frac{2\sigma_L}{P_0 R_0} - \frac{c_\infty}{c_0}} \tag{2.5}$$

where C_0 is the equilibrium concentration of dissolved gas at pressure P_0; C_∞ is the apparent gas concentration in liquid far away from the nucleus.

Besides the vapor and gas filled bubbles, another important part in ultrasonic cavitation is the solid phase involved, such as vessel walls, the emitting surface of ultrasonic radiators, particles suspended in the liquid. The work for cavity formation near the solid surface and the pressure needed for liquid rupture can be determined by (Fisher, 1948; Frenkel, 1945):

$$W_c^s = W_c \phi(\theta) \tag{2.6}$$

$$P_c^s = P_c [\phi(\theta)]^{1/2} \tag{2.7}$$

where $W_c = 16\pi\sigma_L^2 / 3P_c^2$ is the work of cavity formation in a homogeneous liquid; $P_c = -[16\pi\sigma_L^2 / (3kT \ln NkT / h)]^{1/2}$ is the pressure necessary for liquid rupture; k is the Boltzmann constant; N is the Avogadro number; h is Plank's constant; $\Phi(\theta)$ is the trigonometric function of the wetting angle θ.

If assume the cavities as spherical bubbles filled with a gas-vapor mixture and caving dimensions much smaller than the ultrasonic wavelength, the cavity in an incompressible liquid with a constant density and infinitely large sound velocity can be described by (Rayleigh, 1917):

$$R\frac{d^2R}{dt^2} + \frac{3}{2}\left(\frac{dR}{dt}\right)^2 + \frac{1}{\rho_L}\left[P_\infty - P(R)\right] = 0 \tag{2.8}$$

where R is the cavity radius; R is the cavity radius; P_∞ is the pressure infinitely far from the cavity; P(R) is the pressure on the cavity surface.

When P_∞=P_0=const and P(R)=0 (empty bubble), the simplest equation is:

$$U^2 = \frac{dR}{dt} = \frac{2}{3}\frac{P_0}{\rho_L}\left(\frac{R_{\max}^3}{R^3} - 1\right) \tag{2.9}$$

where U is the velocity of the bubble boundary motion; R_{max} is the maximum cavity radius at the collapse onset.

A satisfactory description of stable cavities was proposed by Herring and Flinn that used to estimate the collapse velocity and minimum radius of the cavity (Flinn, 1964):

$$R\left(1-2\frac{U}{c_0}\right)\frac{d^2R}{dt^2} + \frac{3}{2}\left(1-\frac{4U}{3c_0}\right)\left(\frac{dR}{dt}\right)^2 + \frac{1}{\rho_L}$$
$$\left[P_0 - P_v - P_m \sin\omega t + \frac{2\sigma_L}{R} + \frac{4\eta U}{R} - \left(P_0 + \frac{2\sigma_L}{R_0}\right)\left(\frac{R_0}{R}\right)^{3\gamma}\right] + \frac{RU}{\rho_L c_0}\left(1-\frac{U}{c_0}\right)\left(\frac{dP}{dR}\right) = 0 \tag{2.10}$$

With a given velocity the motion of the cavity is described by the Kirwood-Bethe-Gilmore equation (Cole, 1948):

$$R\left(1-\frac{U}{c}\right)\frac{d^2R}{dt^2} + \frac{3}{2}\left(1-\frac{U}{3c}\right)\left(\frac{dR}{dt}\right)^2 + \left(1+\frac{U}{c}\right)H - \frac{U}{c}\left(1-\frac{U}{c}\right)R\frac{dH}{dR} = 0 \tag{2.11}$$

where $H = \int_{P_\infty}^{P(R)} \frac{dP}{\rho_L}$ is the free enthalpy at the surface of a spherical cavity; U is the velocity of bubble boundary motion; R is the cavity radius; P_0 is the environment pressure; P_v is the vapor pressure; P_m is the amplitude; ω is the frequency; c is the sound velocity; γ=1 for isothermal pulsation and 4/3 for adiabatic pulsation.

Cavities make strong shock waves and the amplitude is large only near the collapsing cavity. This is why cavitation-related processes are most pronounces near collapsing cavities. The instantaneous values of pressure in shock waves can be as high as tens of MPa, which make the shock waves to cause microdestruction of solid surfaces and impact a considerable acceleration to particles suspended in liquids. The bubble collapses can also dramatically increase temperature of liquid. The calculation value was up to 10,000 K for water (Abramov, 1998; Crum, 1984).

2.8. Ultrasonic Treatment for Cellulose

2.8.1. Application of ultrasonication in pulp and paper technology

Ultrasound irradiation of cellulose fibers was found to promote fibrillation of the fibers without cutting, and the fibrillation process appeared to occur predominantly at sites on the fiber wall that have already been damaged by the refining process. So that commercial fiber refining could be enhanced by a combination of mechanical and ultrasound refining giving a reduction in cutting and resultant lowering of fiber loss (Manning and Thompson, 2002). Turai and Teng (1978) used ultrasonic generated by a mechanical generator of whistle called a jet-edge generator to deink of waste paper which printed heavily with high-gloss polymeric inks or covered with overprinted varnished (Turai and Teng, 1978). As a pretreatment, ultrasonic irradiation was used to aid a practical high-performance enzymatic hydrolysis of cellulose. The time needed for effective degradation could be markedly reduced by increasing the ultrasonication irradiation power, which made it possible to apply ultrasonication pretreatment in a

practical cellulose saccharification process (Imai et al., 2004). Ultrasonic was uased to distribute the cellulose fibres more uniform in the produced paper web, which made a stronger paper with more even surfaces (Ultra Technology, online). An old review paper discribed the applications of ultrasound in pulp and paper technology before 1977 (Laine et al., 1977).

2.8.2. Cellulose degradation and surface modification by ultrasonication

Simpson and Mason used ultrasonic waves with 500 KHz and 500 wattes to treat cellulose fiberse less than 15 min. The effects were similar to those produced by ordinary beating and there was no measurable chemical degradation of the cellulose (Simpson and Mason, 1950). The ultrasonic irradiation with the equipment of 23 KHz and 11 W affected the morphology of cellulose supended in water, enlarged the cell wall pores and damaged fiber surface without much loss of carbohydrate material. But the chemical changes were of minor importance (Laine and Goring, 1977). Ultrasonication of cellulose caused a strong decrease of the degree of polymerization investigated using equipment with a frequency of 20 kHz and an output power of 22 W (MarxFigini, 1997).

An ultrasound reactor (80 W and 38 kHz) was used to break down the cellulose samples to produce glucose and other chemical species. It could help the further conversion of chemicals into fuel (alcohol) (Aliyu and Hepher, 2000). Ultrasonic treatment can increase the accessibility and improve the regioselective oxidation reactivity of cllulose (Tang et al., 2005). The surface properties of wood fibers were modified by the generation of free radicals using high-frequency ultrasound at 610 kHz.

Thermomechanical pulp fibers (TMP) were sonicated in the aqueous suspensions. The results of FTIR-transmission, FTIR-ATR spectroscopy suggested the number of non-conjugated carbonyl groups in TMP was increased after sonication due to the oxidation of phenolic hydroxyl groups in lignin. And inverse gas chromatography (IGC) results showed an increase in the surface free energy of fibers (Gadhe et al., 2006).

Ultrasound treatment (30 kHz) was used to investigate the fibrillation tendency of viscose and Local fibers determined using a modified and developed microscopic method (Tomljenovic and unko, 2004). Ultrasonic treatment was used for dispersion the fibrils after chemical treatment and fibril dispersion in the fabrication of fibril-reinforced (Choi and Simonsen, 2006).

2.8.3. The challenge of fibril isolation from cellulose by ultrasonication

Some problems and challenges in the isolation of cellulose fibrils and fabrication of fibril-reinforced nanocomposite were mentioned in Chapter 1 (1.1). The challenges in the treatment of cellulose to make fibrils include:

1. The possibility of fibril isolation without severe degradation from cellulose by high intensity ultrasonic treatment because of its instantaneous high shear force and high temperature;

2. How to evaluate the fibril degradation, especially the mechanical properties after isolation;

3. Energy consumption of cellulose treatment by ultrasonic treatment;

4. Cost and scale up of cellulose treatment by ultrasonic treatment;

5. Lack of literature on the cellulose treatment by ultrasonication, especially fibrillation research.

Based on these challenges, this dissertation will focus on developing the fibril isolation method with high intensity ultrasonic treatment, characterizing the fibrils, as well as investigating the reinforcement of these fibrils for some polymers.

2.9. Conclusions

Cellulose fibrils in nano and micro scales, which have high mechanical properties and potential reinforcement for polymers, can be isolated from natural cellulose fibers. Two common methods have been developed to generate fibrils. One is the chemical way mainly by strong acid hydrolysis via removing the amorphous regions of cellulose fiber. This method was used to generate cellulose crystal or nanofibril. The second method is the mechanical way mainly by strong shear force such as using supergrinder or homogenizer to separate cellulose fiber to fibrils and this method was used to generate cellulose microfibril or its bundles. Cellulose fibrils can be used to reinforce polymers to make biodegradable nanocomposites. The high intensity ultrasonication has cavitation behavior in liquid. Cavitations generate strong shock waves, which possess high instantaneous values of pressure. The bubble collapses can also dramatically increase temperature of liquid. Ultrasonic treatments are successfully used in emulsification, catalysis, homogenization, disaggregation, scission, and dispersion.

References

Anonymous, 2002. What are ULTRASONICS and ULTRASONIC PROCESSING? Sonics & Materials, Inc.

Abramov, O. V., 1998. High-intensity ultrasonic theory and industrial applications. Gordon and Breach Science Publishers. ISBN 90-5699-041-1.

Aliyu, M. and Hepher, M.J., 2000. Effects of ultrasound energy on degradation of cellulose material. Ultrasonics Sonochemistry, 7(4): 265-268.

Beck-Candanedo, S., Roman, M. and Gray, D.G., 2005. Effect of reaction conditions on the properties and behavior of wood cellulose nanocrystal suspensions. Biomacromolecules, 6(2): 1048-1054.

Berglund, L., 2005. Cellulose-based nanocomposites. In: L. Drzal (Editor), Natural Fibers, Biopolymers, and Biocomposites. Taylor & Francis, pp. 807-832.

Bhatnagar, A. and Sain, M., 2005. Processing of cellulose nanofiber-reinforced composites. Journal of Reinforced Plastics and Composites, 24(12): 1259-1268.

Blackwel.J, Vasko, P.D. and Koenig, J.L., 1970a. Infrared and Raman spectra of cellulose from cell wall of valonia ventricosa. Journal of Applied Physics, 41(11): 4375-4379.

Blackwel.J, Vasko, P.D. and Koenig, J.L., 1970b. Infrared and Raman spectra of native cellulose from cell wall of valonia ventricosa. Bulletin of the American Physical Society, 15(3): 305.

Blander, M., 1979. Bubble nucleation in liquids. Advances in Colloid and Interface Science, 10(JAN): 1-32.

Bondeson, D., Mathew, A. and Oksman, K., 2006. Optimization of the isolation of nanocrystals from microcrystalline cellulose by acid hydrolysis. Cellulose, 13(2): 171-180.

Chakraborty, A., Sain, M. and Kortschot, M., 2005. Cellulose microfibrils: A novel method of preparation using high shear refining and cryocrushing. Holzforschung, 59(1): 102-107.

Chakraborty, A., Sain, M. and Kortschot, M., 2006. Reinforcing potential of wood pulp-derived microfibres in a PVA matrix. Holzforschung, 60(1): 53-58.

Chaplin M., online. http://www.lsbu.ac.uk/water/hycel.html.

Cheng, Q., Wang, S., Rials, G.T. and Lee, S.H., 2007a. Physical and mechanical properties of polyvinyl alcohol and polypropylene composite materials reinforced with fibril aggregates isolated from regenerated cellulose fibers. Cellulose, online first, DOI: 10.1007/s10570-007-9141-0.

Cheng, Q., Wang, S., Zhou, D., Y., Z. and Rials, T., 2007b. Lyocell-derived cellulose microfibril/nanofibril and its biodegradable nanocomposites. Journal of Nanjing Forestry University, 31(4): 21-26.

Choi, Y.J. and Simonsen, J., 2006. Cellulose nanocrystal-filled carboxymethyl cellulose nanocomposites. Journal of Nanoscience and Nanotechnology, 6(3): 633-639.

Cole, R. H., 1948. Underwater Explosions, Princeton University Press, Princeton, N. J.

Crum, L.A., 1984. Acoustic cavitation series: part five rectified diffusion. Ultrasonics, 22: 215–223.

Dufresne, A., Cavaille, J. and Helbert, W., 1997a. Thermoplastic nanocomposites filled with wheat straw cellulose whiskers. 2. Effect of processing and modeling. Polymer Composites, 18(2): 198-210.

Dufresne, A., Cavaille, J.Y. and Vignon, M.R., 1997b. Mechanical behavior of sheets prepared from sugar beet cellulose microfibrils. Journal of Applied Polymer Science, 64(6): 1185-1194.

Dufresne, A., Dupeyre, D. and Vignon, M.R., 2000. Cellulose microfibrils from potato tuber cells: Processing and characterization of starch-cellulose microfibril composites. Journal of Applied Polymer Science, 76(14): 2080-2092.

Dufresne, A. and Vignon, M.R., 1998. Improvement of starch film performances using cellulose microfibrils. Macromolecules, 31(8): 2693-2696.

Edgar, C.D. and Gray, D.G., 2002. Influence of dextran on the phase Behavior of suspensions of cellulose nanocrystals. Macromolecules, 35(19): 7400-7406.

Eichhorn, S.J. and Young, R.J., 2001. The Young's modulus of a microcrystalline cellulose. Cellulose, 8(3): 197-207.

Favier, V. et al., 1995. Nanocomposite Materials from Latex and Cellulose Whiskers. Polymers for Advanced Technologies, 6(5): 351-355.

Fengel, D., and G. Wegener. 1984. Wood Chemistry, Ultrastructure, Reaction. Walter de Gruyter, Berlin, New York. ISBN 3-11-008481-3. P.234-238.

Finkenstadt, V.L. and Millane, R.P., 1998. Crystal structure of Valonia cellulose I beta. Macromolecules, 31(22): 7776-7783.

Fisher, J.C., 1948. The fracture of liquids. Journal of Applied Physics, 19(11): 1062-1067.

Flinn, G., 1964. Acoustic Principles and Methods, Vol. 1, Methods and Devices, Part B, W. P. Mason Ed., Academic Press, New York.

Franks, A. 1987. "Nanotechnology", J. Phys. E: Sci Instrum 20, pp 1442-1451.

Frenkel, Ya.I., 1945. Kinetic Theory of liquids (in Russian), AN SSSR, Moscow.

Gadhe, J.B., Gupta, R.B. and Elder, T., 2006. Surface modification of lignocellulosic fibers using high-frequency ultrasound. Cellulose, 13(1): 9-22.

Gallagher, P. W., and D. L. Johnson. 1995. Some New Ethanol Technology: Cost, Competition and Adaptation Effects in the Petroleum Market. Staff paper #275. Iowa State University, Ames.

George, J., Sreekala, M.S. and Thomas, S., 2001. A review on interface modification and characterization of natural fiber reinforced plastic composites. Polymer Engineering and Science, 41(9): 1471-1485.

Gindl, W. and Keckes, J., 2005. All-cellulose nanocomposite. Polymer, 46(23): 10221-10225.

Hepworth, D.G. and Bruce, D.M., 2000. The mechanical properties of a composite manufactured from non-fibrous vegetable tissue and PVA. Composites Part a-Applied Science and Manufacturing, 31(3): 283-285.

Herrick, F.W., Casebier, R.L., Hamilton, J.K. and Sandberg, K.R., 1983. Microfibrillated cellulose: morphology and accessibility. Journal of Applied Polymer Science: Applied Polymer Symposium, 37: 797-813.

Hsieh, D.Y. and Plesset, M.S., 1961. Theory of rectified diffusion of mass into gas bubbles. Journal of the Acoustical Society of America, 33(2): 206-215.

Imai, M., Ikari, K. and Suzuki, I., 2004. High-performance hydrolysis of cellulose using mixed cellulose species and ultrasonication pretreatment. Biochemical Engineering Journal, 17(2): 79-83.

Iwamoto, S., Nakagaito, A.N., Yano, H. and Nogi, M., 2005. Optically transparent composites reinforced with plant fiber-based nanofibers. Applied Physics A-Materials Science & Processing, 81(6): 1109-1112.

Jordan, J., Jacob, K.I., Tannenbaum, R., Sharaf, M.A. and Jasiuk, I., 2005. Experimental trends in polymer nanocomposites - a review. Materials Science and Engineering a-Structural Materials Properties Microstructure and Processing, 393(1-2): 1-11.

Kornfeld, M., 1951. Elasticity and Strength of Liquids (Russian translation), GINTL, Moscow, Leningrad.

Kvien, I., Tanem, B.S. and Oksman, K., 2005. Characterization of cellulose whiskers and their nanocomposites by atomic force and electron microscopy. Biomacromolecules, 6(6): 3160-3165.

Laine, J.E. and Goring, D.A.I., 1977. Influence of ultrasonic irradiation on properties of cellulosic fibers. Abstracts of Papers of the American Chemical Society, 173(MAR20): 45-45.

Laine, J.E., Macleod, J.M., Bolker, H.I. and Goring, D.A.I., 1977. Applications of ultrasound in pulp and paper technology. Paperi Ja Puu-Paper and Timber, 59(NA4): 235.

Laka, M., Chernyavskaya, S., Treimanis, A. and Faitelson, L., 2000. Preparation and properties of microcrystalline cellulose gels. Cellulose Chemistry and Technology, 34(3-4): 217-227.

Levandoski, R., J. Norman, G. Pepelnjak, and T. Drnovsek, 1999. Ultrasonic deinking and fiber properties. Progress in Paper Recycling, p. 53-57.

Lilaseca, F. and Peijs, T., 2005. Cellulose-based nanocomposites. The 8th International Conference on Woodfiber-Plastic Composites: 283-295.

Lima, M.M.D. and Borsali, R., 2004. Rodlike cellulose microcrystals: Structure, properties, and applications. Macromolecular Rapid Communications, 25(7): 771-787.

Ljungberg, N. et al., 2005. New nanocomposite materials reinforced with cellulose whiskers in atactic polypropylene: Effect of surface and dispersion characteristics. Biomacromolecules, 6(5): 2732-2739.

Ljungberg, N., Cavaille, J.Y. and Heux, L., 2006. Nanocomposites of isotactic polypropylene reinforced with rod-like cellulose whiskers. Polymer, 47(18): 6285-6292.

Lu, Y.S., Weng, L.H. and Cao, X.D., 2005. Biocomposites of plasticized starch reinforced with cellulose crystallites from cottonseed linter. Macromolecular Bioscience, 5(11): 1101-1107.

Lu, Y.S., Weng, L.H. and Cao, X.D., 2006. Morphological, thermal and mechanical properties of ramie crystallites - reinforced plasticized starch biocomposites. Carbohydrate Polymers, 63(2): 198-204.

Manning, A. and Thompson, R., 2002. The influence of ultrasound on virgin paper fibers. Progress in Paper Recycling, 11(4): 6-12.

Marcovich, N.E., Auad, M.L., Bellesi, N.E., Nutt, S.R. and Aranguren, M.I., 2006. Cellulose micro/nanocrystals reinforced polyurethane. Journal of Materials Research, 21(4): 870-881.

MarxFigini, M., 1997. Studies on the ultrasonic degradation of cellulose - Macromolecular properties. Angewandte Makromolekulare Chemie, 250: 85-92.

Matsuo, M., 1990. General-analysis of the measurement of the crystal-lattice modulus of semicrystalline polymers by X-ray-diffraction. Macromolecules, 23(13): 3261-3266.

Matsuo, M., Sawatari, C., Iwai, Y. and Ozaki, F., 1990. Effect of orientation distribution and crystallinity on the measurement by X-ray-diffraction of the crystal-lattice moduli of cellulose-I and cellulose-II. Macromolecules, 23(13): 3266-3275.

Meyer, K.H. and Misch, L., 1937. Positions of atoms in the new spatial model of cellulose (On the constitution of the crystallized part of the cellulose IV). Helvetica Chimica Acta, 20: 232-244.

Mott, L., Shaler, S.M. and Groom, L.H., 1996. A technique to measure strain distributions in single wood pulp fibers. Wood and Fiber Science, 28(4): 429-437.

Nakagaito, A.N., Iwamoto, S. and Yano, H., 2005. Bacterial cellulose: the ultimate nano-scalar cellulose morphology for the production of high-strength composites. Applied Physics a-Materials Science & Processing, 80(1): 93-97.

Nakagaito, A.N. and Yano, H., 2005. Novel high-strength biocomposites based on microfibrillated cellulose having nano-order-unit web-like network structure. Applied Physics a-Materials Science & Processing, 80(1): 155-159.

Orts, W.J. et al., 2005. Application of cellulose microfibrils in polymer nanocomposites. Journal of Polymers and the Environment, 13(4): 301-306.

O'Sullivan, A. C., 1997. Cellulose: the structure slowly unravels. Cellulose, 4, 173-207.

Page, D.H., Winkler, K., Bain, R. and Elhossei.F, 1972. Mechanical properties of single wood-pulp fibers .1. New approach. Pulp and Paper Magazine of Canada, 73(8): 72.

Panshin, A. J. and Carl de Zeeuw, 1980. Textbook of wood technology: structure, identification, properties, and uses of the commercial woods of the United States and Canada. New York: McGraw-Hill.

Podsiadlo, P. et al., 2005. Molecularly engineered nanocomposites: Layer-by-layer assembly of cellulose nanocrystals. Biomacromolecules, 6(6): 2914-2918.

Pohler, E., Zimmermann, T., and Geiger, T., online. Cellulose-Nanofibrils for polymer reinforcement. http://www.empa.ch/plugin/template/empa/*/27303/---/l=1.

Pu, Y.Q. et al., 2007. Investigation into nanocellulosics versus acacia reinforced acrylic films. Composites Part B-Engineering, 38(3): 360-366.

Rayleigh, 1917. On the pressure developed in a liquid during the collapse of a spherical cavity. Philosophical Magazine, 34(199-04): 94-98.

Rooney, T. 1998. Lignocellulosic feedstock resource assessment. Report SR-580-24189. Golden, Colo.: National Renewable Energy Laboratory.

Sakurada, I., Nukushina, Y. and Ito, T., 1962. Experimental determination of elastic modulus of crystalline regions in oriented polymers. Journal of Polymer Science, 57(165): 651-660.

Salvetat, J.P., Briggs, G.A.D., Bonard, J.M., Bacsa, R.R., Kulik, A.J., Stockli, T., Burnham, N.A. and Forro, L., 1999a. Elastic and shear moduli of single-walled carbon nanotube ropes. Physical Review Letters, 82(5): 944-947.

Salvetat, J.P., Kulik, A.J., Bonard, J.M., Briggs, G.A.D., Stockli, T., Metenier, K., Bonnamy, S., Beguin, F., Burnham, N.A. and Forro, L., 1999b. Elastic modulus of ordered and disordered multiwalled carbon nanotubes. Advanced Materials, 11(2): 161-165.

Salvetat-Delmotte, J.P. and Rubio, A., 2002. Mechanical properties of carbon nanotubes: a fiber digest for beginners. Carbon, 40(10): 1729-1734.

Samir, M., Alloin, F. and Dufresne, A., 2005. Review of recent research into cellulosic whiskers, their properties and their application in nanocomposite field. Biomacromolecules, 6(2): 612-626.

Samir, M., Alloin, F. and Dufresne, A., 2006. High performance nanocomposite polymer electrolytes. Composite Interfaces, 13(4-6): 545-559.

Samir, M., Alloin, F., Sanchez, J.Y. and Dufresne, A., 2004. Cross-linked nanocomposite polymer electrolytes reinforced with cellulose whiskers. Macromolecules, 37(13): 4839-4844.

Sarko, A. and Muggli, R., 1974. Packing analysis of carbohydrates and polysaccharides. 3. Valonia cellulose and cellulose-II. Macromolecules, 7(4): 486-494.

Simpson, F.W. and Mason, S.G., 1950. Note on the treatment of cellulose fibers with ultrasonic waves. Pulp and Paper Magazine of Canada, 51: 70-72.

Sjostrom, E., 1993. Wood chemistry fundamentals and applications; Academic Press: New York.

Sriupayo, J., Supaphol, P., Blackwell, J. and Rujiravanit, R., 2005. Preparation and characterization of alpha-chitin whisker-reinforced chitosan nanocomposite films with or without heat treatment. Carbohydrate Polymers, 62(2): 130-136.

Strasberg, M., 1961. Rectified diffusion - Paper of Hsieh and Plesset. Journal of the Acoustical Society of America, 33(3): 359.

Sturcova, A., Davies, G.R. and Eichhorn, S.J., 2005. Elastic modulus and stress-transfer properties of tunicate cellulose whiskers. Biomacromolecules, 6(2): 1055-1061.

Svagan, A.J., Samir, M. and Berglund, L.A., 2007. Biomimetic polysaccharide nanocomposites of high cellulose content and high toughness. Biomacromolecules, 8(8): 2556-2563.

Tan, E.P.S. and Lim, C.T., 2004. Physical properties of a single polymeric nanofiber. Applied Physics Letters, 84(9): 1603-1605.

Tan, E.P.S. and Lim, C.T., 2005. Nanoindentation study of nanofibers. Applied Physics Letters, 87(12): No. 123106.

Tan, E.P.S. and Lim, C.T., 2006. Mechanical characterization of nanofibers - A review. Composites Science and Technology, 66(9): 1102-1111.

Tang, A.M., Zhang, H.W., Chen, G., Xie, G.H. and Liang, W.Z., 2005. Influence of ultrasound treatment on accessibility and regioselective oxidation reactivity of cellulose. Ultrasonics Sonochemistry, 12(6): 467-472.

Taniguchi, T., 1996. Microfibrillation of natural fibrous materials. J. Soc. Mat. Sci. Japan, 45(4): 472-473.

Taniguchi, T. and Okamura, K., 1998. New films produced from microfibrillated natural fibres. Polymer International, 47(3): 291-294.

Thielemans, W., Belgacem, M.N. and Dufresne, A., 2006. Starch nanocrystals with large chain surface modifications. Langmuir, 22(10): 4804-4810.

Tombler, T.W., Zhou, C.W., Alexseyev, L., Kong, J., Dai, H.J., Lei, L., Jayanthi, C.S., Tang, M.J. and Wu, S.Y., 2000. Reversible electromechanical characteristics of carbon nanotubes under local-probe manipulation. Nature, 405(6788): 769-772.

Tomljenovic, A. and R., C., 2004. Reducing fibrillation tendency of man-made cellulose fibres employing ultrasound treatment. J. Text. Inst., 95(1/6): 327-340.

Tsuchikawa, S., H. W. Siesler. 2006. Near infrared spectroscopic monitoring of the diffusion process of deuterium-labeled molecules in wood. In Characterization of the Cellulose Cell Wall, Chapter 10, P.134. Blackwell Publishing.

Turai, L.L. and Teng, C.H., 1978. Ultrasonic deinking of waste paper. Tappi, 61(2): 31-34.

Turbak, A.F., Snyder, F.W. and Sandberg, K.R., 1983. Microfibrillated cellulose, a new cellulose product: properties, uses, and commercial potential. Journal of Applied Polymer Science: Applied Polymer Symposium, 37: 815-827

Ultra technology, online. http://www.ultratechnology.se/

Wan, W.K., Hutter, J.L., Millon, L. and Guhados, G., 2006. Bacterial cellulose and its nanocomposites for biomedical applications. Cellulose Nanocomposites: Processing, Characterization, and Properties. Acs Symposium Series, pp. 221-241.

Wang, B. and Sain, M., 2007. Isolation of nanofibers from soybean source and their reinforcing capability on synthetic polymers. Composites Science and Technology, 67(11-12): 2521-2527.

Wang, Y.X., Cao, X.D. and Zhang, L.N., 2006. Effects of cellulose whiskers on properties of soy protein thermoplastics. Macromolecular Bioscience, 6(7): 524-531.

Wiley, J.H. and Atalla, R.H., 1987. Band assignments in the Raman-spectra of celluloses. Carbohydrate Research, 160: 113-129.

Wong, E.W., Sheehan, P.E. and Lieber, C.M., 1997. Nanobeam mechanics: Elasticity, strength, and toughness of nanorods and nanotubes. Science, 277(5334): 1971-1975

Wood, R.W. and Loomis, A.L., 1927. The physical and biological effects of high-frequency sound-waves of great intensity. Philosophical Magazine, 4(22): 417-436.

Woodcock, C. and Sarko, A., 1980. Packing analysis of carbohydrates and polysaccharides. 11. Molecular and crystal-structure of native ramie cellulose. Macromolecules, 13(5): 1183-1187.

Xing, C., Wang, S., Pharr, G.M. and Groom, L.H., 2007. Effect of thermo-mechanical refining pressure on the properties of wood fiber cell walls: measured by nanoindentation and AFM. Holzforschung (in print).

Xu, W., Mulhern, P.J., Blackford, B.L., Jericho, M.H. and Templeton, I., 1994. A new atomic-force microscopy technique for the measurement of the elastic properties of biological-materials. Scanning Microscopy, 8(3): 499-506.

Yano, H. and Nakahara, S., 2004. Bio-composites produced from plant microfiber bundles with a nanometer unit web-like network. Journal of Materials Science, 39(5): 1635-1638.

Yano, H., Sugiyama, J., Nakagaito, A.N., Nogi, M., Matsuura, T., Hikita, M. and Handa, K., 2005. Optically transparent composites reinforced with networks of bacterial nanofibers. Advanced Materials, 17(2): 153-155.

Yuan, H.H., Nishiyama, Y., Wada, M. and Kuga, S., 2006. Surface acylation of cellulose whiskers by drying aqueous emulsion. Biomacromolecules, 7(3): 696-700.

Zimmermann, T., Pohler, E. and Geiger, T., 2004. Cellulose fibrils for polymer reinforcement. Advanced Engineering Materials, 6(9): 754-761.

Zimmermann, T., Pohler, E. and Schwaller, P., 2005. Mechanical and morphological properties of cellulose fibril reinforced nanocomposites. Advanced Engineering Materials, 7(12): 1156-1161.

CHAPTER 3. DEVELOPMENT OF A NOVEL PROCESS TO ISOLATE FIBRILS FROM CELLULOSE FIBERS BY HIGH-INTENSITY ULTRASONICATION

3.1. Abstract

Cellulose fibrils in micro and nano scales have high strength and possibility to reinforce polymers. Fibrils can be isolated from natural cellulose fibers by chemical or mechanical methods. The chemical way removes the amorphous regions mainly by strong acid hydrolysis and produces nano-size fibrils called cellulose whisker or cellulose nanocrystal. The mechanical methods generate bundles of microfibrils called cellulose microfiber or microfibrillated cellulose. However, the existing procedures produce low yields, severely degrade cellulose, and are not environmental friend or energy efficient. The purpose of this study was to develop a novel process using high-intensity ultrasonication to isolate fibrils from several cellulose resources. Several factors that may affect the efficiency of fibrillation were considered and discussed. High intensity ultrasound can produce very strong mechanical oscillating power, so the separation of cellulose fibrils from biomass is possible by the action of hydrodynamic forces of ultrasound. The geometrical characteristics of the fibrils were investigated using polarized light microscopy (PLM), scanning electron microscopy (SEM) and atomic force microscopy (AFM). Results show that small fibrils with diameter ranging from thirty nanometers to several micrometers were peeled from the fibers. Some fibrils were still on the surfaces of the big ones, while some were already isolated from the fibers. The degree of fibrillation of the fibers was significantly increased and evaluated by water retention value (WRV) using a centrifuge system. The crystallinities of some cellulose fibers were evaluated by wide angle X-ray diffraction (WAXD) and Fourier transform infrared spectroscopy (FTIR). This novel technique is an environmental benign method

and a simplified process that may make fiber isolation and chemical modification simultaneously and could significantly reduce production cost of cellulose nanofibers and their composites.

Keywords: cellulose, geometry, fiber, fibril, high intensity ultrasonication, isolation, micro, nano

3.2. Introduction

Cellulose fibrils in micro and nano scales are suitable for reinforcement of some polymers to fabricate renewable and biodegradable nanocomposites because small fibrils may have much higher mechanical properties than individual fibers because small fibrils include higher cellulose crystal regions that have very high elastic modulus than fibers (Sakurada et al., 1962). To isolate fibrils from cellulose fibers without severe degradation and with low cost and environmental friend is still challengeable. It is one of the most important steps in the field of fabrication of nanocomposites reinforced with cellulose fibrils. Although many methods have been developed to make fibrils, e.g. chemical and mechanical, none of them are high yield, environmental friend, and/or energy efficient.

The chemical method, mainly by strong acid hydrolysis, removes the amorphous regions of cellulose fiber and produces nano-size fibrils. Cellulose whisker and cellulose nanocrystal have been used to describe nano-size cellulose fibrils. Many sources have been used for fibril isolation by chemical methods, such as wood fibers (Beck-Candanedo et al., 2005; Bondeson et al., 2006), cotton (Choi and Simonsen, 2006), tunicate mantles

(Sturcova et al., 2005), sugar beet pulp (Dufresne et al., 1997), and potato tuber cells (Dufresne et al., 2000). The mechanical method can be used to separate fibrils with high shear force. It includes several ways, such as a high-pressure refiner treatment (Chakraborty et al., 2005), a grinder treatment (Taniguchi, 1996), a microfluidizer (Zimmermann et al., 2004), and a high-pressure homogenizer treatment (Dufresne et al., 1997; Herrick et al., 1983; Nakagaito and Yano, 2005; Turbak et al., 1983). Main product generated by these mechanical methods is bundle of single microfibrils and has been referred as mcirofibrillated cellulose (MFC).

In this study, high intensity ultrasonication, as a novel method for fibril isolation, was developed and used to treat several cellulose materials to generate small fibrils in nano and micro scales. Ultrasound is a part of the sonic spectrum that ranges from 20 kHz to 10 MHz, and generated by a transducer that converts mechanical or electrical energy into high frequency acoustical energy. High intensity ultrasound can produce very strong mechanical oscillating power, so the separation of cellulose microfibril from cellulose may be possible by the action of hydrodynamic forces of ultrasound. They are widely used in many processes, especially in emulsification, catalysis, homogenization, disaggregation, scission, and dispersion (Anonymous, 2001 and 2002a).

Ultrasonic liquid treatment uses high frequency energy to cause vibration in liquids to produce physical or chemical effects. The sound energy is then fed to a horn that transmits the energy as high frequency vibrations to the liquid being processed. Cavitation is a physical phenomenon, which may make both physical and chemical changes when liquids are exposed to these high frequency vibrations. Cavitation includes

the formation, expansion, and implosion of microscopic gas bubbles in liquid as the molecules in the liquid absorb ultrasonic energy. Compression and rarefaction waves rapidly move through the liquid media and will break the attractive forces in the existing molecules and create gas bubbles. The gas bubbles grow as additional ultrasound energy enters the liquid. After reaching a critical size, the gas bubbles implode or collapse. The energy that exists within the cavity and in the immediate vicinity of the gas bubbles just before collapse causes both physical and chemical effects in the liquid. Physical effects occur when cavitation is intense enough to rupture cell membranes, free particulates from solid surfaces, and destroy particles and organisms through particulate collisions or by forcing them apart. Chemical effects occur because the conditions immediately proceeding collapse of a cavitation bubble are similar in magnitude to ultra-high energy combustion conditions. Within the cavitation bubble and the immediate surrounding area, violent shock waves result in a high temperature of up to 5000°C and a high pressure of more than 500 atm at the implosion sites (Suslick, 1990). These extreme temperatures and pressures, which last only microseconds, do not exist long enough to heat the liquids being processed. However, the localized temperature and pressure increases are sufficient to increase chemical reactivity, polymer degradation, and chemical free-radical production (Anonymous, 2001).

Ultrasound was helpful for commercial pulp fiber refining by giving a reduction in cutting and lowering of fiber loss. The irradiation of cellulose fibers with ultrasound was found to promote fibrillation of the fibers without cutting, but the fibrillation process appears to occur predominantly at sites on the fiber wall that have already been damaged

by the refining process (Manning and Thompson, 2002). Turai and Teng (1978) used ultrasonic generated by a mechanical generator of whistle called a jet-edge generator to deink of waste paper which printed heavily with high-gloss polymeric inks or covered with overprinted varnished. As a pretreatment, ultrasonic irradiation was used to aid a practical high-performance enzymatic hydrolysis of cellulose. Pretreatment of the cellulose fibers with ultrasonic irradiation prior to initiating the enzyme reaction further improved the reaction rate, which might support the possibility of applying ultrasonication pretreatment in a practical cellulose saccharification process (Imai et al., 2004).

The goals of this research were to investigate the fundamentals of the isolation of cellulose fibrils from biomass by using high-intensity ultrasonication (HIUS) as a highly effective approach without any chemical treatment, to characterize the fibrils and potential by-products. Several factors that may influence cellulose fibrillation during ultrasonic treatment were considered and tested. A homogenizer and fiber pretreatment with sodium hydroxide were also tried to compare the fibrillation efficiency of cellulose treated by HIUS only. The geometric characteristics of the fibrils were investigated using polarized light microscopy (PLM), scanning electron microscopy (SEM), and atomic force microscopy (AFM). The degree of fibrillation of the fibers was evaluated indirectly by water retention value (WRV). Energy dispersive X-ray spectrometer (EDS) and Fourier transform infrared spectroscopy (FTIR) were used to check the possible by-products that made during ultrasonic treatment. The crystallinities of treated and untreated cellulose fibers were studied by WAXD and FTIR.

3.3. Experimental

3.3.1 Materials

Four cellulose resources were used as raw materials: Regenerated cellulose fiber (Lyocell fiber), pure cellulose fiber (TC40, 180, and 2500), microcrystalline cellulose (MCC), and pulp fiber. Microfibrillated cellulose (MFC, 10% solid slurry, Daicel Chemical Industries, LTD., Japan) was also used as reference. Sodium hydroxide (97.9%, Fisher Scientific) and acetate buffer (pH4.0, Ricca Chemical Company) were used to pretreat some fibers.

Lyocell fiber was about 11 μm in diameter and 12.7 mm in length (provided by Lenzing, Austria). Pulp fiber was about 30 μm in width and 2~5 mm in length (provided by Kimberly-Clark Worldwide, Inc.). Both Lyocell fiber and pulp fiber were cut to pass a screen (room temperature and relative humidity of 30%) with holes of 1 mm in diameter by a Willey mill before treatment. Three different sizes of pure cellulose fiber were used: TC40, TC180, and TC2500 (provided by CreaFill Fibers Corp.). They include 99.5% (minimum) alpha cellulose content. Their average width and length is shown in Table 3.1. As fiber appears in a flat shape with only 1-2 μm in thickness, the average width does not mean fiber thickness or diameter. MCC was donated by the FMC BioPolymer as Avicel PH-101. The air jet particle sizes in wt % were NMT 1.00 of +60 Mesh and NMT 35 of +200 Mesh.

Table 3.1 Average width and length of pure cellulose fiber

	TC40	TC180	TC2500
Average width (μm)	18	20	20
Average Length (μm)	30	200	900

3.3.2. Setups of cellulose treatment by high intensity ultrasonic processor (HIUS)

Batch process treatment

The cellulose materials were soaked in distilled water for more than 24 hours before ultrasonic treatment. High intensity ultrasonic processor **(**HIUS, 1500 Watt Model, SONICS Newtown, CT) was directly applied to cellulose fibers suspended in distilled water. The apparatus and treatment scheme are shown in Figures 3.1 and 3.2. The fibers were immersed in 60 mL of distilled water in a 100-mL beaker. The fiber concentrations were from 0.5% to 2% W/W according to different fiber dimensions. The ultrasonic treatment time and temperature can be controlled by time controller and by ice/water bath or without bath (Figure 3.2). The factors that may affect the cellulose fibrillation and characterization of the treated fibers will be listed in the following sections.

Continuous process treatment by a flow cell system

Continuous HIUS treatment will be conducted with a high-volume continuous flow cell. The flow cell includes a high amplitude hollow probe inside of a chamber, so the fiber can be continuously exposed with HIUS. Throughput rate is variable because of

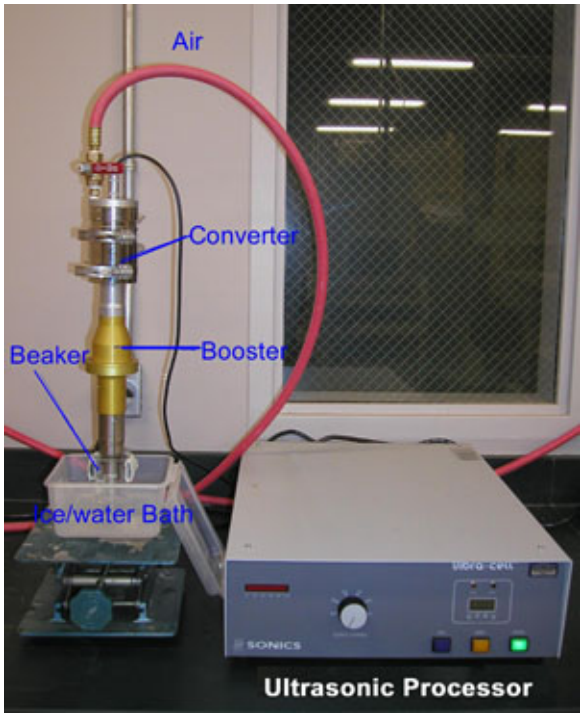

Figure 3.1 Apparatus of 1500-watt model high intensity ultrasonic processor

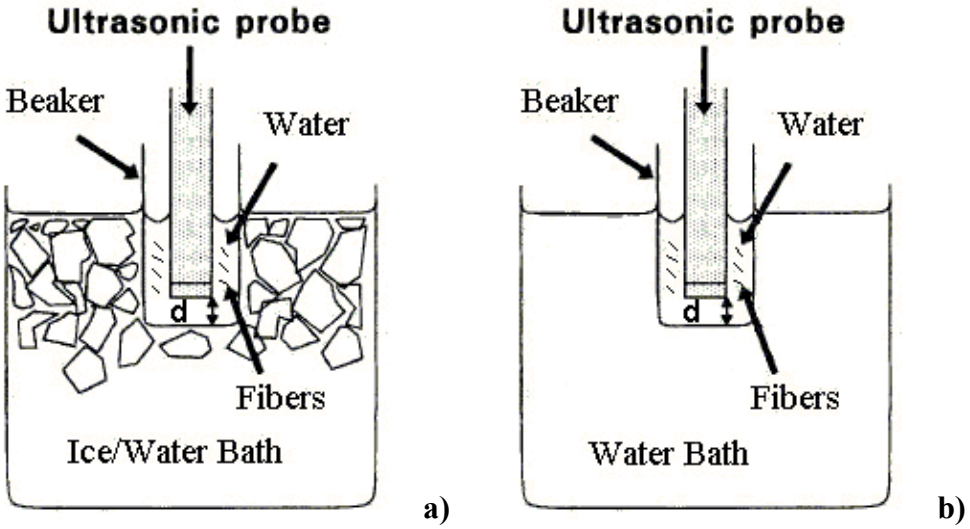

Figure 3.2 A scheme of HIUS treatment for fibers with ice/water (a) or water (b) bath

the viscosity of samples and desired degree of processing, which shows the exposure time of fibers to HIUS and is typically 100 liters/hour when used in conjunction with the VCF 1500 ultrasonic processor and a booster. The apparatus and treatment scheme are shown in Figures 3.3 and 3.4. The flow cell is recommended for the treatment of low viscosity samples and designed primarily for dispersing and homogenizing. High-energy efficiency is expected for the continuous process. The efficiency of cellulose fibrillation will be compared with batch process by some characterizations of the treated fibers.

3.3.3. Factors affecting cellulose fibrillation

There are many factors may influence the efficiency of cellulose fibrillation during ultrasonic treatment. In batch process, six factors Power (P), Time (t), Temperature (T), Concentration (C), Fiber size (FS), and Distance from tip to beaker bottom (d) were considered and three or four levels were used for each factor to check the effects of cellulose fibrillation (Table 3.2). Water retention value (WRV) measured by a centrifuge system and morphological observation investigated by polarized light microscopy (PLM, Olympus-BX51), which will be described in the following sections, were used to evaluate and compare the effects of different factors.

Power can be controlled by the output control button and can be shown in percent of power resistance signal (Figure 3.5). Time controller can be used to adjust time from 1 sec to 60 min. For temperature control, ice/water bath, water bath only, and no bath cooling were used. HOBO Type J Thermocouple was used to record the temperature during treatment (Figure 3.6). Concentration is the solid weight percent of cellulose fiber

Figure 3.3 VCF 1500 ultrasonic processor with a flow cell system

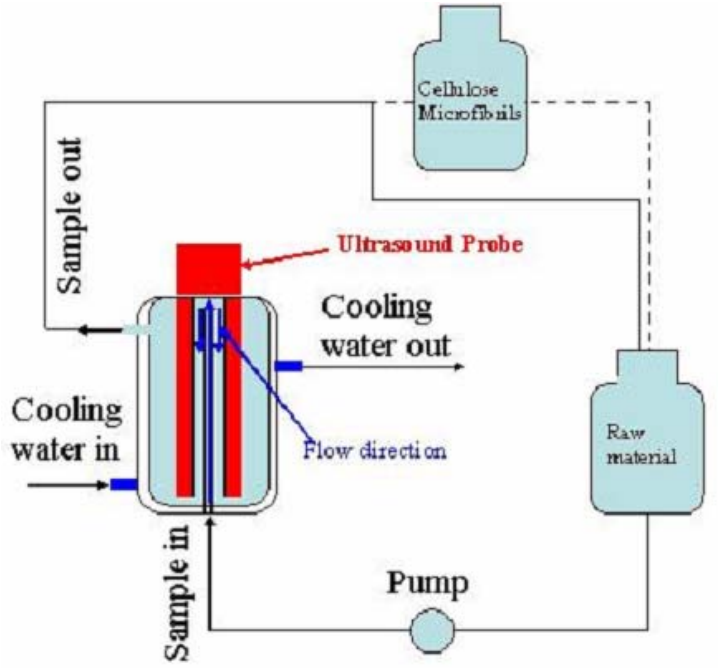

Figure 3.4 A scheme of HIUS treatment with high-volume continuous flow cell apparatus

Figure 3.5 Power output control of HIUS

Figure 3.6 HOBO Type J thermocouple for temperature record during HIUS treatment

Table 3.2 Factors and levels influencing the efficiency of cellulose fibrillation

	Factor	Level	Note (other factors)
1	Power (P, %)	40, 60, 80	t=10, T=W, C=2, FS=30, d=7
2	Time (t, min)	10, 20, 30, 60	P=80, T=W, C=2, FS=30, d=7
3	Temperature (T)	I/W, W, N*	P=80, t=10, C=2, FS=30, d=7
4	Concentration (C, %)	1, 2, 3, 4	P=80, t=10, T=W, FS=30, d=7
5	Fiber Size (FS, μm)	30, 200, 900**	P=80, t=10, T=W, C=2, d=7
6	Distance (d, mm)	4, 7, 10, 15	P=80, t=10, T=W, C=2, FS=30

* I/W=Ice/Water bath, W=Water bath only, N=No bath cooling

** 30=TC40, 200=TC180, 900=TC2500

in distilled water mixture. For fiber size, the three different pure cellulose fibers with different lengths (TC40, TC180, and TC2500) were used. Three levels of distance (d) from tip to beaker bottom were chosen (d in Figure 3.2). For each factor testing, other factors were kept as constants (Table 3.2).

3.3.4. Power consumption of HIUS treatment

The nominal power of the HIUS processor is 1.5KW. To record the real power consumption during treatment, a clamp power meter (EXTECH, 1000Amp HVAC True RMS Power Clamp-On Model 380975) was used to measure the total power (Figure 3.7). The power consumptions of unloading (the power was on but without sample processing), process with different power controls, and process with different sample concentrations were measured and discussed.

Figure 3.7 A clamp power meter for measurement of the total power consumption

3.3.5. Characterizations of potential by-products

Energy dispersive X-ray spectrometer (EDS) SEM (LEO 1525, Figure 3.8) with an Oxford energy dispersive X-ray spectrometer (EDS) used to check the black particles made during HIUS treatment. EDS is a chemical microanalysis technique performed in conjunction with a SEM. The x-rays emitted from the sample during bombardment by the electron beam are utilized to characterize the elemental composition of the analyzed volume.

Fourier transform infrared spectroscopy (FTIR)

PerkinElmer Molecular Spectroscopy (Spectrum One, Figure 3.9) with an ATR (Attenuated Total Reflectance) accessory was used to obtain spectra for the fibers before and after treatment. Untreated Lyocell and pulp fibers were cut to pass the screen with 1

Figure 3.8 SEM with energy dispersive X-ray spectrometer (EDS)

Figure 3.9 Fourier transform infrared spectroscopy (FTIR)

mm holes, while untreated TC180 and Avicel cellulose fibers were scanned as they were. FTIT samples were from the materials used for WRV measurements, which were filtered by 0.2 μm filter and will be discussed in section 3.3.8. Some Lyocell samples were prepared by drying treated fiber suspension on aluminum foil. To check if there were some soluble contents in the suspensions of treated fibers, water from the top of centrifuged suspensions was scanned by FTIR. Mid infrared spectra were recorded in the wavenumbers range of 4000 to 600 cm^{-1}. Spectra were taken at the resolution of 4 cm^{-1} with a total of 16 scans for each sample. To compare different spectra, all the water spectra were normalized on the peak at 3322 cm^{-1}. The fiber spectra were normalized on the peak at about 1019 cm^{-1} attributed to a CO stretching mode (Kataoka and Kondo, 1998). Then all the spectra were corrected by ATR correction with the contact factor of 0, which was assumed that the degree of contact between the sample and the ATR crystal was perfect. After normalized and ATR corrected, two ratios of peak absorbance to nearby valley, 1156/1141 cm^{-1} and 1419/1405 cm^{-1} for Lyocell fiber, 1105/1087 cm^{-1} and 1429/1397 cm^{-1} for Avicel and TC180, respectively, were compared to estimated the changes between treated and untreated cellulose fibers. The absorbance ratios were used to compare the cellulose crystallinities (Schultz et al., 1985). At least three samples were scanned for each cellulose resource.

3.3.5. Effect of abrasive powder on cellulose fibrillation

Abrasive powders with diameters of several μm or under μm may helpful for cellulose fibrillation because the microbubbles generated by the ultrasonic tip could

accelerate the powders, which may hit the cellulose surfaces. Pure cellulose fiber TC40 was treated with alumina (d=0.3, 1.0, and 7.0 μm) by HIUS in batch process. Other factors were: t=10 min, T=Water cooling, C=2%, d=7 mm. Three percents of abrasive powder were tried: 5%, 10%, and 20% of cellulose fiber in weight to check the effect of abrasive powder on cellulose fibrillation.

3.3.6. Effect of cellulose pretreatment by sodium hydroxide

Lyocell and TC180 pure cellulose fibers were pretreated by 2.5 M sodium hydroxide (NaOH) for 6 h. This NaOH concentration was the best one for Lyocell fiber splitting (Ozturk et al., 2006). After washed by distilled water and neutralized by acetate buffer, the fibers were then treated by HIUS for 20 min (Figure 3.10). Fiber geometry changes and water retention values were used to evaluate the effects of alkali pretreatment on cellulose fibrillation by HIUS.

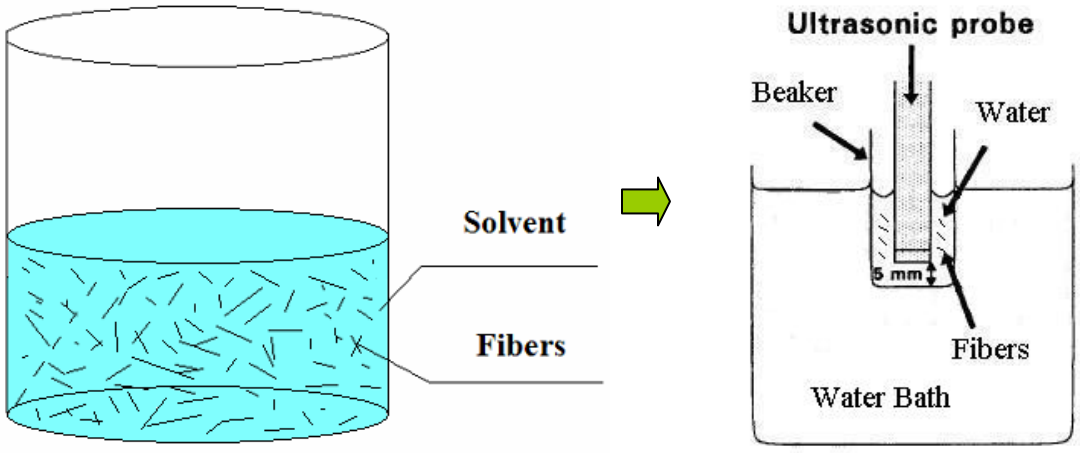

Figure 3.10 Scheme of solvent pretreatment followed by HIUS

3.3.6. Combination of ultrasonication and homogenizer treatment

High Pressure Homogenizer (HPH) is a common device used to mechanically isolate fibrils from cellulose fibers. To compare the efficiency of cellulose fibrillation of ultrasonication and homogenizer treatments, a homogenizer (Stansted Ultrahigh Pressure Homogenizer Model nG12500, Figure 3.11) was used to treat pure cellulose TC40 with different pressures. Combinations of ultrasonication and homogenizer treatments included ultrasonic treatment first, then homogenizer treatment and reverse. Figure 3.12 shows the principle scheme of homogenizer (Stansted, 2007). Table 3.3 shows some factors and levels for homogenizer treatment.

To combine ultrasonication and homogenizer treatments, TC40 were treated 30 min by HIUS in a batch and then HPH (3, 5, 8 passes) with 110MPa, T=~50-70˚C. And TC40 were treated by HPH (8 passes, 220 MPa, ~80˚C), then HIUS treatment for 30 min in batch process.

3.3.7. Fibril separation from treated fibers

Centrifuge (Figure 3.13) was used to separate fibrils from the treated materials with relative centrifugal force (RCF) of about 900 g (g is the earth gravity acceleration) and time of 5 min for Lyocell and 10 minutes for others. RCF is given in multiples of the earth gravity g. It is a dimensionless number that allows one to compare the efficiency of separation or sedimentation of diverse instruments because it is independent of the instrument used. RCF is only related to radius and speed of the centrifugation (Equation 3.1).

Figure 3.11 Stansted ultrahigh pressure homogenizer (Model nG12500)

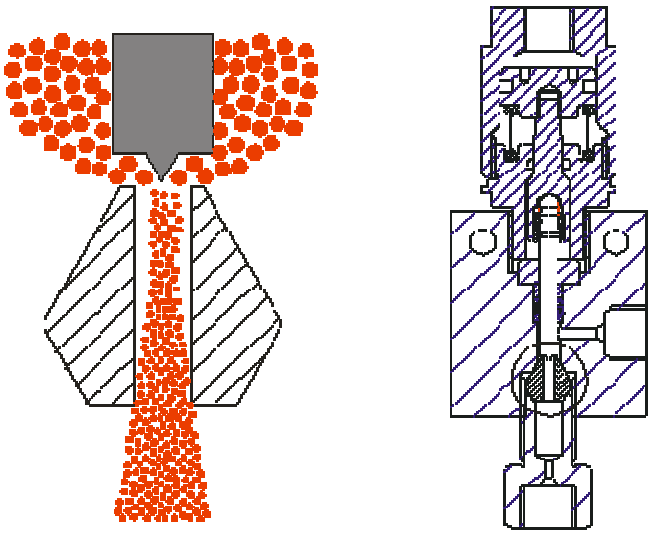

Figure 3.12 Figure 3.12 Principle scheme of homogenizer

Table 3.3 Factors and levels for homogenizer treatment

	Pressure (MPa)	Pass Times	Temperature (°C)
1	55	5, 10, 15	~40
2	110	5, 10, 15	50-70
3	220	3, 5, 8	50-80

Figure 3.13 Centrifuge (Accuspin 400)

$$\mathrm{RCF} = 11.18 \times \left(\frac{n}{1000} \right)^2 \times r \qquad (3.1)$$

where r=radius of centrifugation in cm and n=speed in rpm.

After setting 5 minutes, the top portion was used as small fibrils to reinforce polymers and for further analysis.

3.3.8. Characterizations of fiber and fibrils

Cellulose fibers of untreated and treated by HIUS or HPH, and fibrils separated by centrifuge were characterized by fiber size analyzer, yield, volume change, water retention value (WRV), crystallinity, polarized light microscopy (PLM), scanning electron microscopy (SEM), and atomic force microscopy (AFM).

Dimension analyses of fibers and fibrils

A fiber size analyzer (Kajaani FiberLab 3, done by Buckeye Technologies Inc., Memphis, TN) was used to analyze the dimensions of untreated and treated cellulose fibrils (Lyocell and TC180). This analyzer may measure Kajaani fiber length, fine fiber length, average fiber width, cross sectional area (CSA) measured in square microns, and Kajaani % curl, which is a mathematical function of the continuous fiber length (measures the fibers "pixel-to-pixel" along the center line of the fiber) to the projected fiber length (not take into account curves and bends in the fiber). Each sample was run in triplicate. The continuous fiber length distributions were also analyzed.

Yield measurement

The effect of HIUS on yield of treated cellulose or cellulose fibrils was gravimetrically determined in two ways. First, the treated cellulose by HIUS was filtered by a filter membrane with 0.2-μm pore-size (Whatman Nuclepore) and then dried. The yield was gravimetrically determined as percentage of the weight of 'starting' material (Equation 3.2).

$$\text{Yield} = \frac{W_{DryAfterTreated}}{\text{W}_{\text{DryBeforeTreated}}} \times 100\% \tag{3.2}$$

Second, after separated by centrifuge as described in part of 3.3.7, the fibril portion were dried and weighed. The cellulose fibril yield was gravimetrically determined as percentage of the weight of 'starting' material (Equation 3.3).

$$\text{Yield} = \frac{W_{DryFibril}}{\text{W}_{\text{DryBeforeTreated}}} \times 100\% \tag{3.3}$$

Volume change

The degree of homogenization or microfibrillation is related to fibril and microfibril surface and volumetric phenomena (Herrick et al., 1983). Several methods may be used to evaluate the cellulose fibrillation. One way is to investigate the volume changes of the same weight of cellulose fibers suspended in certain weight of water. It was observed optically by optical images after the cellulose was treated certain time and deposited in beakers or bottles. Some cellulose suspensions, including before and after treatment, different treatment time, were analyzed.

Water retention value (WRV)

Water retention value (WRV) is another way that can be used to measure the degree of homogenization or microfibrillation, which is related to fibril and microfibril surface and volumetric phenomena (Herrick et al., 1983). The higher WRV, the more fibrils could be isolated or more voids among small microfibrils were obtained. WRV is a percent ratio of the water contained in the sample after centrifuged in certain force and time to the dry weight of the sample. Figure 3.14 shows the scheme of water retention value measurement. A 25-mm diameter stainless steel cap with diameter of 1 mm holes and a filter membrane with 0.2-μm pore-size (Whatman Nuclepore) were used to hold and filter the wet mass. Two or four caps were filled with the wet sample (about 0.5 g in dry weight) and placed inside the carriers. After centrifuged (AccuSpin 400, Figure 3.13) for 30 minutes and a relative centrifugal force (RCF) of 900 g (RCF is given in multiples of the earth gravity g and a dimensionless number, RCF is calculated by Equation 3.1 as described in Section 3.3.7) at room temperature, the samples were weighed and oven dried at 80 °C for 24 hours and then dried at 103 °C until they reached constant weight. Equation (3.4) was used to calculate WRV.

$$\mathrm{WRV} = \frac{W_{Wet} - W_{Dry}}{\mathrm{W_{Dry}}} \times 100\% \qquad (3.4)$$

where W_{Wet} is the weight of the sample after centrifugation and W_{Dry} is the dry weight of the sample.

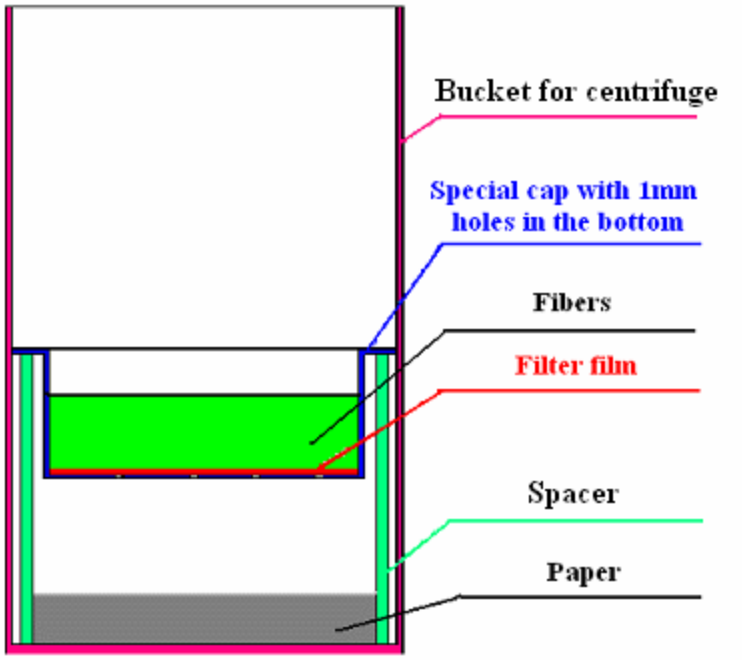

Figure 3.14 Scheme of water retention value measurement setup for centrifuge

Cellulose crystallinity

a. Wide angle X-ray diffraction (WAXD)

The crystallinities of treated and untreated Lyocell fibers were studied by Wide angle X-ray diffraction (WAXD). The equipment (Molecular Metrology) was a pinhole type camera that recorded the patterns on Fuji image plates. The operating voltage was 45 kV, current was 0.66 mA, and the exposed period was 50 minutes using CuKa radiation with a wavelength of 0.15418 nm (Figure 3.15). The crystallinity is defined as the ratio of the amount of crystalline cellulose to the total amount of sample material, including crystalline and amorphous parts. The Segal method was used to calculate the crystallinity of the samples (Thygesen et al., 2005). Two to three samples were tested for each

composition. A typical WAXD curve used to determine the crystallinity by Segal method is shown in Figure 3.16. Equation (3.5) was used to calculate the sample crystallinity (X_{CR}).

$$X_{CR} = \frac{I_{200} - I_{AM}}{I_{200}} \times 100\% \tag{3.5}$$

where I_{200} is the height of the 200 peak, which represents both crystalline and amorphous material; and I_{AM} is the lowest height between the 200 and 110 peaks, which represents amorphous material only.

b. Fourier transform infrared spectroscopy (FTIR)

PerkinElmer Molecular Spectroscopy (Spectrum One, Figure 3.9) was used to obtain spectra to estimate the crystallinities of the treated and untreated cellulose fibers (as described in 3.3.5). Mid inferred spectra were recorded in the wavelength range of 4000 to 600 cm^{-1}. Spectra were taken at the resolution of 4 cm^{-1} with a total of 16 scans for each sample. The fiber spectra were normalized on the peak at about 1019 cm^{-1} attributed to a CO stretching mode and then modified by ATR (Attenuation Total Reflection) correlation the contact factor of 0. The cellulose IR crystallinity index was evaluated as the intensity ratio between IR absorptions at 1419 and 895 cm^{-1} for Lyocell fiber and 1429 and 898 cm^{-1} for Avicel and TC180, which are assigned to CH_2 bending mode and deformation of anomeric CH respectively (Kataoka and Kondo, 1998). At least three samples were scanned for each cellulose source.

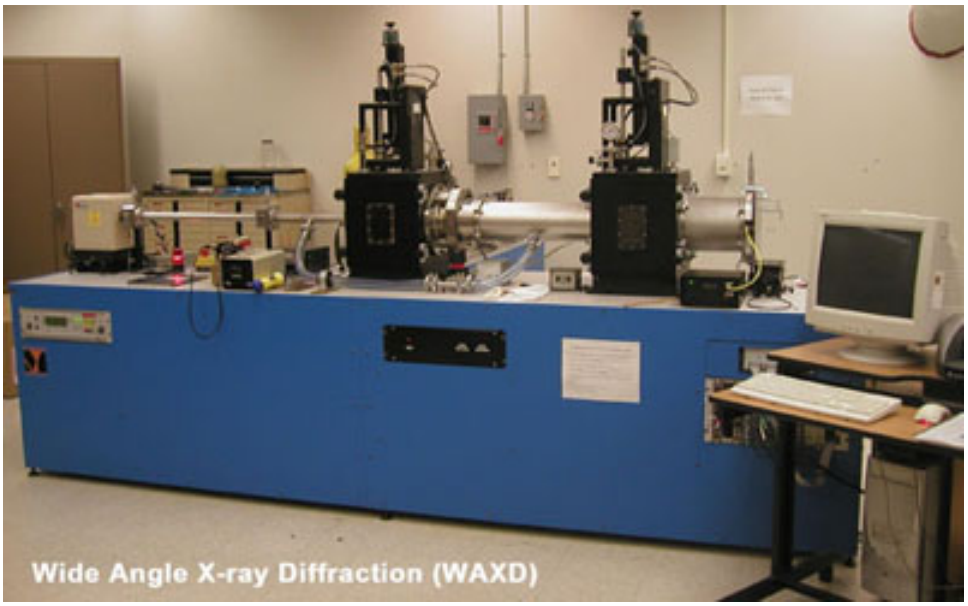

Figure 3.15 Equipment wide angle X-ray diffraction (Molecular Metrology)

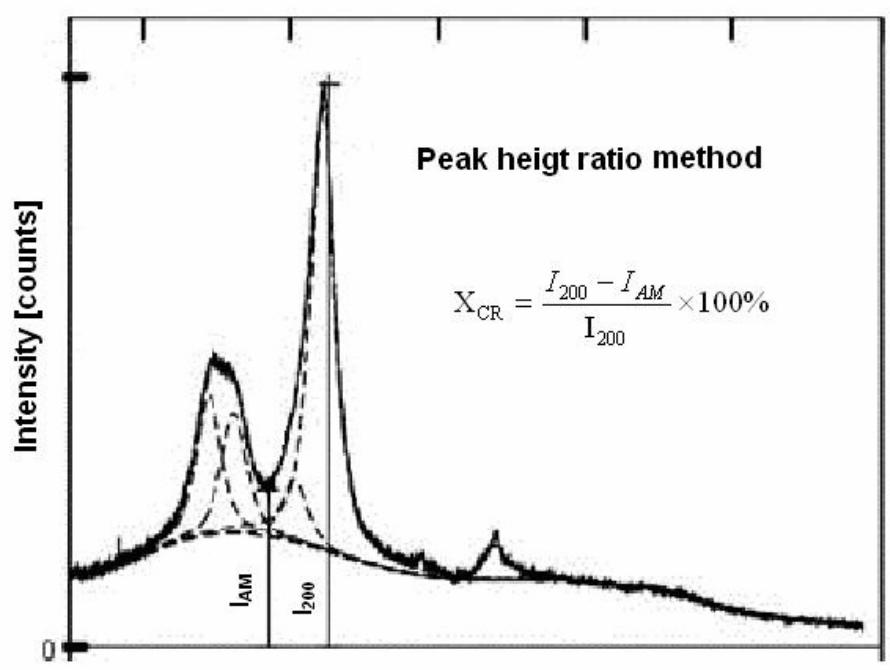

Figure 3.16 Segal method used to determine cellulose crystallinity using WAXD

Morphology observations

a. Polarized light microscopy (PLM)

The appearance and dimensions of the treated and untreated cellulose fibers were studied by a polarized light microscopy (PLM) (Figure 3.17). Some fibers and fibrils were measured by the software package ImageJ using pixels in the images, such as 4.32 pixels/μm for 200 magnification images.

b. Scanning electron microscopy (SEM)

The morphology of the fibers and fibrils were also examined using a scanning electron microscopy (SEM, LEO 1525) (Figure 3.8). Some dried samples of fibril suspension on silicon wafers were observed by SEM. The operating voltages of SEM were 5 to 10 kV and various magnification levels were used to obtain images. At least three images (for both PLM and SEM) were taken and chosen to observe the morphology of all samples, but just some of the features selected randomly in the micrographs were measured because the features could not be precisely measured easily and the big fibrils with diameter of more than 1 μm dominate in the treated fiber material.

c. Atomic force microscopy (AFM)

An AFM (PSIA, XE-100) was also used to observe the morphology of the small fibrils. AFM is not only possible to measure non-conductors in air, but also to measure the physical, chemical, mechanical, electrical, and magnetic properties of a sample's surface, and even measure live cells in solution. It consists of four primary components: a stage, control electronics, a computer, and a video monitor

(Figure 3.18). The AFM uses a micro-machined cantilever with a sharp tip to measure a sample's surface. Figure 3.19 shows a diagram of conventional AFM's scanning. It is typically used to measure samples with relatively small roughness. By measuring the deflection of the cantilever, the force between the atoms at the sample's surface and those at the cantilever's tip can be detected (Anonymous, 2002b).

3.4. Results and Discussion

3.4.1. Comparison of batch process and continuous process

The continuous process was not high-energy efficiency as expected. Compared with batch process, the efficiency of cellulose fibrillation for continuous process was lower. Pure cellulose fiber TC180 was treated by HIUS in the flow cell system. The suspension temperature was about 40~50 ˚C with water cycle cooling. It equaled about

Figure 3.17 Polarized light microscopy (PLM)

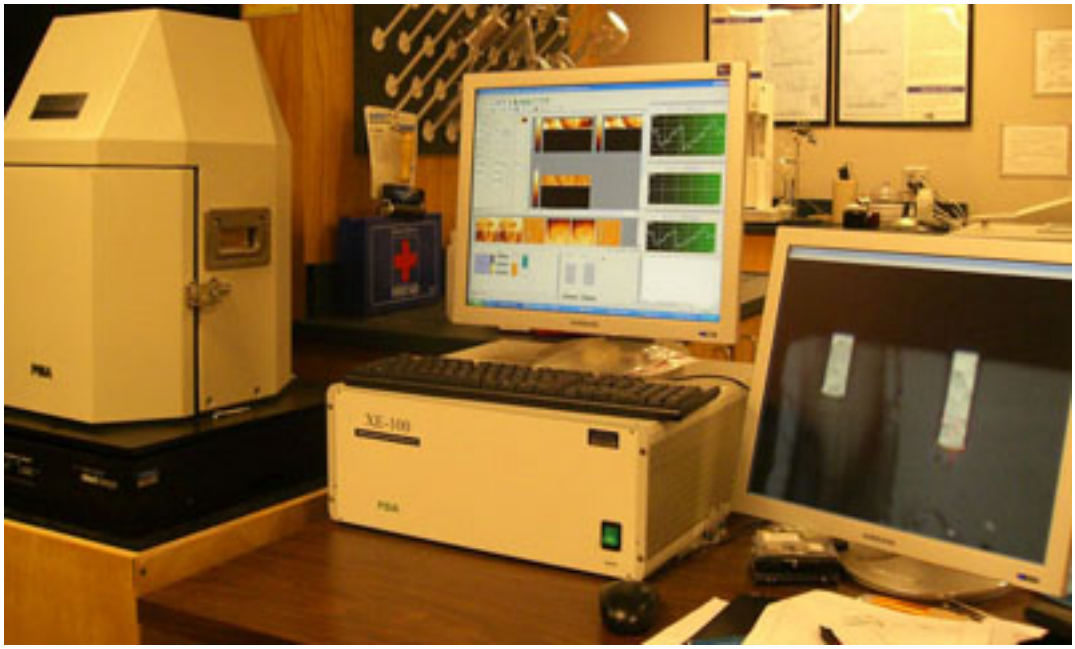

Figure 3.18 The XE-100 AFM System

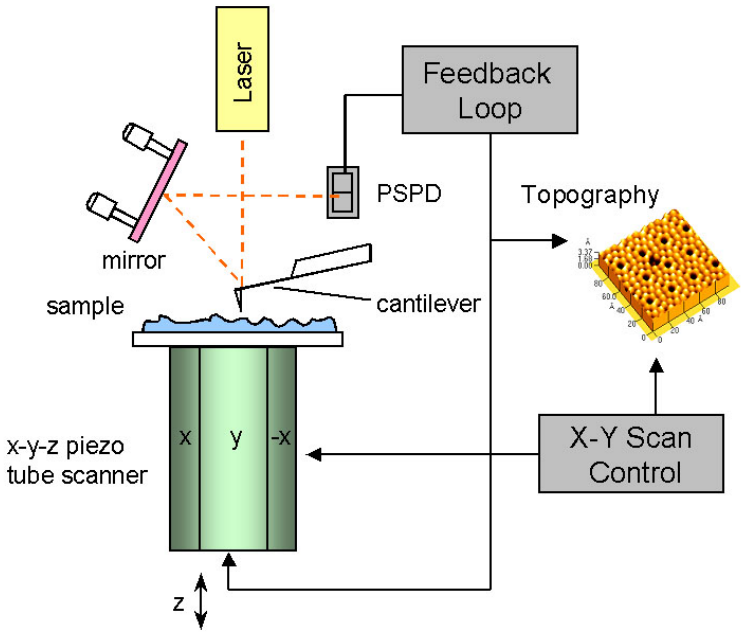

Figure 3.19 Diagram of conventional AFM's scanning

54 min treatment by batch process (about 6 min for a cycle, treated 10 times per hour). Even after 9 h treatment with 2% concentration (12g in 600ml water), the suspension was not gel like, while a good suspension was obtained after 30 min treatment by batch process (Figure 3.20). Figure 3.21 shows the PLM images of pure cellulose TC180 after treated by continuous flow cell (9 h) and batch processes (30 min). The fibers treated by batch process had more fibrillations than those treated by continuous flow cell process. This was why their suspensions were different (Figure 3.20).

The cellulose was not fibrillated well by continuous flow cell treatment maybe because (1) the temperature was not high enough, (2) the distance between the tip and the bottom of the chamber was too big. Batch process was used for further study in this research.

3.4.2. Power consumption and temperature change

The nominal power of the HIUS processor is 15KW/h. The real power consumption was only from 0.10 to 0.40 KW/h measured by a clamp power meter. It may change according to power used, the viscosity and concentration of the samples. If one batch is 2.4 g dry sample and treatment time is one hour, the power consumption could be 167 KW for one kg dry sample. The power cost could be about $11.7/kg (dry weight) if the price of power is 7 cents per KW.

The temperature of water suspension during HIUS treatment changed a lot according to the used power and cooling methods. Figure 3.22 shows the temperature changes with different powers and cooling methods during HIUS treatment measured by

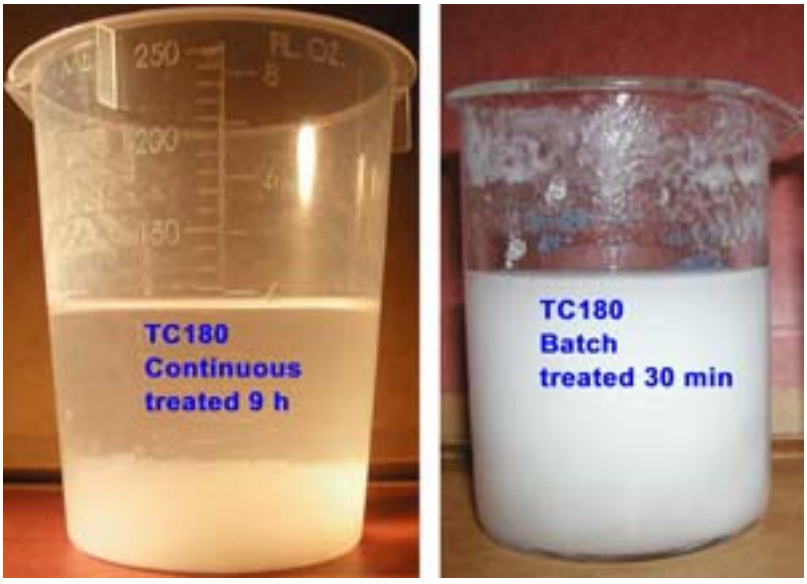

Figure 3.20 Pure cellulose TC180 treated by continuous (left) and batch (right) processes

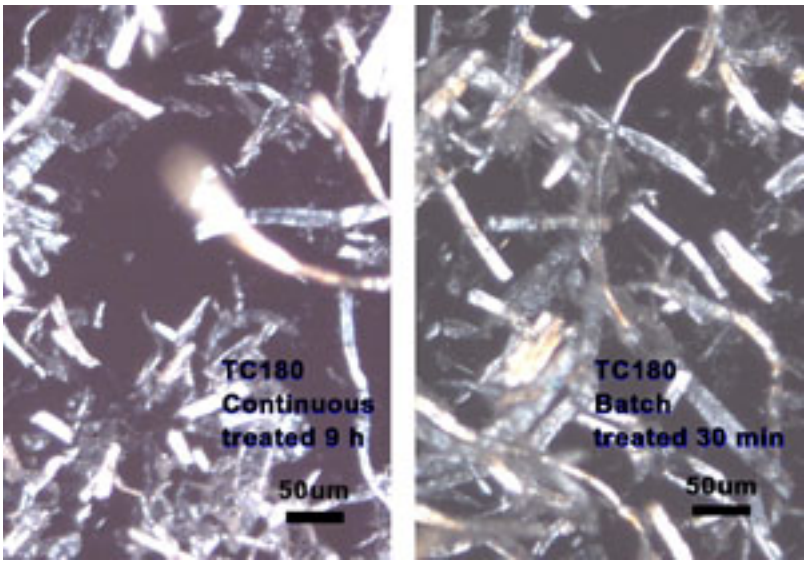

Figure 3.21 PLM images of TC180 treated by continuous (left) and batch (right)

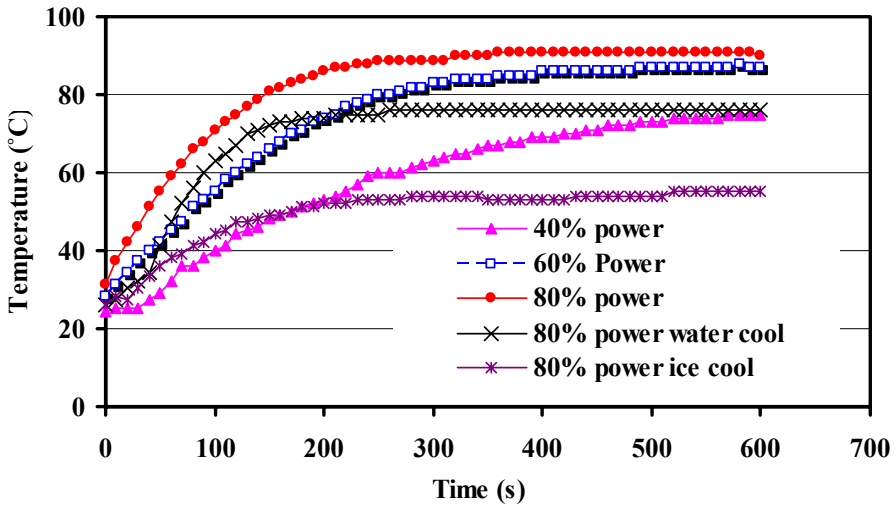

Figure 3.22 Temperature changes with different powers and cooling methods during HIUS treatment

HOBO Type J Thermocouple. It is clear that the higher used power, the higher temperature can be reached and higher speed of temperature increase can be obtained. When ice/water bath was used for cooling with power of 80%, the maximum temperature was only 55 ˚C, while it was about 75 ˚C and 91 ˚C when water bath and without cooling were used as temperature control, respectively.

3.4.3. Characterization of black particles generated during treatment

The black particles generated during HIUS treatment (Figure 3.23) were only Titanium (Ti) analyzed by energy dispersive X-ray spectrometer (EDS) (Figure 3.24). This demonstrated that cellulose fibers did not oxidized and degraded to carbon. When treatment time was more than 30 min continuously, or the tip was used too long (about more than 30 h application), black particles could be observed in the suspension. This

indicated that the Titanium tip is easy to be eroded if the continuous treatment time is too long or the tip is too old.

3.4.4. FTIR analysis of treated fibers and water

Figure 3.25 shows the Mid FTIR spectra of distilled water and water from treated Avicel and Lyocell cellulose suspensions. There were not significant differences among them. It indicated that there were not soluble components in the suspensions after the cellulose materials were treated by HIUS. FTIR spectra were significantly changed by visual inspection after normalized and ATR correction (Figure 3.26).

Figures 3.27 to 3.29 show the Mid FTIR spectra of untreated and treated regenerated cellulose fiber (Lyocell), MCC (Avicel), and pure cellulose (TC180), respectively. There were some changes for some peaks after treated for most of the cellulose fibers. Two ratios of peak absorbance to nearby valley were used to check the changes because the chemical structure of amorphous and crystalline cellulose are identical and differences in the physical environment of the bonds will give FTIR spectra with slightly different characteristics (Schultz, et al., 1985). Two ratios of peak absorbance to nearby valley, 1156/1141 cm^{-1} and 1419/1405 cm^{-1} for Lyocell fiber are shown in Figure 3.30. The ratio of 1419/1405 cm^{-1} was significantly different between the WRV samples and samples dried on aluminum foil. And there were not significant differences for the ratio of 1156/1141 cm^{-1} between the two kinds of samples, except 10 min treatment. This may be because the WRV samples were filtered by o.2 μm filter, which could get rid of some small fibrils with higher crystallinity.

Figure 3.23 Some black particles generated during HIUS

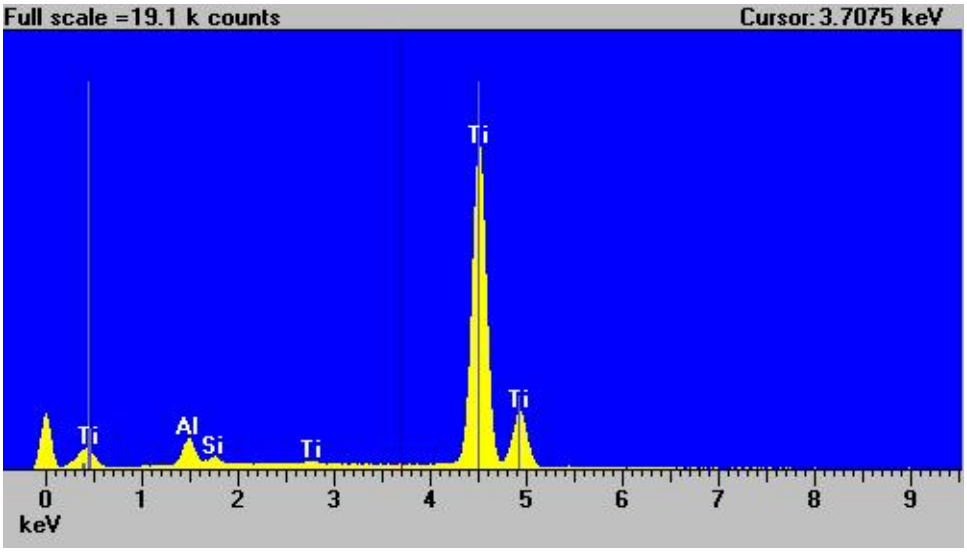

Figure 3.24 Elemental compositions of the black particles were only Titanium analyzed by energy dispersive X-ray spectrometer (EDS)

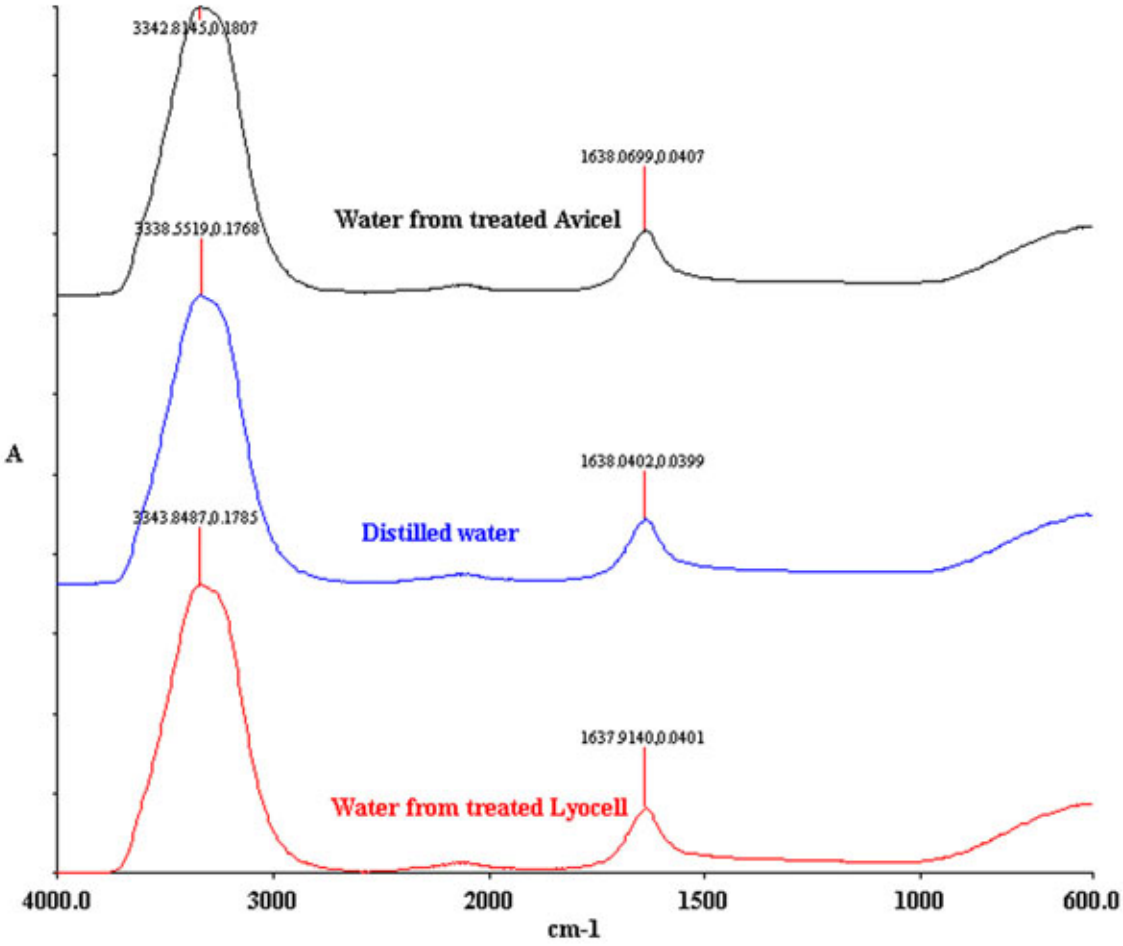

Figure 3.25 Mid FTIR spectra of distilled water and water from treated Avicel and Lyocell cellulose suspensions

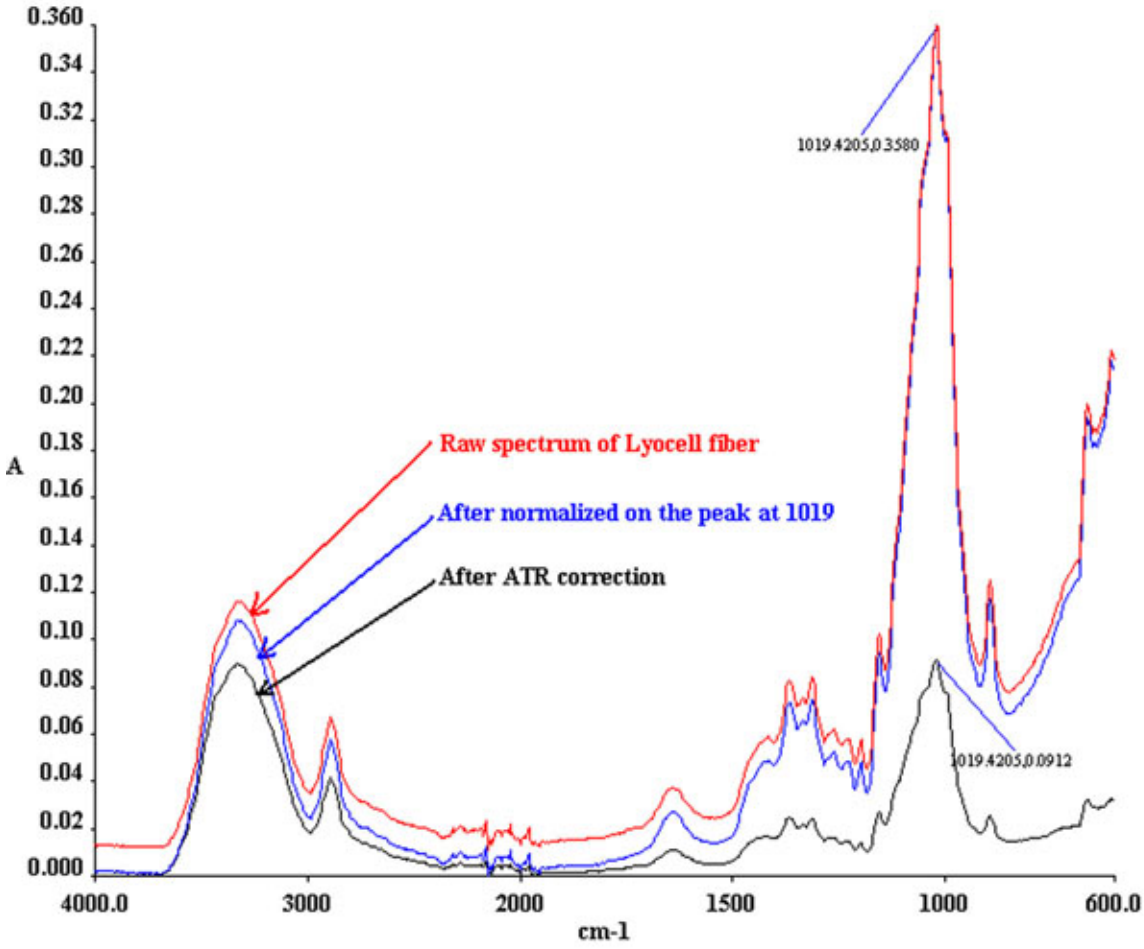

Figure 3.26 Typical FTIR spectra of Lyocell fiber after normalized and ATR correction

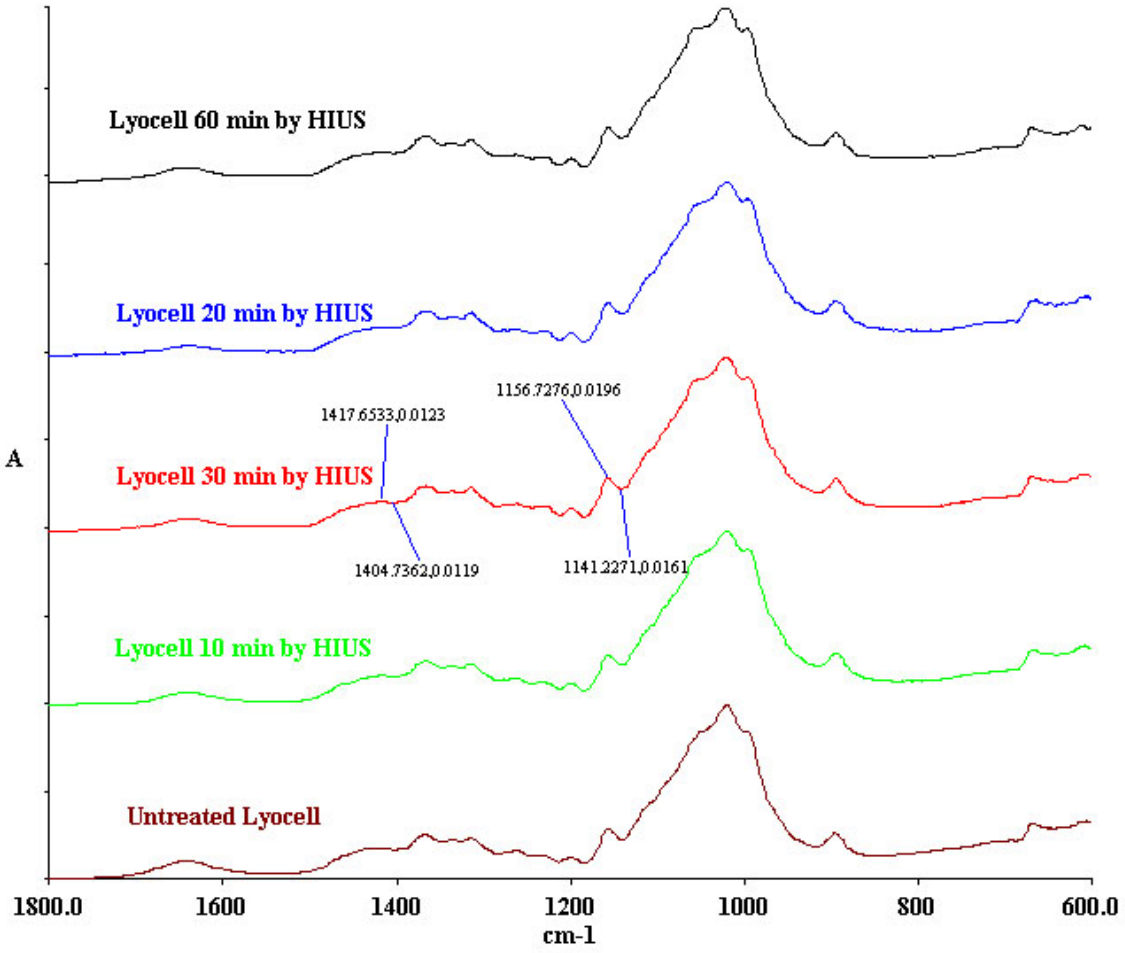

Figure 3.27 Mid FTIR spectra of untreated and treated regenerated cellulose fiber (Lyocell) between 1800 and 600 cm^{-1}

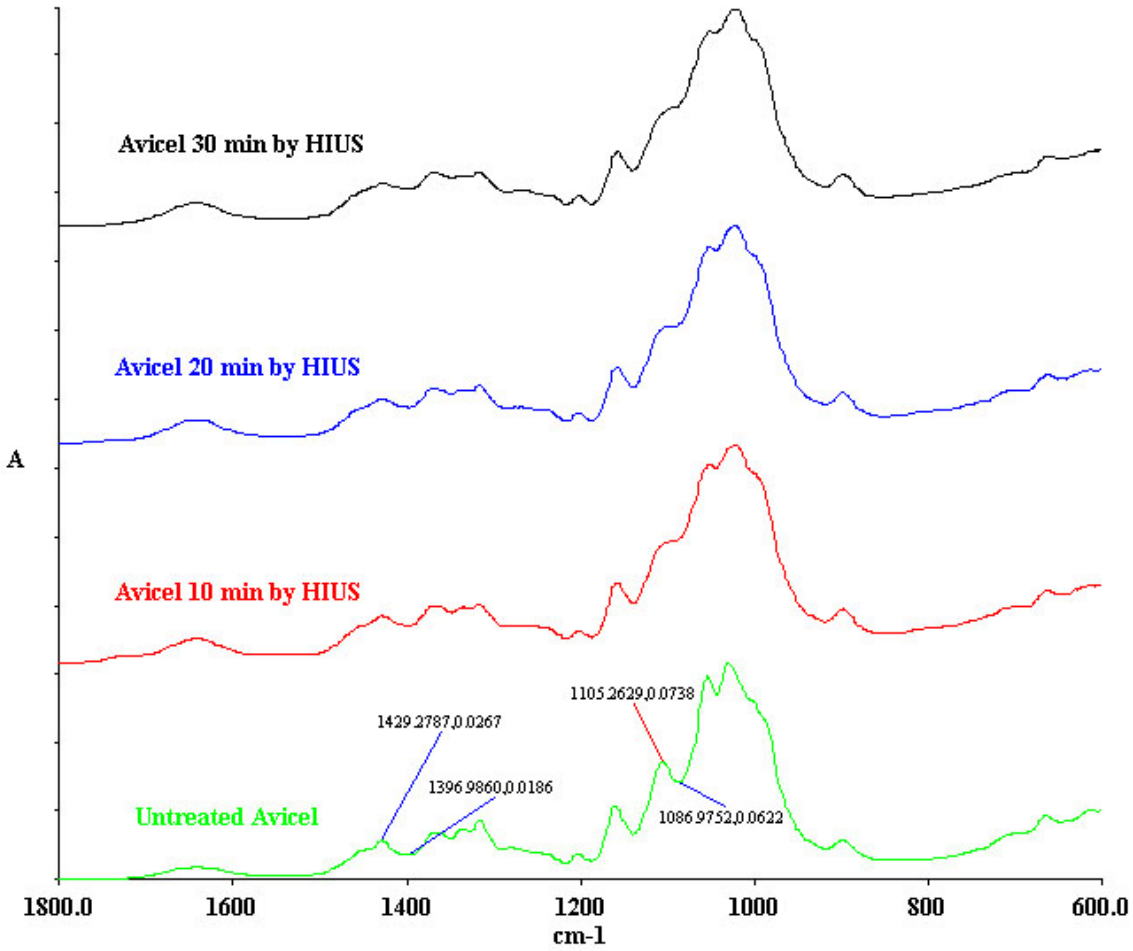

Figure 3.28 Mid FTIR spectra of untreated and treated MCC (Avicel) between 1800 and 600 cm^{-1}

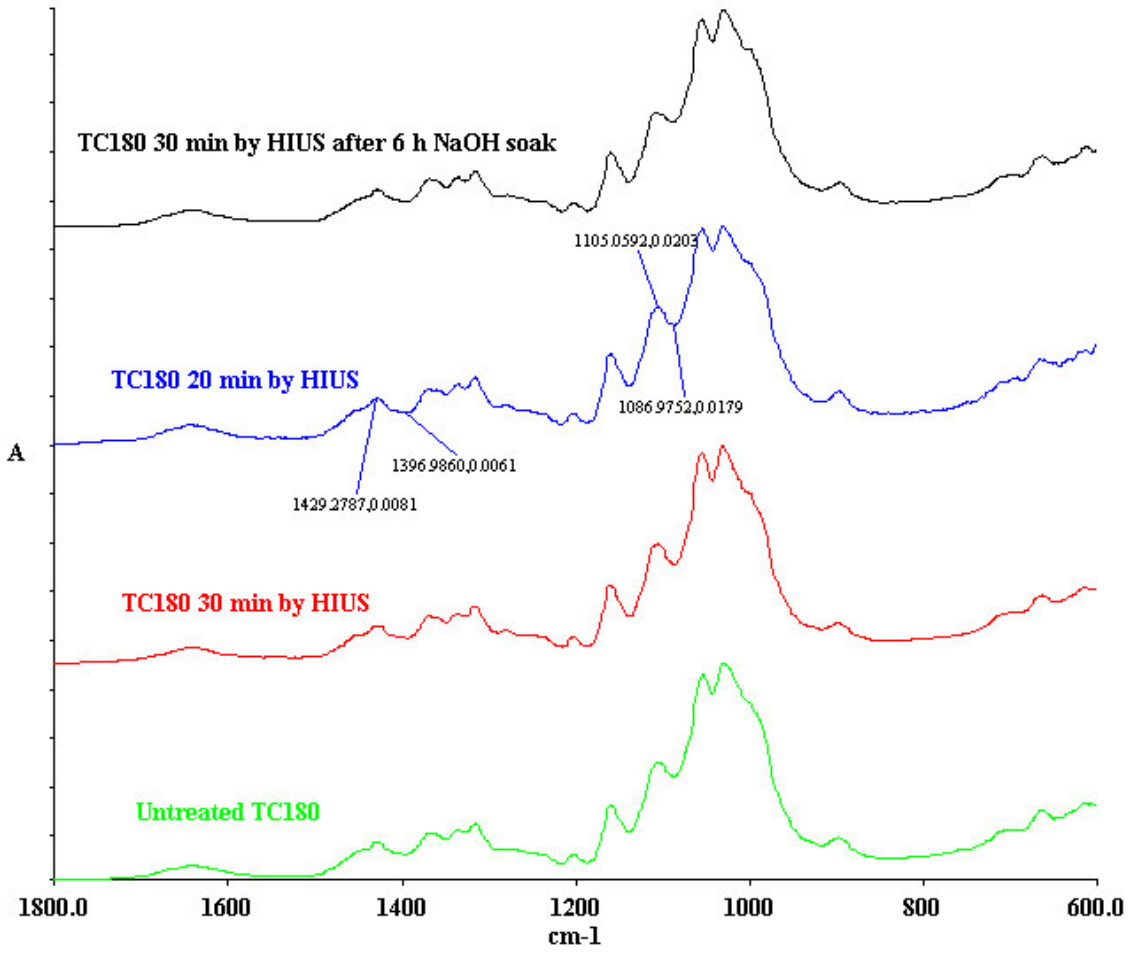

Figure 3.29 Mid FTIR spectra of untreated and treated pure cellulose (TC180) between 1800 and 600 cm^{-1}

The two ratios of peak absorbance to nearby valley, 1105/1087 cm^{-1} and 1429/1397 cm^{-1} for Avicel and TC180, respectively, are shown in Figures 3.31 and 32. Both ratios for Avicel were significantly decreased after treatment, and there were not significant differences among the three treatments. This indicated that HIUS treatment changed the Avicel molecular structure. For TC180, the two ratios had not many differences before and after treatment, while they decreased when NaOH pretreatment was used. Their FTIR crystallinity indices will be discussed in Section 3.4.11.

3.4.5. Effect of abrasive powder on cellulose fibrillation

After treated for 20 min by HIUS with 0%, 5%, 10%, and 20% Alumina powder (1 μm), all the four samples of TC40 were good suspensions (after 24h deposition) (Figure 3.33). There were not big different appearances among them in volume change because the treatment times were too long. Figure 3.34 shows samples of TC40 treated only 5 min by HIUS with 0%, 5%, 10%, and 20% Alumina powder (0.3, 1, and 7 μm). In this case, it was easier to compare the effects of the abrasive powders on cellulose fibrillation because all the samples did not have good suspensions after 24h deposition.

Compared with the untreated sample suspension, the volumes of all the treated sample suspensions were significantly increased, and there were not big differences among the both the abrasive powder loading amount (0%, 5%, 10%, and 20%) and different abrasive powder sizes (0.3, 1, and 7 μm). The powders may make the fibrillation a little bit fast especially for 0.3 μm powder because the small powders may be easier to be accelerated by the microbubbles generated by the cavitations and the powder may hit

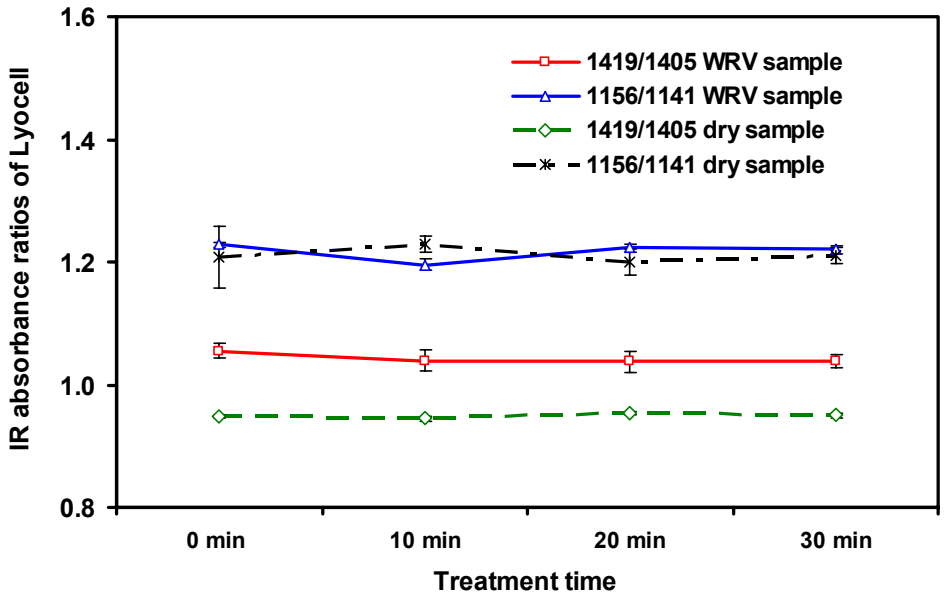

Figure 3.30 FTIR absorbance ratios of untreated and treated Lyocell fiber

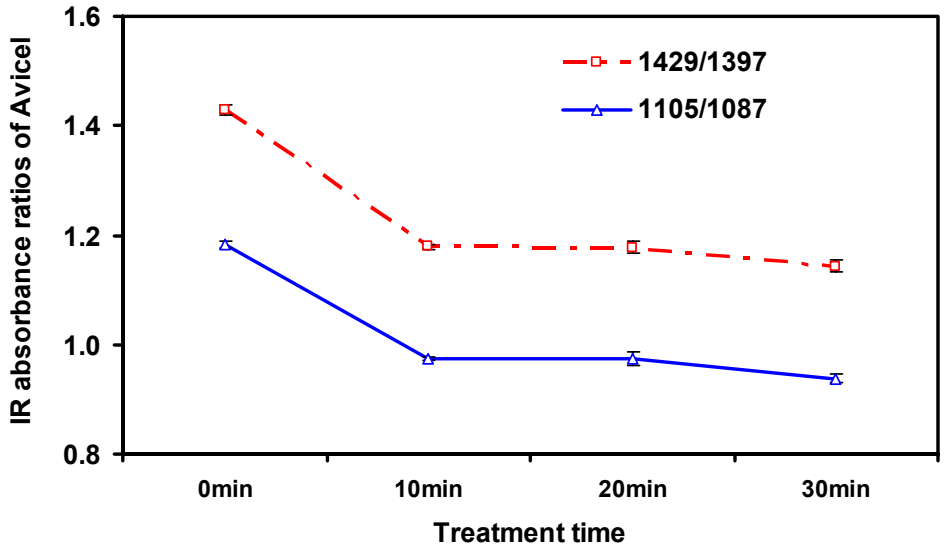

Figure 3.31 FTIR absorbance ratios of untreated and treated Avicel

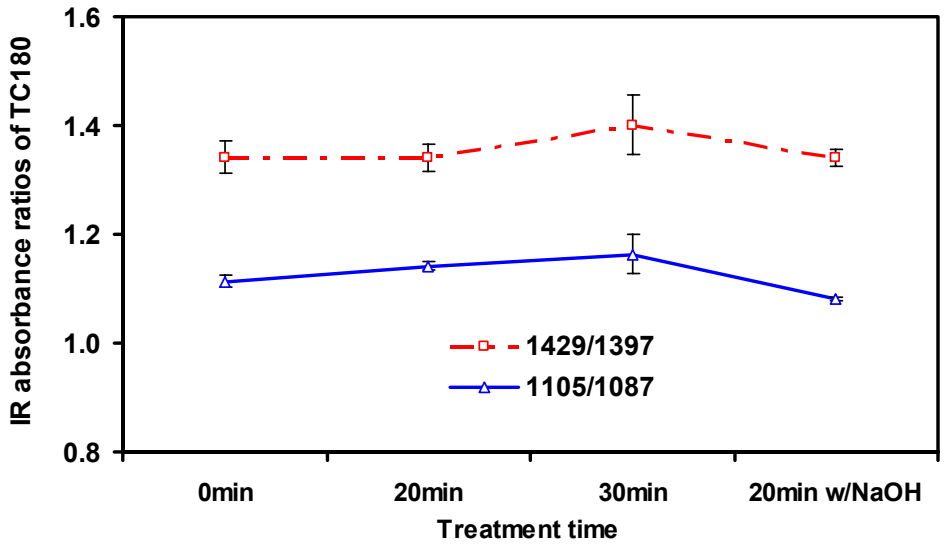

Figure 3.32 FTIR absorbance ratios of untreated and treated TC180

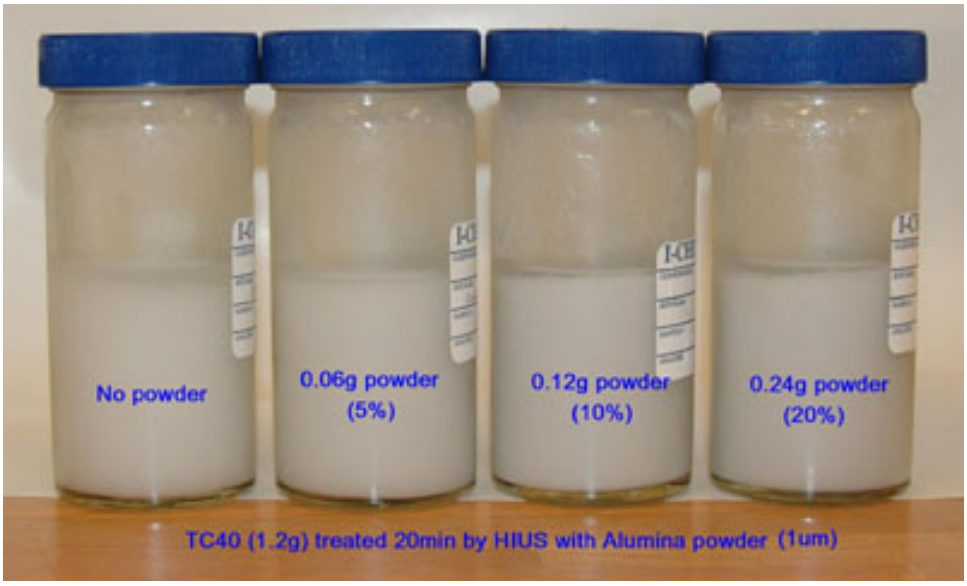

Figure 3.33 Volume changes of TC40 treated 20 min by HIUS with abrasive powders

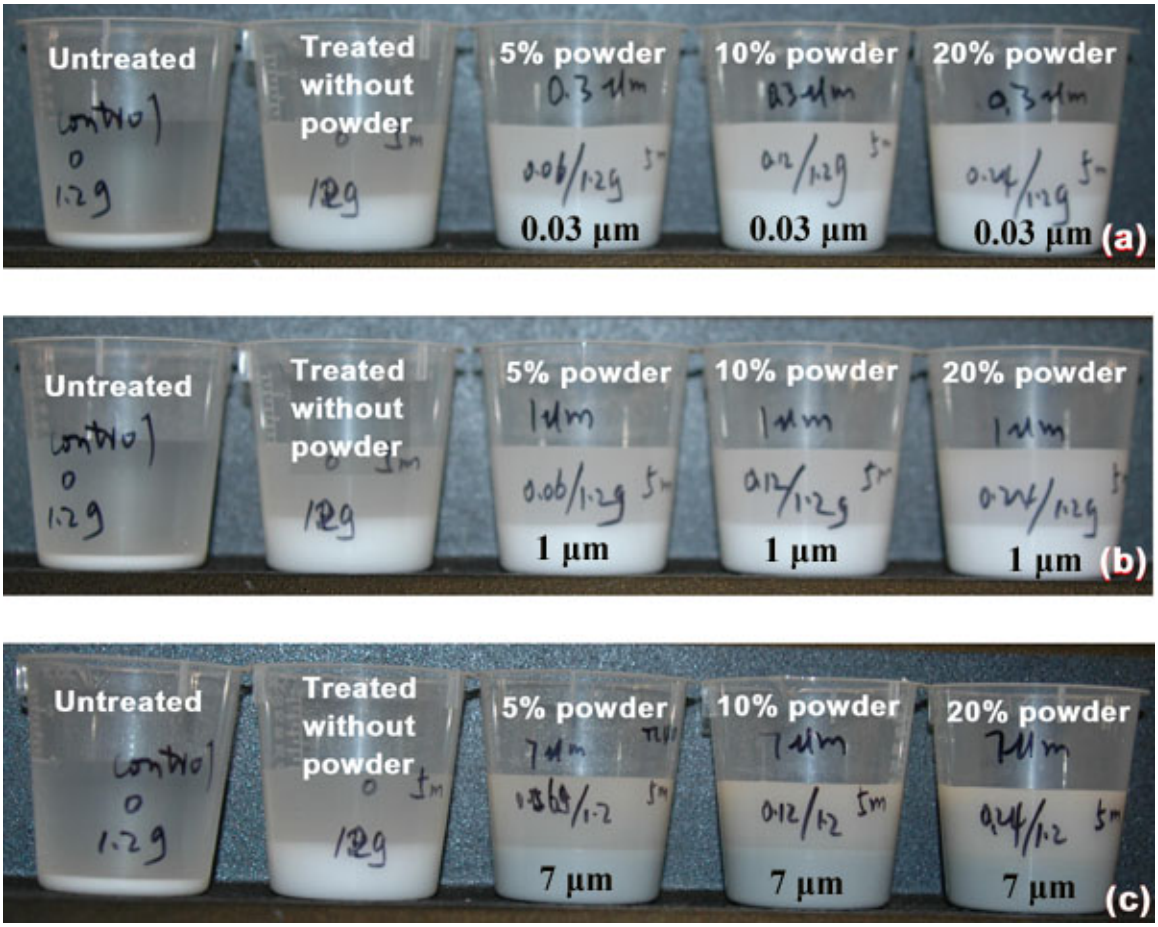

Figure 3.34 Volume changes of TC40 (1.2 g) treated 5 min by HIUS with abrasive powders

the cellulose to accelerate the fibrillation, but it was very difficult to separate the powder and cellulose fiber and fibrils even centrifuge was used. So no further study about abrasive powder application was performed in this study.

3.4.6. Effect of cellulose pretreatment by sodium hydroxide

Figures 3.35 and 3.36 show water retention values (WRV) of Lyocell fibers and TC180 pure cellulose fiber soaked in water or NaOH and treated by HIUS for 20 min. WRV were increased significantly after just soaked in NaOH about 6 h for both Lyocell and TC180 fibers. This indicates that the pretreatment by NaOH swell the fibers and the fibers were easier to fibrillation (Ozturk et al., 2006), so that the WVR of fibers, which were soaked by NaOH and treated for 20 min by HIUS, were higher than those of fibers without NaOH immersion. The swollen Lyocell fibers could be observed by PLM images (Figure 3.37). A PLM image of treated Lyocell is shown in Figure 3.38. It is clear that the fibers were fibrillated and many small fibrils were split from big fibers. Although alkali pretreatment made fibrillation easier, especially for Lyocell fibers, no further study in this research was carried out because of the chemical involvement and time consumption.

3.4.7. Combination of ultrasonication and homogenizer treatment

After treated by High Pressure Homogenizer (HPH) by different pressures, good suspensions of TC40 could be obtained (Figure 3.39). The higher pressure, the better fibrillations of fiber were observed. Some PLM images of treated fibers are shown in Figure 3.40 for 55 MPa and Figure 3.41 for 110 and 220 MPa. The dimensions of fibrils

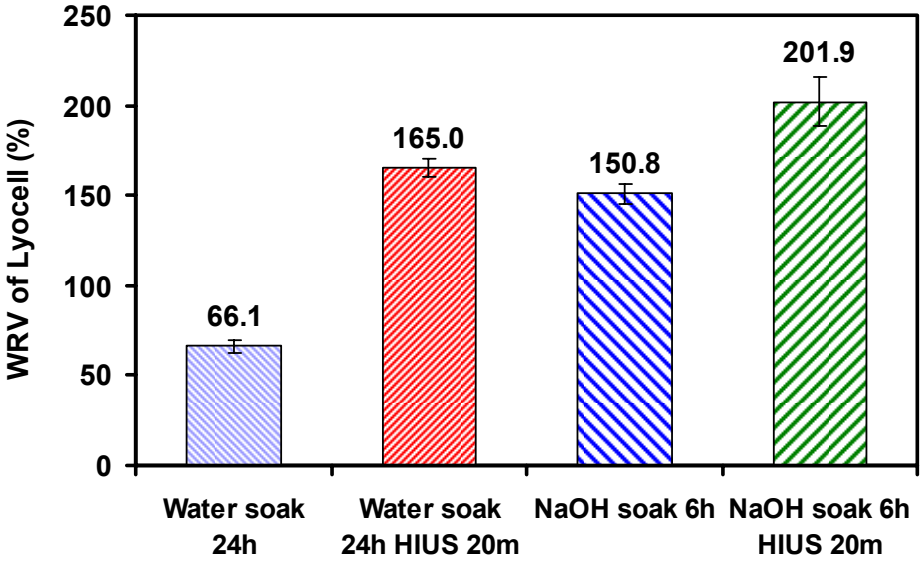

Figure 3.35 WRV of Lyocell fibers soaked in water or NaOH and treated by HIUS for 20 min

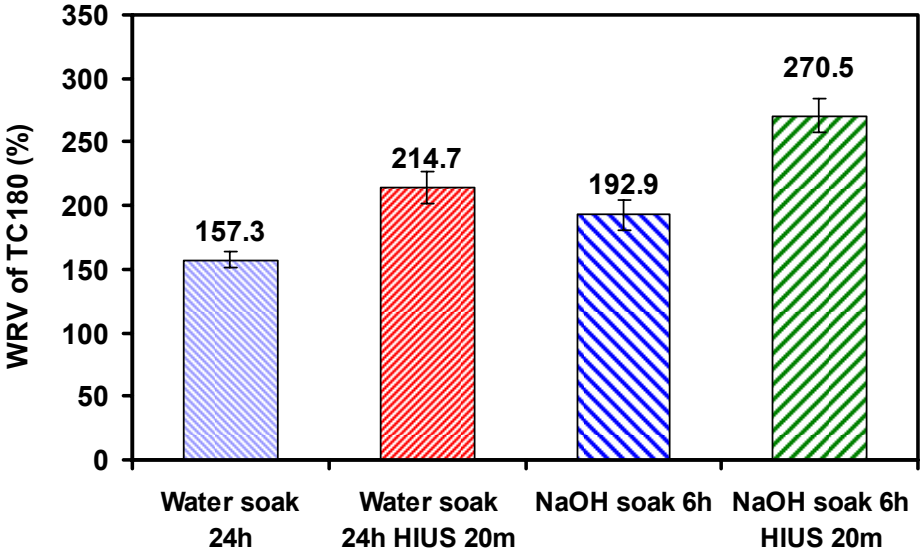

Figure 3.36 WRV of TC180 soaked in water or NaOH and treated by HIUS for 20 min

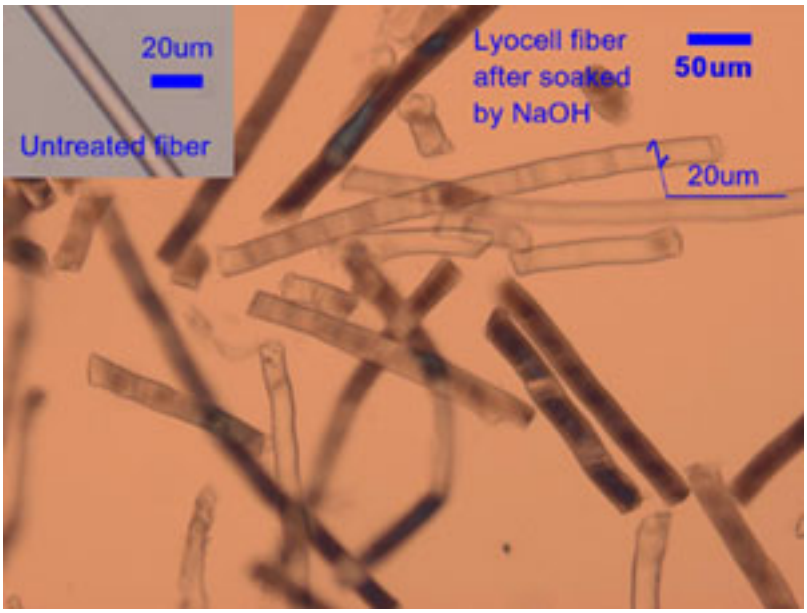

Figure 3.37 PLM image of swollen Lyocell fibers pretreated by NaOH

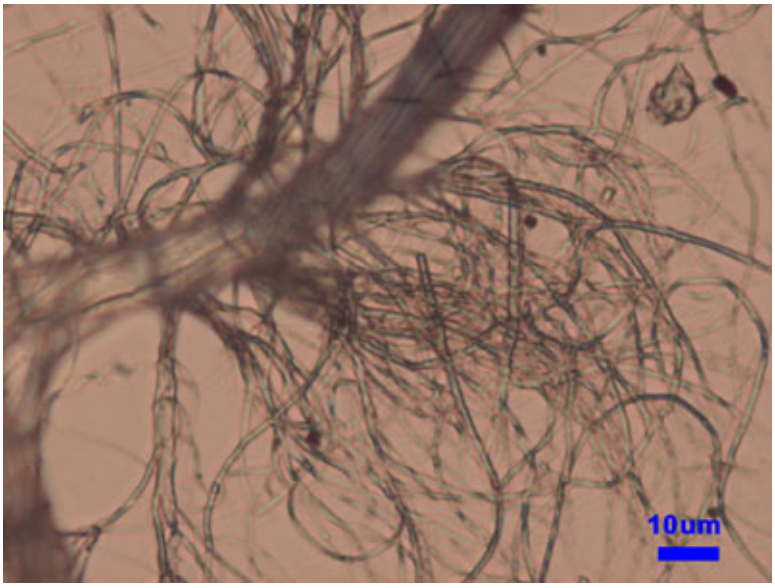

Figure 3.38 PLM image of Lyocell treated 30 min by HIUS after pretreated by NaOH

Figure 3.39 TC40 suspensions treated by High Pressure Homogenizer (HPH)

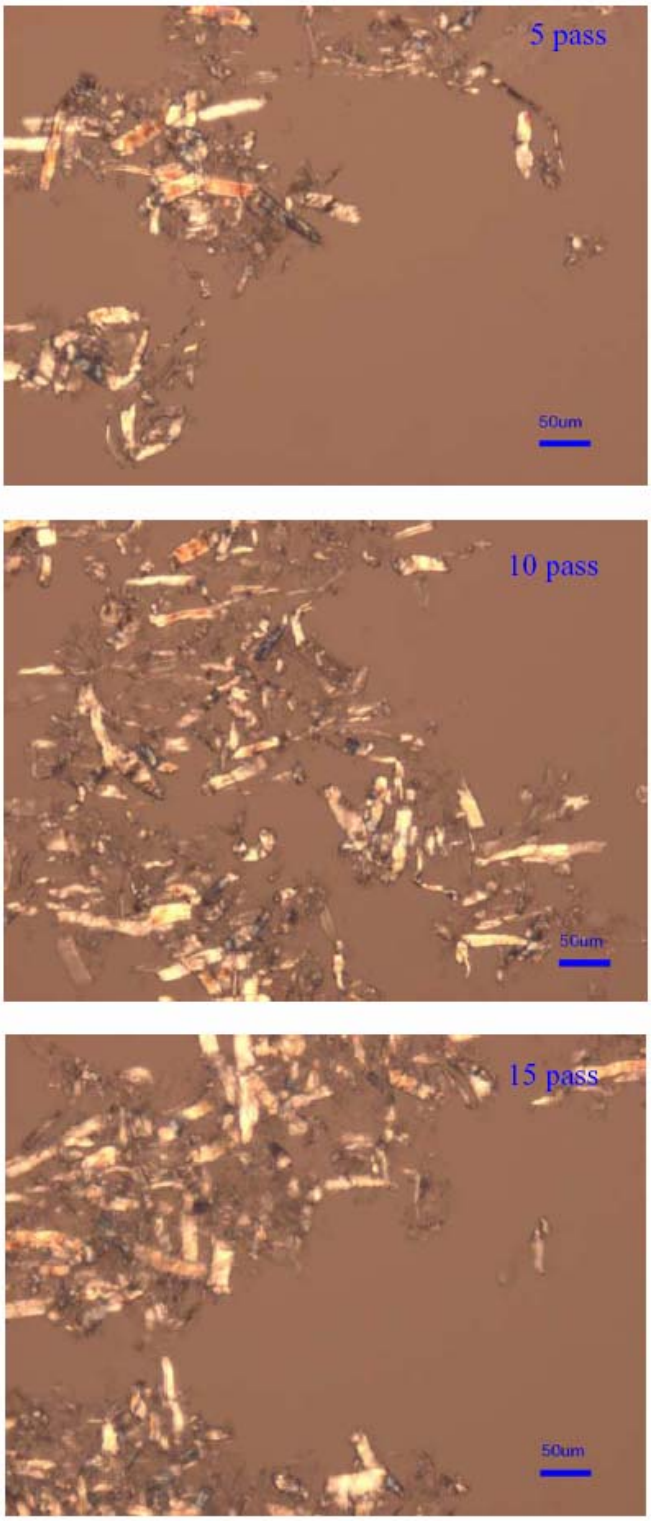

Figure 3.40 TC40 treated by HPH with pressure of 55MPa

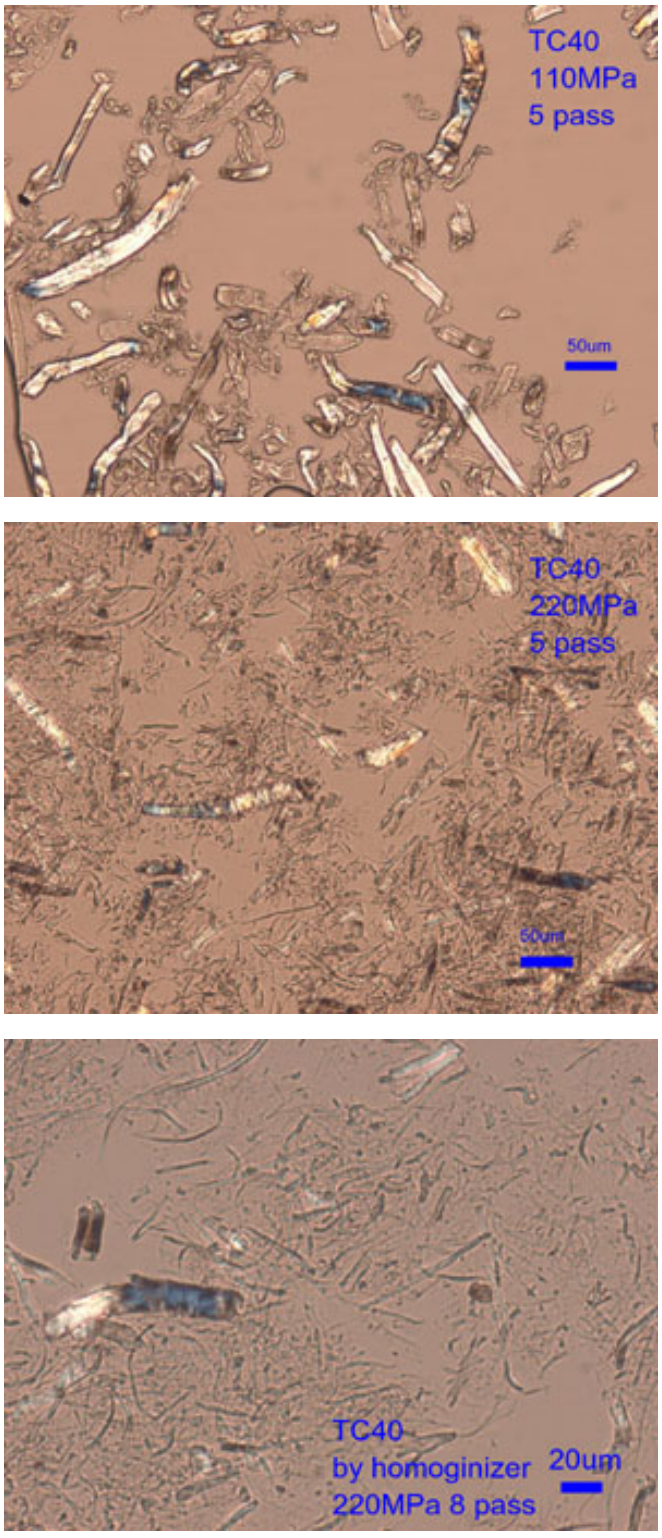

Figure 3.41 TC40 treated by HPH with pressure of 110 and 220 MPa

were getting smaller with higher pressure. The suspension temperature was increased faster for higher-pressure process, which was also helpful for fibrillation of cellulose fibers (Herrick et al., 1983; Turbak et al., 1983).

Further fibrillation of cellulose fibers was observed in the combination of ultrasonication (HIUS) and homogenizer (HPH) treatments for both HPH followed by HIUS (Figure 42) and HIUS followed by HPH (Figures 43). The process of HIUS treatment first then by HPH treatment for only several times may be better than the process of HPH followed by HIUS because homogenizer could make the suspension more uniform. HIUS treatment was focused in this study.

3.4.8. Fibril separation from treated fibers

After centrifuged 5 or 10 min and deposited for about 5 min, the top portion was defined as fibrils used to reinforce polymers and for further analysis. The fibrils still had a wide range of diameters from several μm to tens of nm. If deposited longer time, more big fibrils might sink to the tube bottom, especially for Lyocell fibers, pulp fibers, and big pure cellulose fibers. Figure 3.44 shows images of the suspensions of treated Lyocell fiber before (left) and after (right) centrifuged with 5 min and deposited 5 min.

3.4.9. Dimension analyses of fibers and fibrils

Table 3.4 shows a summary of dimension analyses of fibers and fibrils (Lyocell and TC180) measured by Kajaani FiberLab 3. By definition, Kajaani fiber length is defined as fibers having a fiber length of 0.25 - 7.60 mm (fiber length being length

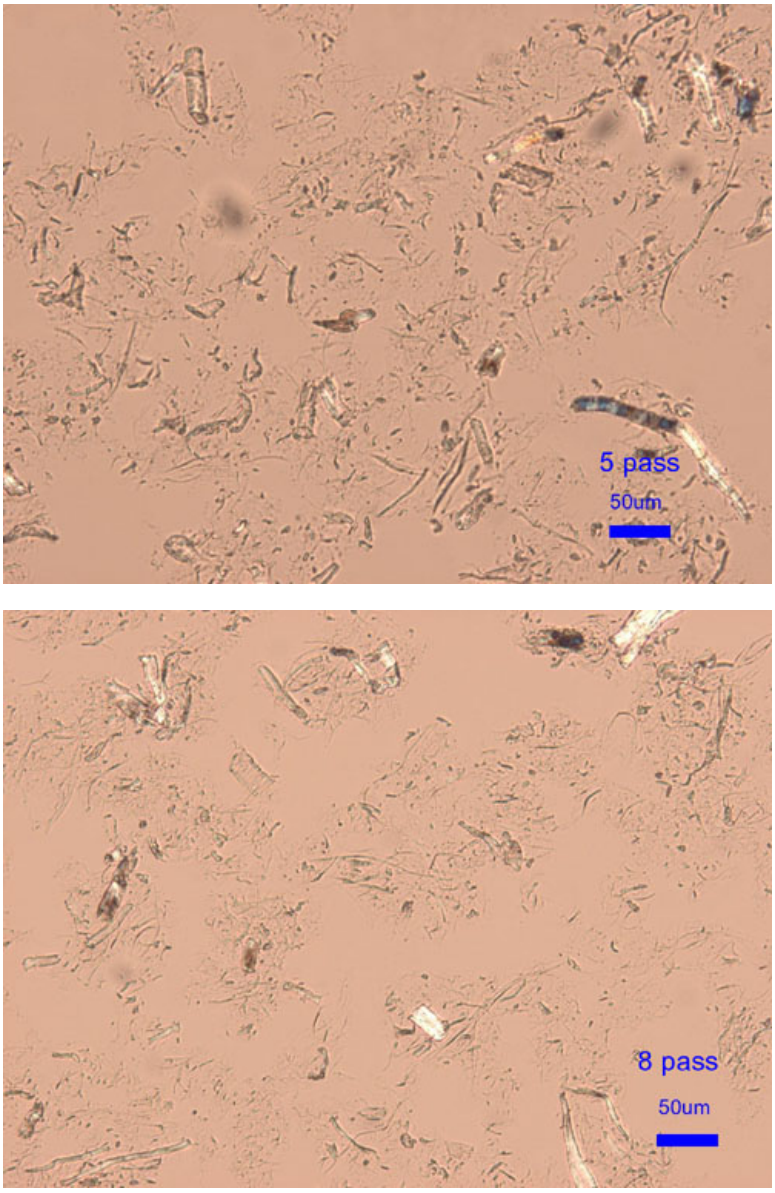

Figure 3.42 TC40 treated by HPH with 110 MPa after HIUS 30 min

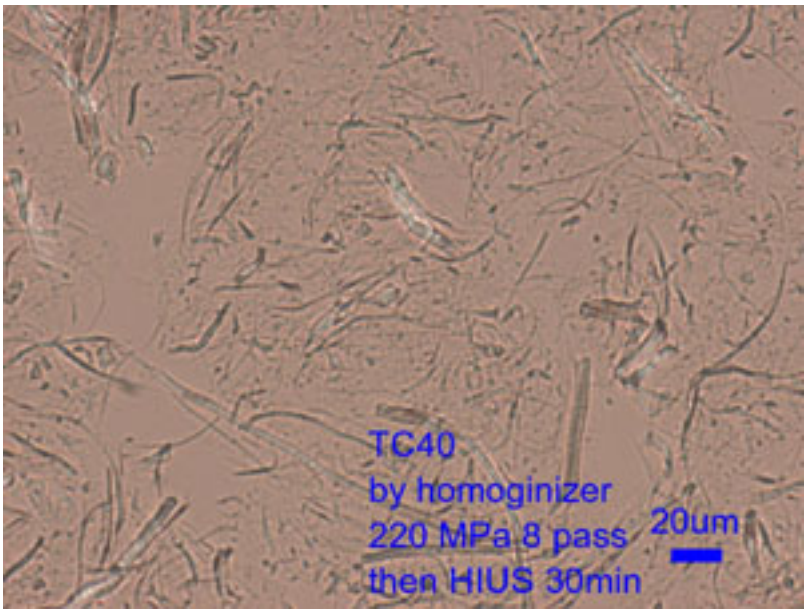

Figure 3.43 TC40 treated by HIUS for 30 min after HPH with 220MPa and 8 passes

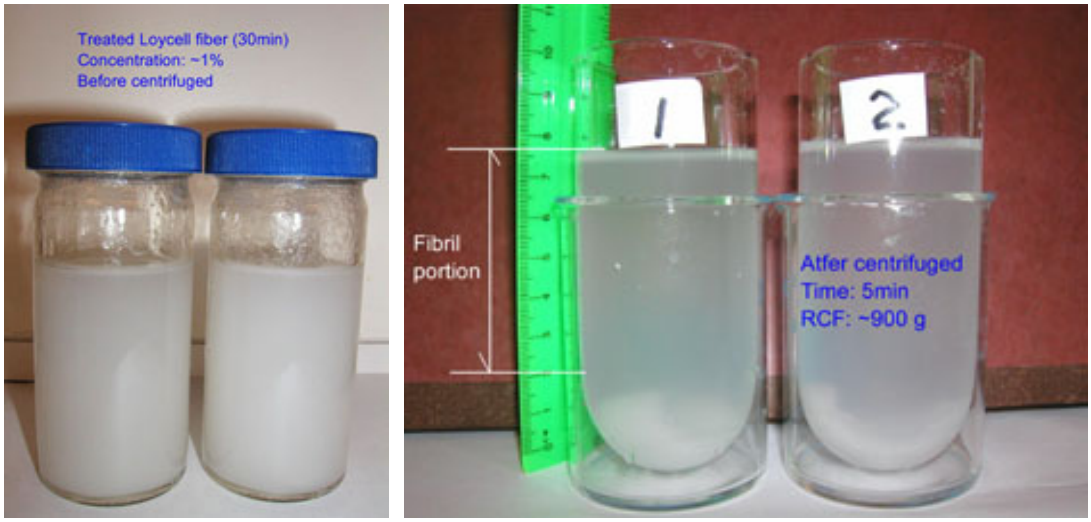

Figure 3.44 Suspensions of treated Lyocell fiber before and after centrifugation

Table 3.4 A summary of dimension analyses of fibers and fibrils measured by Kajaani FiberLab 3

Fiber	Sample	Continuous L.Wt. Av.[4] (0.00-7.60mm) (mm)	Continuous L.Wt. Av.[4] (0.25-7.60mm) (mm)	Continuous % Fines (0.00-0.25mm) (%)	Width (um)	% Curl (%)	CSA[5] (um^2)
Lyocell	Raw fiber	0.97	1.04	8.06	16.4	10.0	160
Lyocell	Mixture[1]	0.87	0.95	10.29	17.7	11.2	201
Lyocell	Separated fibrils[2]	0.27	0.53	67.99	13.1	4.9	174
Lyocell	Separated fibrils[3]		no	detect			
TC180	Raw fiber	0.26	0.42	62.56	12.5	5.9	166
TC180	Mixture[1]	0.23	0.42	67.66	11.6	4.5	156
TC180	Separated fibrils[2]	0.17	0.56	87.96	8.2	2.8	133

1. Mixture after HIUS 30min, 2. Separated fibrils after centrifuge 5m (HIUS 30m),

3. Separated fibrils after centrifuge 5m and set > 3 days (HIUS 30min),

4. L. Wt. Av.=length weighted average, 5. CSA=cross sectional area.

weighted average). Two fiber length (FL) measurements were shown: one with the fines included (0.00 – 7.60-mm) and one with the fines excluded (0.25 – 7.60-mm). Fines are defined as having a measurement of 0.00 - 0.25mm. Width is the average fiber width and CSA is the cross sectional area measured in square microns. The advantage of new Kajaani FiberLab 3 compared with old FiberLab 1 is that FiberLab 3 has an additional source and camera, and it measures the fibers "pixel-to-pixel" along the center line of the fiber, which is called a "continuous" fiber length, while FiberLab 1 gave a "projected" fiber length measurement (Length Weighted Average). Hence, it would not take curves and bends in the fiber into account. The FiberLab 3 also gives the projected length, which is used to calculate Kajaani % curl. The % curl is a mathematical function of the continuous fiber length to the projected fiber length. The straighter fibers would have a similar projected and continuous FL. The curlier the fiber, like cotton or mercerized wood, the greater the difference in projected and continuous FL. As the difference between projected and continuous FL approaches zero, the % curl approaches zero. The disadvantage of this machine for this research is that it can't detect or measure too fine fibrils with less than 1 μm of length. The smaller separated fibrils after centrifuged 5 min and deposited more than 3 days (Lyocell HIUS 30 min) did not run because there were too many fibers below detection limits.

The average width of untreated Lyocell (16.4 μm) was higher than original width of dry fiber (11 μm) because of the swelling after soaked in water, while the average width of treated Lyocell (17.7 μm) was higher than that of untreated Lyocell. This indicates that the fibers were getting looses, some small fibrils might be on the surfaces

of big fibers and big fibers still dominated the treated Lyocell fibers. For TC180, the average width before treatment (12.5 μm) was much less than original width of dry fiber (20 μm). This was unexpected maybe because the original fiber was too thin (only 1-2 μm).

The continuous fiber length distributions of the two materials including before and after treatment, and separated fibrils are showing in Figures 3.45-50, respectively. The results indicate that there were more short fibers in the treated materials.

3.4.10. Fiber and fibril yields

Figures 3.51 and 52 shows the yields of pulp and Lyocell fibers treated by HIUS for different time, separately. The yield of treated fiber was about 100%. This means that there were not water soluble components in the water suspensions treated by HIUS, which accorded with the results of FTIR tests (see 3.4.4).

It is hard to define the small fibril yield after separated by centrifuge as described in part of 3.3.7 because the fibril portion on the top of the suspension could affect by the centrifuge time and deposition time after centrifuge, as well as the concentration of suspensions. The centrifuge time of 5 min for Lyocell and 10 min for others and deposition time of 5 min after centrifuge were used in this study. The yields of fibrils from Lyocell and Avicel fibers treated by HIUS for 30 min and 60 min are shown in Table 4. After treated 30 min and centrifuged, the big fibers were treated for another 30 min, which was marked as the second 30 min. Longer fibers such as Lyocell were much more difficult to be fibrillated than shorter fibers such as Avicel fiber.

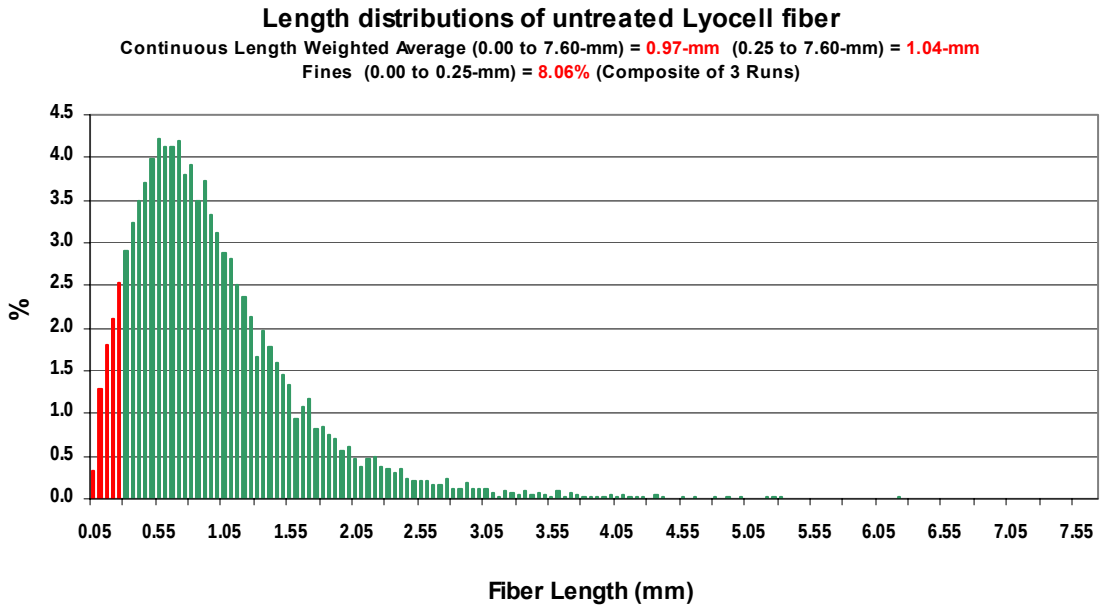

Figure 3.45 Continuous fiber length distributions of untreated Lyocell fibers

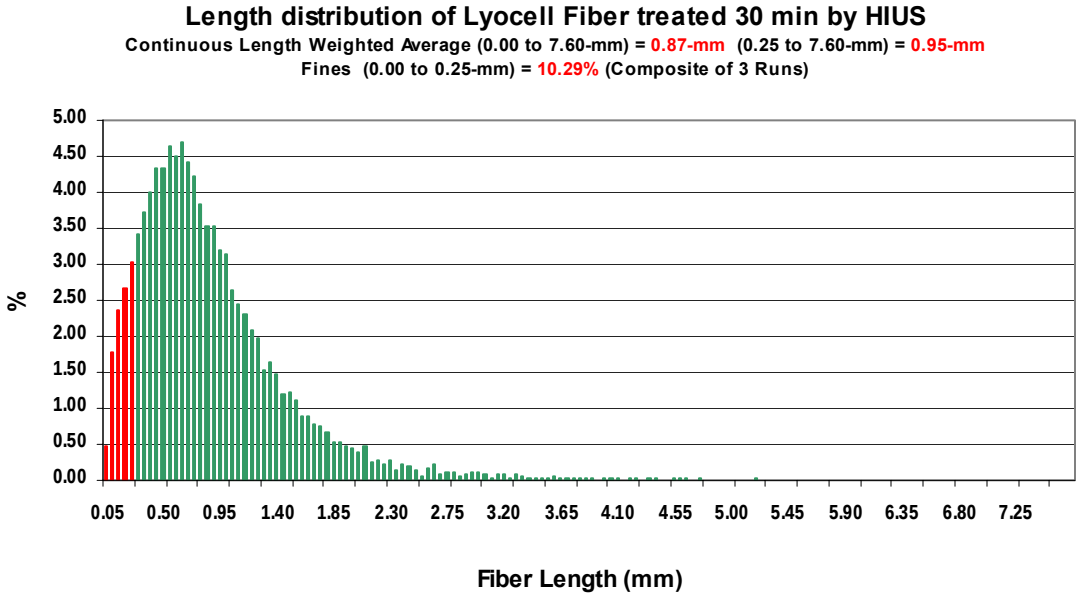

Figure 3.46 Continuous fiber length distributions of treated Lyocell fibers

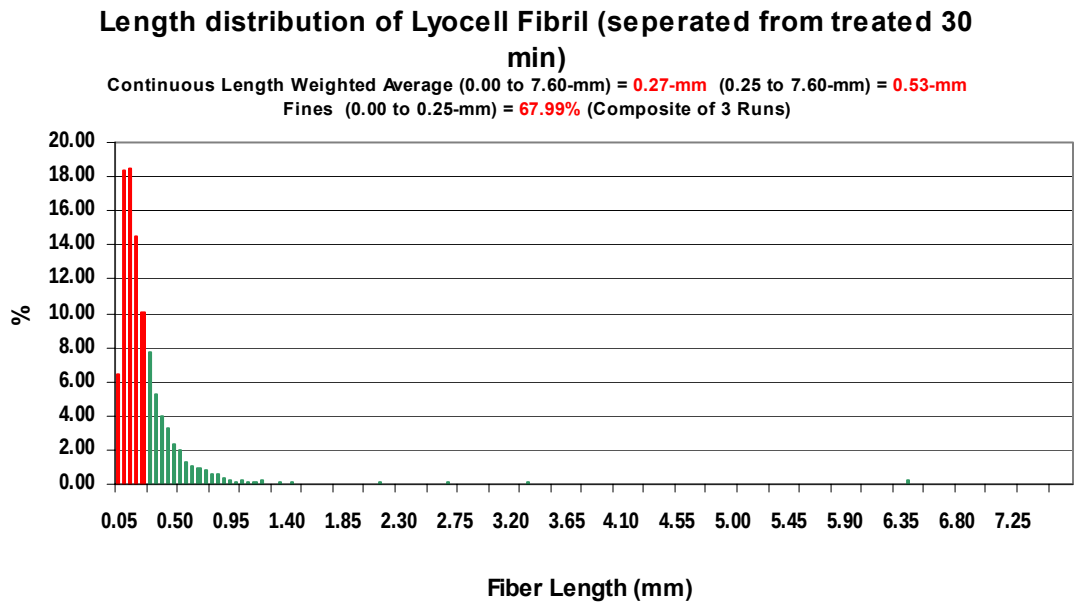

Figure 3.47 Continuous fiber length distributions of separated Lyocell fibrils

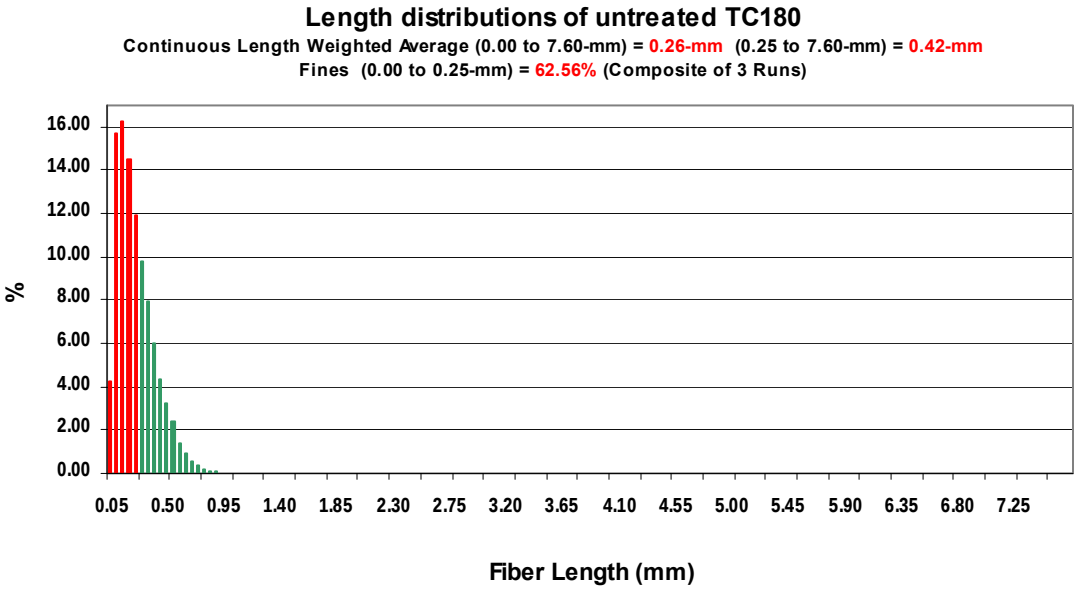

Figure 3.48 Continuous fiber length distributions of untreated TC180

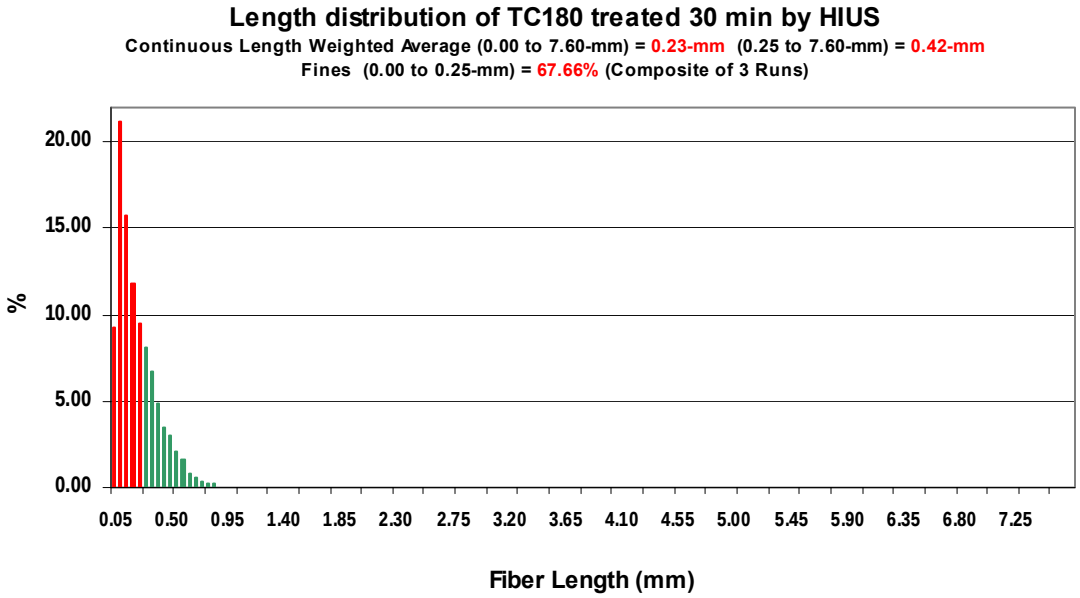

Figure 3.49 Continuous fiber length distributions of treated TC180

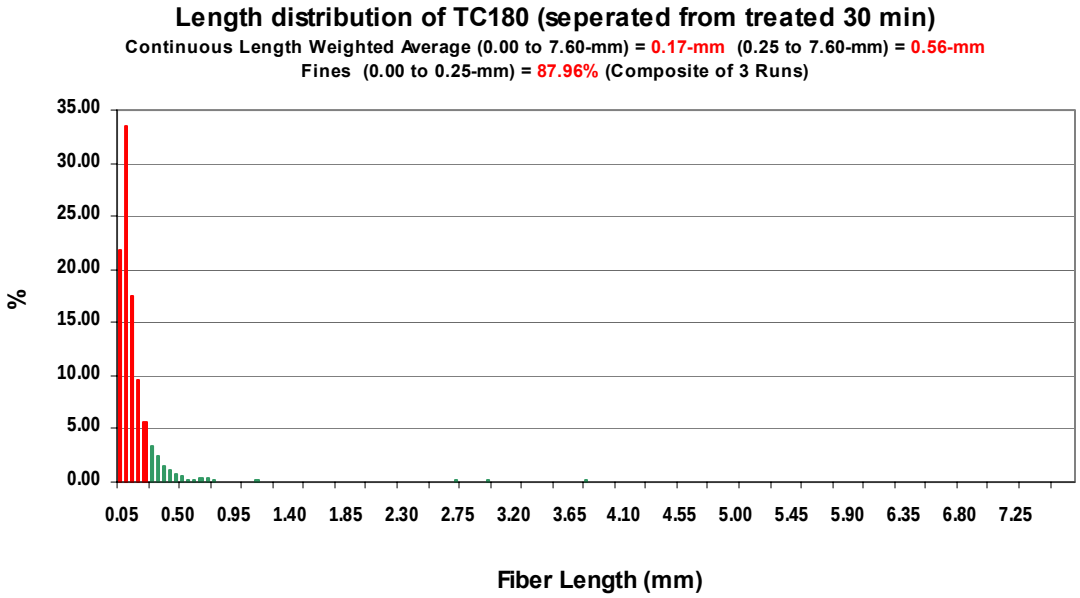

Figure 3.50 Continuous fiber length distributions of separated TC180 fibrils

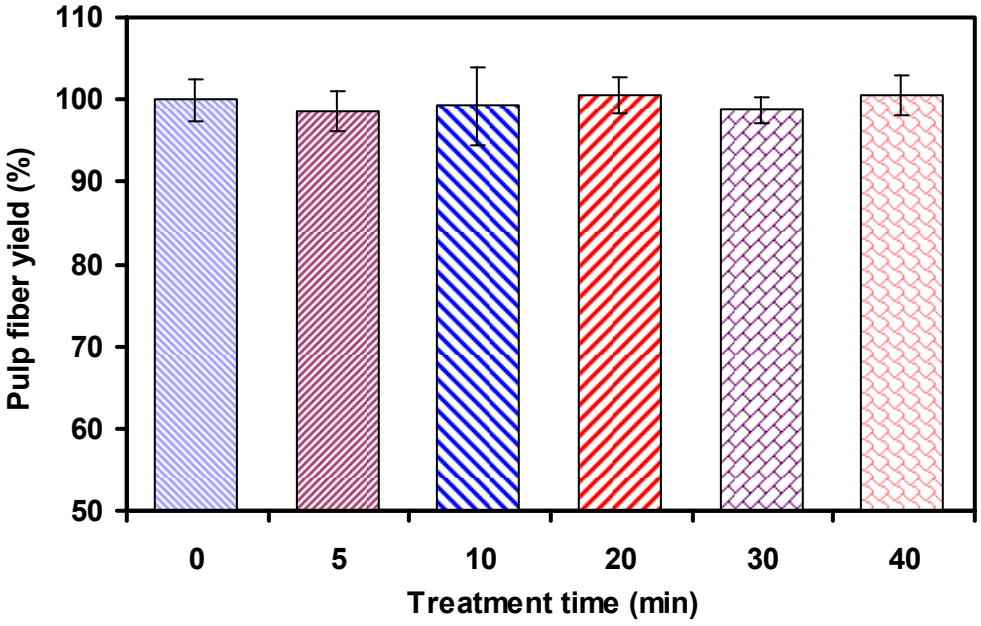

Figure 3.51 Fiber yields of pulp fibers treated by HIUS

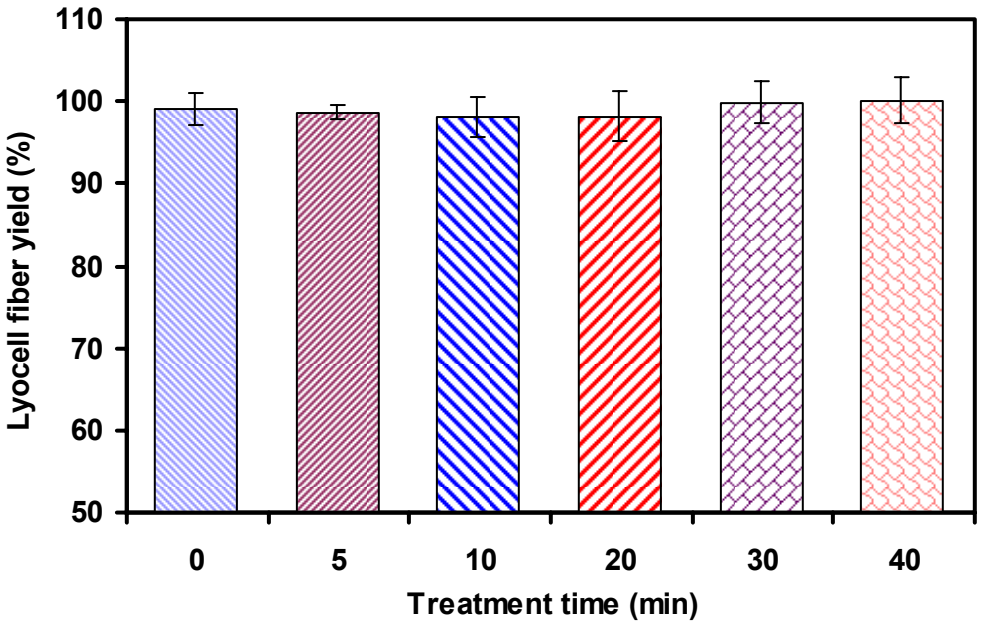

Figure 3.52 Fiber yields of Lyocell fibers treated by HIUS

Table 3.5 Small fibril yields of Lyocell and Avicel fibers treated by HIUS

	First 30 min	Second 30 min	Continuous 60 min
Lyocell fiber (%)	3±2	4±2	5±2
Avicel Fiber (%)	~40	~40	~52

3.4.11. Efficiency of cellulose fibrillation evaluated by water retention values

Water retention value (WRV) was mainly used to estimate the efficiency of cellulose fibrillation during ultrasonic treatment. The six factors that may influence cellulose fibrillation including Time (t), Temperature (T), Power (P), Concentration (C), Fiber size (FS), and Distance from tip to beaker bottom (d) were discussed using WRV. When one factor was variable, the others were kept as constants (Table 3.2).

Time and temperature

Figure 3.53 shows the WRV with standard deviations of the untreated and treated Lyocell fibers for different treatment time and temperature. The degree of microfibrillation of the treated fibers increased as the treatment time increased. It indicates that the fibers became smaller and more surface area on the fibrils as treatment time and temperature increased because WRV is related to fibril and microfibril surface and volumetric phenomena (Herrick et al., 1983). The longer the treatment time, the smaller the fibrils can be obtained in the suspension mixture. Higher temperature of the suspension was very helpful for cellulose microfibrillation. It was 91˚C without cooling and 55˚C with ice cooling (Figure 3.22).

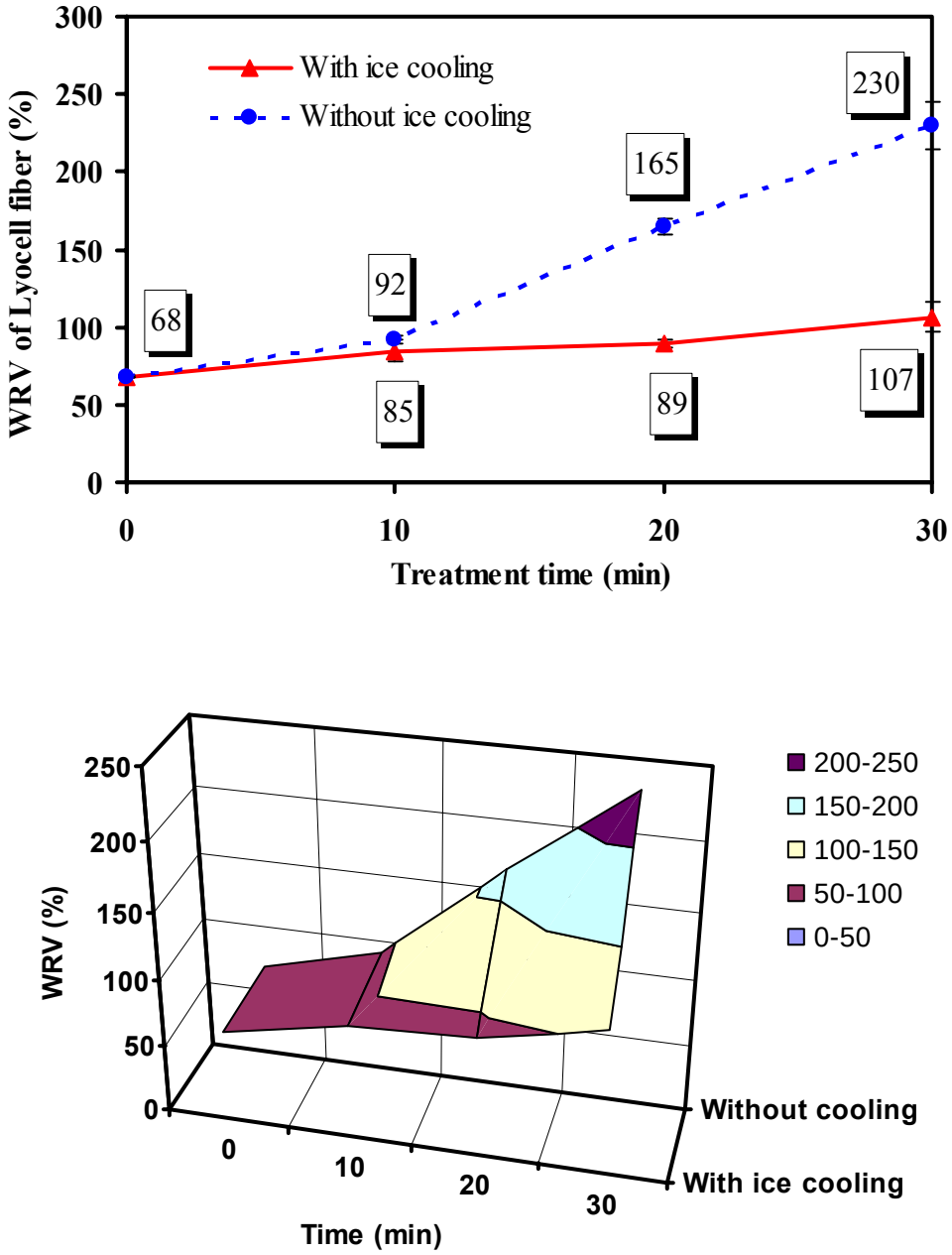

Figure 3.53 WRV of Lyocell fibers treated by HIUS with different treatment time and temperature: 2D (top) and 3D (bottom)

Power

Figure 3.54 shows the WRV of TC40 treated by HIUS with different treatment power. It was clear that higher operation power made cellulose microfibrillation easier. This was because higher operation power transferred more energy to the probe and the temperature of the suspension increased faster (Figure 3.22), which helped cellulose microfibrillation.

Concentration

Figure 3.55 shows the WRV of TC40 treated by HIUS with different fiber concentrations. Higher concentrations of cellulose suspensions operation had lower WRV as the aquatic force generated by microbubble could not agitate and stir the cellulose fiber well in the suspensions, so that the fibers had less chance to pass the tip.

Fiber size

Figure 3.56 shows the WRV of different sizes of pure cellulose fibers treated by HIUS. Treated smaller fiber (TC40) had much higher WRV than that of treated bigger fiber (TC2500), but the increase percentage from untreated fiber for each fiber had not much difference among the three fibers.

Distance from tip to beaker bottom

Figure 3.57 shows the WRV of TC40 treated by HIUS with different distances from tip to beaker bottom. If d was more than 10 mm, WRC significantly decreased. This

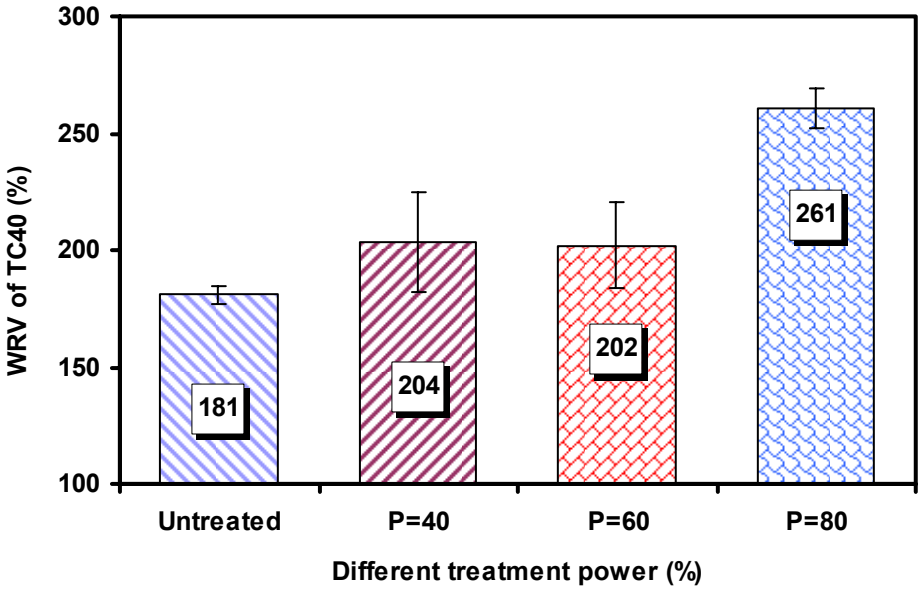

Figure 3.54 WRV of TC40 treated by HIUS with different treatment power

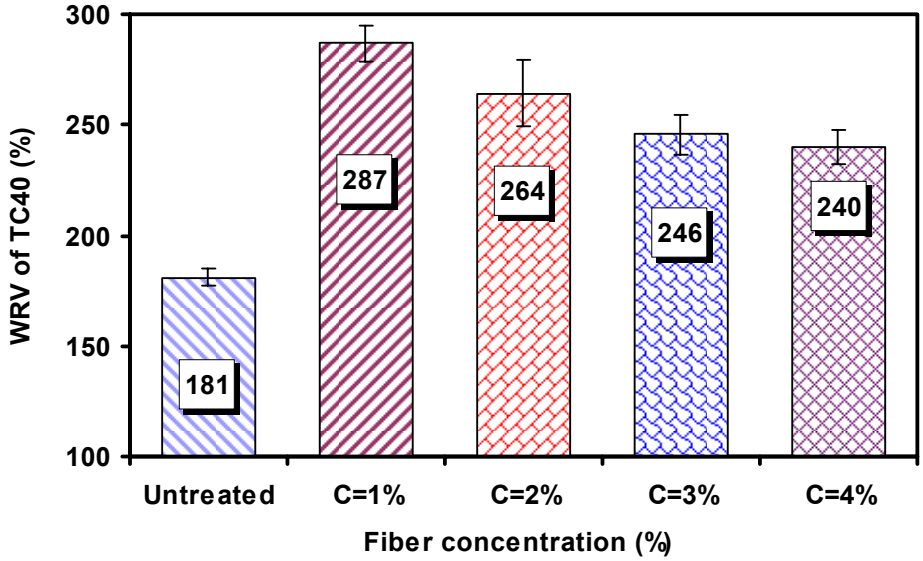

Figure 3.55 WRV of TC40 treated by HIUS with different fiber concentrations

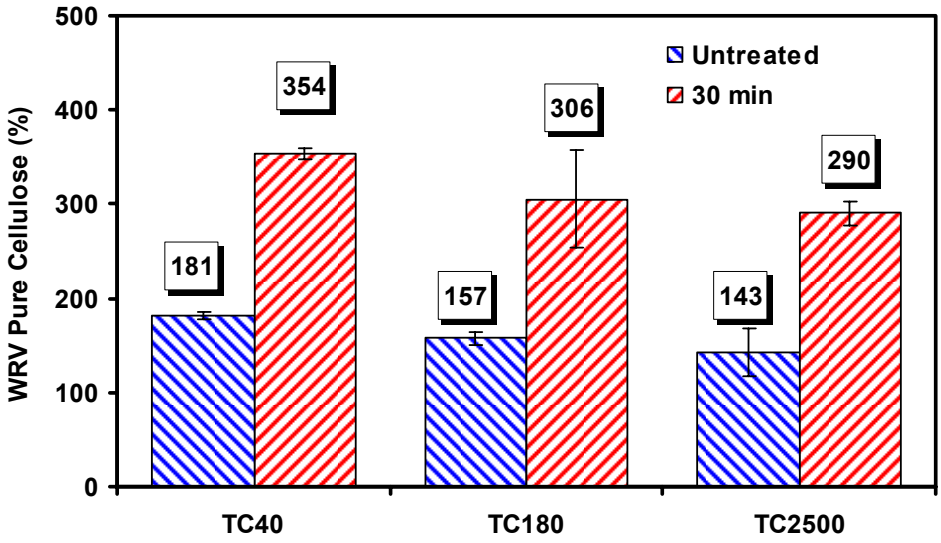

Figure 3.56 WRV of different pure cellulose fibers before and after treated by HIUS

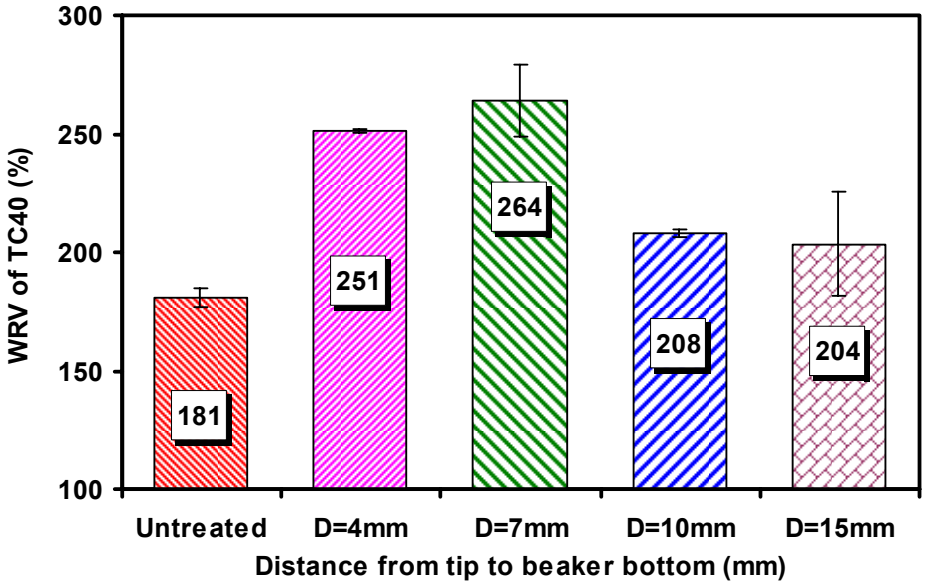

Figure 3.57 WRV of TC40 treated by HIUS with different distances from tip to beaker bottom

may be because less accelerated fibers by the aquatic force generated by microbubbles reached the bottom of the beaker, so that the suspension did not agitate and stir very well, and subsequently the fibers had less chance to pass the tip.

According to WRV measurements, the optimum process of HIUS for TC40 could be: P=80%, T=without cooling, C=1%, t=7 mm, t>30 min, but longer treatment time could make higher cellulose degradation.

3.4.12. Crystallinity changes

The crystallinity of the treated Lyocell fibers increased as the treatment time increased. The results measured by WAXD are shown in Figure 5.58 (average of two or three samples). All the four cellulose samples have a narrow peak at 2θ of about 20° and a lower peak at 2θ of about 12° (Figure 59). The crystallinity of untreated Lyocell cellulose was calculated to be 61% from the X-ray diffraction patterns, which was reasonable according to the published values of about 64.04% and 72.56% for Lyocell-I and Lyocell-II respectively (Peng et al., 2003). A reason that the crystallinity of fiber and fibril aggregate mixture went up with the treatment time increasing may be that some of the amorphous cellulose were degraded during the mechanical treatment and removed during filtration for WRV measurement. High crystalline fibers and fibril aggregates could be more effective in achieving higher reinforcement for composite materials (Eichhorn and Young, 2001).

The crystallinity index of Lyocell fiber was also evaluated by FT-IR as the intensity ratio between IR absorptions at 1419 and 895 cm^{-1}. Figure 3.60 shows the

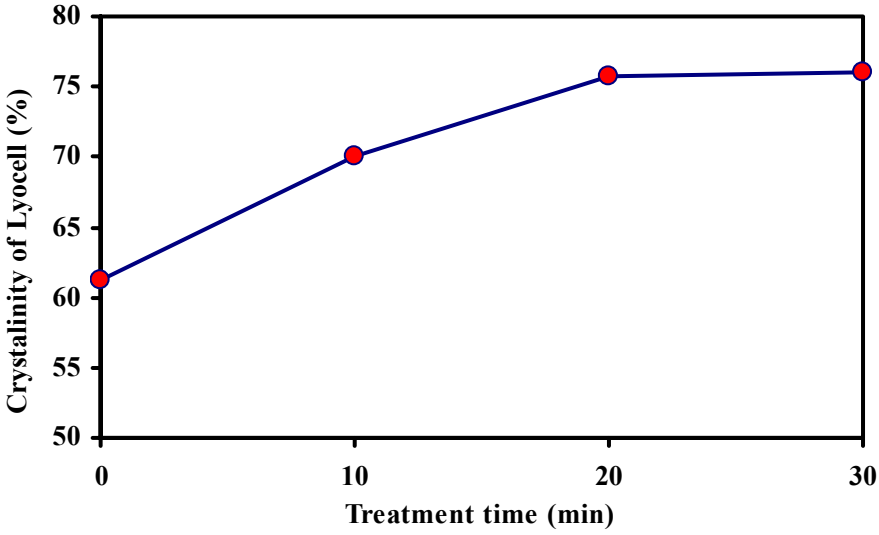

Figure 3.58 Crystallinities of untreated and treated Lyocell fibers measured by WAXD

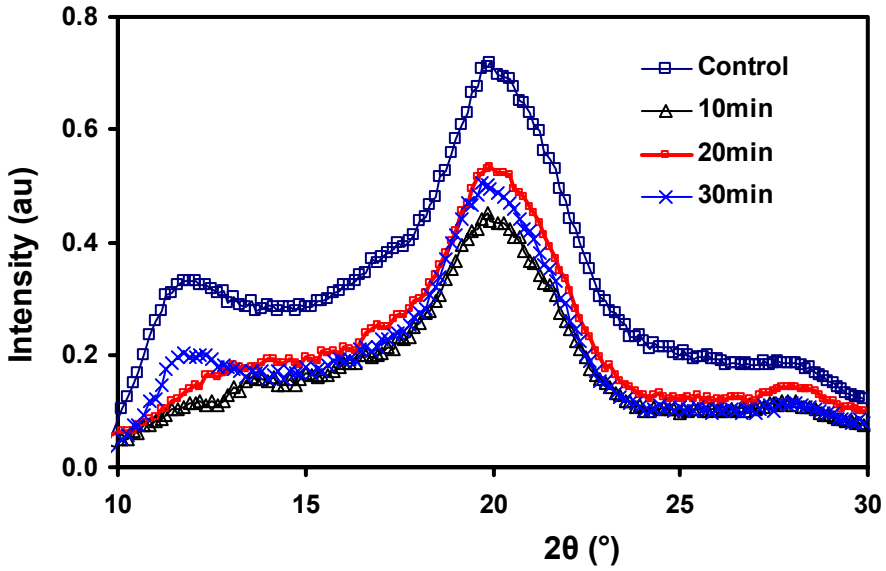

Figure 3.59 WAXD curves for untreated and treated Lyocell fibers

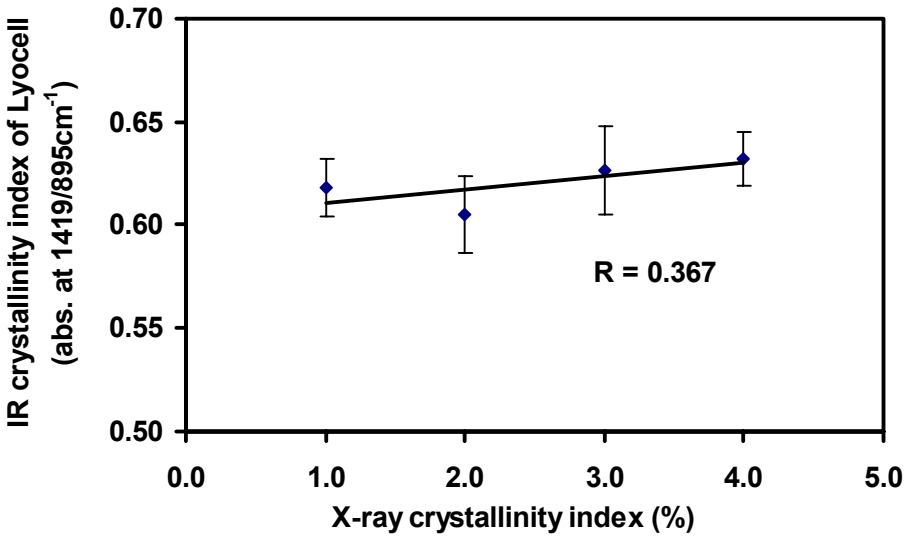

Figure 3.60 Correlation between X-ray and FT-IR crystallinity indices of cellulose for Lyocell

correlation between X-ray and IR crystallinity indices of cellulose for Lyocell. The correlation coefficient (R) vales was only 0.367. This may be because only four points were used and the correlation may be not linear at all. The correlation between X-ray and FT-IR crystallinity indices of cellulose for cotton and V. Ventricosa was like power function (Kataoka and Kondo, 1998). The FT-IR crystallinity indices of Lyocell fiber for different samples (WRV sample vs. dried directly on aluminum foil) were different, especially when the sample was treated for 10 min (Figure 3.61). This indicated that the filtration for WRV measurement may get rid of some small fibrils that included more crystalline parts.

The FT-IR crystallinity indices of Avicel and TC180 for different treatment time are shown in Figures 3.62 and 3.63, respectively. HIUS treatment significantly decreased the FT-IR crystallinity index of Avicel fibers. This may be because Avicel has very high

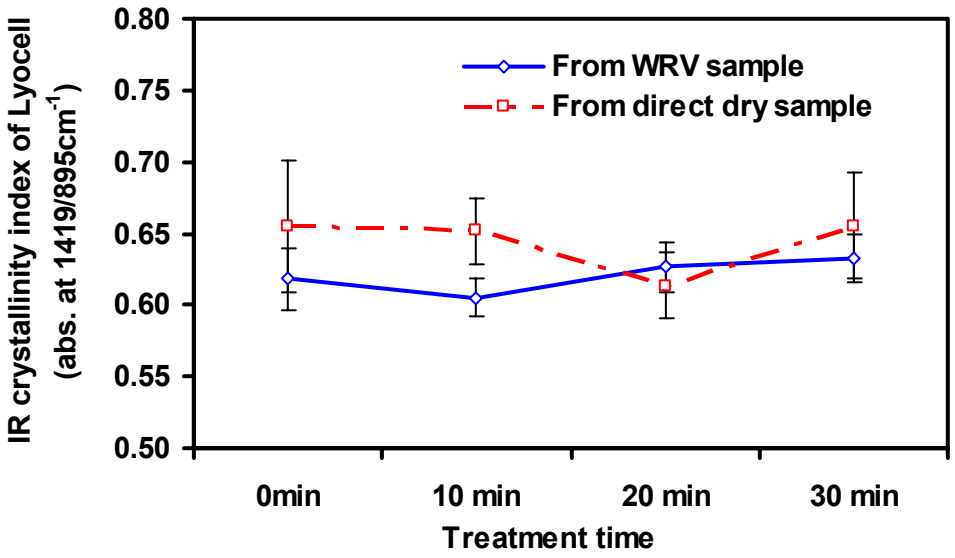

Figure 3.61 FT-IR crystallinity indices of Lyocell fiber for different treatment time and sample preparation

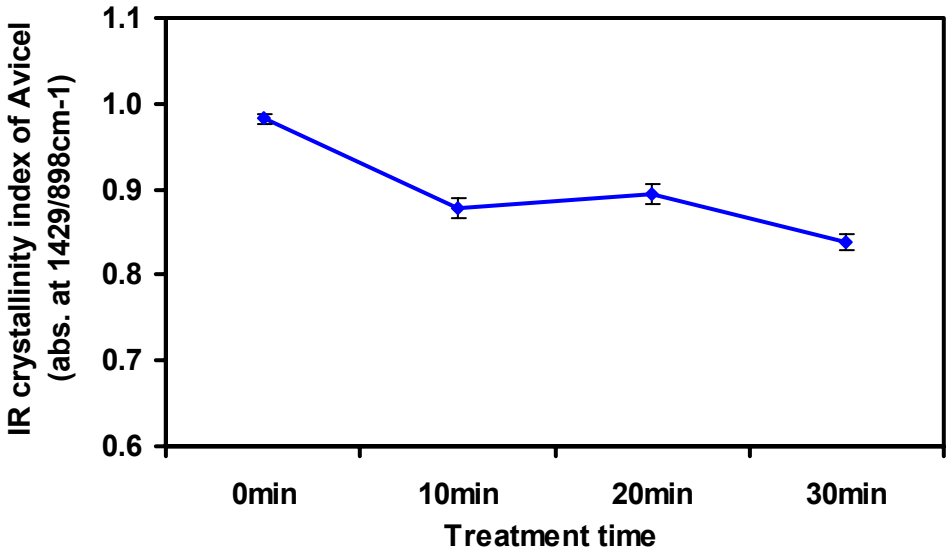

Figure 3.62 FT-IR crystallinity indices of Avicel for different treatment time

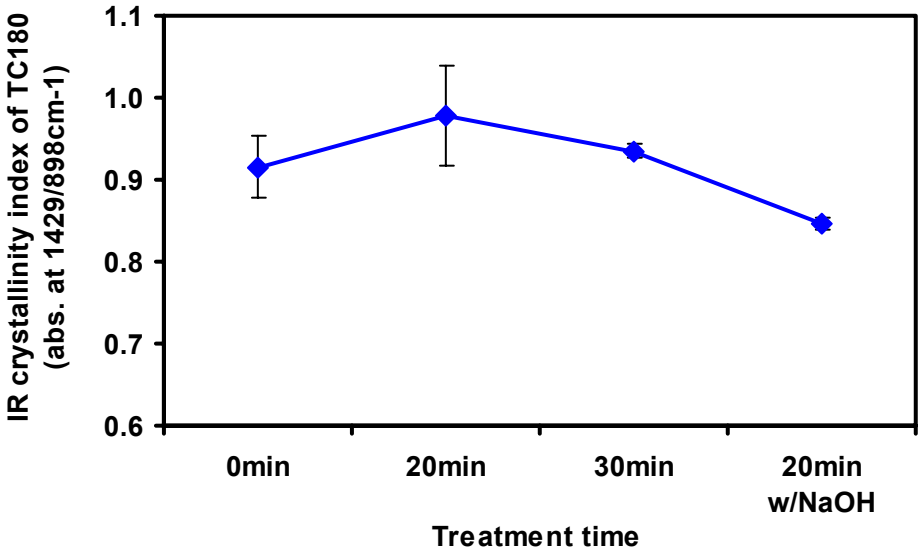

Figure 3.63 FT-IR Crystallinity indices of TC180 for different treatment time

crystallinity and HIUS treatment changed some molecular structure of Avicel cellulose. For pure cellulose fiber (TC180), HIUS treatment did not change FT-IR crystallinity index too much, while it decreased for the pretreated TC180 by NaOH. This indicated that NaOH pretreatment could change some molecular structure of pure cellulose fiber.

3.4.13. Morphological analysis of fibers and fibrils

The geometrical characteristics of the untreated and treated fibers by high intensity ultrasonication (HIUS) and fibrils separated from treated fibers, including regenerated cellulose fiber (Lyocell), pure cellulose fiber, pulp fiber, microcrystalline cellulose (Avicel), as well as commercial microfibrillated cellulose (MFC), were investigated by polarized light microscopy (PLM), scanning electron microscopy (SEM) and atomic force microscopy (AFM).

Regenerated cellulose fiber (Lyocell)

The PLM overview appearance of a single untreated Lyocell fiber (inset figure) and some fibers treated for 10, 20, and 30 min by HIUS are shown in Figure 3.64. The longer treatment time, the higher fibrillation was obtained. This is why the WRV was increased along with the treatment time incensement. After 30 minutes treatment, a mixture suspension of fiber and fibril aggregates with diameter ranging from microns to tens of nanometers was obtained. Figures 3.65 and 3.66 show more PLM images of treated Lyocell fibers and fibrils separated with centrifuge. Many small fibril aggregates with diameter less than 1μm were peeled from the fibers. Some fibril aggregates were still on the surfaces of the big ones that dominate the treated fibers, while some were already isolated from the big fibers as shown in Figure 3.66.

The structure and appearance of the Lyocell fibers and fibrils (treated 30 min) on silicon wafers observed by SEM are shown in Figures 3.67 and 3.68. Figure 3.69 shows fibrils isolated from Lyocell fiber after treated for 90 min. The diameters or widths of the fibrils isolated from Lyocell fibers were in a wide range of tens to hundreds nm, and have a wide range of aspect ratio (length/diameter). The AFM images of fibrils (Figures 3.70 and 3.71) show some small fibrils with diameters of 20 to 30 nm. Some fibril diameters were at the range of 100 to 200 nm. Compared with commercial microfibrillated cellulose (MFC) (Figures 3.72 to 3.74), which was obtained by mechanical treatment (mainly by homogenizer), the fibrils generated by HIUS after 30 min treatment and separated by centrifuge had a similar range of diameters from tens of nm to several μm, and also included a small amount of big fibers more than 10 μm in diameter (Figure 3.72).

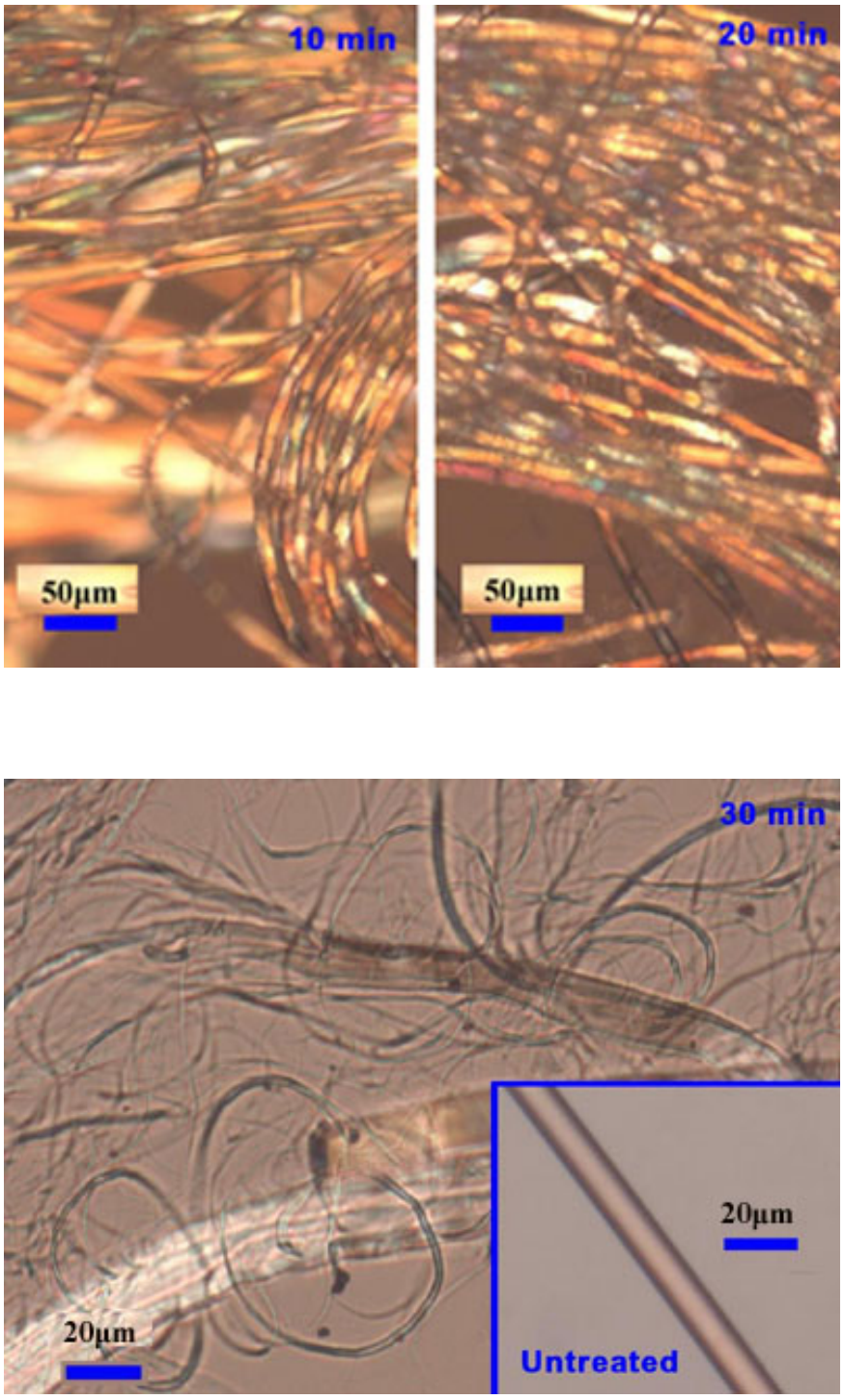

Figure 3.64 PLM images of Lyocell fibers treated 10, 20, and 30 min by HIUS

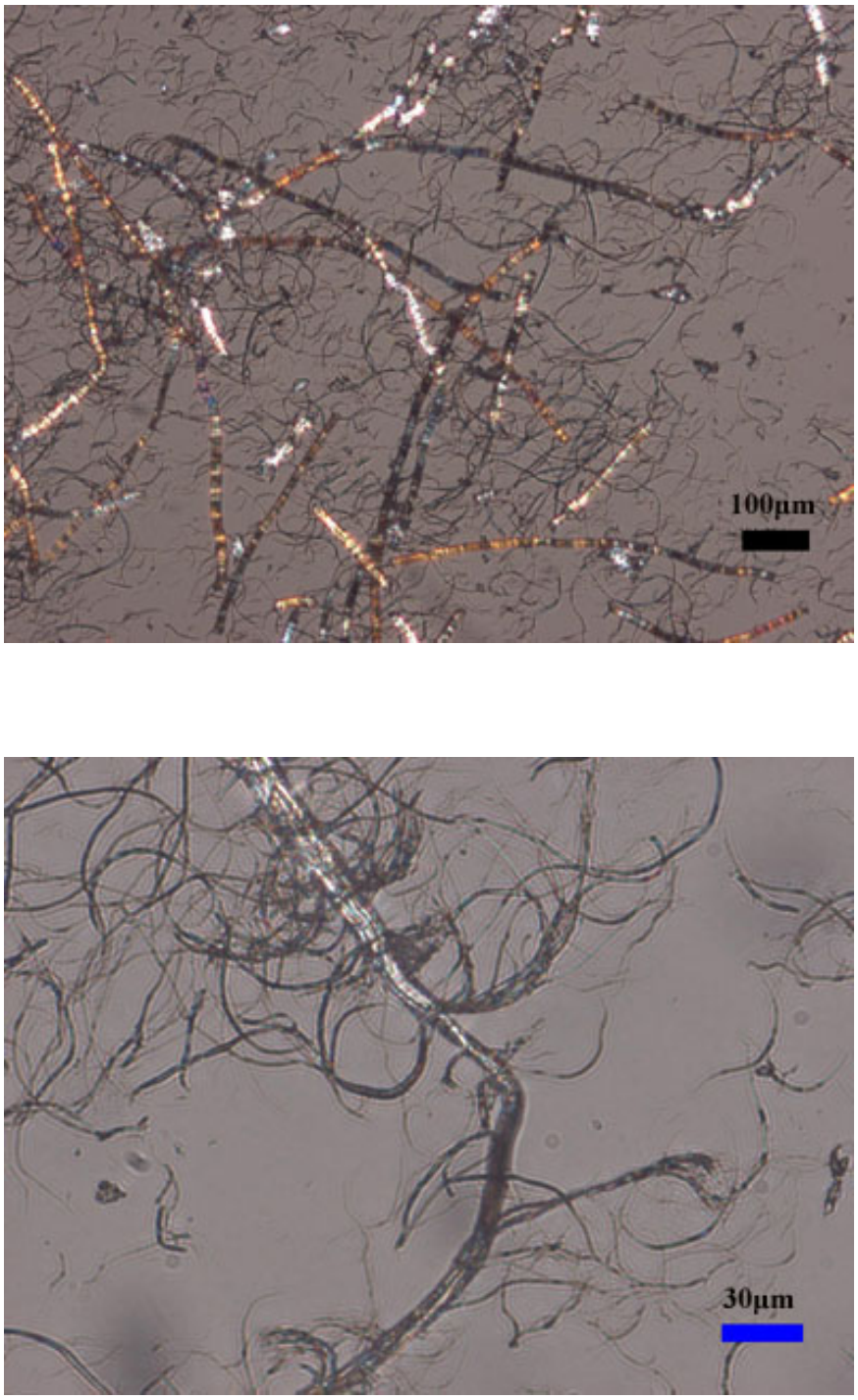

Figure 3.65 PLM images of Lyocell fibers treated 30 min by HIUS (a)

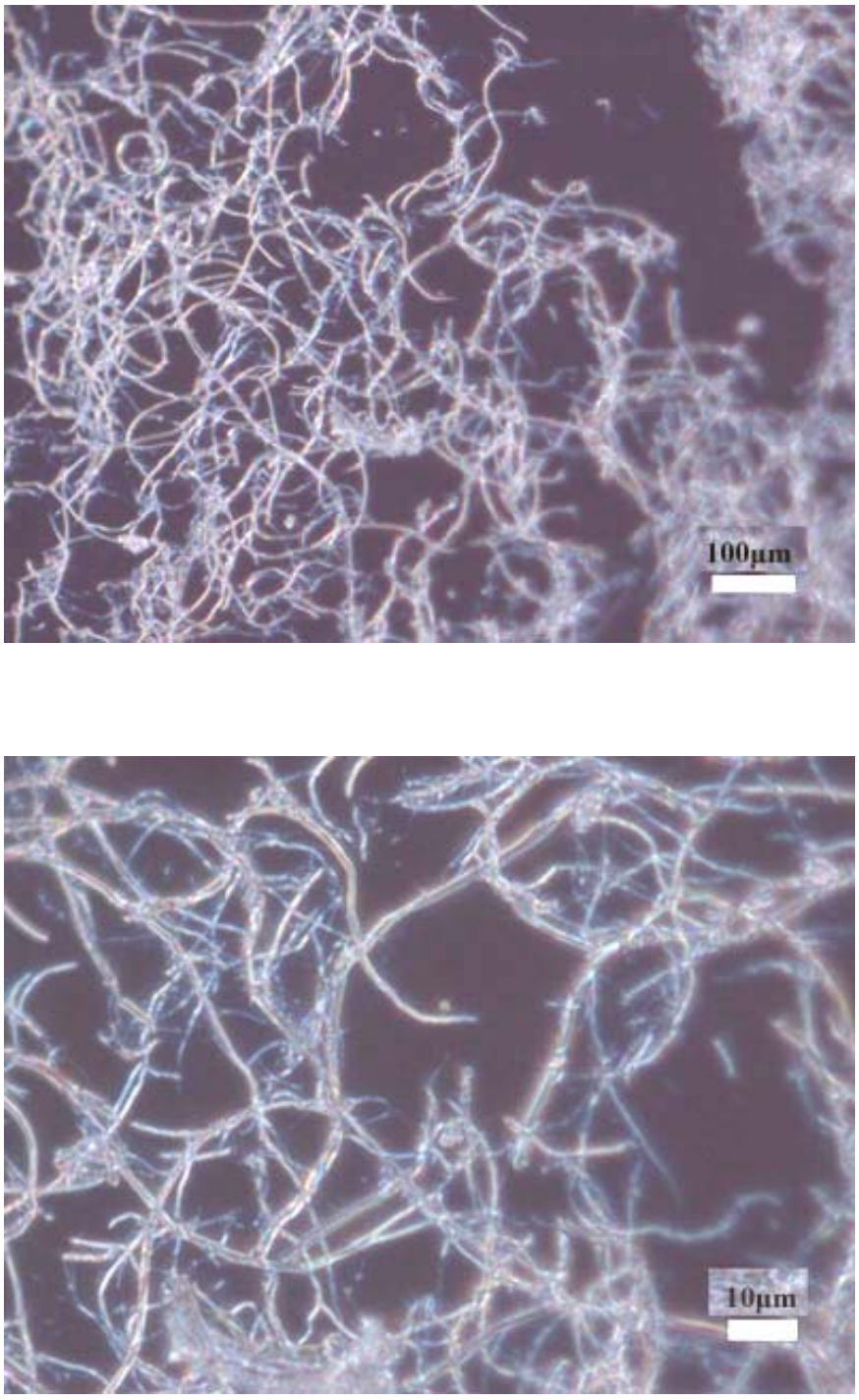

Figure 3.66 PLM images of Lyocell fibers treated 30 min by HIUS (b)

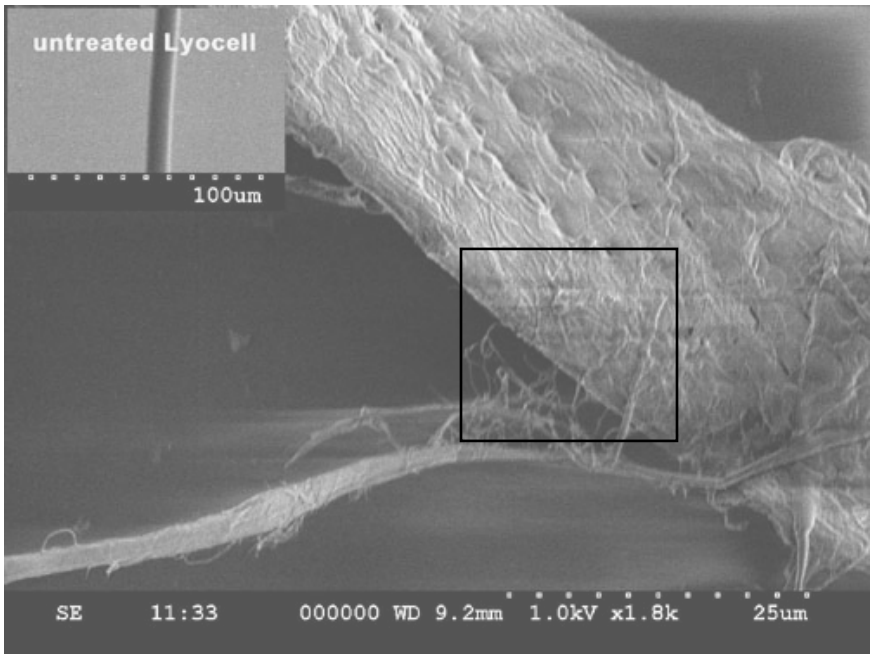

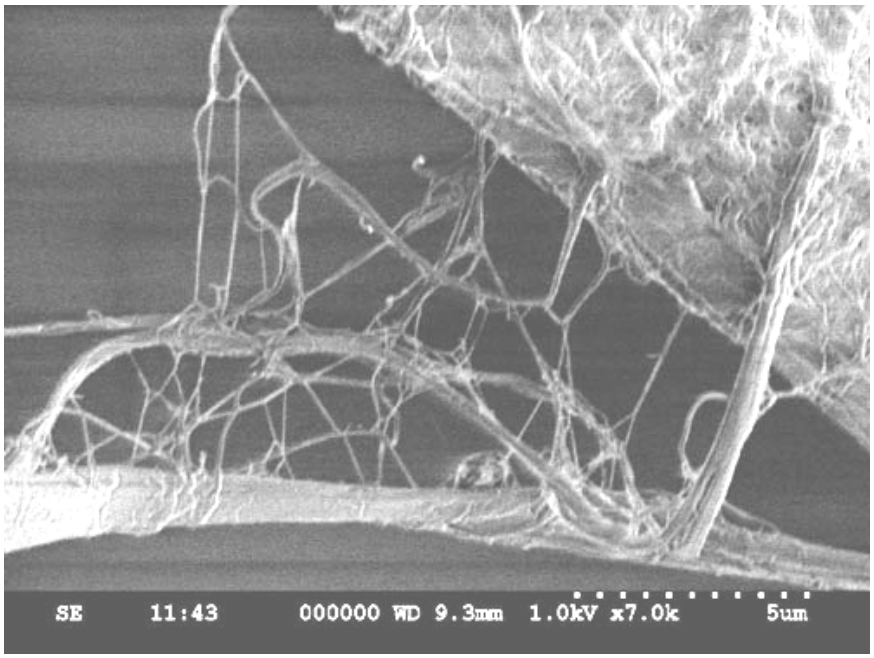

Figure 3.67 SEM images of Lyocell fibers treated 30 min by HIUS (a)

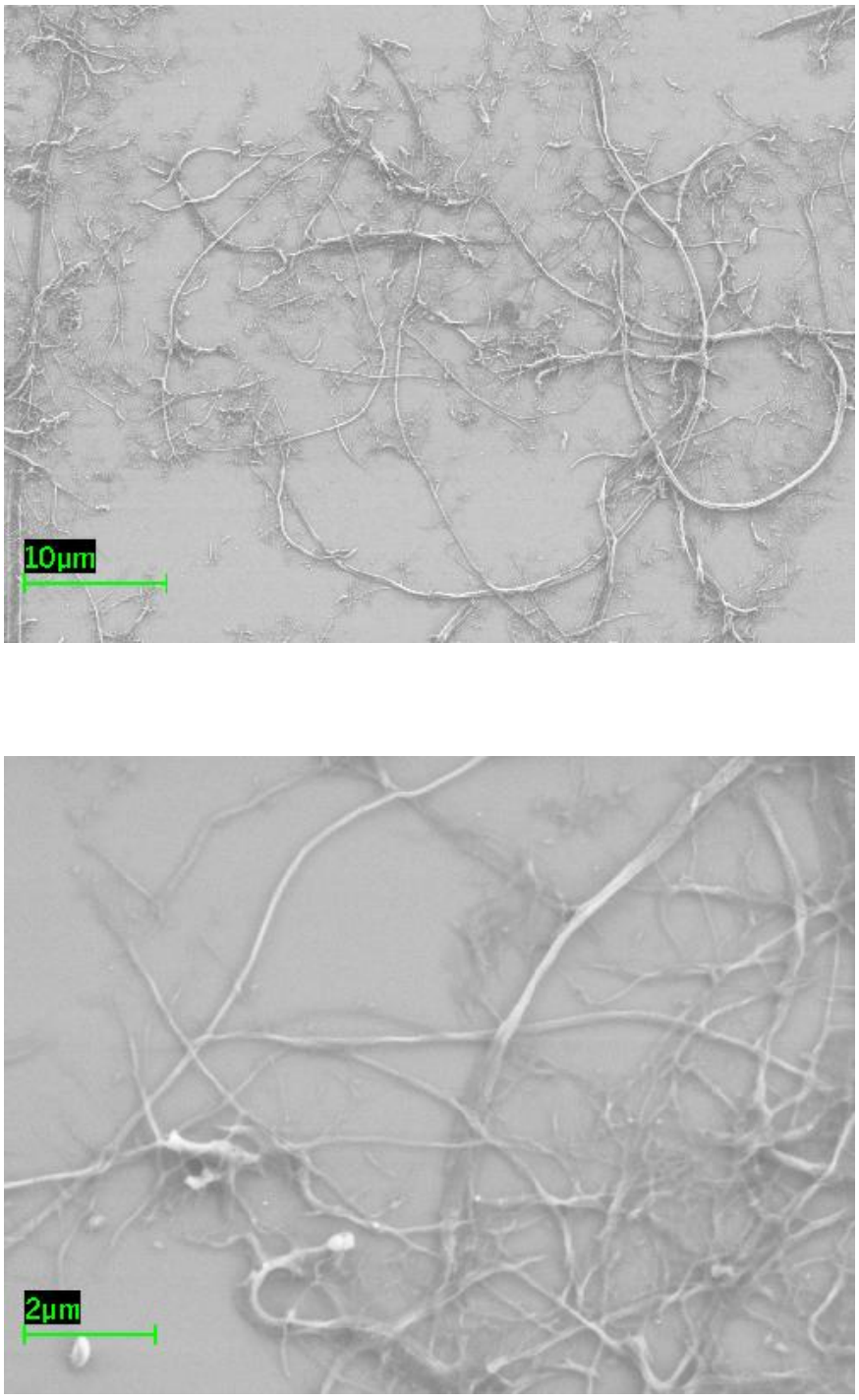

Figure 3.68 SEM images of Lyocell fibers treated 30 min by HIUS (b)

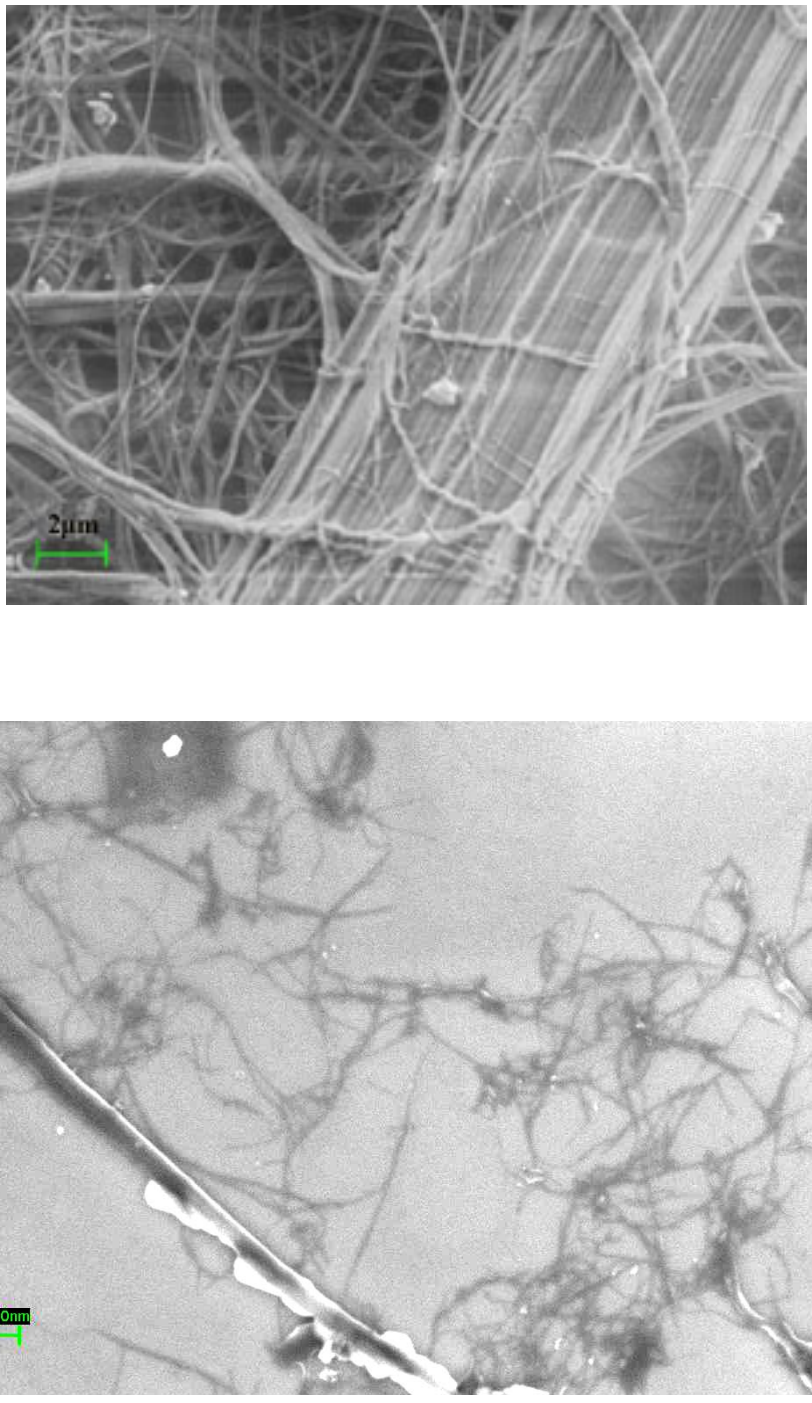

Figure 3.69 SEM images of Lyocell fibers treated 90 min by HIUS

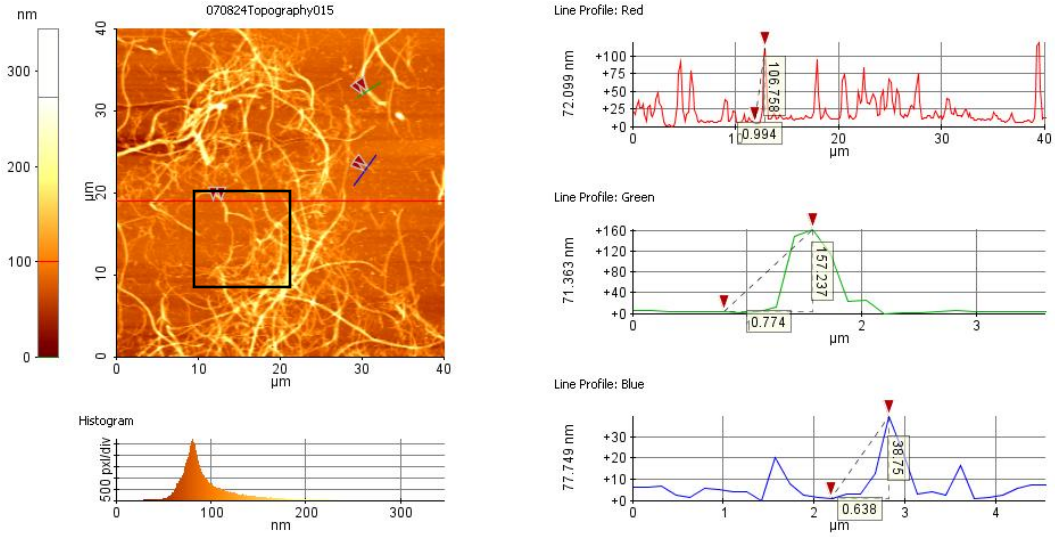

Statistics

Line	Min(nm)	Max(nm)	Mid(nm)	Mean(nm)	Rpv(nm)	Rq(nm)	Ra(nm)	Rz(nm)	Rsk	Rku
Red	72.099	191.641	131.870	93.574	119.542	20.498	14.488	32.387	-2.265	8.850
Green	71.363	233.833	152.598	94.785	162.470	46.641	30.851	24.357	-2.224	6.247
Blue	77.749	117.630	97.690	84.589	39.881	8.245	5.361	4.639	-2.517	9.632

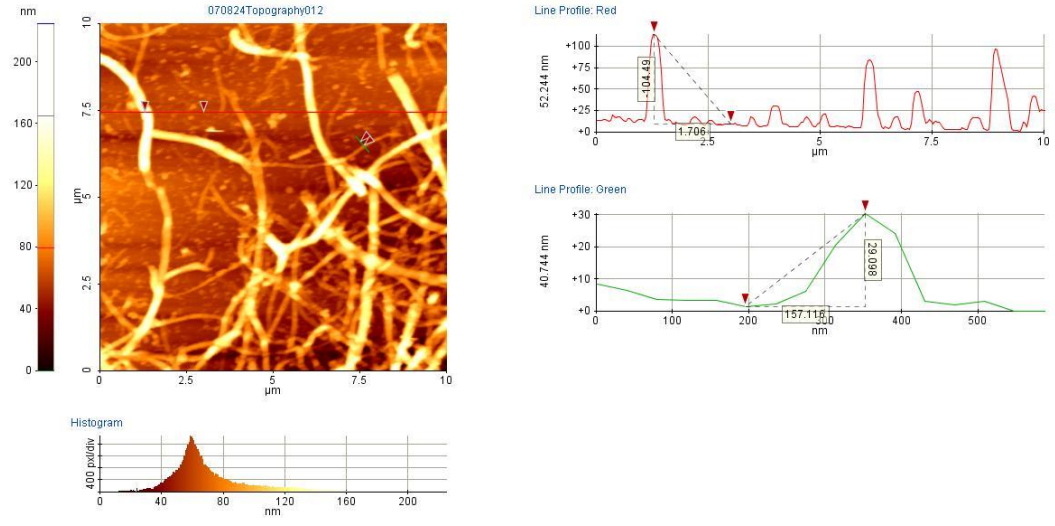

Statistics

Line	Min(nm)	Max(nm)	Mid(nm)	Mean(nm)	Rpv(nm)	Rq(nm)	Ra(nm)	Rz(nm)	Rsk	Rku
Red	52.244	166.454	109.349	70.964	114.210	23.058	14.840	37.541	-2.532	8.970
Green	40.744	71.207	55.976	48.536	30.463	9.039	6.980	2.006	-1.478	3.704

Figure 3.70 AFM images of Lyocell fibers treated 30 min by HIUS (a)

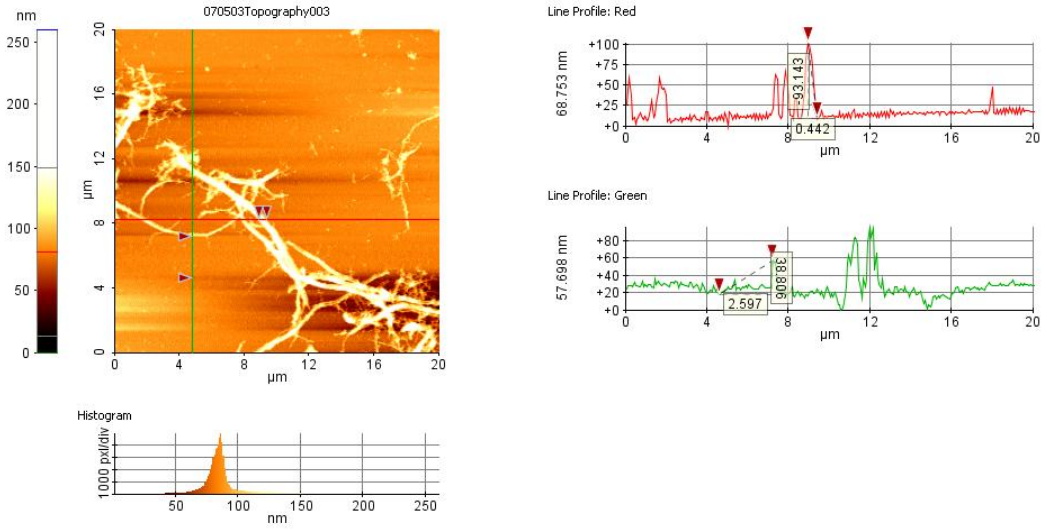

Statistics

Line	Min(nm)	Max(nm)	Mid(nm)	Mean(nm)	Rpv(nm)	Rq(nm)	Ra(nm)	Rz(nm)	Rsk	Rku
Red	68.753	171.116	119.934	86.558	102.363	14.735	8.391	28.338	-3.177	14.629
Green	57.698	153.974	105.836	84.154	96.276	13.336	7.539	18.857	-2.619	12.662

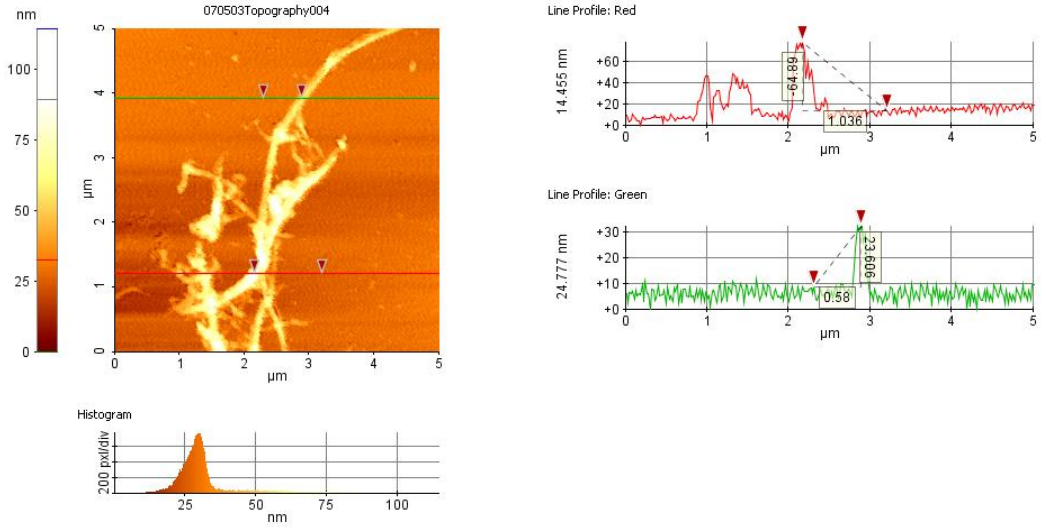

Statistics

Line	Min(nm)	Max(nm)	Mid(nm)	Mean(nm)	Rpv(nm)	Rq(nm)	Ra(nm)	Rz(nm)	Rsk	Rku
Red	14.455	92.553	53.504	31.314	78.099	13.845	8.889	21.737	-2.403	9.170
Green	24.777	56.981	40.879	31.314	32.203	4.561	2.627	9.080	-3.437	18.485

Figure 3.71 AFM images of Lyocell fibers treated 30 min by HIUS (b)

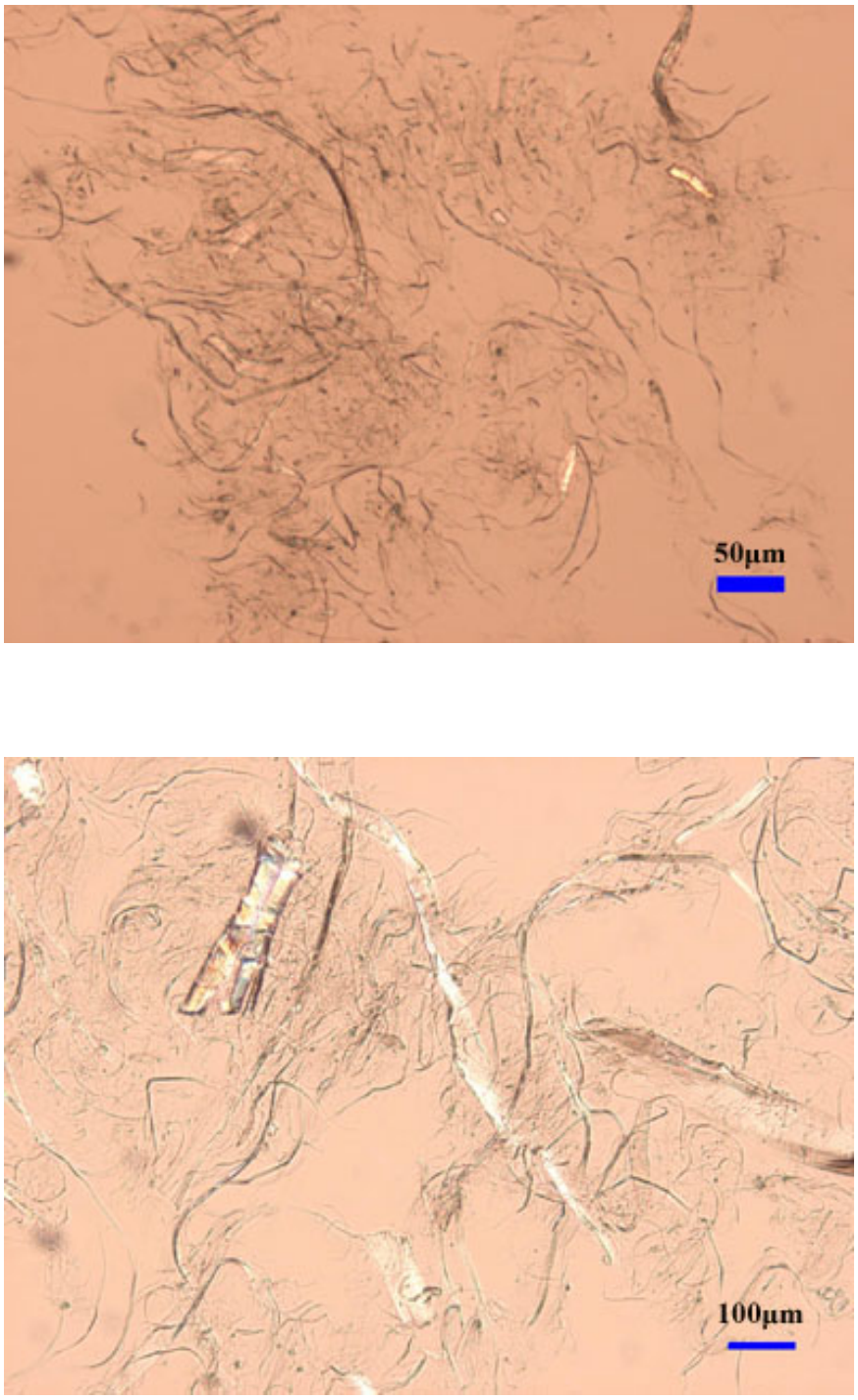

Figure 3.72 PLM images of MFC

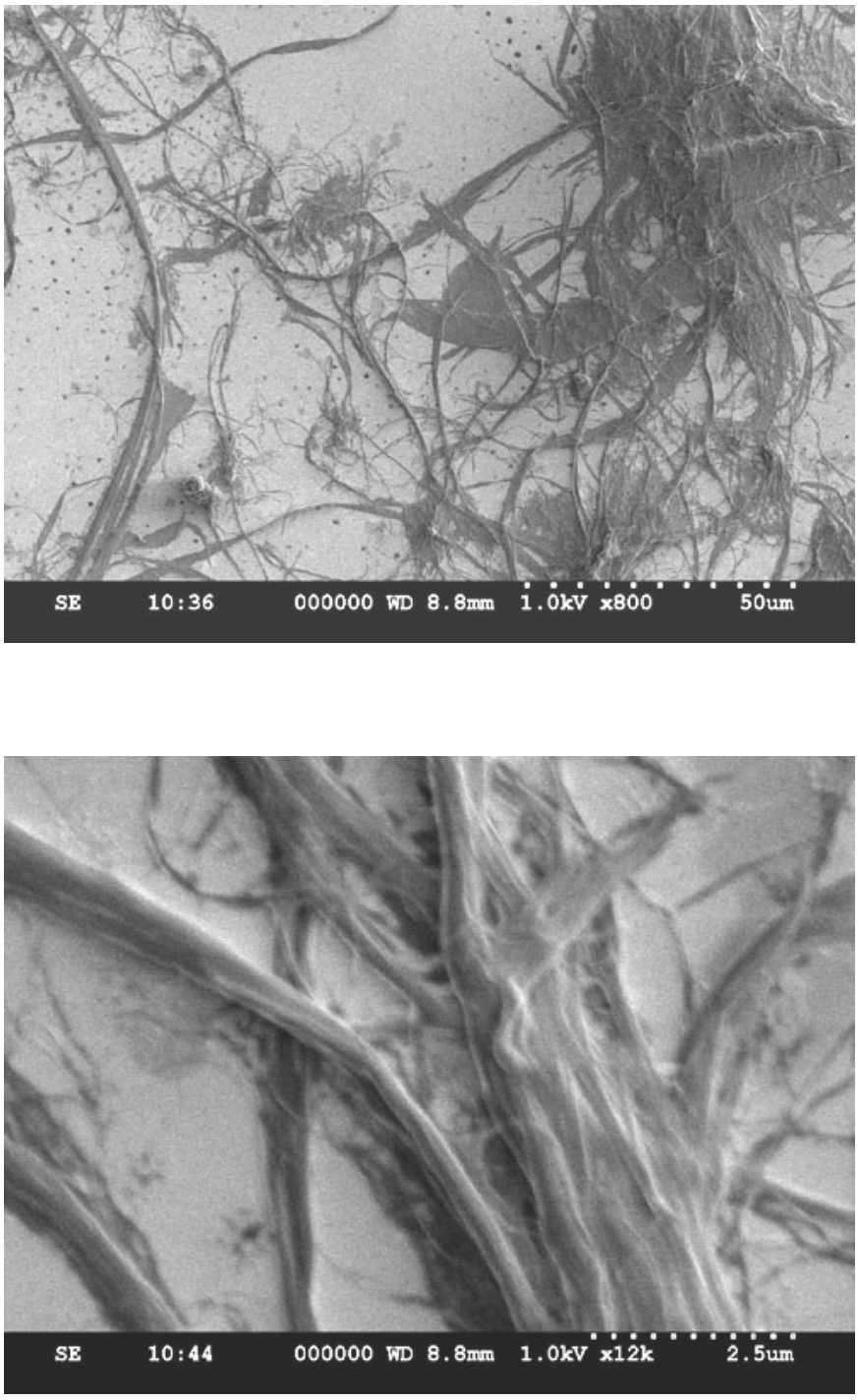

Figure 3.73 SEM images of MFC

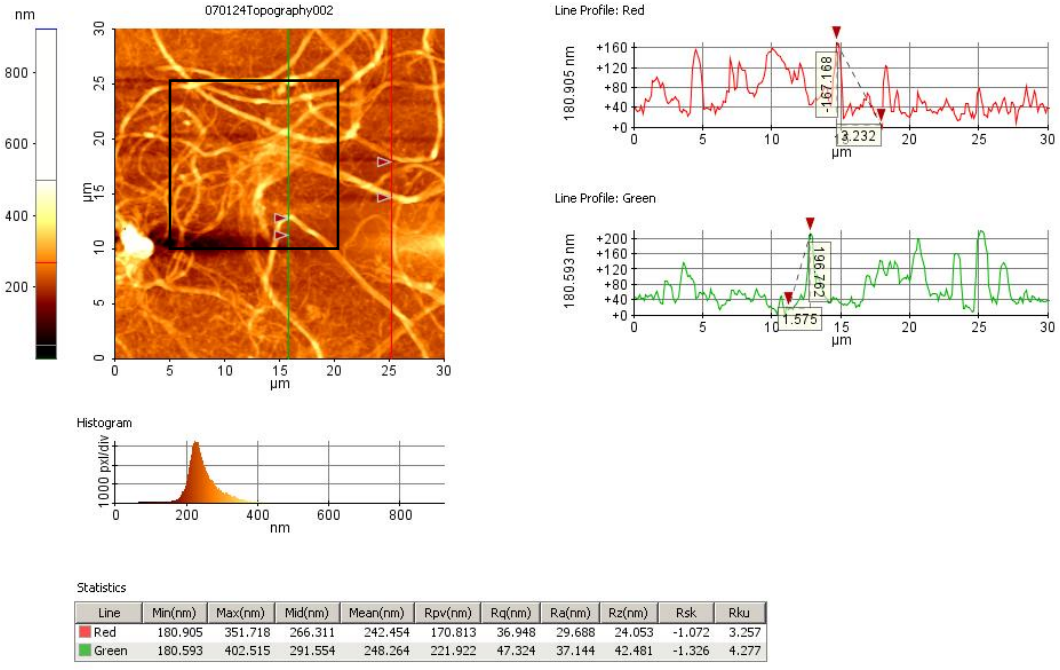

Statistics

Line	Min(nm)	Max(nm)	Mid(nm)	Mean(nm)	Rpv(nm)	Rq(nm)	Ra(nm)	Rz(nm)	Rsk	Rku
Red	180.905	351.718	266.311	242.454	170.813	36.948	29.688	24.053	-1.072	3.257
Green	180.593	402.515	291.554	248.264	221.922	47.324	37.144	42.481	-1.326	4.277

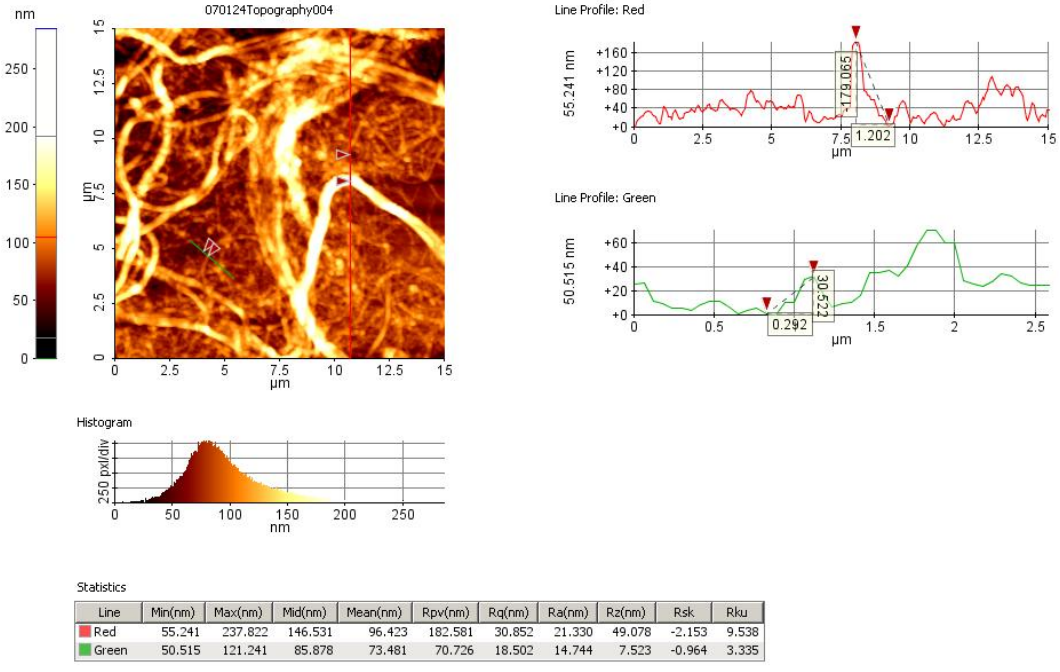

Statistics

Line	Min(nm)	Max(nm)	Mid(nm)	Mean(nm)	Rpv(nm)	Rq(nm)	Ra(nm)	Rz(nm)	Rsk	Rku
Red	55.241	237.822	146.531	96.423	182.581	30.852	21.330	49.078	-2.153	9.538
Green	50.515	121.241	85.878	73.481	70.726	18.502	14.744	7.523	-0.964	3.335

Figure 3.74 AFM images of MFC

Pure cellulose fiber

The PLM overview appearance of untreated pure cellulose fibers (TC40, TC180 and TC2500) and fibers treated by HIUS for 30 min are shown in Figures 3.75 and 3.76, respectively. Short fibers (TC40) were much easier to fibrillation than longer fibers (TC2500). This is why the WRV of treated TC40 increased much more compared with that of untreated TC40 than those of TC180 and TC2500 (Figure 3.56). The longer treatment time, the higher fibrillation was obtained (Figure 3.77). Figure 3.78 shows PLM images of fibrils separated with centrifuge from TC180 treated 30 min. It can be seen from the figures that many small fibril aggregates with diameter less than 1μm were peeled from the big fibers.

AFM images of TC40 and TC180 fibrils treated 30 min by HIUS are shown in Figure 3.79. Smaller fibrils with diameters around 20-30 nm can be observed and the aspect ratios of fibrils were much bigger than the untreated cellulose and it could be helpful for polymer reinforcement.

Pulp fiber

PLM images of untreated and treated (20 min) pulp fibers, and fibrils separated by centrifuge from pulp suspensions (30 min by HIUS) are shown in Figure 3.80. After 20 min HIUS treatment, only small amount of fibers were fibrillated. Most fibrils in the top portion after centrifugation were in microns and less. Some particles with very small aspect ratios were observed, which was not like the fibrils generated from Lyocell fiber (Figure 3.66) and this may be because pulp fiber has less crystallinity than Lyocell fiber.

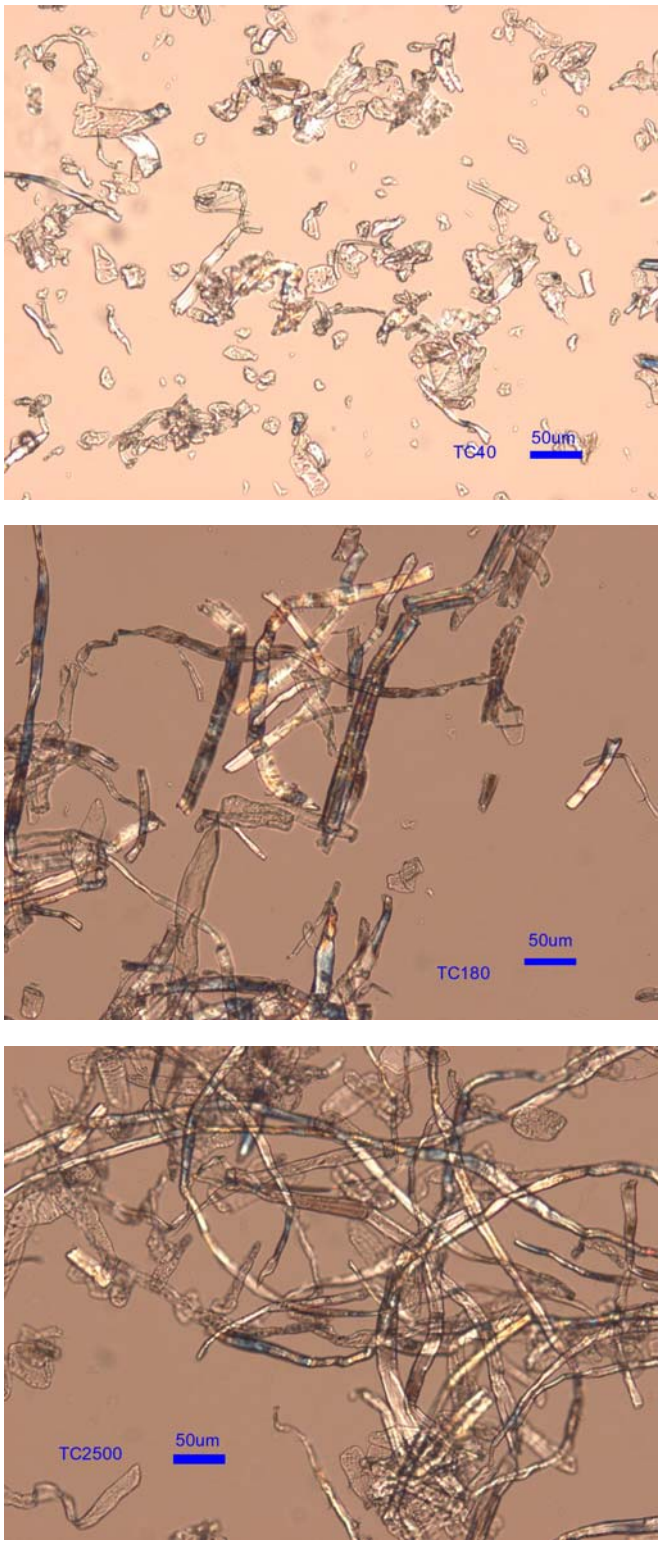

Figure 3.75 PLM images of untreated TC40, TC180 and TC2500

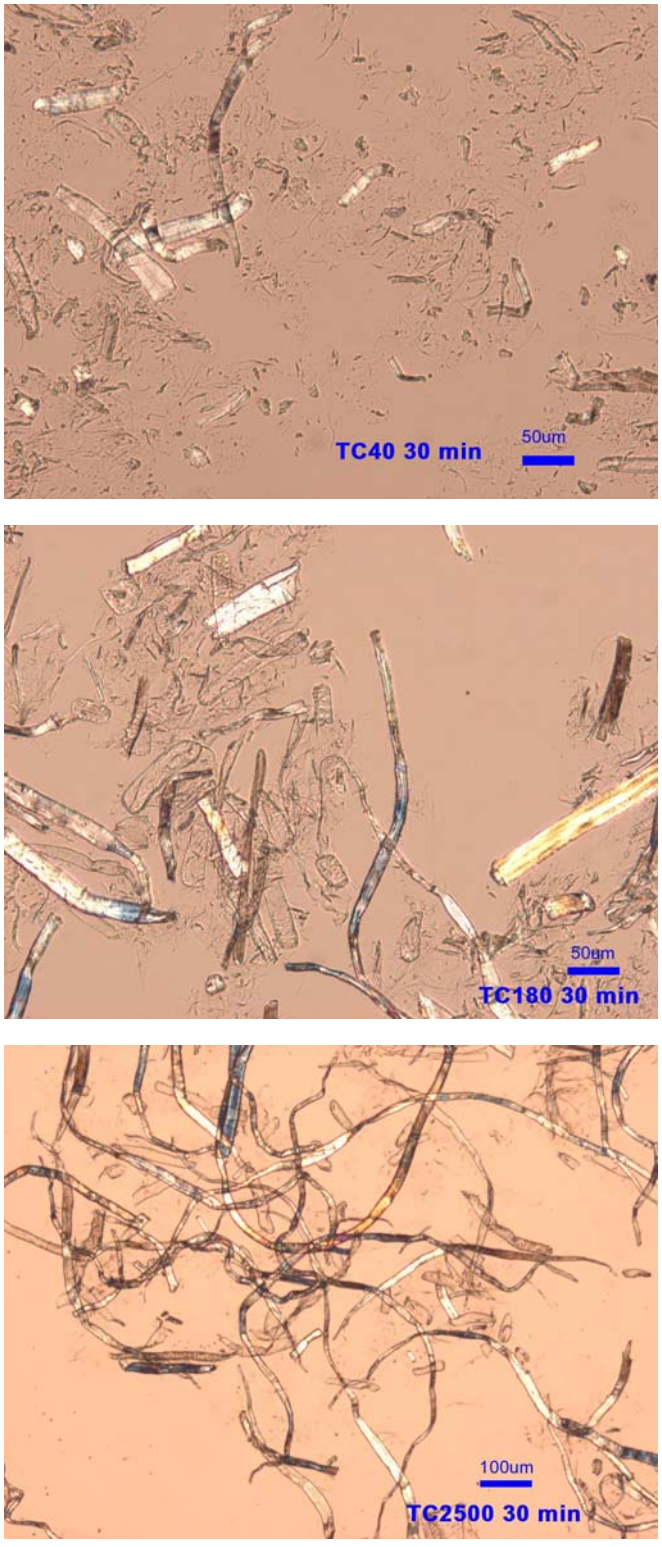

Figure 3.76 PLM images of treated TC40, TC180 and TC2500 by HIUS

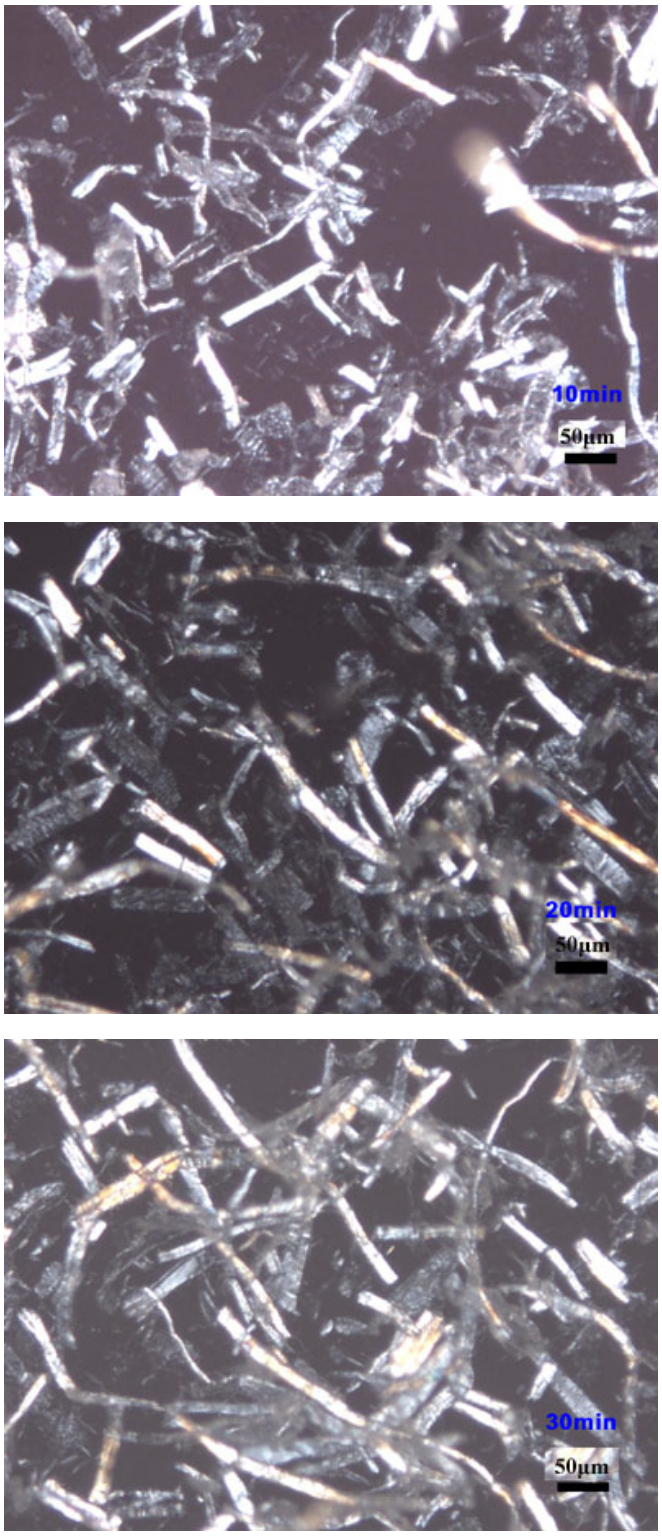

Figure 3.77 PLM images of TC180 treated 10, 20, and 30 min by HIUS

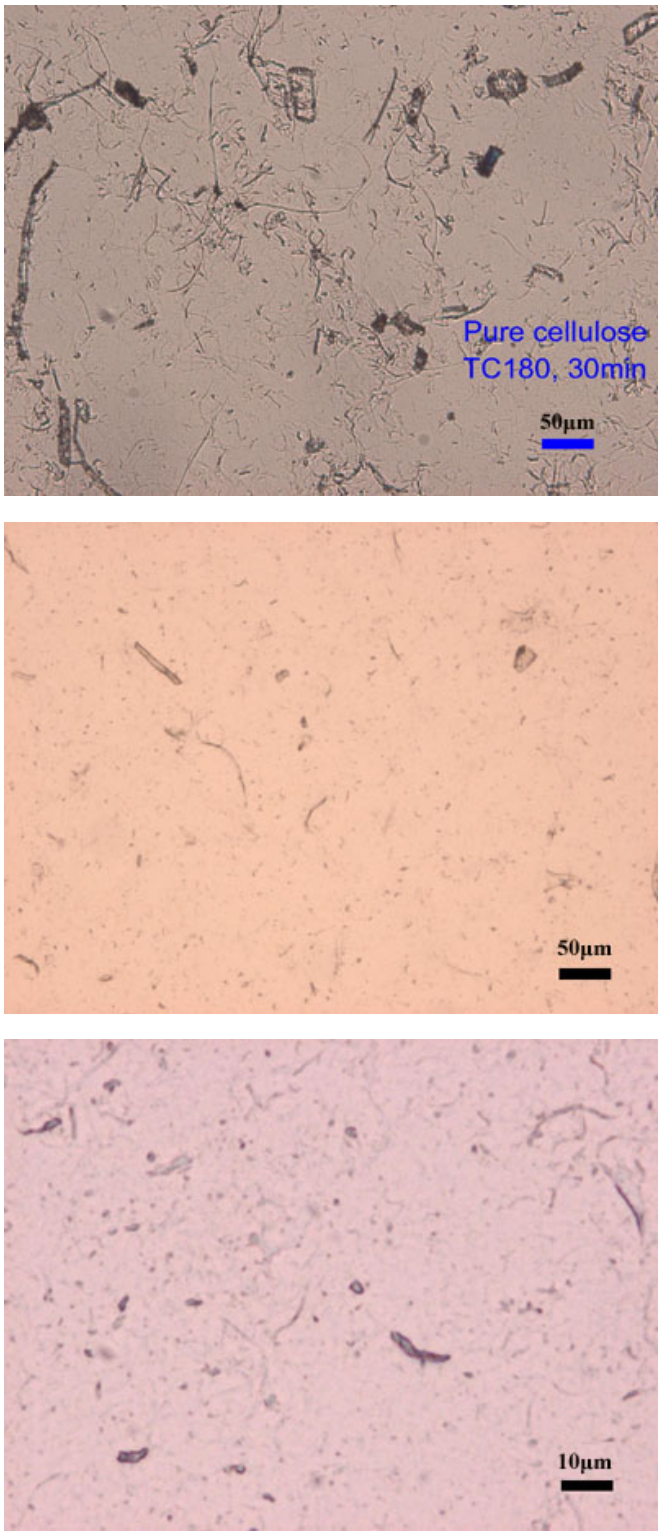

Figure 3.78 PLM images of TC180 fibrils treated 30 min by HIUS

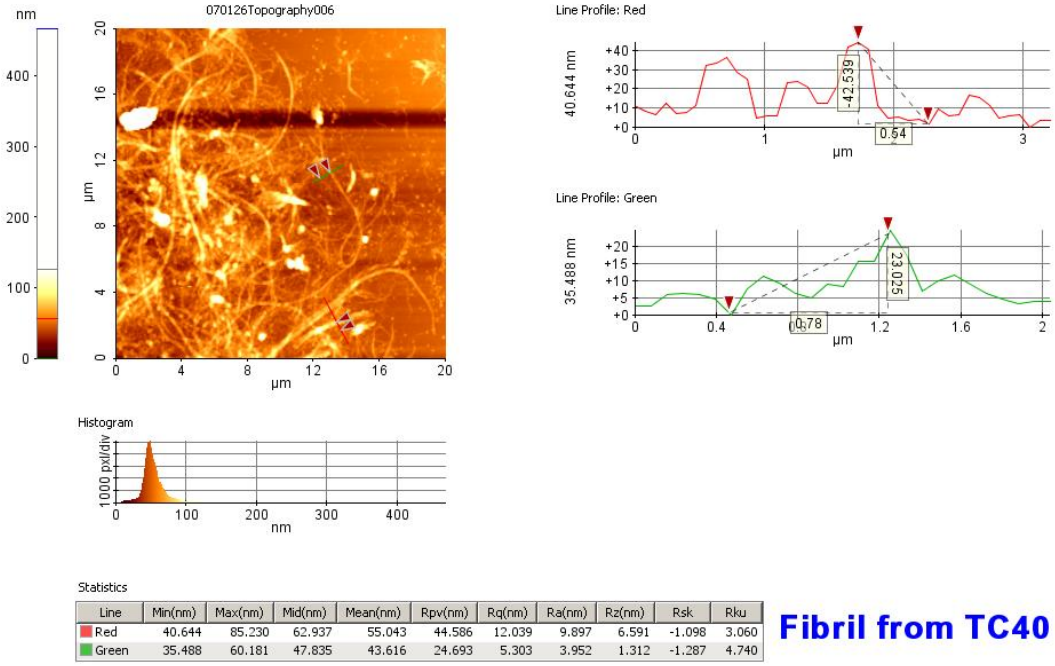

Line	Min(nm)	Max(nm)	Mid(nm)	Mean(nm)	Rpv(nm)	Rq(nm)	Ra(nm)	Rz(nm)	Rsk	Rku
Red	40.644	85.230	62.937	55.043	44.586	12.039	9.897	6.591	-1.098	3.060
Green	35.488	60.181	47.835	43.616	24.693	5.303	3.952	1.312	-1.287	4.740

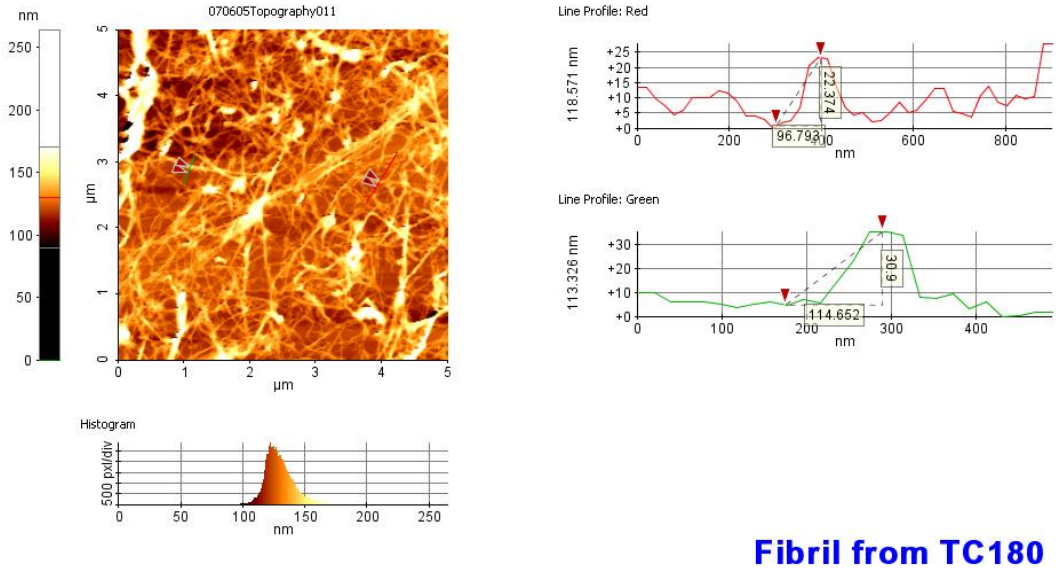

Statistics

Line	Min(nm)	Max(nm)	Mid(nm)	Mean(nm)	Rpv(nm)	Rq(nm)	Ra(nm)	Rz(nm)	Rsk	Rku
Red	118.571	146.568	132.569	127.518	27.997	5.849	4.392	2.763	-1.246	4.667
Green	113.326	148.939	131.132	123.468	35.613	10.249	7.361	2.449	-1.658	4.444

Figure 3.79 AFM images of TC 40 & TC180 fibrils treated 30 min by HIUS

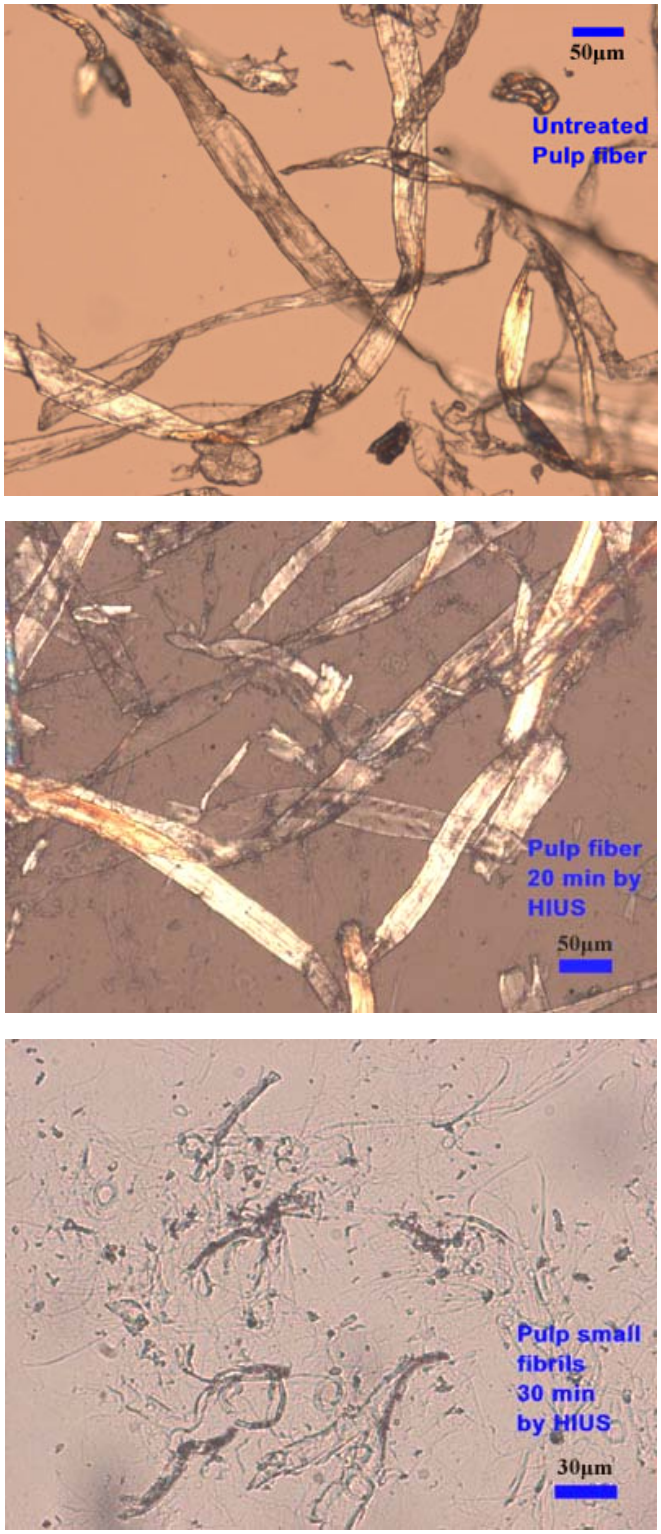

Figure 3.80 PLM images of pulp fibers and fibrils

SEM images of pulp fibrils in the top portion after centrifugation, including treatment of 30 min, 60 min, and 90 min, were in Figures 3.81 to 3.83, respectively. It is clear that the longer treatment time, the higher fibrillation and smaller fibrils were obtained. Some fibrils with diameter less than 50 nm were observed after treatment time of 90 min (Figure 3.83).

Microcrystal cellulose (Avicel)

Figure 3.84 shows the PLM images of untreated and treated (10 min and 30 min) Avicel cellulose. And Figure 3.85 shows the PLM images of Avicel fibrils separated by centrifuge process from Avicel suspensions treated 30 min by HIUS. The aspect ratio (length/diameter) of untreated Avicel cellulose is around 1. After HIUS treated, even only 10 min, most particles were split to smaller fibers. This is why a very stable suspension was obtained after 30 min treatment. The dimensions of fibrils in the top portion after centrifugation were in microns and less. Most of them were several hundreds of nm and some of them around 100 nm and less. This can be observed clearly in the AFM images (Figure 3.86). The aspect ratios of fibrils were much bigger than the untreated cellulose and it could be helpful for polymer reinforcement.

3.5 Conclusions

High intensity ultrasonication (HIUS) by batch process can be used to isolate fibrils from several cellulose resources: regenerated cellulose fiber (Lyocell), pure cellulose fiber (TC40, 180, and 2500), microcrystalline cellulose (Avicel), and pulp fiber.

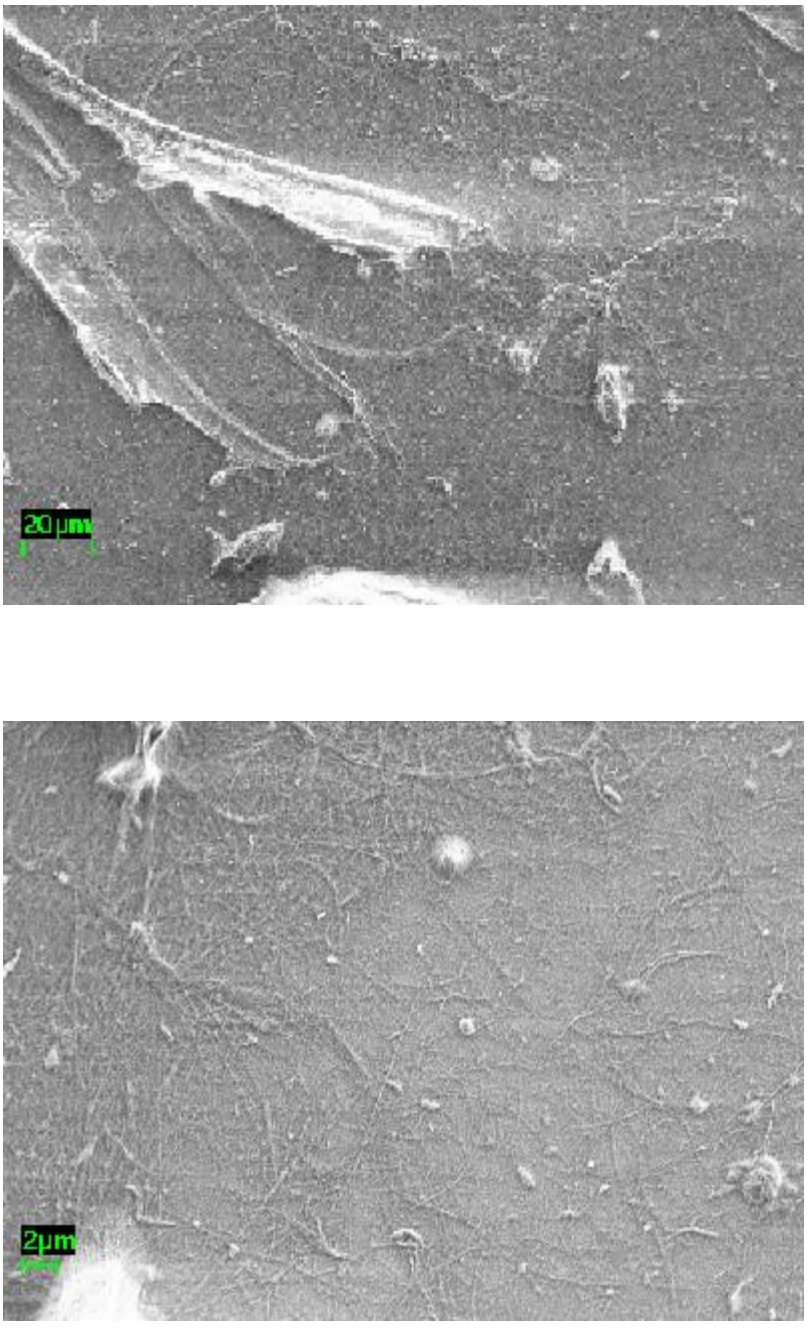

Figure 3.81 SEM images of pulp fibers treated 30 min by HIUS

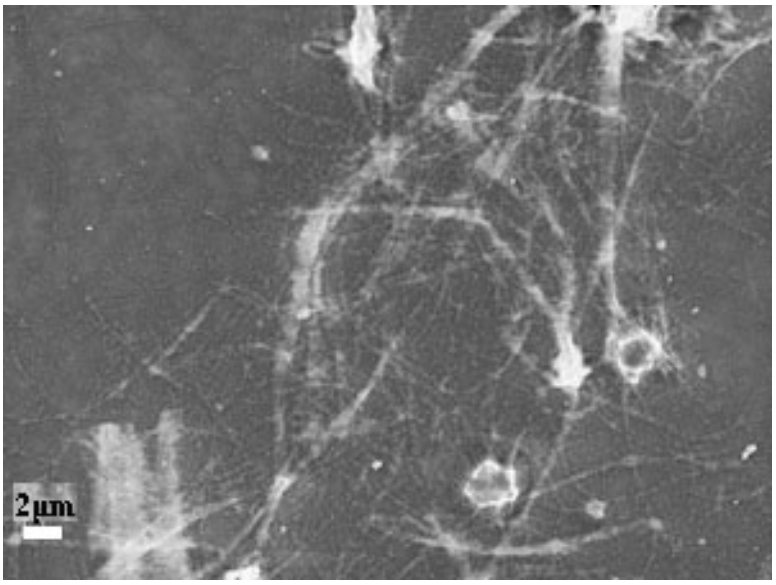

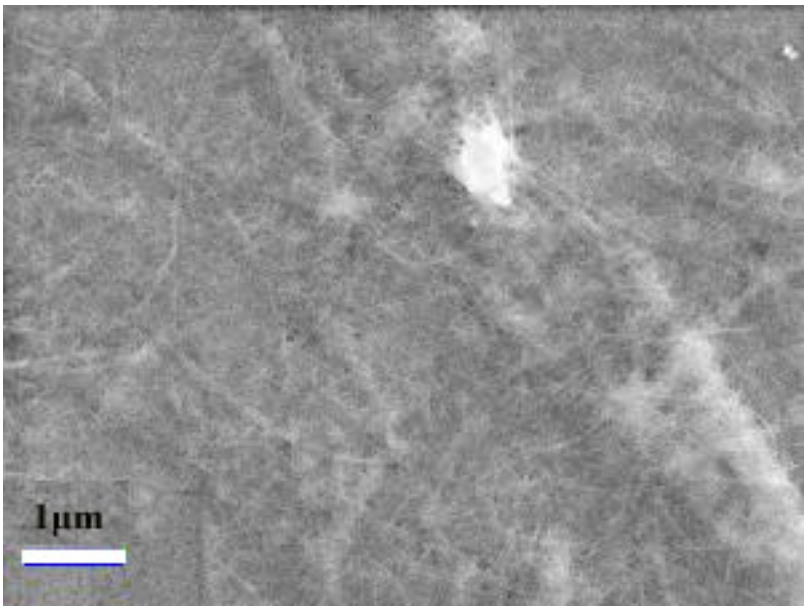

Figure 3.82 SEM images of pulp fibers treated 60 min by HIUS

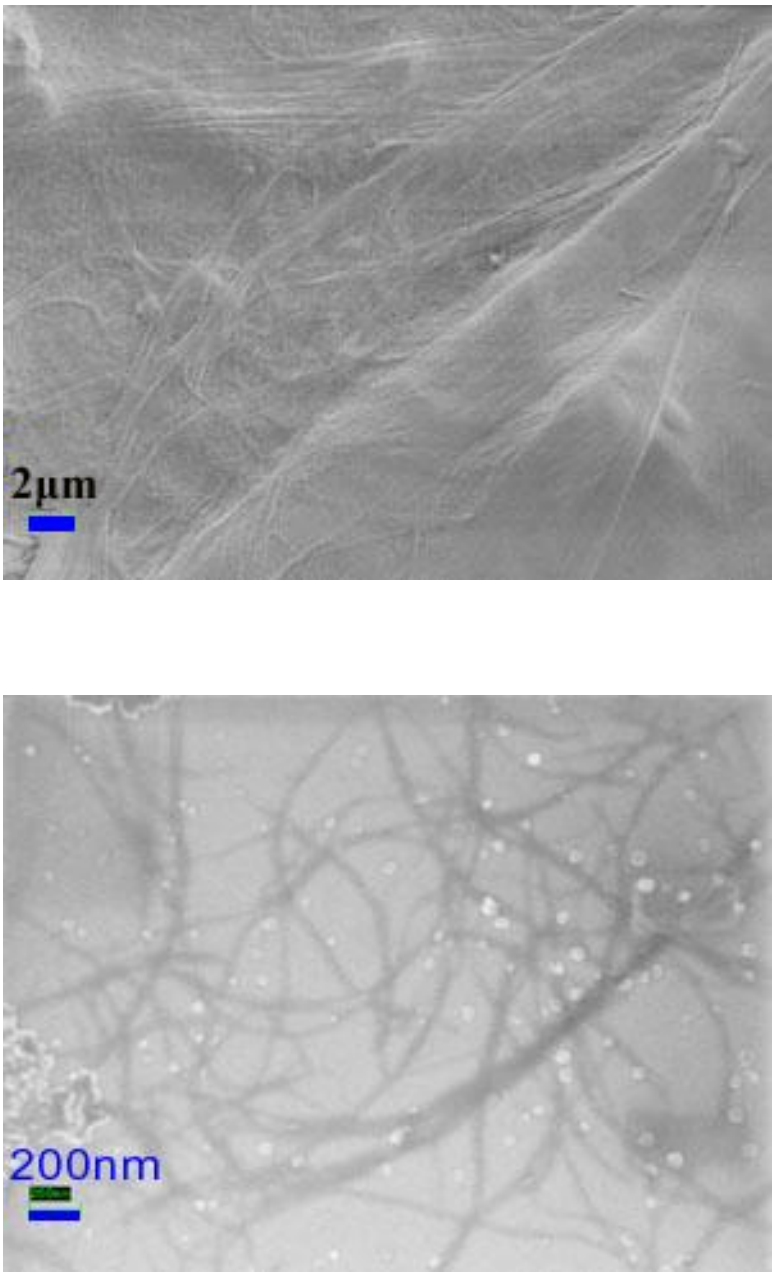

Figure 3.83 SEM images of pulp fibers treated 90 min by HIUS

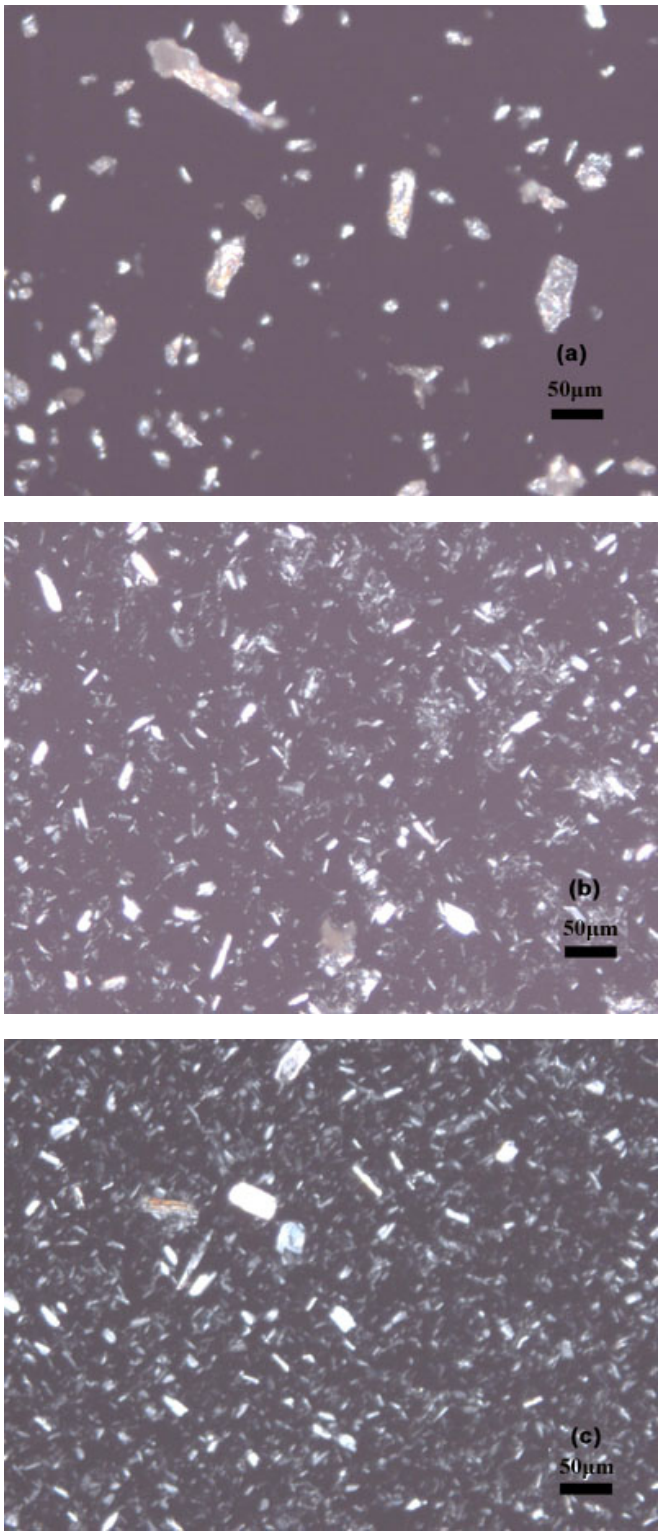

Figure 3.84 PLM images of untreated Avicel (a), treated 10 min (b), and 30 min (c)

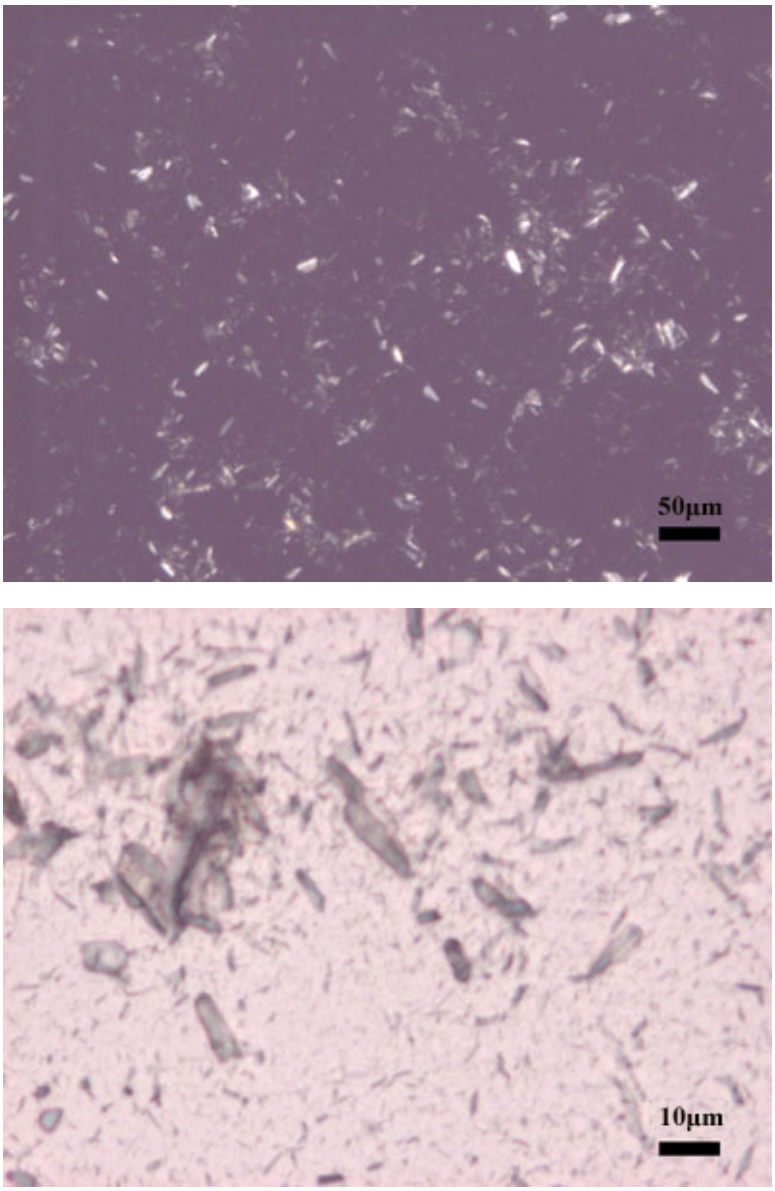

Figure 3.85 PLM images of Avicel fibrils after treated 30 min by HIUS

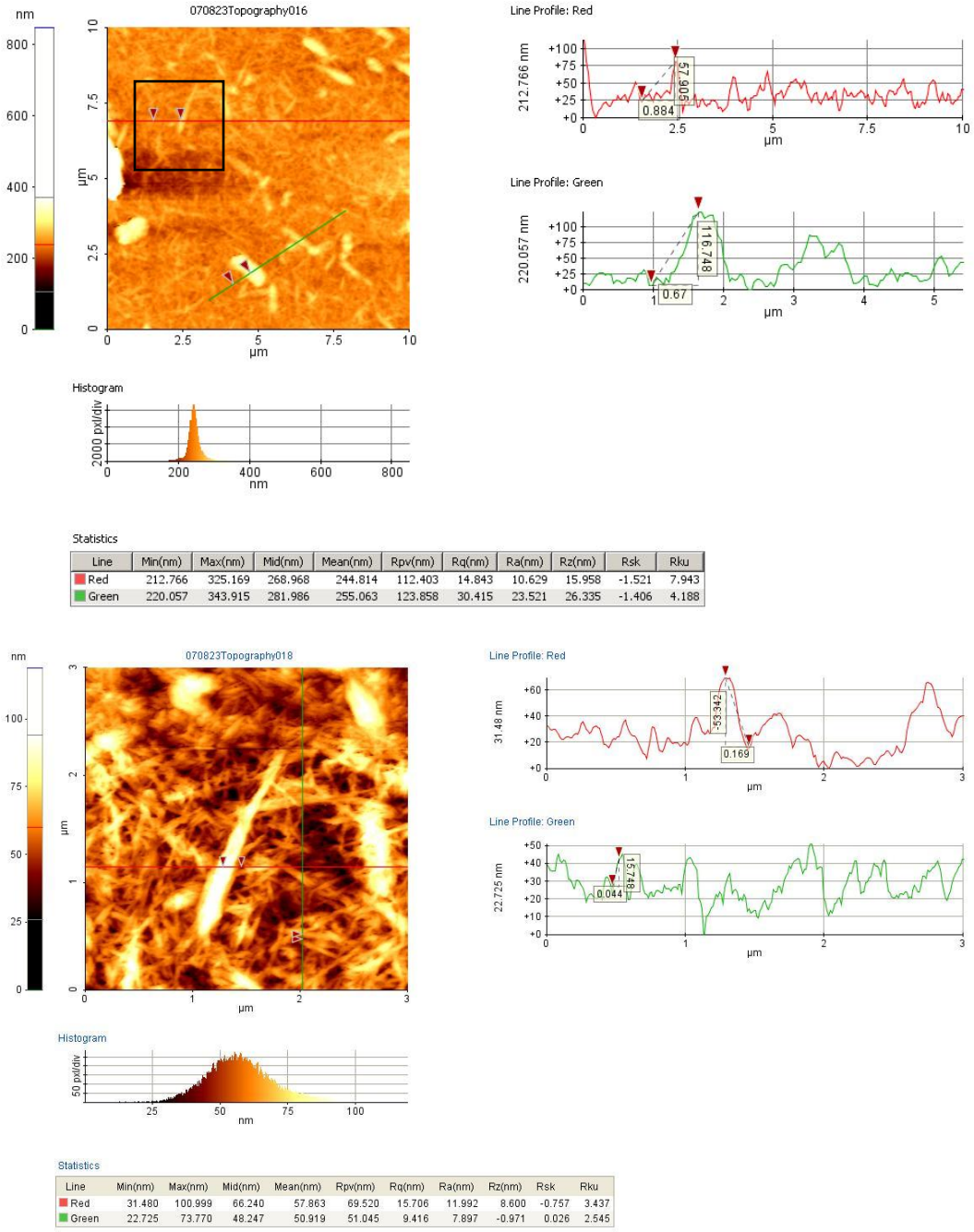

Line	Min(nm)	Max(nm)	Mid(nm)	Mean(nm)	Rpv(nm)	Rq(nm)	Ra(nm)	Rz(nm)	Rsk	Rku
Red	212.766	325.169	268.968	244.814	112.403	14.843	10.629	15.958	-1.521	7.943
Green	220.057	343.915	281.986	255.063	123.858	30.415	23.521	26.335	-1.406	4.188

Line	Min(nm)	Max(nm)	Mid(nm)	Mean(nm)	Rpv(nm)	Rq(nm)	Ra(nm)	Rz(nm)	Rsk	Rku
Red	31.480	100.999	66.240	57.863	69.520	15.706	11.992	8.600	-0.757	3.437
Green	22.725	73.770	48.247	50.919	51.045	9.416	7.897	-0.971	0.026	2.545

Figure 3.86 AFM images of Avicel fibrils treated 30 min by HIUS

A mixture of fibrils in micro and nano scales was obtained. Some fibrils were still on the surfaces of the big ones, while some were isolated from the fibers. Small fibrils can be separated from HIUS treated water suspension by centrifuge. The observations of polarized light microscopy, SEM and AFM showed that the size of the fibrils had a wide diameter range from about thirty nm to several μm. The cellulose crystallinity or molecular structure evaluated by WAXD and FTIR was changed by ultrasonic treatment, and the changes were different for different cellulose resources. Water retention value is used to evaluate the cellulose fibrillation, which was significantly increased by HIUS treatment for all cellulose resources.

The power consumption of HIUS treatment was low according to its nominal power level. Temperature increased faster when power is higher, and the higher power the better fibrillation. Temperature of the water suspension can reach up to 91 ºC without water cooling. The higher temperature the better cellulose fibrillation, while the longer raw fiber, the lower fibrillation. Cellulose concentration is important and it depends on the dimensions of cellulose fiber, which should be lower if the fiber is longer. Shorter distance from tip to beaker bottom may not have benefit to fibrillation. Pressure and pass time are very important for high pressure homogenizer (HPH). Only several passes using HPH after HIUS treatment can make very good cellulose suspension and more uniform cellulose fibrils than those treated by HIUS or HPH only. The Titanium (Ti) tips of HIUS were eroded quickly and Ti black particles were found in the cellulose suspensions if the cellulose treated continually more than 30 min or the tip was too old. It is very helpful to use a new tip material with less erosion for this application.

References

Anonymous, 2001. Ultrasonic Treatment Technology Description. http://www.nemw.org/Balsurv3_US.htm

Anonymous, 2002a. What are ULTRASONICS and ULTRASONIC PROCESSING? Sonics & Materials, Inc.

Anonymous, 2002b. XE-100 User's Manual. PSIA Corporation.

Beck-Candanedo, S., Roman, M. and Gray, D.G., 2005. Effect of reaction conditions on the properties and behavior of wood cellulose nanocrystal suspensions. Biomacromolecules, 6(2): 1048-1054.

Bondeson, D., Mathew, A. and Oksman, K., 2006. Optimization of the isolation of nanocrystals from microcrystalline cellulose by acid hydrolysis. Cellulose, 13(2): 171-180.

Chakraborty, A., Sain, M. and Kortschot, M., 2005. Cellulose microfibrils: A novel method of preparation using high shear refining and cryocrushing. Holzforschung, 59(1): 102-107.

Choi, Y.J. and Simonsen, J., 2006. Cellulose nanocrystal-filled carboxymethyl cellulose nanocomposites. Journal of Nanoscience and Nanotechnology, 6(3): 633-639.

Dufresne, A., Cavaille, J.Y. and Vignon, M.R., 1997. Mechanical behavior of sheets prepared from sugar beet cellulose microfibrils. Journal of Applied Polymer Science, 64(6): 1185-1194.

Eichhorn, S.J. and Young, R.J., 2001. The Young's modulus of a microcrystalline cellulose. Cellulose, 8(3): 197-207.

Herrick, F.W., Casebier, R.L., Hamilton, J.K. and Sandberg, K.R., 1983. Microfibrillated cellulose: morphology and accessibility. Journal of Applied Polymer Science: Applied Polymer Symposium, 37: 797-813.

Imai, M., K. Ikari, and I. Suzuki, 2004. High-performance hydrolysis of cellulose using mixed cellulose species and ultrasonication pretreatment. Biochemical Engineering Journal, 17(2): p. 79-83.

Kataoka, Y. and Kondo, T., 1998. FT-IR microscopic analysis of changing cellulose crystalline structure during wood cell wall formation. Macromolecules, 31(3): 760-764.

Manning, A. and R. Thompson, 2002. The influence of ultrasound on virgin paper fibers. Progress in Paper Recycling, 11(4): p. 6-12.

Nakagaito, A.N. and Yano, H., 2005. Novel high-strength biocomposites based on microfibrillated cellulose having nano-order-unit web-like network structure. Applied Physics a-Materials Science & Processing, 80(1): 155-159.

Ozturk, H.B., Okubayashi, S. and Bechtold, T., 2006. Splitting tendency of cellulosic fibers - Part 1. The effect of shear force on mechanical stability of swollen lyocell fibers. Cellulose, 13(4): 393-402.

Peng, S.J., Shao, H.L. and Hu, X.C., 2003. Lyocell fibers as the precursor of carbon fibers. Journal of Applied Polymer Science, 90(7): 1941-1947.

Sakurada, I., Nukushina, Y. and Ito, T., 1962. Experimental determination of elastic modulus of crystalline regions in oriented polymers. Journal of Polymer Science, 57(165): 651-660.

Schultz, T.P., McGinnis, G.D. and Bertran, M.S., 1985. Estimation of cellulose crystallinity using fourier transform-infrared spectroscopy and dynamic thermogravimetry. Journal of Wood Chemistry and Technology, 5(4): 543-557.

Stansted, 2007. http://www.sfp-4-hp.demon.co.uk/.

Sturcova, A., Davies, G.R. and Eichhorn, S.J., 2005. Elastic modulus and stress-transfer properties of tunicate cellulose whiskers. Biomacromolecules, 6(2): 1055-1061.

Suslick, K.S., 1990. Sonochemistry. Science, 247(4949): 1439-1445.

Taniguchi, T., 1996. Microfibrillation of natural fibrous materials. J. Soc. Mat. Sci. Japan, 45(4): 472-473.

Thygesen, A., Oddershede, J., Lilholt, H., Thomsen, A.B. and Stahl, K., 2005. On the determination of crystallinity and cellulose content in plant fibres. Cellulose, 12(6): 563-576.

Turai, L.L. and C.H. Teng, 1978. Ultrasonic Deinking of Waste Paper. Tappi, 61(2): p. 31-34.

Turbak, A.F., Snyder, F.W. and Sandberg, K.R., 1983. Microfibrillated cellulose, a new cellulose product: properties, uses, and commercial potential. Journal of Applied Polymer Science: Applied Polymer Symposium, 37: 815-827.

Zimmermann, T., Pohler, E. and Geiger, T., 2004. Cellulose fibrils for polymer reinforcement. Advanced Engineering Materials, 6(9): 754-761.

CHAPTER 4. A METHOD FOR TESTING THE ELASTIC MODULUS OF SINGLE CELLULOSE FIBRILS VIA ATOMIC FORCE MICROSCOPY

4.1. Abstract

Understanding the mechanical properties of cellulosic fibrils in micro and nano scales is important when the fibrils are used as polymer reinforcement materials. The measurement of mechanical properties of single fibrils is difficult because of the very small forces and dimensions involved. In this study, atomic force microscope (AFM) was used to measure the nano Newton forces and nanometer deflections of fibrils by nanoscale three-point bending test, and the elastic moduli of single fibrils were evaluated by a model. Data mining, AFM tip selection, and the testing position of the reference were chosen to observe and discuss the determination of the fibril deflections in bending test. The results indicated that it was necessary to consider the penetration of AFM tips to the cellulosic fibril surfaces. The AFM cantilever deflection for the tip was loaded on the fibril laid on the wafer was better as reference to calculate the deflection of the fibril suspended above a silicon groove than the cantilever deflection for the tip was loaded on the wafer as reference. The elastic modulus of cellulosic fibril with diameter of about 170 nm isolated from Lyocell fiber by high intensity ultrasonication was evaluated to be 93 GPa. AFM nanoindentation test with a diamond-coating tip was also used to estimate the elastic modulus of same cellulose fibrils. The results calculated from the unmodified Hertz theory model did not match the results obtained from three-point bending test.

Keywords: Atomic force microscope (AFM), cellulose, deflection, elastic modulus, fibril, indentation, micro, nano, three-point bending

4.2. Introduction

Cellulose fibrils in micro and nano scales isolated from natural fibers may have much higher mechanical properties than individual fibers, so that much attention have been paid in the past two decades to study how to make small fibrils and how to combine them with polymers to make nanocomposites (Herrick et al. 1983, Turbak et al. 1983; Berglund 2005; Cheng et al. 2007a; Cheng et al. 2007b). Mechanical method with high shear force was used to separate fibrils, which includes high-pressure homogenizer treatment (Herrick et al. 1983; Turbak et al. 1983; Dufresne et al. 1997) and high-pressure refiner or supergrinder treatment (Taniguchi 1996; Chakraborty et al. 2005). Chemical method mainly by strong acid hydrolysis removes the amorphous regions of cellulose fiber and obtained crystal parts or called nano whiskers (Dufresne et al. 1997; Choi and Simonsen 2006).

Although many studies have been focused on how to make small fibrils and how to use fibrils to reinforce polymers, mechanical properties of individual fibril are rarely studied. Understanding the mechanical properties of single cellulosic fibrils is very important, especially when the ultimate aim of the fibrils is for reinforcement in composite materials. The mechanical properties of single wood fiber have been studied by several researchers (Page et al. 1972; Mott et al. 1996; Xing et al., 2007 a and b). For smaller fibrils, it is difficult to measure the mechanical properties directly due to the difficulty in isolating individual cellulosic fibrils without severe degradation, measuring the very tiny forces and deformations involved, as well as characterizing the complex and uneven diameters or widths. The obtained elastic modulus of the crystalline region of

ramie fiber measured by X-ray diffraction was 137 GPa (Sakurada et al. 1962). The Young's modulus of microcrystalline cellulose (flax and hemp) was estimated to be 25±4 GPa from the values of the shift rate of the 1095cm^{-1} band using Raman spectroscopy (Eichhorn and Young 2001).

A nanoscale three-point bending test using AFM is a relative new method to obtain the elastic modulus of nano scale fibrils. It has been used in several fields, especially for carbon nanotubes. An AFM cantilever tip is used to apply a small load at the midpoint along the suspended length of a single nanofiber, which is suspended over a small groove. This method has been used to obtain the elastic modulus of nanosized beams, such as silicon carbide nanorods and multiwall carbon nanotubes (Wong et al. 1997, Salvetat et al. 1999a, Salvetat, et al. 1999b, Salvetat-Delmotte and Rubio 2002), β-chitin fibers (Xu et al. 1994), and PLLA nanofibers (Tan and Lim 2004). A model was used to calculate the elastic modulus of the fiber after a force and deflection curve is obtained. As the three-point bending test for bulk specimens, the deflection of the specimens along with boundary conditions during the loading is a key factor to determine the elastic moduli of the specimens. The measurement methods and accuracy could significantly affect the calculation results, which are more important for the nanoscale three-point bending test using AFM because of the very tiny forces and deflections. Ignore the bending deflection of a nanofiber was determined by measuring the difference between the cantilever deflections over the *Z*-piezo displacement on a silicon wafer substrate and on the nanofiber (Tombler et al. 2000, Tan and Lim 2004), no details about the factors that affected the determination of the deflection were found in the references.

And furthermore, the factors that affect the determination of bending deflection may be different for different materials to be tested.

In this study, the nanoscale three-point bending test setup in AFM (PSIA, XE-100) was used to study some factors that may affect the determination of bending deflections and mechanical properties of individual cellulose fibrils. Several factors including data mining by the software, different tips with same nominal spring constant, the condition of the tips, tips with different spring constant, the test position of the reference were used to observe and discuss the determination of the bending deflection during the nanoscale three-point bending test using AFM. Cellulosic fibrils isolated mechanically from Lyocell fiber were tested to evaluate their elastic moduli. Nanoindentation study of this single fibril was also performed using an AFM cantilever tip to compare the results of AFM three-point bending test.

4.3. Experimental

4.3.1. Materials and sample preparations

Lyocell fiber was used as raw material (provided by Lenzing). After the fibers were cut and passed a screen with holes of 1 mm in diameter by a Willey mill, they were soaked in distilled water for more than 24 hours and treated by high intensity ultrasonication to isolate fibrils (Chapter 3). Smaller fibrils with diameters less than 300 nm were separated from the treated fibers by centrifuging with about 500 g force for 5 min. After centrifugations, the top layers were kept for further morphological analysis and AFM three-point bending tests. A drop of fibril suspension was first dried on silicon

wafers with and without grooves at room temperature and then dried at 40~50 ºC in an oven more than 2 hours to make sure the fibrils were dried. A scanning electron microscope (SEM, LEO 1525) was used to investigate the appearance of the fibrils.

4.3.2. Three-point bending and nanoindentation tests in AFM

A schematic of the measurement of mechanical property using AFM is shown in Figure 4.1 (not in scale). An AFM cantilever tip was used to apply a small load at the midpoint (L/2) or at a quarter (L/4) along the suspended length of the fibrils (Figure 4.2) (Gere and Timoshenko, 1997). The silicon wafer has grooves with 5 μm in width and 1350 nm in depth (standard grating, MicroMasch). Two silicon cantilevers with nominal spring constant of 0.16 N/m (CSC17, MicroMasch) and 1.6 N/m (ZEILR, Nanosensor), and resonant frequency of 12 KHz and 27 KHz respectively, were used. The radius of the tip is less than 10 nm. AFM measurements were performed in ambient conditions under contact mode and the upper force limit was set to 10 nN (0.16 N/m) and 200/400 nN (1.6 N/m) with a loading rate of 1 μm/s. The tip for nanoindentation study was silicon (DT-NCHR, Nanosensor) with real diamond tip-side coating, spring constant of 44 N/m, and resonant frequency of 356 KHz. The typical macroscopic tip radius of curvature lies is between 100 and 200 nm. The nanoindentation tests were performed in ambient conditions under contact mode and the upper force limit was set to 500, 1000, and 2000 nN with a loading rate of 1 μm/s.

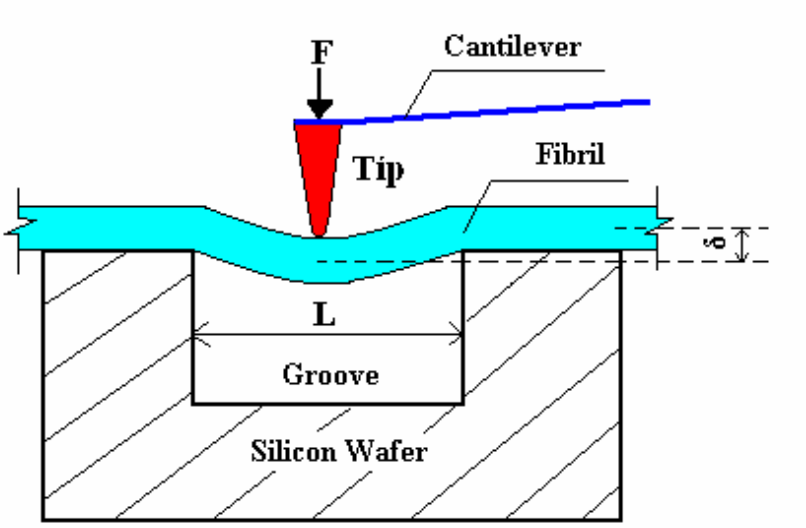

Figure 4.1 Schematic of the measurement of mechanical property using AFM

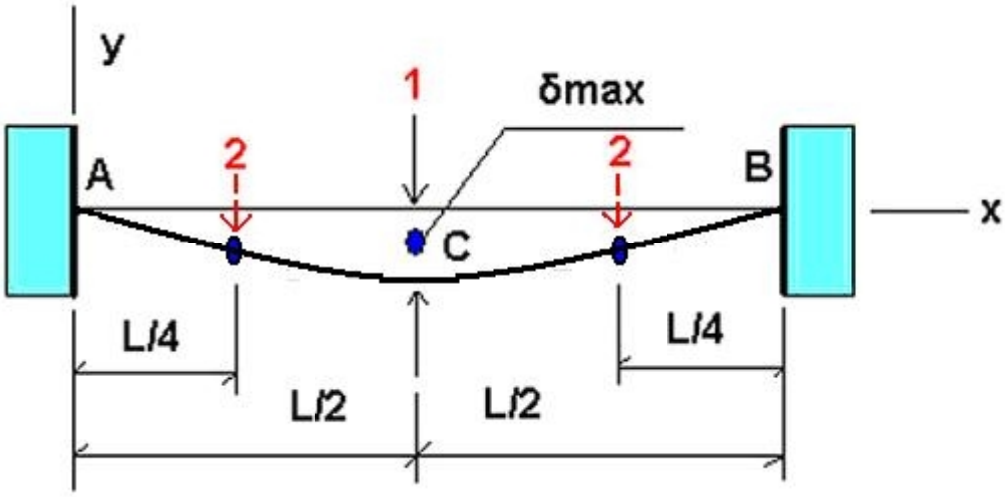

Figure 4.2 Deflection curve for a fixed-end beam

4.3.3. Determination of the deflection

The most important step is how to obtain the fibril deflection δ (Figure 4.1). The common method uses the force deflection curves obtained using AFM (Figure 4.3). The difference of the cantilever deflections between the tips loaded on the fibril above a groove (Figure 4.1) and loaded on the reference (such as silicon wafer substrate) was defined as the sample deflection δ. The test position of the reference may include testing on clear wafer, on the wafer after the sample were dried, or testing on fibril laid on the wafer substrate, which is described in the following section 4.3.4.

4.3.4. Considered factors influencing the deflection determination

Many factors may influence the deflection determination during the nanoscale three-point bending test using AFM. In this study, two groups of factors were chosen to observe and discuss the determination of the bending deflection: (1) data mining and AFM tip selection, including data mining by the software (Z-Scan or Z-Detector Fit), different tips with same spring constant but different conditions (new or used after 25 scans and ~400 bending tests), tips with different spring constant, different force applied to the fibrils, and (2) the testing position of the reference (Figure 4.4). The test position of the reference may include testing on wafer or testing on fibril laid on wafer after the sample were dried on the wafer, and test on clear wafer before the sample were dropped on the wafer because the fibril suspension may include some small particles in nanometer scale and the tip may penetrate into the fibrils.

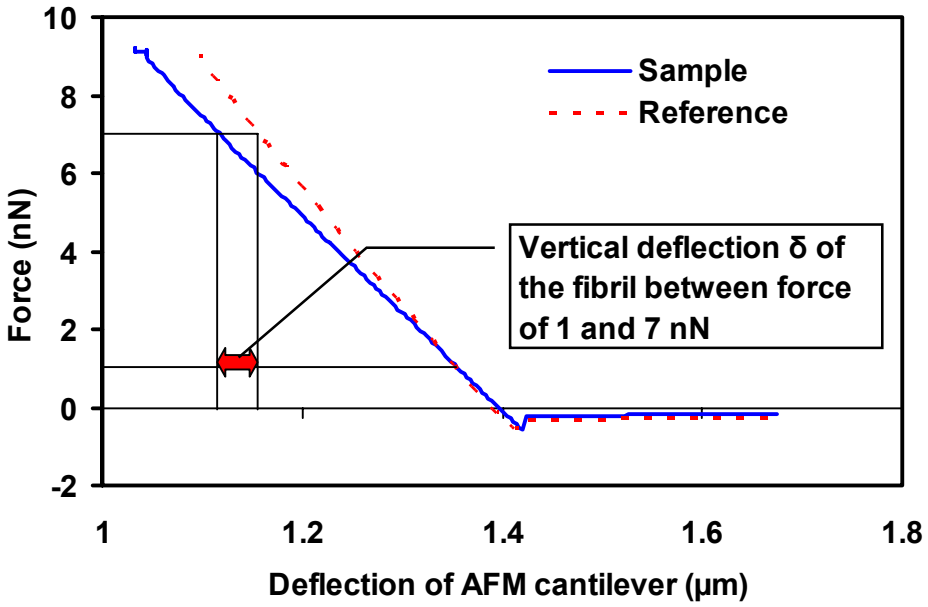

Figure 4.3 Typical curves used to determine the fibril deflection δ

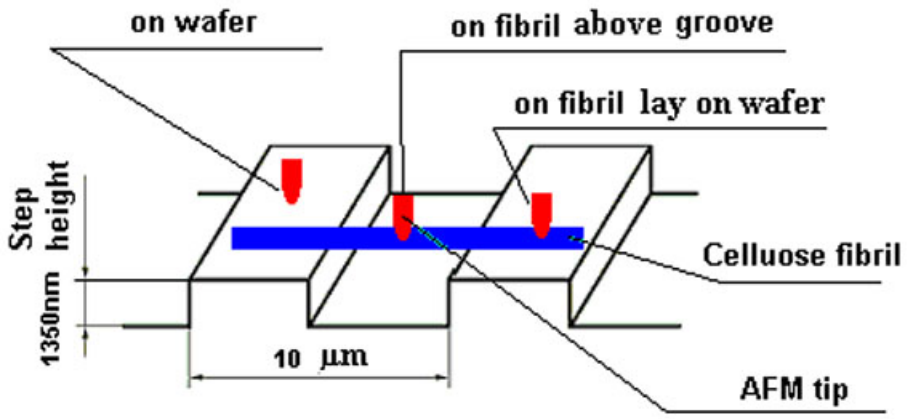

Figure 4.4 Three AFM tip testing positions during bending test

The modified extensions of Z scanner (Z-Detector Fit) from different factors were calculated between the two forces (such as 1 and 7 nN in Figure 4.5). Multiple comparisons by the Statistical Analysis System (SAS) (t Tests (LSD)) were used to detect the overall significant differences of the influences on the extensions of Z scanner (α=0.05).

4.3.5. Determination of the elastic modulus

Generally, the deflections of beams under certain force include both bending and shear deformations. The total deflection is the sum of the deflection due to bending and shears. When a concentrated force F is loaded in the midpoint of a beam, the maximum deflection can be calculated by Equation (4.1) (Gere and Timoshenko, 1997):

$$\delta = \frac{FL^3}{192EI} + f_s \frac{FL}{4GA} \tag{4.1}$$

where L is the span, E is the elastic modulus, I is the second moment of area of the beam (I= πD^4/64 for a filled cylinder with diameter of D), f_s is the shape factor, G is the shear modulus and A is the cross-sectional area.

The shear deformation decreases with the ratio of beam length to diameter, and it becomes important only for relatively short beams. In this case, the contribution of shear is negligible because the fibril worked as a long beam with the length to diameter ratio of more than 20, so that the elastic modulus can be determined by Equation (4.2) as the pure bending formula.

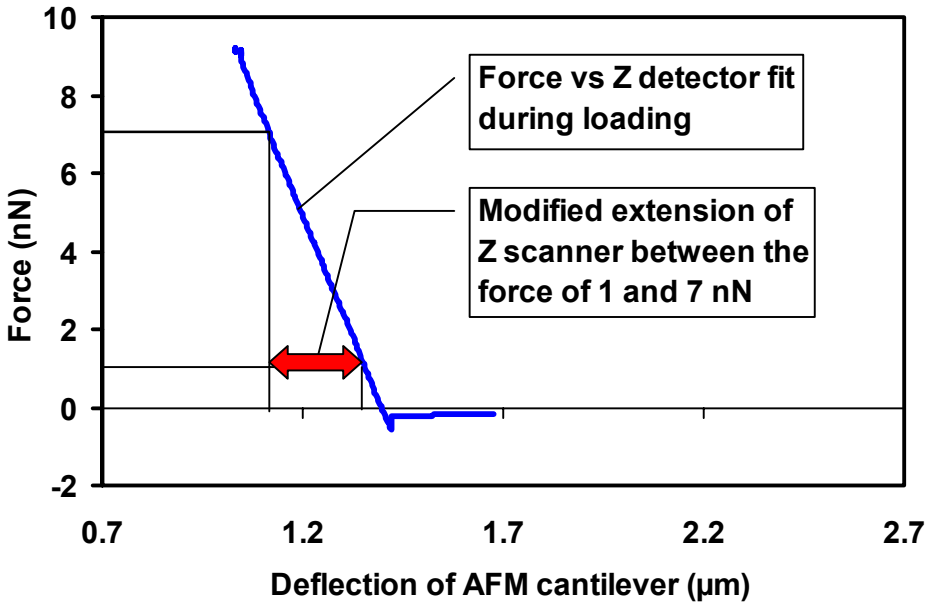

Figure 4.5 A typical force deflection curve during loading using AFM

$$E = \frac{FL^3}{192\delta I} \tag{4.2}$$

To check the reliability of midpoint test, the tip can be loaded on one quarter (L/4) of the span, the deflection should be half of the maximum deflection because the modulus is constant (Figure 4.2), and the elastic modulus can be determined by Equation (4.3).

$$E = \frac{FL^3}{384\delta I} \tag{4.3}$$

Some other assumptions for Equation (4.2) need to be noted here. First the fibril was assumed to be a pure elastic beam with both ends fixed (fixed-end beam) (Figure 4.2). This means the adhesion between the fiber and the silicon substrate was high enough for the small load. And second, the fibrils were assumed to have cylinder cross-section.

The maximum stress (σ_{max}) in the fibrils could be estimated by equation 4.4 (Gere and Timoshenko, 1997).

$$\sigma_{\max} = \frac{4F_{\max}L}{\pi D^3} \tag{4.4}$$

where F_{max}, L, and D are maximum force, groove span, fibril diameter, respectively.

Normal contact of elastic solids (Hertz theory) was used to analyze the force-indentation data. The fibril was assumed as a cylinder and the AFM tip as a sphere. The relative elastic modulus *Er* is given by (Johnson, 1992, Tan and Lim, 2005)

$$E_r = \sqrt{\frac{9P^2}{16R_e\delta^3}} \tag{4.5}$$

where *P* is the force applied, δ is the indentation depth (determined as bending test shown as in Figure 4.3), and *Re* is the equivalent radius for a spherical indenter in contact with an infinitely long cylinder, which is given by:

$$R_e = \sqrt{\frac{R_t^2 R_f}{R_t + R_f}} \tag{4.6}$$

where R_t is the AFM tip radius and R_f is the radius of the fibril. The vertical distance between the highest point of the fibril cross section and the wafer surface was taken to be the fibril diameter. The elastic modulus of the fibril (E_f) is related to the relative elastic modulus (E_r) by the following relation:

$$E_f \approx E_r(1-\nu_f^2) \tag{4.7}$$

where ν_f is Poisson's ratio of the fibril (assume 0.25 here).

The concentrated force F is related to Photodetector Voltage in AFM and is calculated by equation (4.3) (Anonymous, PSIA Corporation).

$$F = M\left(\frac{3}{A+B}\right)1000k\left(\frac{PSPD_{DC}}{10}\right) \tag{4.8}$$

where M is the MicrometerPerErrorSignalADC (different for every cantilever), A+B is the laser intensity, k is the spring constant of the cantilever N/m, $PSPD_{DC}$ is the DC voltage signal from the photodetector (A-B).

4.4. Results and Discussions

After the morphology of fibrils on silicon wafer was observed by SEM and AFM, the results and discussion focused on the factors that may influence the deflection determination during the nanoscale three-point bending test using AFM. The extension of Z-Scanner (Figure 4.5) was used to study and compare the influences of the two-group factors. Then the elastic modulus of cellulose fibrils isolated from Lyocell fibers was calculated and discussed as one sample. AFM nanoindentation results of the cellulose fibrils were also discussed.

4.4.1. Morphology observations of fibrils on silicon wafer

The fibrils isolated from Lyocell fiber were bundles of smaller nanofibrils. The suspensions of the treated Lyocell fibers were mixtures of fibrils in micro and nano scales. SEM images show the fibrils on silicon wafer with (Figure 4.6 top) and without (Figure 4.6 bottom) grooves. Both diameter and length of the fibrils had a very large range. During AFM three-point bending test, only the fibrils suspended well on the

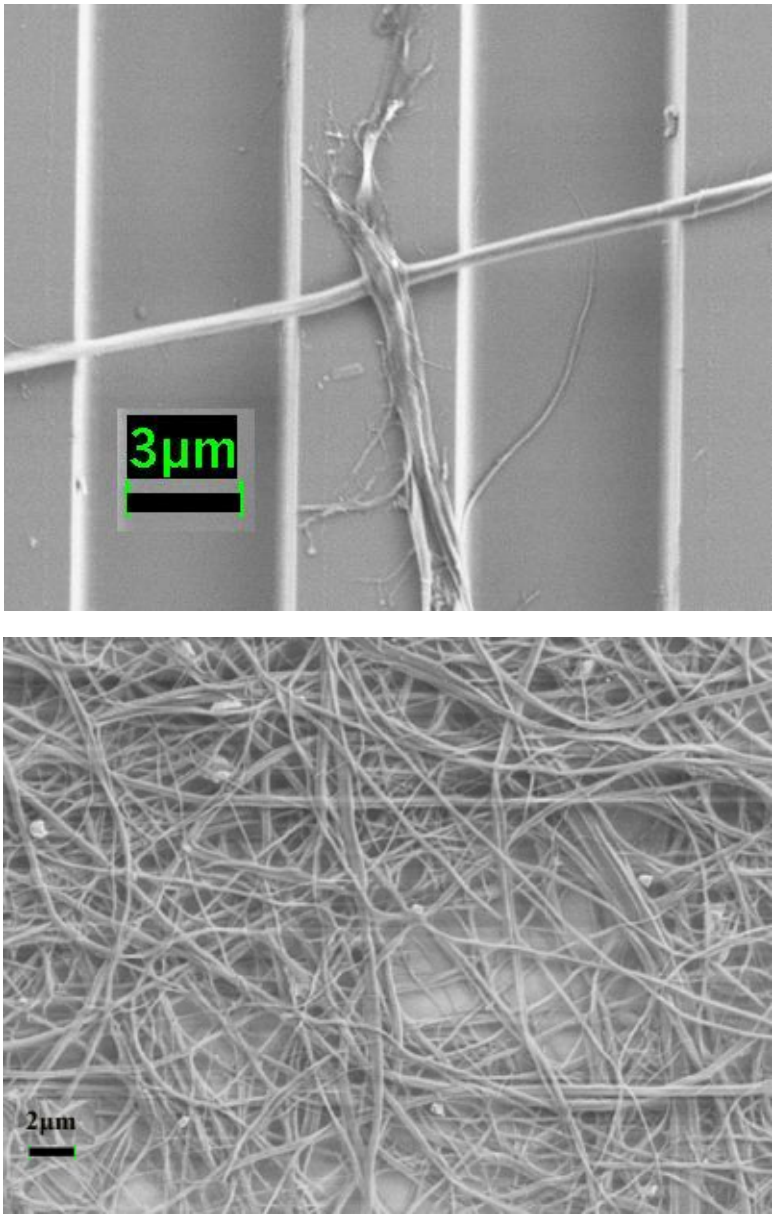

Figure 4.6 SEM images of fibrils isolated from Lyocell fiber on silicon wafer

grooved silicon wafer were chosen to scan and tested (Figure 4.6, bottom). And Figure 4.7 shows an AFM image of a single Lyocell fibril suspended well on a grooved silicon wafer.

4.4.2. Effects of data mining and tip conditions on deflection

The F/D curves (Force vs. Distance) obtained from the F/D spectroscopy mode (PSIA, XE-100) include two types: F vs. Z-Scan and F vs. Z-Detector Fit (Figure 4.8). Extension of Z-Scanner was used to describe the distance in the curves (modified extension in Figure 4.5). Z-Scan is the distance traveled as measured by the voltage to the z piezo. The problem with using the raw z-scan data is that for large distance, piezos are not linear and hysteresis exists in the travel (Figure 4.8). Z-Detector Fit takes into account the problems with noise and hysteresis; and the software takes the Z-Scan values and normalizes it with the Z-Detector data. So Z-Detector Fit is the Z-Scan distance corrected by the strain gauge feedback. It is better to use Z-Detector Fit as the extension of the F/D curve. The data of Z-Scan and Z-Detector Fit as shown in Table 4.1 were significantly different for all the three tips ($\alpha=0.5$, $p<0.0001$).

The extensions of Z-Scanner (distance between the force of 1 and 7 nN tested on silicon wafer as shown in Figure 4.5) of data mined by the software (Z-Scan or Z-Detector Fit) from different tips with same nominal spring constant (tip A and B), the condition of the tip A (new or used) are shown in Table 4.1. The extensions of Tip A and B were significantly different ($\alpha=0.5$, $p<0.0001$). Although the two tips were made from same condition and had the same spring constant, the extensions of Z-Scanner were

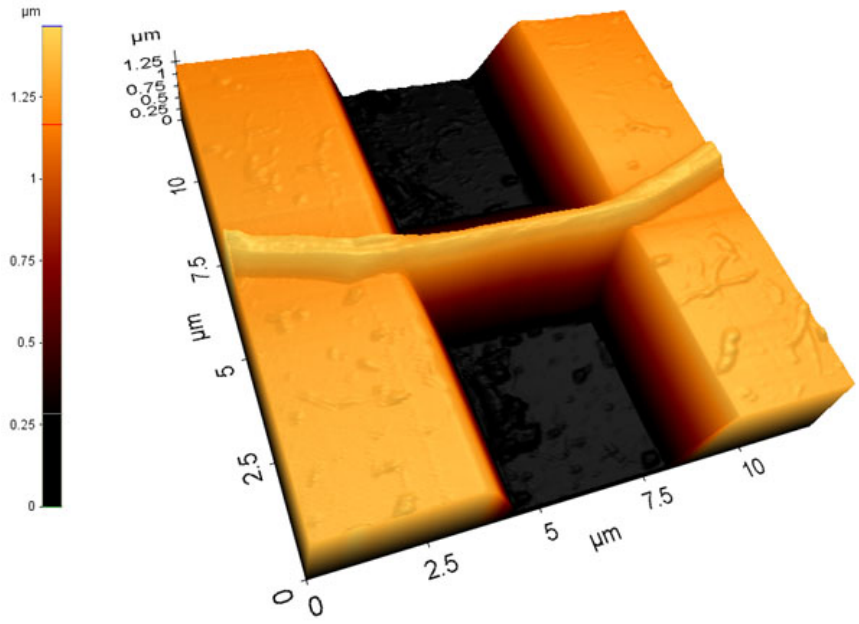

Figure 4.7 AFM image of a single fibril isolated from Lyocell fiber on grooved silicon wafer

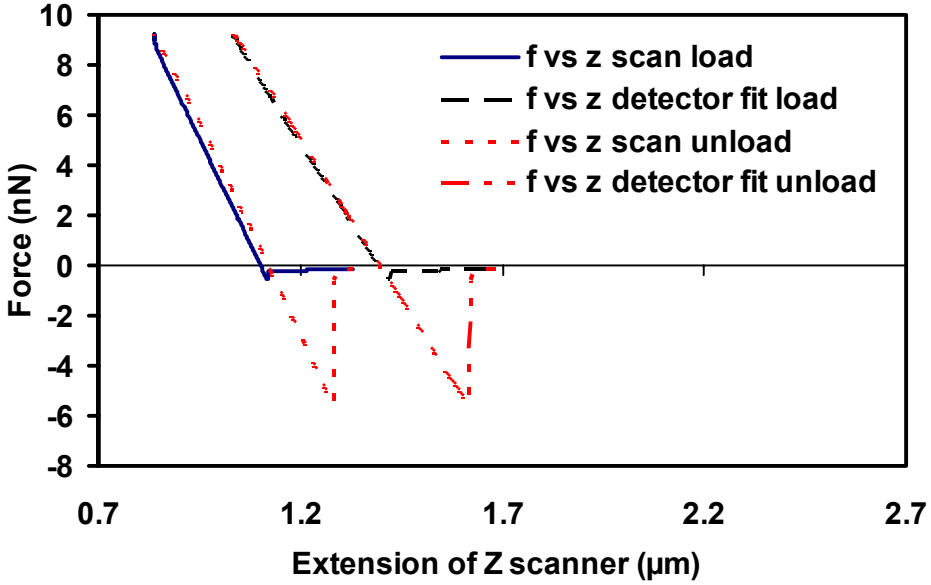

Figure 4.8 Two types of F/D curves from the AFM data mining

Table 4.1 Extensions of Z-Scanner between the force of 1 and 7 nN of three tips

	New Tip A (μm)		Old Tip A (μm)		New Tip B (μm)	
	Z-Scan	Z-Detector Fit	Z-Scan	Z-Detector Fit	Z-Scan	Z-Detector Fit
1	0.1607	0.2132	0.2173	0.2734	0.1410	0.1874
2	0.1649	0.2158	0.2179	0.2738	0.1395	0.1835
3	0.1646	0.2147	0.2174	0.2737	0.1404	0.1855
4	0.1630	0.2143	0.2161	0.2724	0.1407	0.1851
5	0.1648	0.2150	0.2163	0.2724	0.1404	0.1847
6	0.1654	0.2156	0.2178	0.2748	0.1389	0.1847
7	0.1633	0.2144	0.2171	0.2741	0.1407	0.1849
8	0.1650	0.2150	0.2174	0.2748	0.1400	0.1836
9	0.1666	0.2165	0.2196	0.2774	0.1406	0.1841
Mean	0.1643	0.2150	0.2174	0.2741	0.1402	0.1848
COV*	1.04	0.44	0.47	0.55	0.47	0.63

* Coefficient of Deviation

different when they were used to test on wafer surface with same force. The extension of old tip A was significantly different compared with that of new tip A (α=0.5, $p<0.0001$). These indicate that it is necessary to use the same tip to test the fibrils above grooves, fibrils laid on wafer and/or silicon wafer to obtain the fibril deflection δ.

4.4.3. Effects of test position on deflection

To measure the extensions of Z-Scanner used as reference to calculate the fibril deflection δ, three testing positions of AFM tip were considered: testing on wafer and on fibril laid on wafer after the sample were dried, as well as testing on clear wafer.

The results of two tips are shown in Table 4.2. The extensions of testing on clear wafer and on wafer with samples for both tips were significantly different (α=0.5) in this case. One reason may be that the fibril suspension may include some small particles in nanometer scale. The extensions tested on fibrils laid on wafer were higher than those tested on wafer with samples (significantly for tip A, not significantly for tip B (α=0.5)), but the differences were only several nanometers. This indicates that the AFM tip may penetrate into the fibril but the penetration was very small when the tip force was only less than 10 nN (max for this tip). This force may be not enough to bend the fibril because the fibril was expected very stiff and most of all the fibril surfaces were not smooth enough. The roughness was at least several nm as shown in Figure 4.9. The COV of the extensions testing on fibrils was higher than that of the testing on wafer with samples. It indicates again that the fibril surfaces were not smooth enough.

Table 4.2 Extensions of Z-Scanner between the force of 1 and 7 nN for different testing positions

	Tip A (μm)			Tip B (μm)		
	On clear wafer	On wafer with sample	On fibril laid on wafer	On clear wafer	On wafer with sample	On fibril laid on wafer
1	0.2132	0.1975	0.1872	0.1874	0.2073	0.2094
2	0.2158	0.1969	0.2073	0.1835	0.2020	0.2073
3	0.2147	0.1946	0.1845	0.1855	0.2036	0.2090
4	0.2143	0.1961	0.1947	0.1851	0.2081	0.2133
5	0.2150	0.1967	0.2313	0.1847	0.2053	0.2104
6	0.2156	0.1976	0.2333	0.1847	0.2046	0.2021
7	0.2144	0.2001	0.2402	0.1849	0.2095	0.2053
8	0.2150	0.1955		0.1836	0.2085	0.2032
9	0.2165	0.1960		0.1841	0.2053	0.2088
Mean	0.2150	0.1968	0.2112	0.1848	0.2060	0.2076
COV*	0.44	0.80	11.13	0.60	1.21	1.72

* Coefficient of Deviation

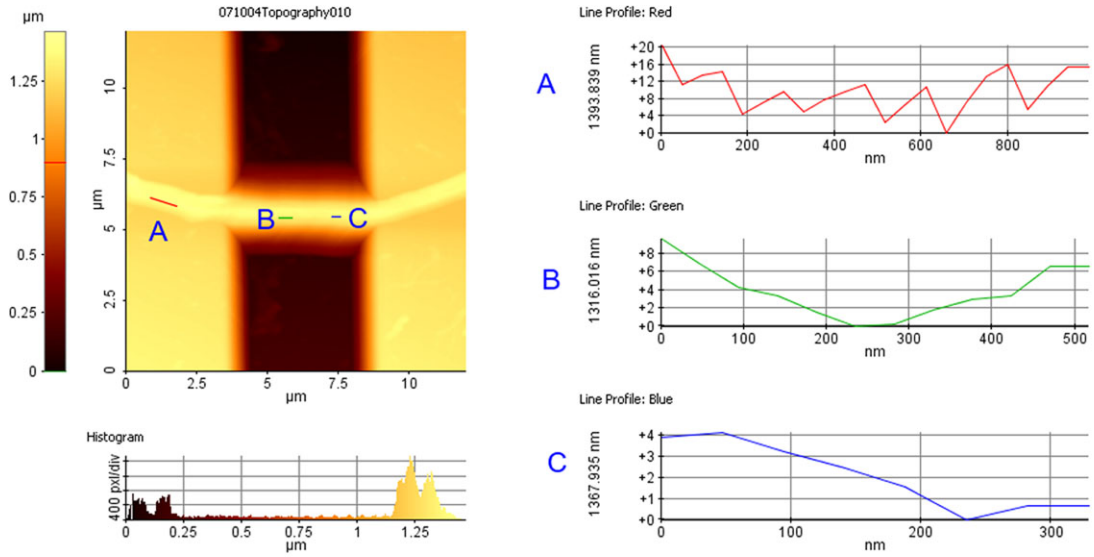

Statistics

Line	Min(µm)	Max(µm)	Mid(µm)	Mean(µm)	Rpv(µm)	Rq(µm)	Ra(µm)	Rz(µm)	Rsk	Rku
Red	1.394	1.414	1.404	1.403	0.020	0.005	0.004	0.000	-0.140	2.696
Green	1.316	1.326	1.321	1.320	0.010	0.003	0.002	0.000	-0.649	2.526
Blue	1.368	1.372	1.370	1.370	0.004	0.001	0.001	0.000	0.216	1.598

Figure 4.9 The surface roughness of a single Lyocell fibril in an AFM image

4.4.4. Effects of cantilever stiffness on deflection

To decide the suitable tip cantilever for cellulosic fibril measurement, two kind tips with spring constant of 0.16 N/m (tip0.16) and 1.6 N/m (tip1.6) were used. The extensions of Z-scanner testing on clear wafer, on fibril laid on wafer, and on fibril above grooves for tip0.16 and tip1.6 are shown in Figures 4.10 and 4.11, respectively. There was no significant difference (α=0.5) between the extensions on clear wafer and on fibril laid on wafer, which means no penetration into the fibril. And there were not significantly difference (α=0.5) between the extensions on fibril laid on wafer and on fibril above grooves, which means no bending on the fibril above the grooves. It was clear in this case that the force of less than 10 nN was not enough to bend the fibril.

For high spring constant tip, much higher forces can be applied to the tips, so that the cantilever extensions could be higher (Figures 4.11). The max force for tip1.6 was about 500 ~ 600 nN and 200nN was used in this case and the tip was on one quarter span of the fibril. There were significantly differences (α=0.5) among the extensions of Z-scanner testing on clear wafer, on fibril laid on wafer, and on fibril above grooves. The results demonstrated that the tip penetrated into the fibril and the bending deflection of the fibril above the groove was about 20 nm in this case.

4.4.5. Elastic modulus of single cellulose fibrils

According to the above results and discussion, tip1.6 with high spring constant was used and the fibril deflection (δ) during three-point bending test using AFM could be determined by subtracting the extension of Z-Scanner testing on wafer after sample dried

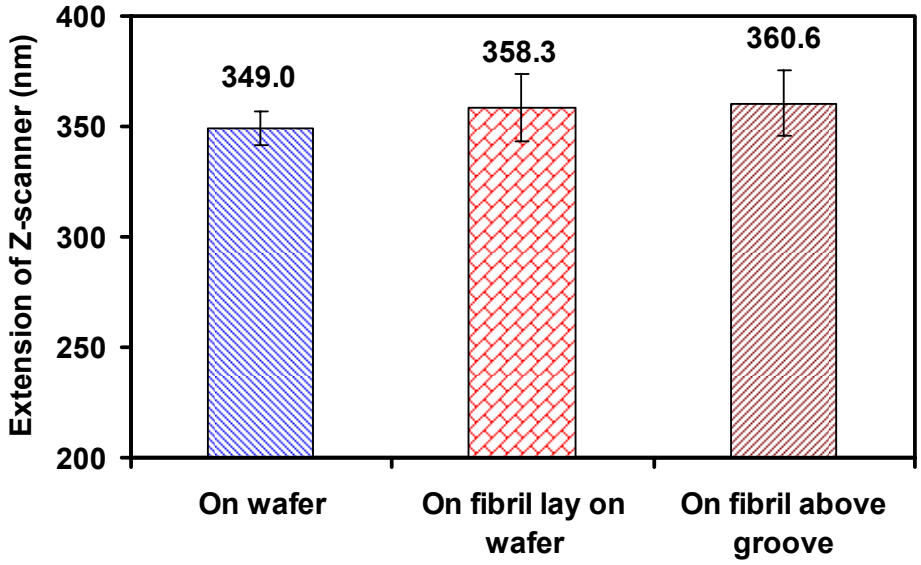

Figure 4.10 Cantilever extension of z-scanner for different testing position using low spring constant tip (tip0.16)

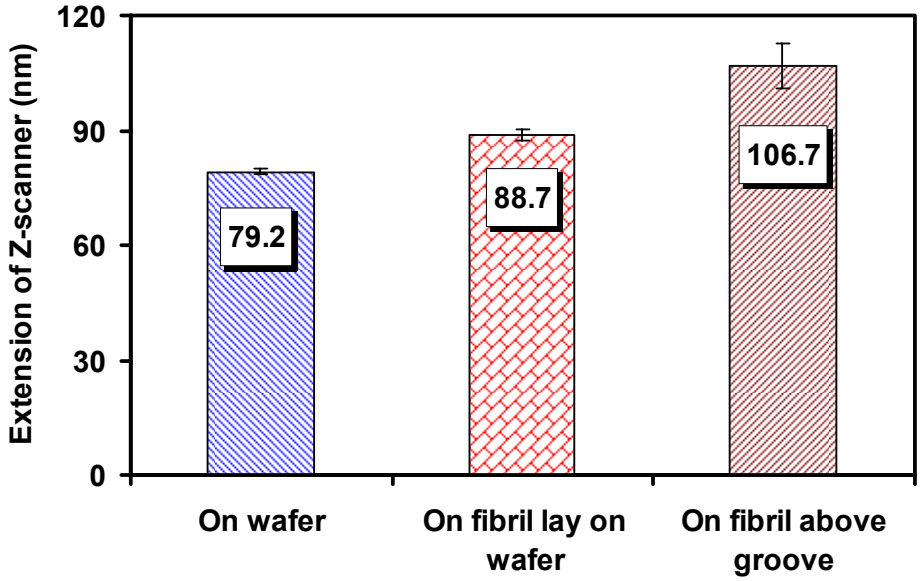

Figure 4.11 Cantilever extension of z-scanner for different testing position using high spring constant tip (tip1.6)

or on the fibril laid on the wafer (as reference) from the extension of Z-Scanner testing on the fibril suspended above a groove. There was some difference of the modulus calculated from them and it was higher if the fibril laid on the wafer was used as reference (Figure 4.12). The position on the fibril laid on the wafer was chosen as reference because the sharp tips with radius of less than 10 nm penetrated into the fibrils in most cases. Several fibrils with similar diameter (±5 nm) may be tested as one sample. At least six points on the fibril laid on the wafer were tested, and the mean of deflections was used as reference to calculate the deflection of each fibril tested in the same sample. After deflection δ of each fibril was determined and the fibril diameter was obtained by measuring the height of fibrils in AFM images, the elastic modulus of the fibril was calculated using Equation (4.2).

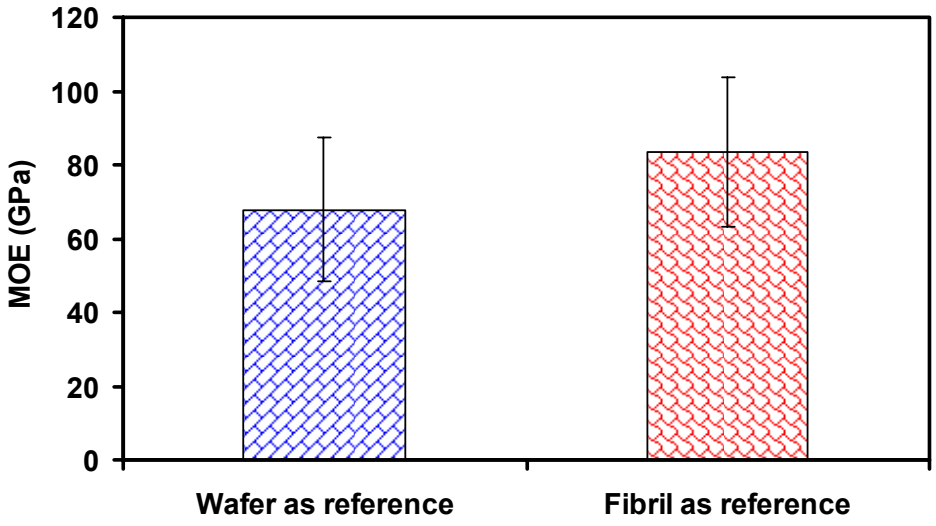

Figure 4.12 Elastic of moduli of single cellulosic fibril (d≈170 nm) tested by tip1.6 and calculated using different testing positions as the reference to determine the reflection

Figure 4.13 shows elastic of moduli of single cellulosic fibrils with diameter of about 170 nm tested by tip1.6 on midpoint and a quarter (L/4) of the fibril span (Figure 4.2) with force limitations of 200 nN and 400 nN. The elastic modulus should be the same when the tip is loaded on one quarter (L/4) and midpoint of the span (Gere and Timoshenko, 1997). The result shows that modulus obtained from one quarter (L/4) of the fibril span was a little lower and had much higher variation than those obtained from midpoint of the span. One reason may be that the deflection variations were much higher when the tip is loaded on L/4 span because the fibril surface was not very smooth and the fibril was not flat during bending test (Figure 4.2). The none-perpendicular tip load to the sample surface could cause slip and friction between the AFM tip and the sample surface

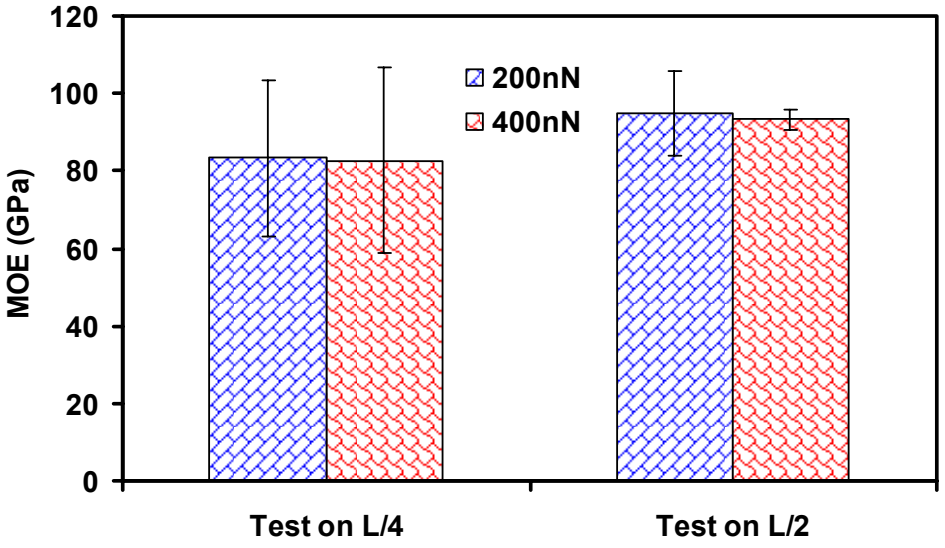

Figure 4.13 Elastic of moduli of single cellulosic fibrils (d≈170 nm) tested by tip1.6 on m idpoint and a quarter (L/4) of the fibril span with different force limitations

during test (Li et al., 2003). There was no significant difference between the 200nN and 400nN forces, but the variation may be less for higher force.

The modulus for the Lyocell small fibril (d≈170 nm) was estimated to be about 93 GPa obtained from the reference testing position on fibril laid on the wafer. It is much higher than the elastic modulus of Lyocell fibers was about 11 to 13 GPa evaluated by nanoindentation (Lee et al. 2007), but it may be reasonable because smaller fibril may have less defects and higher stiffness. It is needed to notice that nanoindent is compression, but the obtained data here were from bending. The correlation between them is not known.

The maximum stress (σ_{max}) in the fibrils estimated by equation 4.4 were 13, 260, and 520 MPa for the fibril diameter of 170 nm and the maximum forces of 10, 200, and 400 nN, respectively. It was high stress, especially for 200 and 400 nN forces, but the force displacement curves were linear (similar as Figure 4.8) and no broken fibrils, permanent indents, and fibril movements were observed after bending tests. This indicated that the fibril bend and AFM tip penetration into the fibril surface were elastic and the fibrils had high strength.

The elastic moduli of Lyocell fibrils estimated by nanoindentation were much less than those obtained from three-point bending test. Figure 4.14 shows elastic of moduli of single cellulosic fibrils (d≈170 nm) estimated with Equations 4.4 to 4.6 by AFM nanoindentation for different maximum forces loaded on the fibrils. It was unexpected that the modulus decreased with the load increasing and this may be because of the viscoelastic effect. The Hertz models used for the calculation of small fibril elastic

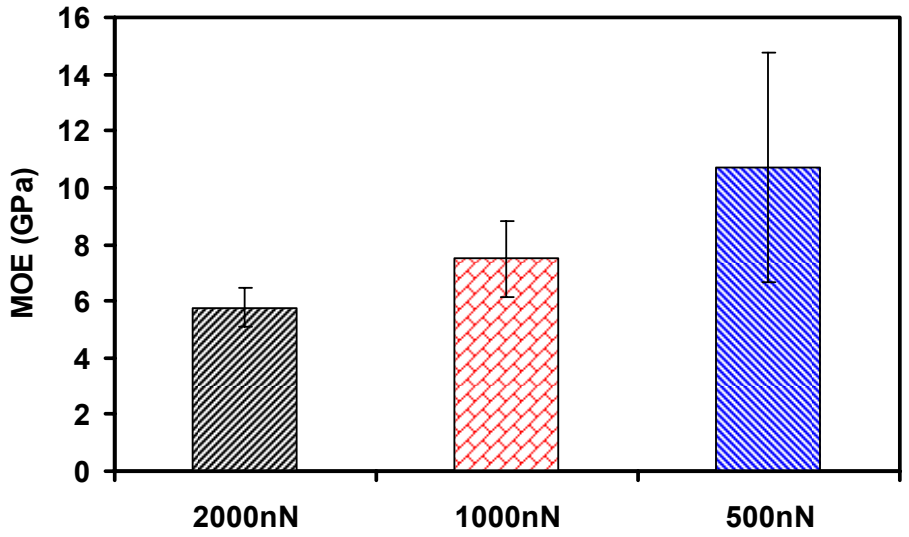

Figure 4.14 Elastic of moduli of single cellulosic fibrils (d≈170 nm) estimated by AFM n anoindentation with diamond coating tip from different maximum forces

modulus assume that either the fiber surface is flat or the AFM tip and fiber are two spherical bodies in elastic contact. Both assumptions were valid because the tip radius may be much smaller than the fiber radius, and the tip and fibril shape were not exactly spherical. Other factors that may influence the nanoindentation results include ambiguous tip shape and cantilever spring constant, fiber surface roughness, curvature of fibril surface, and the tip could be serious worn or damaged after used (Figure 4.15). The results were in an underestimation of the elastic modulus values because the rough fibril surface resulted in the increase in contact area and reduction of contact pressure for a given load. The none-perpendicular tip load to the sample surface could cause slip and friction between the AFM tip and the sample surface during indentation (Li et al., 2003, Tan and Lim, 2005). The Hertz theory without modification for nanoindentation test by a

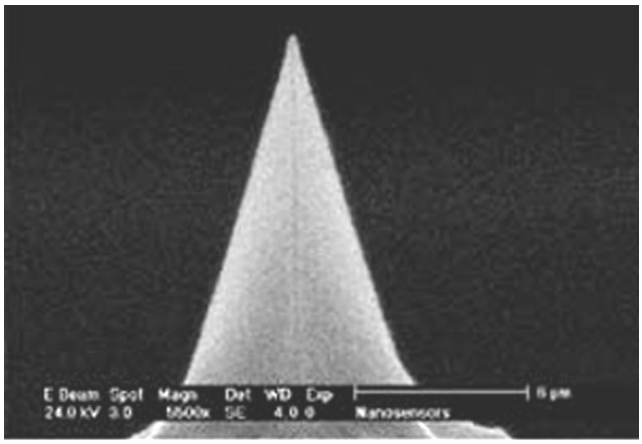

a)

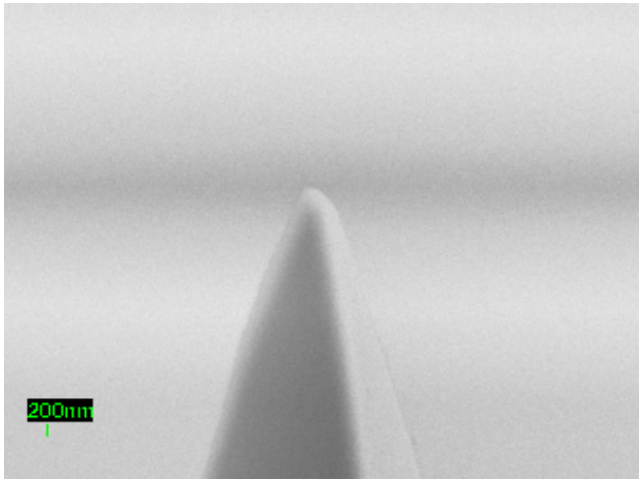

b)

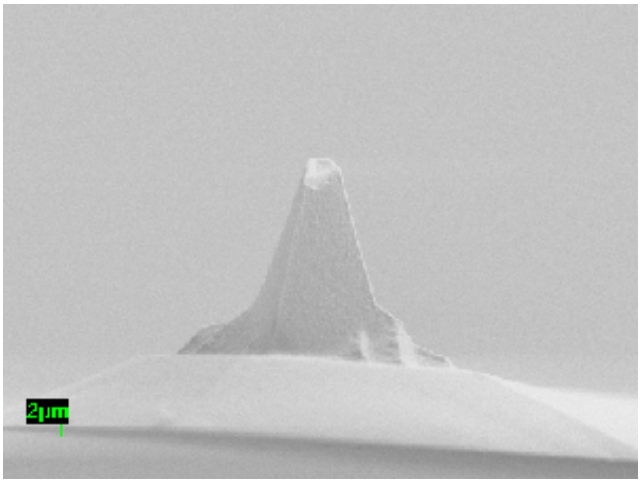

c)

Figure 4.15 SEM images of AFM nanoindentation tip with diamond coating: a) un-used, b) worn, c) damaged

high spring constant AFM tip may be not suitable to estimate the elastic modulus of this cellulosic fibril. The modulus of Lyocell fibril tested here could be much higher than the nanoindentation results, which was only about 10 GPa in maximum. Further study and more factors that may influence the indentation test are needed for this model to be used in this material.

4.5. Conclusions

The nanoscale three-point bending test performed by AFM can be used to determine the elastic moduli of single cellulosic fibrils. Many factors influenced the determination of the fibril deflections during bending tests, which subsequently affected the calculation of elastic modulus. Most of the considered factors including data mining, AFM tip selection, and the testing position of the reference influenced the deflections, especially the different stiffness AFM tips and the choice of the testing position of the reference to determine the fibril deflections. The results indicated that the penetration of AFM tips to the cellulosic fibril surfaces should be considered for the bending deflection of fibrils suspended above a silicon groove. The AFM cantilever deflection when the tip was loaded on the fibril laid on the wafer was better as reference to calculate the deflection of the fibril suspended above a silicon groove than that obtained on the wafer as reference. The elastic modulus of Lyocell fibril with diameter of about 170 nm isolated by high intensity ultrasonication was evaluated to be 93 GPa. The Hertz theory for nanoindentation test may be not suitable to estimate the elastic modulus of this kind of cellulosic fibril before it is modified using more factors.

References

Anonymous, PSIA Corporation. Technical Support & Service Department.

Berglund, L., 2005. Cellulose-based nanocomposites. In: A.K.M. Mohanty, M.; Drzal, L. (Editor), Natural Fibers, Biopolymers, and Biocomposites. Taylor & Francis, pp. 807-832.

Chakraborty, A., Sain, M. and Kortschot, M., 2005. Cellulose microfibrils: A novel method of preparation using high shear refining and cryocrushing. Holzforschung, 59(1): 102-107.

Cheng, Q., Wang, S., Zhou, D., Zhang, Y. and Rials, T.G., 2007a. Lyocell-derived cellulose microfibril/nanofibril and its biodegradable nanocomposites. Journal of Nanjing Forestry University, 31(4): 21-26.

Cheng, Q., Wang, S., Rials, T.G. and Lee, S.H., 2007b. Physical and mechanical properties of polyvinyl alcohol and polypropylene composite materials reinforced with fibril aggregates isolated from regenerated cellulose fibers. Cellulose, online first, DOI: 10.1007/s10570-007-9141-0.

Choi, Y.J. and Simonsen, J., 2006. Cellulose nanocrystal-filled carboxymethyl cellulose nanocomposites. Journal of Nanoscience and Nanotechnology, 6(3): 633-639.

Dufresne, A., Cavaille, J.Y. and Vignon, M.R., 1997. Mechanical behavior of sheets prepared from sugar beet cellulose microfibrils. Journal of Applied Polymer Science, 64(6): 1185-1194.

Eichhorn, S.J. and Young, R.J., 2001. The Young's modulus of a microcrystalline cellulose. Cellulose, 8(3): 197-207.

Gere, J.M. and Timoshenko, S.P., 1997. Mechanics of materials. PWS Publishing Company, Boston, MA.

Herrick, F.W.C., R. L.; Hamilton, J. K. and Sandberg, K. R., 1983. Microfibrillated cellulose: morphology and accessibility. Journal of Applied Polymer Science: Applied Polymer Symposium, 37: 797-813.

Johnson, K. L., 1992. Contact mechanics. Cambridge University Press, Cambridge.

Lee S.H., Wang, S., Pharr G.M., Kant M. and Penumadu D., 2007. Mechanical properties and creep behavior of lyocell fibers by nanoindentation and nano-tensile testing. Holzforschung, 61(3): 254-260.

Li, X.D., Hao, H.S., Murphy, C.J. and Caswell, K.K., 2003. Nanoindentation of silver nanowires. Nano Letters, 3(11): 1495-1498.

Mott, L., Shaler, S.M. and Groom, L.H., 1996. A technique to measure strain distributions in single wood pulp fibers. Wood and Fiber Science, 28(4): 429-437.

Page, D.H., Winkler, K., Bain, R. and Elhossei, F, 1972. Mechanical properties of single wood-pulp fibers. 1. New approach. Pulp and Paper Magazine of Canada, 73(8): 72.

Sakurada, I., Nukushina, Y. and Ito, T., 1962. Experimental determination of elastic modulus of crystalline regions in oriented polymers. Journal of Polymer Science, 57(165): 651-660.

Salvetat, J.P., Briggs, G.A.D., Bonard, J.M., Bacsa, R.R., Kulik, A.J., Stockli, T., Burnham, N.A. and Forro, L., 1999a. Elastic and shear moduli of single-walled carbon nanotube ropes. Physical Review Letters, 82(5): 944-947.

Salvetat, J.P., Kulik, A.J., Bonard, J.M., Briggs, G.A.D., Stockli, T., Metenier, K., Bonnamy, S., Beguin, F., Burnham, N.A. and Forro, L., 1999b. Elastic modulus of ordered and disordered multiwalled carbon nanotubes. Advanced Materials, 11(2): 161-165.

Salvetat-Delmotte, J.P. and Rubio, A., 2002. Mechanical properties of carbon nanotubes: a fiber digest for beginners. Carbon, 40(10): 1729-1734.

Tan, E.P.S. and Lim, C.T., 2004. Physical properties of a single polymeric nanofiber. Applied Physics Letters, 84(9): 1603-1605.

Tan, E.P.S. and Lim, C.T., 2005. Nanoindentation study of nanofibers. Applied Physics Letters, 87(12): No. 123106.

Taniguchi, T., 1996. Microfibrillation of natural fibrous materials. J. Soc. Mat. Sci. Japan, 45(4): 472-473.

Tombler, T.W., Zhou, C.W., Alexseyev, L., Kong, J., Dai, H.J., Lei, L., Jayanthi, C.S., Tang, M.J. and Wu, S.Y., 2000. Reversible electromechanical characteristics of carbon nanotubes under local-probe manipulation. Nature, 405(6788): 769-772.

Turbak, A.F.S., F. W. and Sandberg, K. R., 1983. Microfibrillated cellulose, a new cellulose product: properties, uses, and commercial potential. Journal of Applied Polymer Science: Applied Polymer Symposium, 37: 815-827.

Wong, E.W., Sheehan, P.E. and Lieber, C.M., 1997. Nanobeam mechanics: Elasticity, strength, and toughness of nanorods and nanotubes. Science, 277(5334): 1971-1975

Xing, C., Wang, S., Pharr, G.M. and Groom, L.H., 2007a. Effect of thermo-mechanical refining pressure on the properties of wood fiber cell walls: measured by nanoindentation and AFM. Holzforschung (in print).

Xing, C., Wang, S., Pharr, G.M. and Groom, L.H., 2007b. Comparison of the effects of thermomechanical refining pressure on the properties of refined fibers of juvenile and mature wood (submitted to Cellulose).

Xu, W., Mulhern, P.J., Blackford, B.L., Jericho, M.H. and Templeton, I., 1994. A new atomic-force microscopy technique for the measurement of the elastic properties of biological-materials. Scanning Microscopy, 8(3): 499-506.

CHAPTER 5. EFFECTS OF PROCESS AND SOURCE ON ELASTIC MODULUS OF SINGLE CELLULOSE FIBRILS

5.1. Abstract

Cellulose fibrils in micro and nano scales have potential lightweight and much higher strength than individual wood fibers, but the measurement of mechanical properties of individual fibrils is difficult due to the tiny dimensions and uneven diameters or widths, and the small forces involved. In this study, the test method of measurement of fibril elastic modulus using AFM developed in Chapter 4 was used to investigate the effects of process and cellulose source on elastic moduli of single cellulose fibrils. The fibrils were generated from cellulose by high intensity ultrasonic treatment. Individual fibrils were suspended over a micro scale groove etched on a silicon wafer. A nano-scale three-point bending test was performed to obtain the elastic modulus. The results indicated that the elastic moduli of cellulose fibrils were not significantly different between 30 min and 60 min HIUS treatment for Lyocell fiber, between isolation methods of HIUS and high-pressure homogenizer for pure cellulose fiber. The elastic modulus of Lyocell fibrils with diameters from 150 to 180 nm was evaluated about 98 GPa. It decreased dramatically when the diameter was more than 180 nm.

Keywords: Atomic force microscope (AFM), cellulose, deflection, elastic modulus, fibril, micro, nano, three-point bending

5.2. Introduction

Cellulose fibers are attractive for replacing man-made fibers, such as glass fibers, as reinforcement or fillers to make environmental friendly products because they are

renewable, biodegradable and the most abundant biopolymer in the world. Due to the potential higher mechanical properties than individual wood fibers, fibrils in micro and nano scales have been generated from cellulose fibers and used to reinforce polymers to make nanocomposites in the past two decades (Herrick, 1983; Turbak, 1983; Berglund, 2005; Cheng et al. 2007a; Cheng et al. 2007b). One main method used to isolate cellulose fibrils is a mechanical treatment with high shear force, such as high-pressure homogenizer treatment (Dufresne et al., 1997; Herrick, 1983; Turbak, 1983), and high-pressure refiner or supergrinder treatment (Chakraborty et al, 2005; Taniguchi, 1996). The commercial microfibrillated cellulose (MFC) is used in some industrial applications, such as food, cosmetic, and medicinal products (Lima and Borsali, 2004). The mechanical separated fibrils have a wide range of diameters from tens of nm to several μm, while most of the chemical separated fibrils are much smaller and uniform with diameters from several nm to tens nm (Beck-Candanedo et al., 2005).

The mechanical properties of the fibrils could helpful to evaluate the degradation of fibrils during the isolation process and the potential reinforcement of the fibrils for polymers. To understand the mechanical properties of single cellulosic fibrils is very important for fibril isolation and polymer reinforcement, but mechanical properties of individual fibril are rarely studied. The mechanical properties of single wood fiber have been studied (Mott et al., 1996; Page et al., 1972; Xing et al., 2007 a and b). For smaller fibrils, it is very difficult to measure the mechanical properties directly due to the difficulty in isolating individual cellulose fibrils, measuring the very tiny forces and deformations involved. Estimated by X-ray diffraction, the obtained elastic modulus of

the crystalline region was 137 GPa (Sakurada et al., 1962) and the crystal lattice moduli of cellulose I and II were in the range 122~135 and 106~112 GPa, respectively (Matsuo et al., 1990). The Young's modulus of microcrystalline cellulose was estimated to be 25±4 GPa from the values of the shift rate of the 1095cm^{-1} band using Raman spectroscopy (Eichhorn and Young, 2001).

A nano-scale three-point bending test setup by atomic force microscope (AFM) has been used to obtain the elastic modulus of nano scale fibrils of silicon carbide nanorods and multiwall carbon nanotubes (Salvetat et al., 1999a; Salvetat et al., 1999b; Salvetat-Delmotte and Rubio, 2002; Wong et al., 1997), β-chitin fibers (Xu et al., 1994), PLLA nanofibers (Tan and Lim, 2004), and bacterial cellulose (Wan et al., 2006). In Chapter 4, a protocol of this method was investigated for the measurement of elastic modulus of cellulose fibrils generated by high intensity ultrasonication. The results indicated that it was necessary to use the same AFM tip to test fibrils suspended on grooves and on fibrils laid on silicon wafer surface at the same time to obtain the fibril deflection (Cheng and Wang, 2007).

Following chapter 4 about the test method development, this Chapter was focused on the effects of process and cellulose source on elastic modulus of single cellulose fibrils evaluated by this method. Mechanical properties of individual cellulose fibrils isolated from regenerated cellulose fiber (Lyocell), pure cellulose flours (TC40), and pulp fiber by ultrasonic treatment were investigated. As references, TC40 treated by high-pressure homogenizer (HPH) and commercial microfibrillated cellulose (MFC) were tested and compared. The fibrils produced by mechanical methods have diameters in the wide range

of tens of nm to several μm. Only the fibrils with diameters of 150–300 nm and lengths of more than five micrometers were chosen and investigated.

5.3. Materials and Methods

5.3.1. Materials

Three raw materials were used: Lyocell fiber (a regenerated cellulose fiber, about 11 μm in diameter, provided by Lenzing), pulp fiber (provided by Kimberly-Clark Worldwide, Inc.), and pure cellulose flours (TC40, average fiber width 18 μm and lengths 30 μm, provided by CreaFill Fibers Corp.). As reference, commercial microfibrillated cellulose (MFC, 10% solid slurry, Daicel Chemical Industries, LTD., Japan) was also used. Treatments and resources of the five types of fibrils were shown in Table 5.1.

5.3.2. Isolation and classification of fibrils

Lyocell and pulp fiber were cut to pass screen with holes of 1 mm in diameter by a Willey mill before treatment. After soaked in distilled water for more than 24 hours, they were treated by high intensity ultrasonication (HIUS) to isolate fibrils.

Table 5.1 Treatments and resources of the five types of fibrils

	Lyocell	TC40 A	TC40 B	Pulp	MFC
Resources	Regenerated cellulose	Pure cellulose	Pure cellulose	Paper mill	Wood fiber
Treatments	Ultrasonic	Ultrasonic	Homogenizer	Ultrasonic	Mechanical

The detailed isolation method of ultrasonic treatment was described in Chapter 3. For pure cellulose flours, both mechanical methods of high intensity ultrasonication (the same treatment as Lyocell fiber) and traditional high-pressure homogenizer (Stansted, Model nG12500, 220 MPa, 8 Passes) were used to generate fibrils. A method of classification of fibrils was needed because the diameters of the fibrils ranged from tens of nanometers to several micrometers. In this study, smaller fibrils with diameters less than 300 nm were used. All five types (Table 5.1) of fibril water suspensions were centrifuged with about a relative centrifugal force of 500 g and time for 5 min. After centrifugations and deposited for about 5 min, the most big fibrils of the suspensions with a concentration of 1% had sunk to the bottom of the tubes. The top layers, which had lower concentration of smaller fibrils, were kept for further morphological analysis and AFM three-point bending tests.

5.3.3. Morphology observations and sample preparation

A drop of fibril suspension was first dried on a silicon wafer with or without grooves at room temperature and then dried at 40~50ºC in an oven more than 2 hours to make sure the fibrils were completely dried. A scanning electron microscope (SEM, LEO 1525) and an AFM (PSIA, XE-100) were used to investigate the appearance and dimensions of the fibrils. Some 3D AFM images and optical images taken under microscopy were used to check the situation of fibrils suspended on the grooves of the silicon wafers.

5.3.4. Three-point bending test by AFM

The elastic modulus of the cellulose fibrils was obtained by performing a nanoscale three-point bending test on a single fibril suspended over the etched groove in a silicon wafer. The wafer has grooves with 5 μm in width and 1360 nm in depth (standard grating, MicroMasch). An AFM (PSIA, XE-100) cantilever tip was used to apply a small load at the midpoint along the suspended length of the fibrils. According to testing method described in Chapter 4, a silicon cantilever with nominal spring constant of 1.6 N/m, resonant frequency of 27 KHz was chosen (ZEILR, Nanosensor). The radius of curvature of the tip is less than 10 nm.

Figure 5.1 shows a schematic of the measurement of mechanical property using AFM (not in scale). AFM measurements were performed in ambient conditions under contact mode and the upper force limit was set to 200 nN or 400 nN with a loading rate of 1 μm/s. If the spring constant of the cantilever is too small, only very small force can be applied to the fibrils and the fibrils may be not bending. The F/D (force/displacement) function was used to measure and record the force applied on the tip and the cantilever displacement (Chapter 4).

5.3.5. Determination of the elastic modulus

The total deflection of beams under certain force deflection is the sum of the deflections due to bending and shear. But the shear deformation decreases with the increasing of the ratio of beam length to diameter, and it becomes important only for relatively short beams. In this case, the contribution of shear is negligible because the

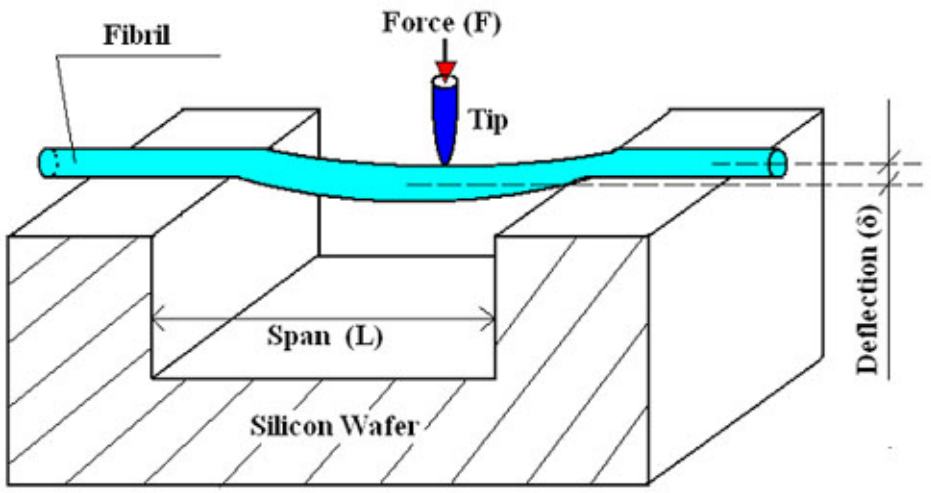

Figure 5.1 Schematic of the measurement of mechanical property using AFM

fibril worked as a long beam with the length to diameter ratio of more than 20. The elastic modulus (E) can be determined by the following equation as the pure bending formula.

$$E = \frac{FL^3}{192\,\delta I} \tag{5.1}$$

where F is the concentrated force loaded in the midpoint of a beam, L is the span, δ is the fibril deflection, I is the second moment of area of the beam ($I = \pi D^4/64$ for a filled cylinder with diameter of D). Testing on quarter spans (L/4 and 3L/4) were also performed (Chapter 4).

For this simplified model, it is assumed that the fibril is a pure elastic beam with both ends fixed (fixed-end beam). This means the adhesion between the fiber and the silicon substrate was high enough for the small load. And the fibrils were assumed to have cylinder cross-section (Gere and Timoshenko, 1997; Cheng and Wang, 2007).

The most important step was how to obtain the fibril deflection δ (Figure 5.1). The common method uses the force displacement curves from AFM (Figure 5.2) (Lee et al., 2005; Tan and Lim, 2004; Cheng and Wang, 2007). From the force displacement curve, the difference of Z-piezo displacement between the load on the fibril and load on reference was defined as the fibril deflection δ. Unlike some literatures using silicon wafer as reference (Tan and Lim, 2004), the testing position on the fibril laid on the wafer was chosen as reference because the sharp tips with radius of less than 10 nm could penetrate into the fibrils in the most cases (Chapter 4). At least six points on the fibril laid on the wafer were tested as reference to calculate the deflection of each fibril tested on the same wafer. The diameters of fibrils were obtained from the heights of fibrils in AFM images and not from the widths of the fibrils because the AFM tip could widely broaden

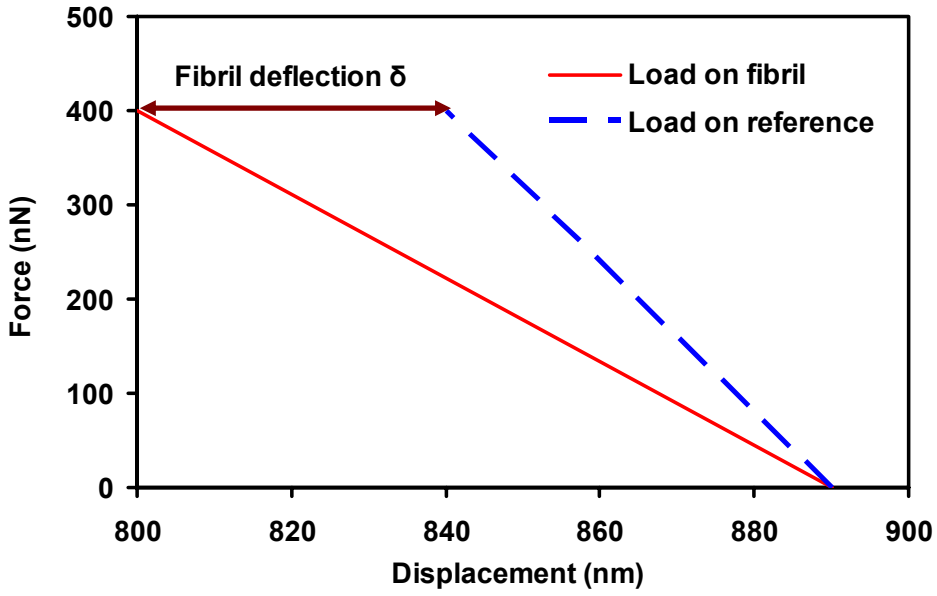

Figure 5.2 Schematic of the determination of fibril deflection during bending by AFM

the fibril widths (Demir et al., 2002; Simonsen, 2007). Two or more fibrils with similar diameter (±5 nm) were tested as one sample because it is very difficult to get two woody fibrils with exactly same diameter. The data of elastic of modulus were average from testing on midpoint and quarter spans of the fibrils above grooves with force limit of 200 nN and 400 nN.

Multiple comparisons by the Statistical Analysis System (SAS) (t Tests (LSD)) were used to detect the significant differences of elastic moduli of the fibrils isolated from different HIUS treatment time (30 or 60 min), from different mechanical treatments for TC40 (ultrasonication and homogenizer), and from different cellulose resources (pulp fiber and MFC) (α=0.05).

5.4. Results and Discussion

5.4.1. Morphology observations

SEM and AFM images (Figure 5.3) show that the fibrils made by mechanical methods had a large range in diameters, as well as the large range in length. The suspensions of the treated cellulose fibers were mixtures of fibrils in micro and nano scales. The fibrils suspended on the grooved silicon wafer are shown in Figure 5.4. Only good suspended fibrils were chosen and scanned (ovals in Figure 5.4, a). After scanned, only the straight fibrils on the grooves (Figure 5.4, b) were tested because the curved ones may have higher deflection variations when the none-perpendicular tip loads to the sample surface could cause slip and friction between the AFM tip and the sample surface during test (Li et al., 2003). Most of the fibrils made by mechanical methods were

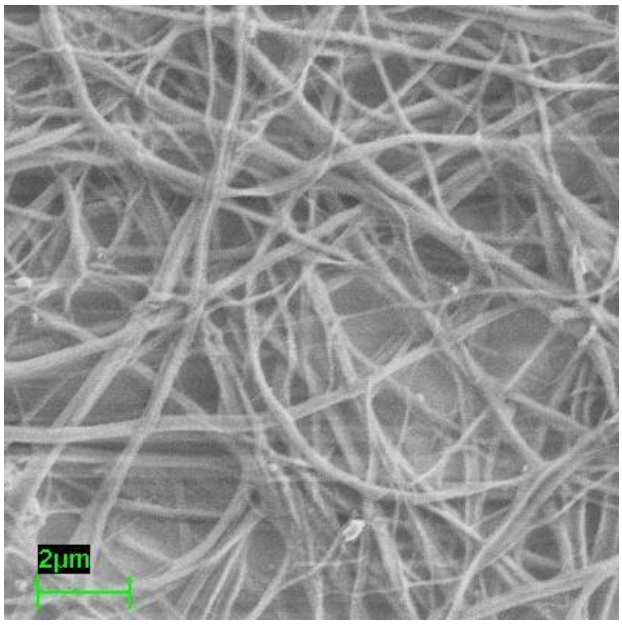

a)

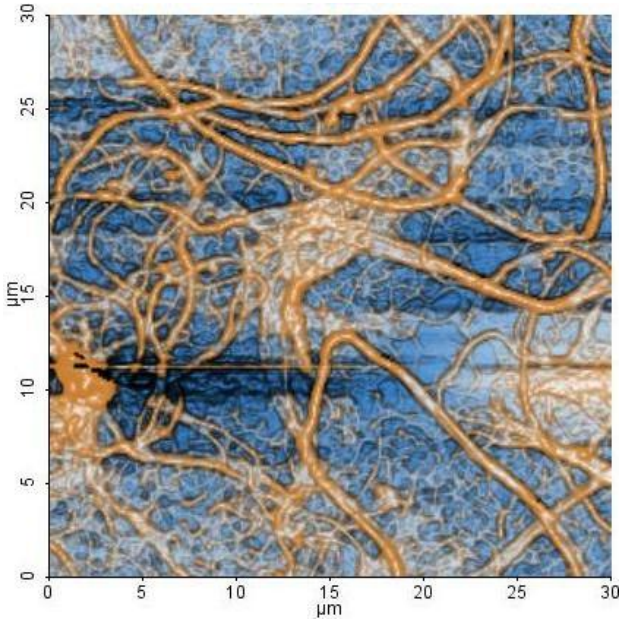

b)

Figure 5.3 SEM image of Lyocell fibrils (a) and AFM image of MFC fibrils (b)

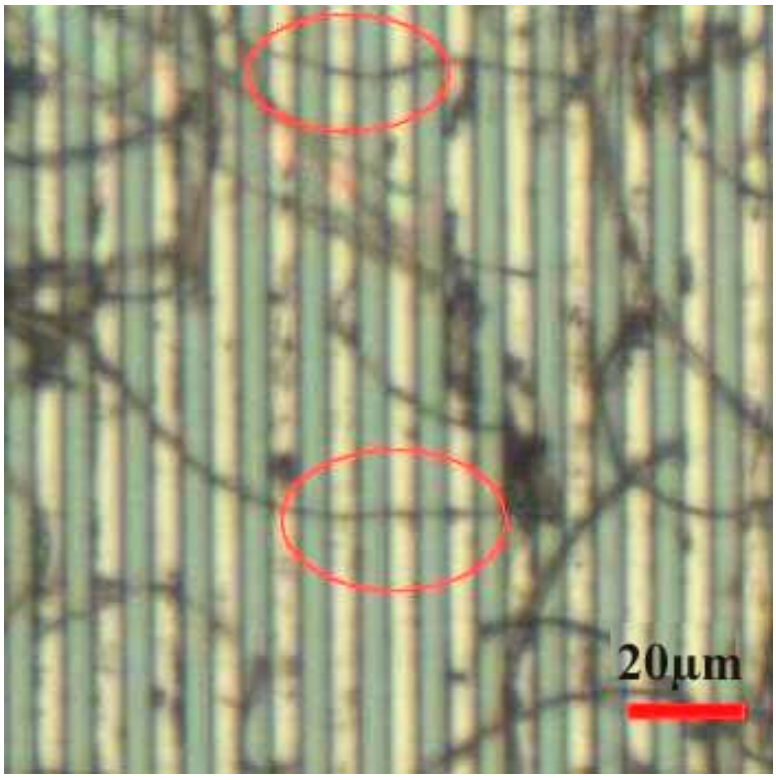

a)

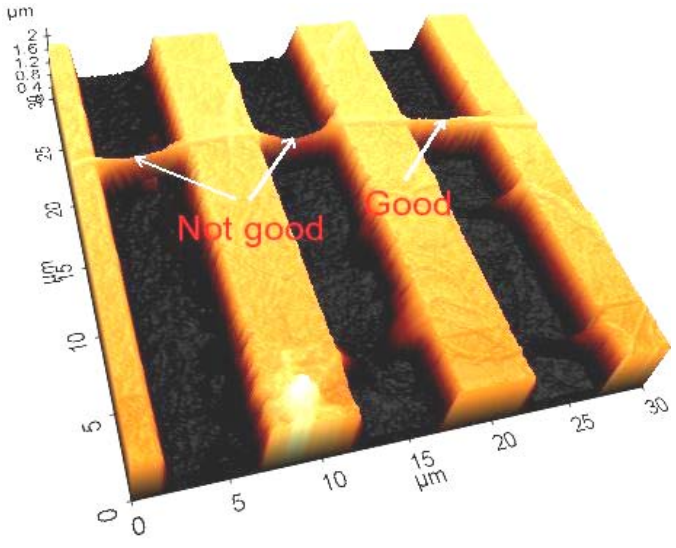

b)

Figure 5.4 Fibrils on grooved silicon wafer: optical image (a), AFM 3D image (b)

bundles of smaller microfibrils that can be observed with AFM images of MFC (Figure 5.5). The microfibrils were almost parallel with the longitudinal direction of the fibrils, which means that the fibrils were from the S_2 layer of the wood cell wall.

5.4.2. Reasonableness of assumptions

To check if the AFM tip penetrated into the fibril surfaces or not, small areas on the fibril surface were scanned before and after test (Figure 5.5). The tip was loaded in the circles in Figure 5.5. There was no significant change observed. This indicates that the maximum force of 400 nN did not cause indents on surface of fibrils so that the load was not used for the permanent deformation of the sample (Salvetat et al., 1999a; Tan and Lim, 2004). The elastic penetration depth was evaluated about 1 to 10 nm depending on the applied forces and surface roughness of fibrils. The force displacement curves of loading both on the tested fibrils above grooves and laid on silicon wafer were perfectly linear. This indicates the assumption that the deformation of the fibrils was purely elastic is reasonable. There were no fibrils that moved after scanned and tested by AFM under contact mode, so that the adhesion between the fiber and the silicon substrate was high enough to ensure the fibrils worked as fixed-end beams (Gere and Timoshenko, 1997).

Although the above assumptions are reasonable, it is necessary to pay attention if these elastic modulus values were used as the absolute value because the fibril surfaces were relatively rough and the diameter of the fibrils was not uniform (Figures 5.3 and 5.5). The cellulose fibril surfaces and diameters with diameter of more than 150nm were more complex than t hose of carbon nanotubes (Salvetat et al., 1999a; Salvetat et al.,

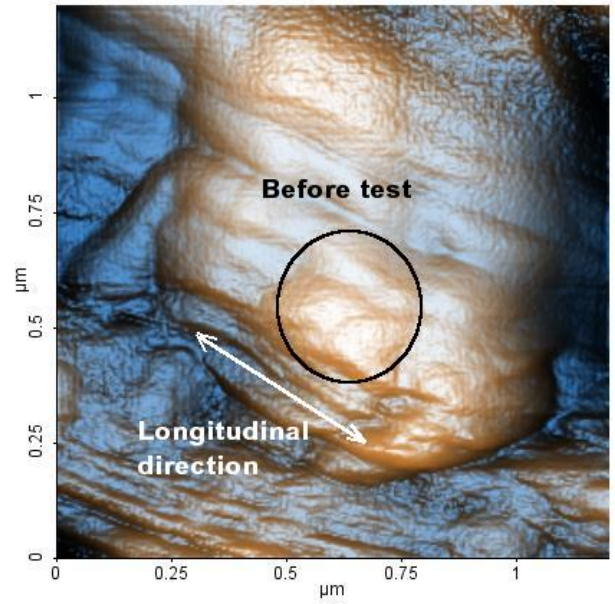

a)

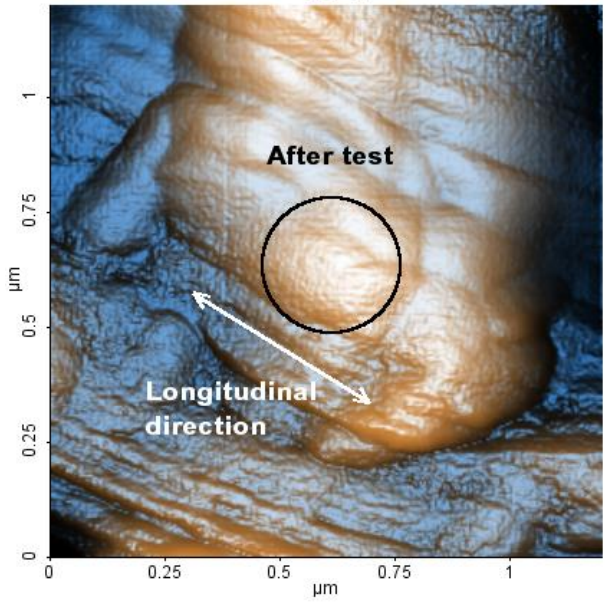

b)

Figure 5.5 AFM images of MFC fibril surface: before test (a) and after test (b)

1999b), PLLA nanofibers (Tan and Lim, 2004), and bacterial cellulose nanofibers (Wan et al., 2006). The shear deformation of the fibrils may have some contribution to the total deflection, although it was very small for long thin beams and could be completely ignored.

5.4.3. Elastic modulus of fibrils

Table 5.2 shows one sample of the diameter, deflection, and modulus of Lyocell fibrils made by 60 min ultrasonic treatment. Figure 5.6 shows the elastic moduli of the Lyocell fibrils with different diameters and different HIUS treatment time. The results indicated that the elastic moduli of Lyocell fibrils were not significantly different between 30 min and 60 min HIUS treatments. The elastic modulus of Lyocell fibrils with diameters from 150 to 180 nm was evaluated about 98 GPa, and decreased dramatically after the diameter was more than 180 nm. The same change trends were obtained for the carbon nanotube ropes that the modulus depends strongly on sample diameter. Because of the significance of shear deformation as span and diameter ratio decreased, the elastic modulus appeared to drop drastically when the diameter of the fibrils was more than 180 nm (Gere and Timoshenko, 1997; Salvetat et al., 1999a; Tan and Lim, 2004).

Another reason could be the size effect, which indicates that the tested mechanical properties of smaller specimens are higher than those of big ones. Size effect is a phenomenon that the volume of the body subjected to stress can influence the measured strength, especially for brittle materials. All materials have flaws at some level. How the material responds to these flaws determines whether a size effect is present. For ductile

Table 5.2 Diameter, deflection, and modulus of Lyocell fibrils by maximum AFM tip force of 200 nN

Group	Diameter (±2 nm)	Deflection (nm)*	Modulus (GPa)*
1	156	35.9±4.3	105.2±12.5
2	172	31.9±4.2	91.2±18.3
3	236	34.7±3.8	25.7±2.8
4	272	38.6±5.7	14.1±2.3

* Average ± standard deviation

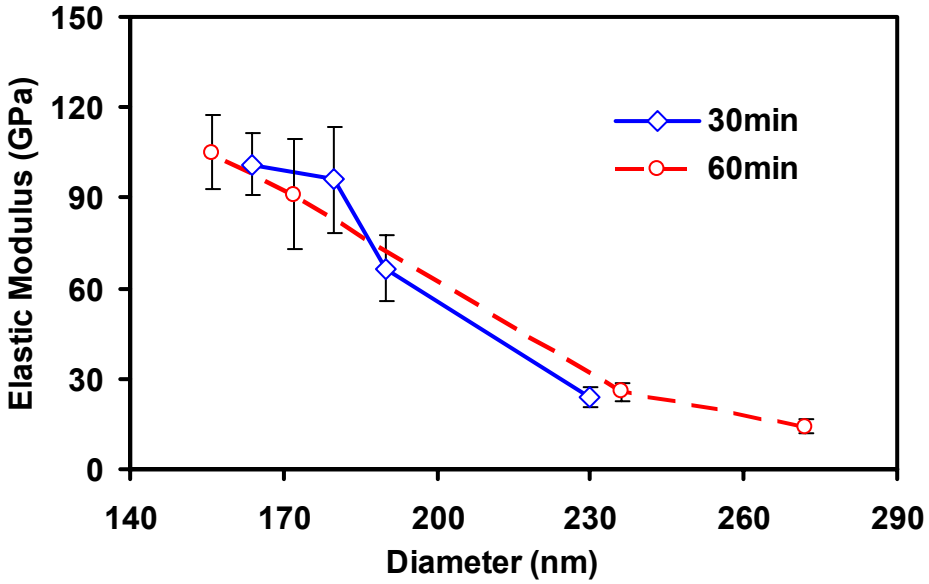

Figure 5.6 Tested elastic moduli of Lyocell fibrils with different diameters and treatment time

materials, a flaw-induced stress concentration is diminished by localized irreversible deformation, which desensitizes the material to the presence of a flaw. But brittle materials are subjected to the entire stress concentration because the stress concentration due to a flaw is not diminished. Initiations and propagations of local fracture lead to global failure of the material. And the local material response leads to the presence of a size effect (Ding et al., 2001; Odom and Adams, 1992). Griffith (1920) provided the support for the occurrence of a size effect for the first time. The presence of flaws was responsible for reducing the strength of isotropic materials. The number of flaws and the likelihood of the presence of larger flaws increases as the specimen size increasing. Material failure at lower overall stresses was leaded by the larger flaws and the associated stress concentration.

The moduli of TC40 fibrils with diameters of 270 and 230 nm treated by homogenizer and ultrasonication are shown in Figure 5.7. There was not significant difference between isolation methods of HIUS and high-pressure homogenizer for TC40. Figure 5.8 shows the moduli of pulp fibrils and MFC with diameters of 180 and 234 nm, and no big difference was observed between them. The Lyocell fibrils (~96 GPa) had higher modulus than pulp fibrils (~81 GPa) and MFC (~83 GPa) at diameter about 180 nm. This may be because regenerated cellulose fiber has higher strength and higher crystallinity than those of natural fibers.

The elastic moduli of Lyocell fibrils with diameters of 150 to 180 nm were lower than those of the crystal regions of cellulose the cellulose, which may be up to 137 GPa (Matsuo et al., 1990; Sakurada et al., 1962), and similar with the bacterial cellulose that

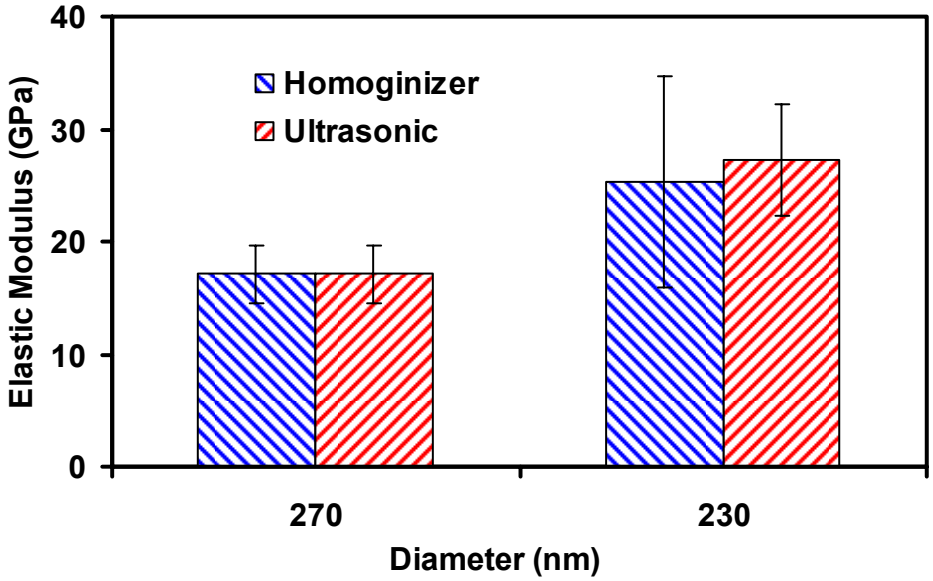

Figure 5.7 Tested elastic moduli of TC40 with different mechanical treatments

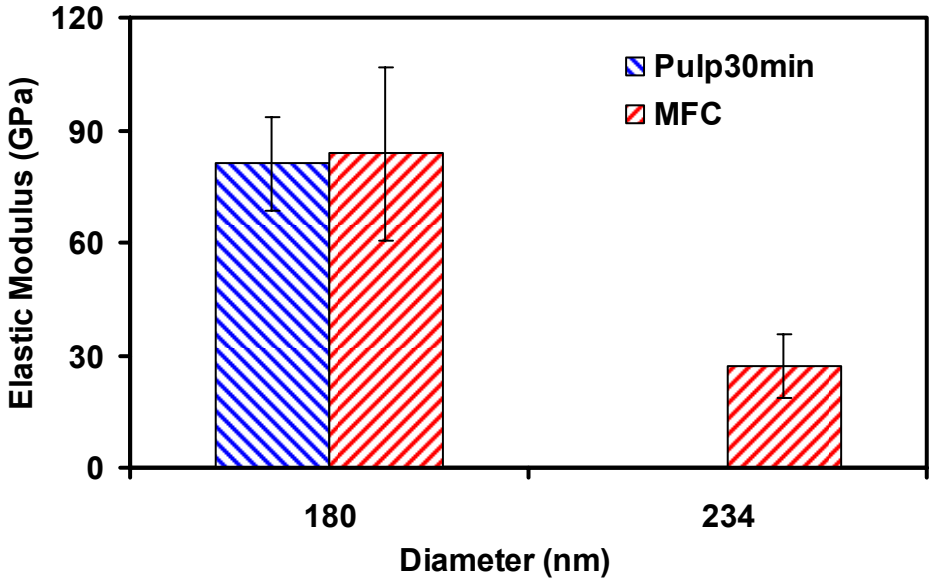

Figure 5.8 Tested elastic moduli of pulp fiber and MFC

had a value of modulus 84±16 GPa for the mean radii ranging from 31~72 nm (Wan et al., 2006). There are several reasons that may cause the moduli decreases besides the effects of different test methods. For example, the fibrils used in this paper were generated by mechanical methods with high shear force, which may degrade the mechanical property of the fibrils (Herrick, 1983; Iwamoto et al., 2007). The fibrils are bundles of microfibrils and the diameters are not small enough, which still includes amorphous regions and may have more defects than smaller fibrils or cellulose crystals. The surfaces of fibrils are relative rough and the diameters of the fibrils were not uniform.

5.5. Conclusions

Elastic moduli of single cellulose fibrils isolated by mechanical treatments can be evaluated by nano-scale three-point bending test performed by AFM. Most of the fibrils generated by mechanical methods were bundles of smaller nanofibrils and the fibrils had complex surfaces and wide range of diameters. The elastic modulus of single fibrils with diameters ranging from 150 to 300 nm can be measured by AFM using a silicon wafer with 5 μm in width of grooves. In this diameter range, the elastic moduli of Lyocell fibrils did not have significant differences between the HIUS treatment time of 30 min and 60 min. The modulus of Lyocell fibrils with diameters from 150 to 180 nm was evaluated about 98 GPa and it decreased dramatically when the diameter was more than 180 nm. The results also indicated that the elastic moduli of cellulose fibrils were not significantly different between isolation methods of HIUS and high-pressure

homogenizer, and between different cellulose sources of pulp fibers treated by homogenizer. The elastic modulus of fibrils from regenerated cellulose fibers was higher than that of natural fibers.

References

Beck-Candanedo, S., Roman, M. and Gray, D.G., 2005. Effect of reaction conditions on the properties and behavior of wood cellulose nanocrystal suspensions. Biomacromolecules, 6(2): 1048-1054.

Berglund, L., 2005. Cellulose-based nanocomposites. In: A.K.M. Mohanty, M.; Drzal, L. (Editor), Natural Fibers, Biopolymers, and Biocomposites. Taylor & Francis, pp. 807-832.

Chakraborty, A., Sain, M. and Kortschot, M., 2005. Cellulose microfibrils: A novel method of preparation using high shear refining and cryocrushing. Holzforschung, 59(1): 102-107.

Cheng, Q. and Wang, S., 2007. A method for testing the elastic modulus of single cellulose fibrils via atomic force microscopy (In preparation).

Cheng, Q., S. Wang, Zhou, D., Zhang, Y. and Rials, T.G., 2007a. Lyocell-derived cellulose microfibril/nanofibril and its biodegradable nanocomposites. Journal of Nanjing Forestry University, 31(4): 21-26.

Cheng, Q., Wang, S., Rials, T.G., Lee, S.H., 2007b. Physical and mechanical properties of polyvinyl alcohol and polypropylene composite materials reinforced with fibril

aggregates isolated from regenerated cellulose fibers. Cellulose, online first, DOI: 10.1007/s10570-007-9141-0.

Demir, M.M., Yilgor, I., Yilgor, E. and Erman, B., 2002. Electrospinning of polyurethane fibers. Polymer, 43(11): 3303-3309.

Ding, J.N., Meng, Y.G. and Wen, S.Z., 2001. Specimen size effect on mechanical properties of polysilicon microcantilever beams measured by deflection using a nanoindenter. Materials Science and Engineering B-Solid State Materials for Advanced Technology, 83(1-3): 42-47.

Dufresne, A., Cavaille, J.Y. and Vignon, M.R., 1997. Mechanical behavior of sheets prepared from sugar beet cellulose microfibrils. Journal of Applied Polymer Science, 64(6): 1185-1194.

Eichhorn, S.J. and Young, R.J., 2001. The Young's modulus of a microcrystalline cellulose. Cellulose, 8(3): 197-207.

Gere, J.M. and Timoshenko, S.P., 1997. Mechanics of materials. PWS Publishing Company, Boston, MA.

Griffith, A.A., 1920. Phenomena of rupture and flow in solids. Philosophical Transactions of the Royal Society of London Phi, 221(A):163–198.

Herrick, F.W.C., R. L.; Hamilton, J. K.; Sandberg, K. R., 1983. Microfibrillated cellulose: morphology and accessibility. Journal of Applied Polymer Science: Applied Polymer Symposium, 37: 797-813.

Iwamoto, S., Nakagaito, A.N. and Yano, H., 2007. Nano-fibrillation of pulp fibers for the processing of transparent nanocomposites. Applied Physics a-Materials Science & Processing, 89(2): 461-466.

Li, X.D., Hao, H.S., Murphy, C.J. and Caswell, K.K., 2003. Nanoindentation of silver nanowires. Nano Letters, 3(11): 1495-1498.

Lee, S.H., Tekmen, C. and Sigmund, W.M., 2005. Three-point bending of electrospun TiO2 nanofibers. Materials Science and Engineering A: Structural Materials Properties Microstructure and Processing, 398(1-2): 77-81.

Lima, M.M.D. and Borsali, R., 2004. Rodlike cellulose microcrystals: Structure, properties, and applications. Macromolecular Rapid Communications, 25(7): 771-787.

Matsuo, M., Sawatari, C., Iwai, Y. and Ozaki, F., 1990. Effect of orientation distribution and crystallinity on the measurement by X-ray-diffraction of the crystal-lattice moduli of cellulose-I and cellulose-II. Macromolecules, 23(13): 3266-3275.

Mott, L., Shaler, S.M. and Groom, L.H., 1996. A technique to measure strain distributions in single wood pulp fibers. Wood and Fiber Science, 28(4): 429-437.

Odom, E.M. and Adams, D.F., 1992. Specimen size effect during tensile testing of an unreinforced polymer. Journal of Materials Science, 27(7): 1767-1771.

Page, D.H., Winkler, K., Bain, R. and Elhossei, F., 1972. Mechanical properties of single wood-pulp fibers. 1. New approach. Pulp and Paper Magazine of Canada, 73(8): 72.

Sakurada, I., Nukushina, Y. and Ito, T., 1962. Experimental determination of elastic modulus of crystalline regions in oriented polymers. Journal of Polymer Science, 57(165): 651-660.

Salvetat, J.P., Briggs, G.A.D., Bonard, J.M., Bacsa, R.R., Kulik, A.J., Stockli, T., Burnham, N.A. and Forro, L., 1999a. Elastic and shear moduli of single-walled carbon nanotube ropes. Physical Review Letters, 82(5): 944-947.

Salvetat, J.P., Kulik, A.J., Bonard, J.M., Briggs, G.A.D., Stockli, T., Metenier, K., Bonnamy, S., Beguin, F., Burnham, N.A. and Forro, L., 1999b. Elastic modulus of ordered and disordered multiwalled carbon nanotubes. Advanced Materials, 11(2): 161-165.

Salvetat-Delmotte, J.P. and Rubio, A., 2002. Mechanical properties of carbon nanotubes: a fiber digest for beginners. Carbon, 40(10): 1729-1734.

Simonsen, J., 2007. Cellulose nanocrystal composites. http://woodscience.oregonstate.edu/faculty/simonsen/.

Tan, E.P.S. and Lim, C.T., 2004. Physical properties of a single polymeric nanofiber. Applied Physics Letters, 84(9): 1603-1605.

Taniguchi, T., 1996. Microfibrillation of natural fibrous materials. J. Soc. Mat. Sci. Japan, 45(4): 472-473.

Turbak, A.F.S., F. W.; Sandberg, K. R., 1983. Microfibrillated cellulose, a new cellulose product: properties, uses, and commercial potential. Journal of Applied Polymer Science: Applied Polymer Symposium, 37: 815-827.

Wan, W.K., Hotter, J.L., Million, L. and Guacos, G., 2006. Bacterial cellulose and its nanocomposites for biomedical applications. Cellulose Nanocomposites: Processing, Characterization, and Properties. Aces Symposium Series, pp. 221-241.

Wong, E.W., Sheehan, P.E. and Libber, C.M., 1997. Nan beam mechanics: Elasticity, strength, and toughness of nanorods and nanotubes. Science, 277(5334): 1971-1975.

Xing, C., Wang, S., Pharr, G.M. and Groom, L.H., 2007a. Effect of thermo-mechanical refining pressure on the properties of wood fiber cell walls: measured by nanoindentation and AFM. Holzforschung (in print).

Xing, C., Wang, S., Pharr, G.M. and Groom, L.H., 2007b. Comparison of the effects of thermomechanical refining pressure on the properties of refined fibers of juvenile and mature wood (submitted to Cellulose).

Xu, W., Muller, P.J., Blackford, B.L., Jericho, M.H. and Templeton, I., 1994. A new atomic-force microscopy technique for the measurement of the elastic properties of biological-materials. Scanning Microscopy, 8(3): 499-506.

CHAPTER 6. COMPOSITE MATERIALS REINFORCED WITH CELLULOSIC FIBRILS ISOLATED FROM LYOCELL FIBERS BY HIGH-INTENSITY ULTRASONICATION

6.1. Abstract

Natural fibers in micro and nano scales may be a potential alternative for man-made fibers because of the comparable mechanical properties to those of glass, carbon, and aramid fibers. Cellulose fibril and fibril aggregate are generally prepared by physical treatments, e.g., high-pressure homogenizer, or chemical treatments, e.g., acid hydrolysis. In this study, fibril aggregates were generated from a regenerated cellulose fiber by ultrasonication treatment. The geometrical characteristics of the fibers and the fibril aggregates were investigated using scanning electron microscopy (SEM) and polarized light microscopy (PLM), and their crystallinities were investigated by wide angle X-ray diffraction (WAXD). The degree of fibrillation of the fibers is indirectly evaluated by water retention value (WRV). Nano-biocomposites of poly(vinyl alcohol) (PVA), poly(lactic acid) (PLA), and polypropylene (PP) reinforced with fibril aggregates were prepared by film casting and compression molding. The mechanical properties of the composites were evaluated by tensile test. The morphological characteristics of the nanocomposites were investigated with SEM and PLM. As reference, commercial microfibrillated cellulose was also used to reinforce biodegradable polymer.

Keywords: Composite, Fibril, Fibril aggregate, Micro, Nano, Morphology, Mechanical property, Regenerated cellulose fiber

6.2. Introduction

The main structural component of plants is cellulose, which is renewable and biodegradable. It is the most abundant natural biopolymer in the world. Natural cellulose fibers are synthesized mainly in plants such as grasses, reeds, stalks, and woody vegetation by photosynthesis. The natural fibers are attractive to replace man-made fibers such as glass and aramid fibers as reinforcement and fillers to make environmentally friendly products because they have many advantages such as renewable, low cost, low density, low energy consumption, high specific strength and modulus, high sound attenuation, nonabrasive, relatively reactive surface (George et al., 2001). Fibrils in nano scales generated from natural fibers have much higher mechanical properties, such as the cellulose crystal regions are a bundle of stretched cellulose chain molecules with Young's modulus of up to 137 GPa (Sakurada et al., 1962), and elastic modulus of Lyocell fibrils with diameter from 150 nm to 180 nm was evaluated about 98 GPa (Chapters 4 and 5). In the past two decades, much attention has been paid to study how to make fibrils and fibril aggregates and how to combine them with polymers to make nanocomposites (Berglund, 2005; Herrick et al., 1983; Turbak et al., 1983). Nanocomposite is a broad concept that includes at least one-dimensional of one component in the composite at the nanometer scale (1-100 nm).

Two main methods have been used to generate cellulose fibrils and fibril aggregates. One is the chemical way, mainly by strong acid hydrolysis, which removes the amorphous regions of cellulose fiber and produces nano-size fibrils. Cellulose whisker and cellulose nanocrystal have been used to describe nano-size cellulose fibrils.

Many sources have been used for fibril isolation by chemical method, such as wood fibers (Beck-Candanedo et al., 2005; Bondeson et al., 2006), cotton (Choi and Simonsen, 2006), sea animals such as tunicate mantles (Sturcova et al., 2005), sugar beet pulp (Dufresne et al., 1997), and potato tuber cells (Dufresne et al., 2000). The other is the mechanical method, which includes a high pressure refiner treatment (Chakraborty et al., 2005), a grinder treatment (Taniguchi, 1996), a microfluidizer (Zimmermann et al., 2004), a high-pressure homogenizer treatment (Dufresne et al., 1997; Herrick et al., 1983; Nakagaito and Yano, 2005; Turbak et al., 1983), and high-intensity ultrasonication (Chapter 3, Cheng et al. 2007 a and b). Main product generated by these mechanical methods is no single fibril and has been referred as cellulose microfibril and mcirofibrillated cellulose (MFC). MFC is used in some industrial applications, such as food, cosmetic, and medicinal products (Lima and Borsali, 2004). The research on nanocomposites reinforced by cellulose fibrils has grown very fast because of its environmentally friendly feature and the improvement of stiffness and/or strength in recent years (Samir et al., 2004; Zimmermann et al., 2004). There are two major fabrications of nanocomposites. One is film casting using water-soluble or solvent-soluble polymers (Chakraborty et al., 2006b; Favier et al., 1995), and the other is freeze drying followed by classical compression or extrusion processes (Hajji et al., 1996).

Lyocell fiber is a regenerated cellulose fiber, which is a 100% cellulose fiber derived from wood-pulp. It is produced by dissolving wood pulp in a solution of hot N-methyl morpholine oxide and then spinning the solution into fibers. It is a biodegradable and extremely strong fiber with industrial uses such as in automotive filters, ropes,

abrasive materials, bandages, protective suiting material, and clothing (Woodings, 2000). Untreated Lyocell was used to reinforce thermoplastic commodity polymers with some coupling agents (Ganster and Fink, 2006). The fibril aggregates were isolated from regenerated cellulose fiber by a novel mechanical process – high intensity ultrasonication (see Chapter 3).

The purpose of this research was to investigate the physical and mechanical properties of poly(vinyl alcohol) (PVA, biodegradable), poly(lactic acid) (PLA, biodegradable), and polypropylene (PP, non-biodegradable) composite materials reinforced with fibril aggregates isolated from Lyocell fiber. The fibers and fibril aggregates were characterized by scanning electron microscopy (SEM), polarized light microscopy (PLM), wide angle X-ray diffraction (WAXD), and water retention value (WRV). PVA composites were prepared by film casting. PLA and PP composites were prepared by compression molding. The tensile properties and morphologies of the composites were evaluated and compared.

6.3. Experimental

6.3.1. Materials

Lyocell fiber (provided by Lenzing) was used as raw material. It was 11 μm in diameter and cut to pass a screen (room temperature and relative humidity of 30%) with holes of 1 mm in diameter by a Willey mill before treatment. Commercial microfibrillated cellulose (MFC 10% solid slurry, Daicel Chemical Industries, LTD., Japan) was used as a reference. Biodegradable polymers: poly(vinyl alcohol) (PVA,

99+% hydrolyzed, typical average M_W 85,000-124,000, purchased from Sigma-Aldrich) and poly(lactic acid) (PLA), and synthetic non-biodegradable polymer: polypropylene fiber (PP, provided by FiberVisions, Georgia), were used as matrixes.

6.3.2. Fibrils isolation and composites preparation

Lyocell fiber was soaked in distilled water for more than 24 hours and then treated 30 min by high intensity ultrasonication. The details of the mechanical method for fibril isolation were described in Chapter 3. The reinforcement material used in this study was different comparing with MFC and single crystal fibril, so a term of fibril aggregate was used. A film casting method was used to make fibril-reinforced PVA composites. PVA water solution (10% W/W) and cellulose fibril aggregate water suspension were mixed and stirred manually and then dispersed by ultrasonic treatment (Sonic Newtown, CT, 20 kHz, Model 1500 W) for about one minute with 50% power level. After degassing in a desiccator by vacuum for more than two days, the mixtures were evaporated in room temperature and relative humidity of 30% until films were formed with a nominal thickness of 150 μm. Then the films were dried in an oven at 70 °C for more than 4 hours (Figure 6.1).

For PLA composites, the fibril aggregates and the PLA polymer were combined together using multiple layers followed by compressive molding (Figure 6.2). Five layers included two fibril mats made by filtration system, which consisted of a set of filtration assemblies (Labglass) and a membrane filter (Millipore isopore, 0.4 μm pore size), and three PLA films made by hot compression press with nominal thickness of 51 or 127 μm

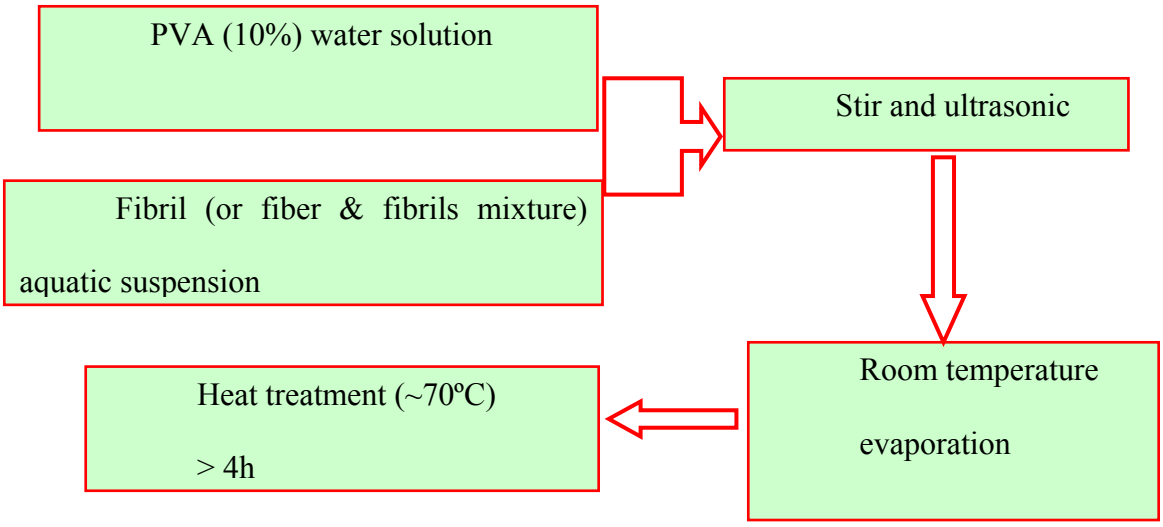

Figure 6.1 Flow chart of the fabrication of PVA and fibril composites by film casting

Figure 6.2 Sandwich structure of PLA and treated fiber composites for compressive molding

and hot pressed at a temperature of 170°C. After the fibril mats were dried, the five layers were put in a round metal mold with nominal thickness of 254 μm and hot pressed at a temperature of 170 °C and a pressure of 5 MPa for about 5 min.

The PP composites were made from filtered mats of cellulose fibril aggregates and PP fibers by compression molding. The mats were made from the well-stirred mixture of cellulose fibril aggregates and PP fibers by a filtration system used the same setup above for fibrils mats. After drying the mats were put in a round metal mold with nominal thickness of 254 μm and hot pressed at a temperature of 170°C and a pressure of 5 MPa for around 5 minutes.

6.3.3. Water retention value

Water retention value (WRV) can be used to measure the degree of homogenization or microfibrillation, which is related to fibril and microfibril surface and volumetric phenomena (Herrick et al., 1983). WRV is a percent ratio of the water contained in the sample after centrifuged in force and time to the dry weight of the sample. A 25-mm diameter stainless steel cap with diameter of 1 mm holes and a filter membrane with 0.2-μm pore-size (Whatman Nuclepore) were used to hold and filter the wet mass. Two caps were filled with the wet sample (about 0.5 g in dry weight) and placed inside the carriers. After centrifuged (AccuSpin 400) for 30 minutes and a relative centrifugal force (RCF) of 900 g (RCF is given in multiples of the earth gravity g and a dimensionless number) at room temperature, the samples were weighed and oven dried at 80°C for 24 hours and

then dried at 103°C until they reached constant weight. Equation (6.1) was used to calculate WRV (Figure 6.3).

$$\mathrm{WRV} = \frac{W_{Wet} - W_{Dry}}{\mathrm{W_{Dry}}} \times 100\% \tag{6.1}$$

where W_{Wet} is the weight of the sample after centrifugation, and W_{Dry} is the dry weight of the sample.

6.3.4. Crystallinity

The crystallinity of the fibers and fibril aggregates was studied by wide angle X-ray diffraction (WAXD) (Cheng et al., 2007; Thygesen et al., 2005). The equipment (Molecular Metrology) was a pinhole type camera that recorded the patterns on Fuji

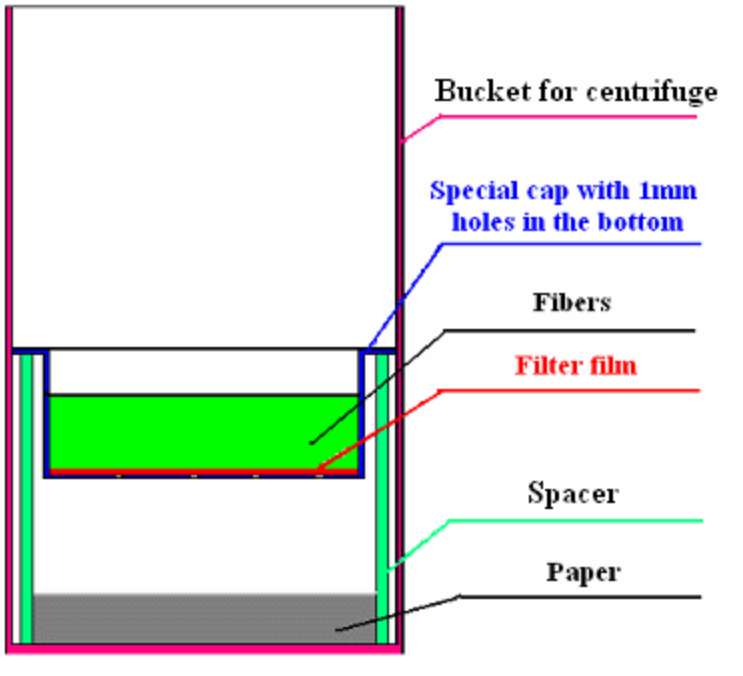

Figure 6.3 Water retention value (WRV) measurement setup for centrifuge

image plates. The operating voltage was 45 kV, current was 0.66 mA, and the exposed period was 50 minutes using CuKa radiation with a wavelength of 0.15418 nm. The crystallinity is defined as the ratio of the amount of crystalline cellulose to the total amount of sample material, including crystalline and amorphous parts. The Segal method was used to calculate the crystallinity of the samples (Thygesen et al., 2005). Three samples were tested for each composition. A typical WAXD curve used to determine the crystallinity by Segal method is shown in Figure 6.4. Equation (6.2) was used to calculate the sample crystallinity (X_{CR}).

$$X_{CR} = \frac{I_{200} - I_{AM}}{I_{200}} \times 100\% \tag{6.2}$$

where I_{200} is the height of the 200 peak, which represents both crystalline and amorphous material; and I_{AM} is the lowest height between the 200 and 110 peaks, which represents amorphous material only.

6.3.5. Morphology observations

The appearance and dimensions of the treated and untreated Lyocell fibers were investigated by polarized light microscopy (PLM, Olympus-BX51) and a digital image analysis software package (ImageJ). Some fibers and fibril aggregates were measured by the software using pixels in the images, such as 4.32 pixels/μm for 200 magnification images. The Morphology of the fibrils and fractured surfaces of the composites were examined using a scanning electron microscopy (SEM, LEO 1525). Some dried samples of fibril aggregate suspension on silicon wafers were observed by SEM. The fractured surfaces of the composites were coated with gold on an ion sputter coater, and operating

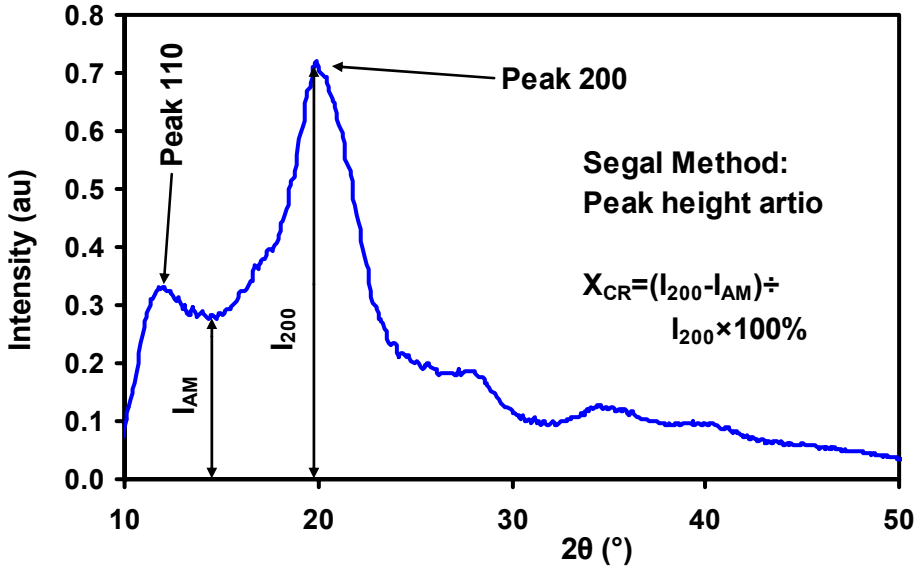

Figure 6.4 A typical WAXD curve used for the crystallinity determination

voltages of SEM were 5 to 10 kV and various magnification levels were used to obtain images. PLM was also used to observe the distributions of the fibers and fibril aggregates in the composites. At least three images (for both PLM and SEM) were taken and chosen to observe the morphology of all samples, but just some of the features selected randomly in the micrographs were measured because the features could not be precisely measured easily and the treated fibers with fibrils on surfaces and the big fibrils with diameter of more than 1 μm dominate in the treated fiber material.

6.3.6. Mechanical testing

The mechanical tests were performed about one week after the composites were fabricated. An Instron testing machine (model 5567) was used to test the mechanical properties of composites with a length of 20 mm between the top and bottom clamps, a

crosshead speed of 1 mm/min, and a load cell of 30 kN (Figure 6.5). The specimens were cut to dogbone shapes with width of 5 mm for the narrow portion and total length of 40 mm. At least five specimens were tested for each composition according to the ASTM D1708 standard for tensile testing on plastics (ASTM, D 1708-2002a). Tensile modulus was tangent modulus from the linear portion in the stress-strain curves. Multiple comparisons by the Statistical Analysis System (SAS) (t Tests (LSD)) were used to detect the overall significant differences of the influences on the tensile elastic modulus and strength of composites reinforced with untreated and treated Lyocell fibers (α=0.05).

6.4. Results and Discussions

First, the morphology, crystallinity, and degree of fibrillation of the untreated and treated Lyocell fibers by HIUS were investigated and discussed. Second, the tensile modulus and strength of PVA, PLA, and PP composites reinforced with the untreated and treated Lyocell fibers were evaluated and compared. Finally, the cross-section morphologies of the composites after tensile tests were observed by SEM, and the distribution of the fiber and fibrils was investigated by PLM.

6.4.1. Morphology of fibers and fibrils

A mixture suspension of fibril aggregates with diameter ranging from microns to tens of nanometers was obtained after 30 minutes treatment. The PLM overview appearance of a single untreated Lyocell fiber (inset figure) and some treated fibers are

Figure 6.5 Instron testing machine (model 5567)

shown in Figure 6.6. It can be seen from the figure that many small fibril aggregates with diameter less than 1μm were peeled from the fibers. Some fibril aggregates were still on the surfaces of the big ones that dominate the treated fibers with about 95% in weight (Figure 6.6), while some were already isolated from the big fibers as shown in Figure 6.7. The structure and appearance of the cellulose fibril aggregates on silicon wafers observed by SEM are shown in Figure 6.7. The diameters or widths of the fibril aggregates isolated from Lyocell fibers were in a wide range of tens to hundreds nm, and have a wide range of aspect ratio (length/diameter); most are more than 50 as evident from the measurements of randomly selected features (Figure 6.7). This aspect ratio is suitable for polymer reinforcement (Chakraborty et al., 2006a). Beck-Candanedo et al.

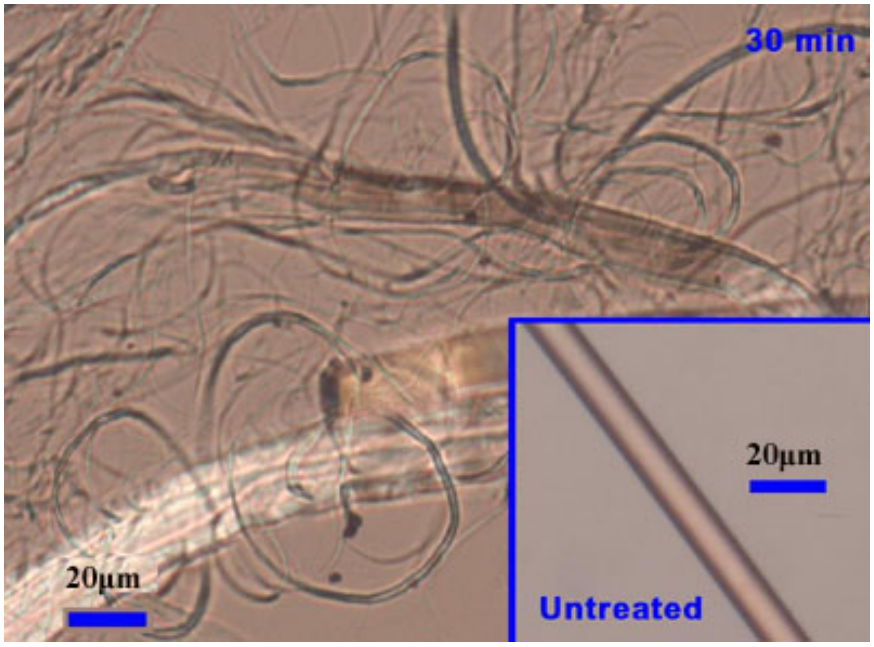

Figure 6.6 Structure and appearance of treated and untreated Lyocell fibers

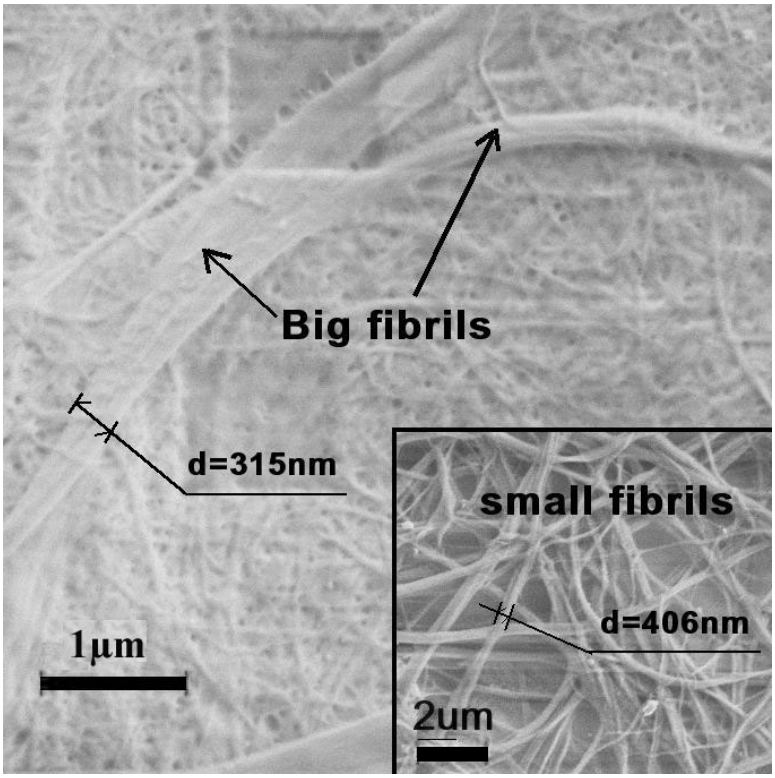

a)

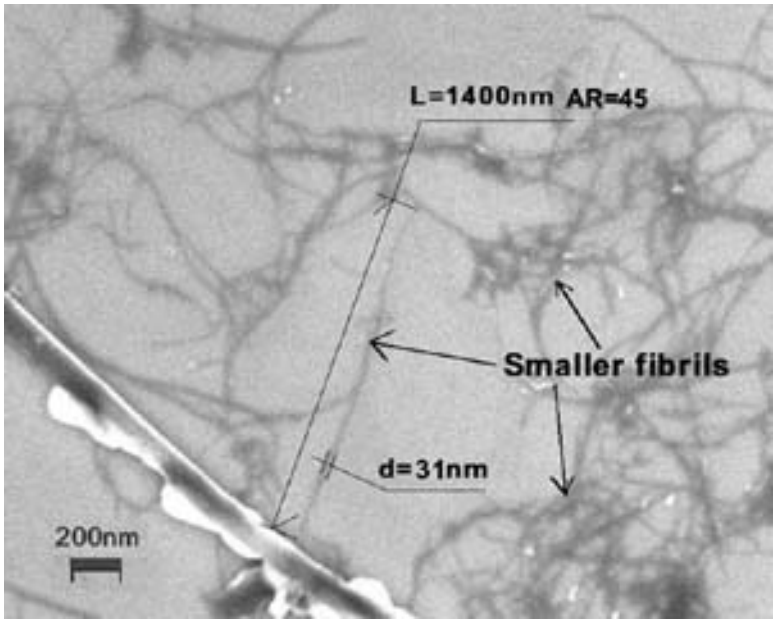

b)

Figure 6.7 SEM images of fibrils isolated from Lyocell fiber (AR=Aspect Ratio)

(2005) reported the diameter of the cellulose nano-crystals to have diameters of 3-5 nm. Therefore the fibers represented in our micrographs must be considered fibril aggregates rather than individual cellulose nano-crystals.

6.4.2. Water retention value of fibers and fibrils

Figure 6.8 shows the WRV with standard deviations of the untreated and treated Lyocell fibers for different treatment time. The degree of microfibrillation of the treated fibers increased as the treatment time increasing because WRV is related to fibril and microfibril surface and volumetric phenomena (Herrick et al., 1983). It indicates that the fibers become smaller and more surface area on the fibrils as treatment time increasing. The longer the treatment time, the smaller the fibril aggregates can be obtained in the suspension mixture.

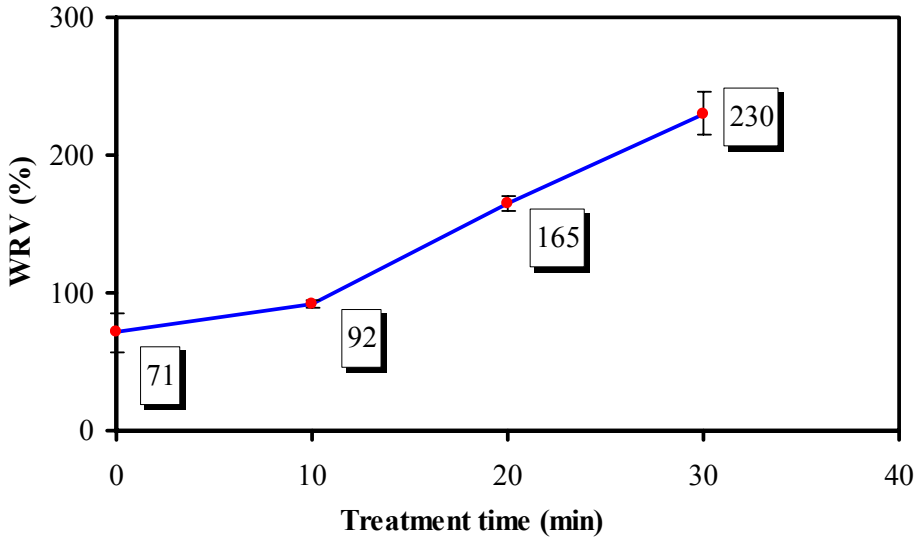

Figure 6.8 WRV of untreated and treated Lyocell fibers with different treatment time

6.4.3. Crystallinity of fibers and fibrils

The crystallinity of the treated Lyocell fibers increased as the treatment time increasing. The results measured by WAXD are shown in Table 6.1 (average of three samples with standard deviation). All the four cellulose samples have a narrow peak at 2θ of about 20° and a lower peak at 2θ of about 12° (Figure 6.4 and 6.9). The crystallinity of untreated Lyocell cellulose was calculated to be 61% from the X-ray diffraction patterns, which was reasonable according to the published values of about 64.04% and 72.56% for Lyocell-I and Lyocell-II respectively (Peng et al., 2003). A reason the crystallinity of fiber and fibril aggregate mixture went up with the treatment time increasing may be that some of the amorphous cellulose were degraded and removed during the mechanical treatment. High crystalline fibers and fibril aggregates could be more effective in achieving higher reinforcement for composite materials (Eichhorn and Young, 2001).

6.4.4. Mechanical properties of the composites

PVA composites by film casting

Figure 6.10 shows typical tensile curves of neat PVA and its composites with 2%, 6%, and 10% of treated Lyocell fibers. The tensile strength of 2% loading reinforced composite was higher than pure PVA. The elongations to break were significantly

Table 6.1 The crystallinities of untreated and treated Lyocell fibers measured by WAXD

Treatment Time (min)	0	10	20	30
Crystallinity	61.0	70.0	75.8	72.4
Standard Deviation	0.4	1.6	1.5	5.1

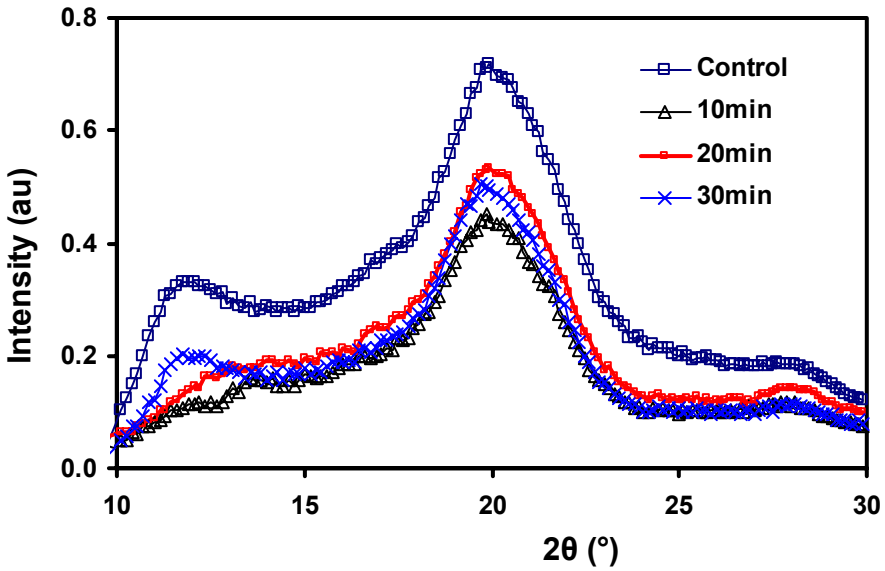

Figure 6.9 WAXD curves for untreated and treated fibers

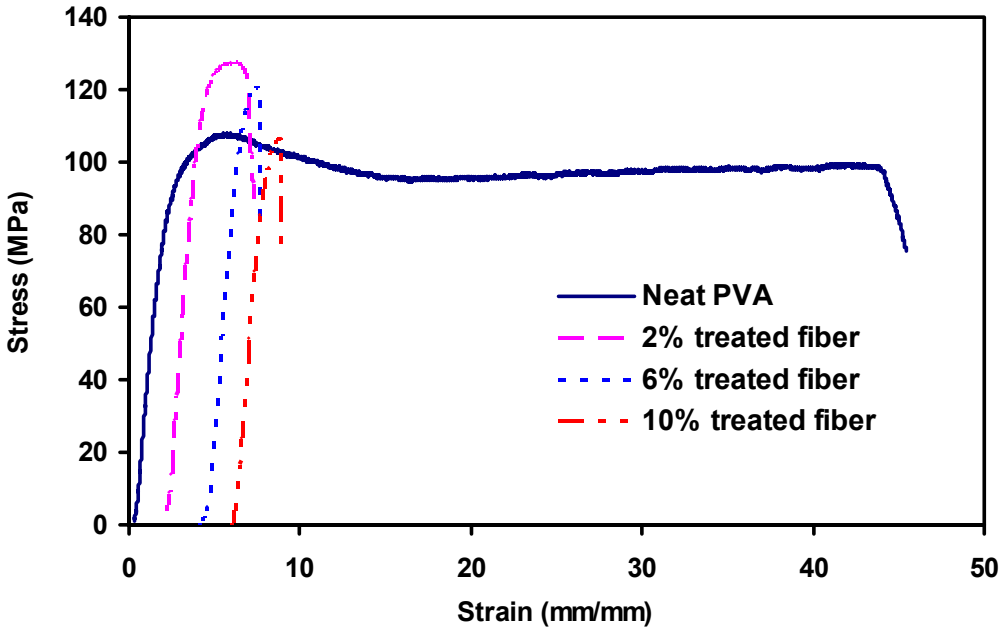

Figure 6.10 Typical stress-strain curves of PVA and its composites

decreased for the composites compared to the pure PVA. This means that the composites are more brittle than the pure PVA.

The tensile modulus and strength of neat PVA and its composites reinforced by untreated and treated Lyocell fibers, and MFC of 2%, 6%, and 10% by weight (W/W) are shown in Figure 6.11 and Figure 6.12, respectively. The tensile modulus of neat PVA was increased by all the three contents of fibers and fibril aggregates, but the modulus changes were not significant (α=0.05) among the loadings of 2%, 6%, and 10% except between the 2% and 6% of MFC (Figure 6.11). The tensile strength of PVA was decreased by untreated Lyocell fiber and MFC, but it was increased by treated Lyocell fibers although the increments were not significant (α=0.05) (Figure 6.12).

For treated Lyocell fibers, both modulus and strength of PVA were improved because of the small fibrils. The reinforcement of MFC was better than untreated Lyocell fibers and similar with treated Lyocell fibers for tensile modulus (Figure 6.11) but not as good as treated Lyocell fibers for tensile strength (Figure 6.12). One reason was that the aspect ratio of the fibrils was smaller for MFC than that of treated Lyocell fibers as discussed in the following part of the composite morphology.

By adding 2% of treated Lyocell fibers, the tensile modulus of the PVA composite was about 15% higher than neat PVA film, and the tensile strength was improved about 6%. The improvements were not as high as those of the films cast with microfibers (0.1-1 μm in diameter) generated from wood pulp in PVA, with doubling (from about 42 to 102 MPa) of tensile strength and a 2.5-fold (from about 2.3 to 5.2 GPa) increase in stiffness by 5% microfiber loading (Chakraborty et al., 2006b). This may be

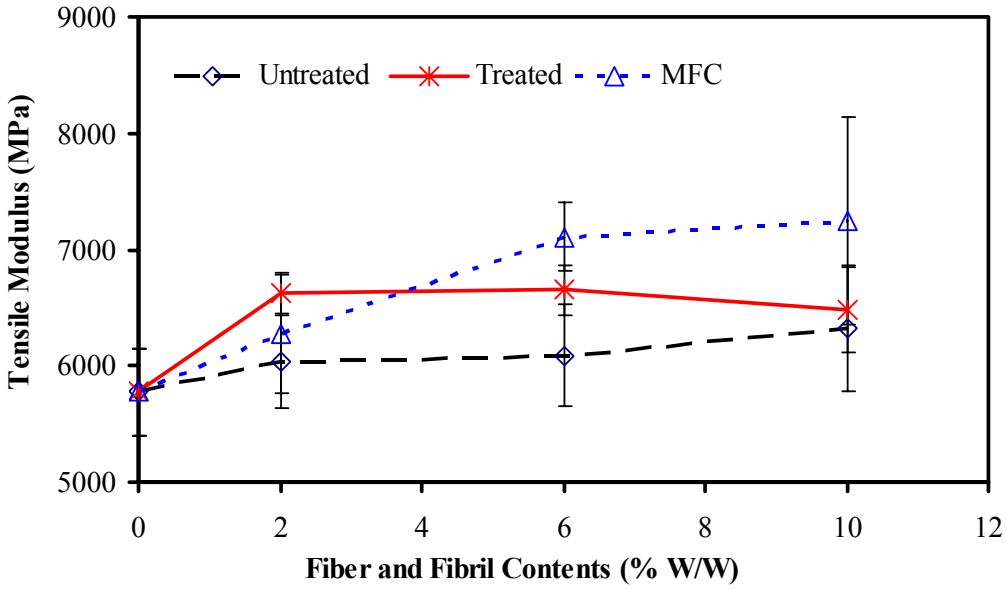

Figure 6.11 Tensile modulus of PVA and its composites reinforced by untreated and treated Lyocell fiber, and MFC

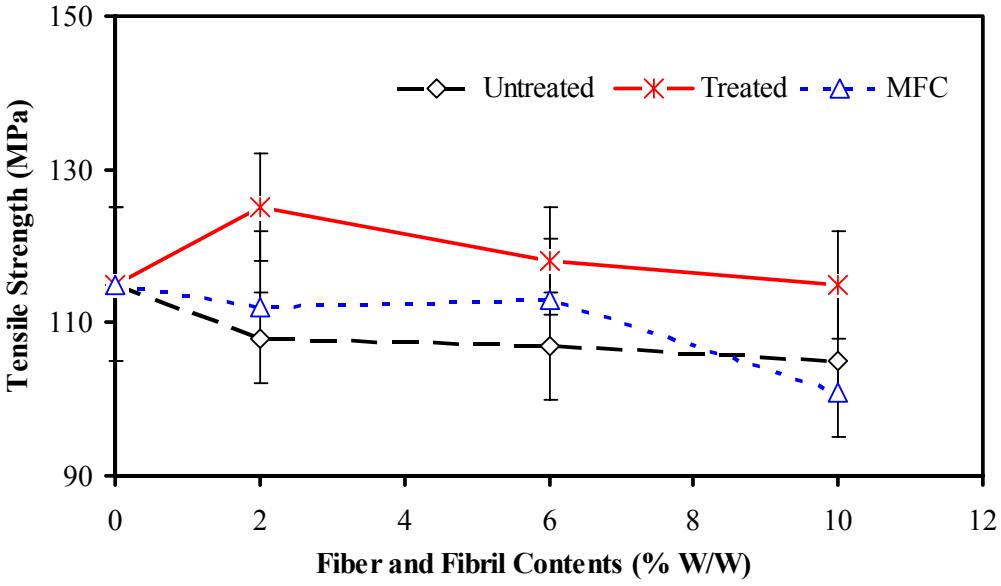

Figure 6.12 Tensile strength of PVA and its composites reinforced by untreated and treated Lyocell fiber, and MFC

caused in several factors. First of all, the resources of neat PVA were different, and film making conditions e.g. dry temperature and time, so that the properties of neat PVA were much different (modulus 2.3 vs. 5.78 GPa, strength 42 vs. 115 MPa). In fact, the results of neat PVA in this paper were similar as those of reinforced composites. Second, the fibril aggregates and MFC used in this study had bigger fibers and fibril aggregates (more than 1 μm) and may not be as even and fine enough as that used by Chakraborty. Others factors may include adhesion between the fibers and the polymer matrix, the uniform distribution of the fibril aggregates, aspect ratio and orientation of the fibers, and the degree of crystallinity of the matrix (Mathew et al., 2005). It could be helpful for understanding the reinforcement mechanism of the fiber and fibril to do further analyses by some micromechanical models to account for different fibers with different aspect ratios and orientation.

PLA composites by compression molding

Figure 6.13 shows typical tensile curves of neat PLA and its composites with 10% and 20% of treated Lyocell fibers. Again the tensile strengths were higher for the composites compared to pure PLA, which is also shown in Figure 14, but the elongations of the composites were decreased dramatically compared to the pure PLA, which indicates that the composites are much more brittle than the pure PLA.

Figure 6.14 compares the tensile modulus and strength of composites reinforced by untreated and treated Lyocell fibers by loading of 10% and 20% (W/W) with those of pure PLA. The result indicates that all composites have tensile modulus higher than that

of pure PLA. The tensile modulus and strength of the composites reinforced by treated fibers were higher than those of the composites reinforced by untreated fibers, which was considered as the contribution of the fibrils in micro and nano scales.

Both of the untreated and treated fibers of 10% loading did not have much influence on tensile strength (Figure 14). When the loading increased to 20%, the tensile strength of the composites with untreated fibers decreased 18%, while the treated fibers increased the tensile strength about 14% compared to pure PLA. Again, this may be considered the contribution of the fibrils isolated from the fibers and microfibrillation on the fiber surface. The results were not as same as the reference that microcrystalline cellulose did not increase the tensile strength of PLA (Mathew et al. 2005).

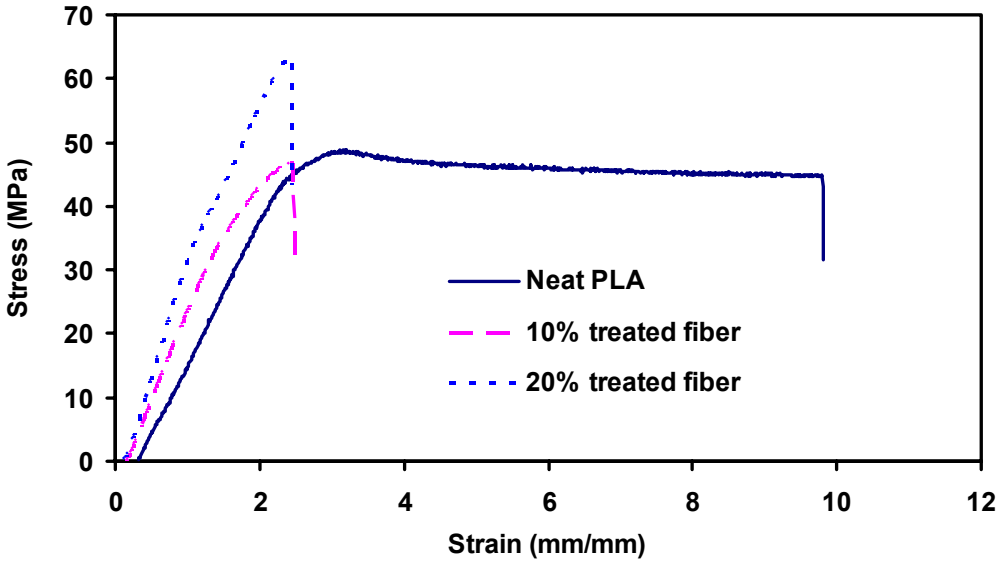

Figure 6.13 Typical stress-strain curves of PLA and its composites

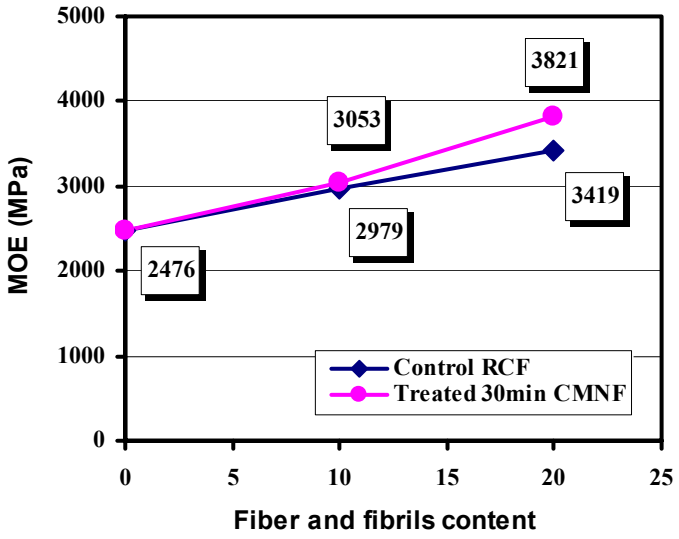

a)

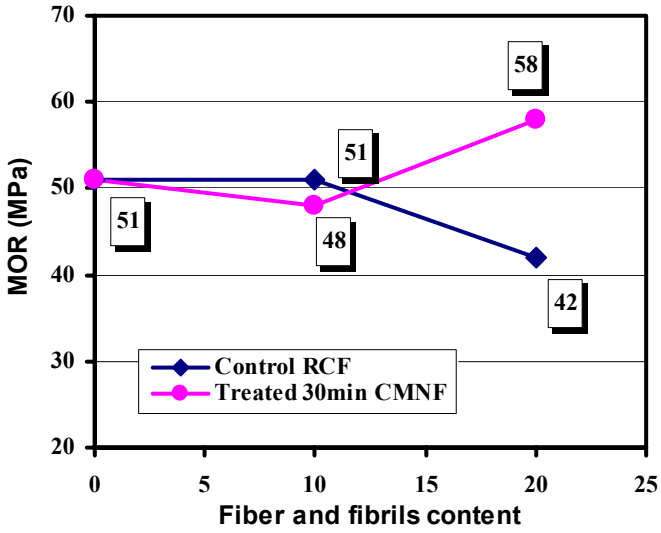

b)

Figure 6.14 Comparison of the mechanical properties of PLA and its composites: modulus (a) and strength (b)

PP composites by compression molding

Figure 6.15 shows typical tensile curves of neat PP and its composites with 10% and 20% of untreated and treated Lyocell fibers. The change trends of tensile strengths and elongations to break of the composites were similar as PVA and PLA composites.

Figure 16 compares the tensile modulus and strength of composites reinforced with untreated (control samples) and treated Lyocell fibers by loadings of 10% and 20% in weight with those of neat PP. The results indicate that all composites have higher tensile modulus and strength than those of neat PP. For control samples compared with the neat PP, the tensile moduli were significantly (α=0.05) increased 81% and 96% by loadings of 10% and 20% respectively. For the composites reinforced with the treated fibers, the tensile moduli were significantly (α=0.05) increased 93% and 130% by adding

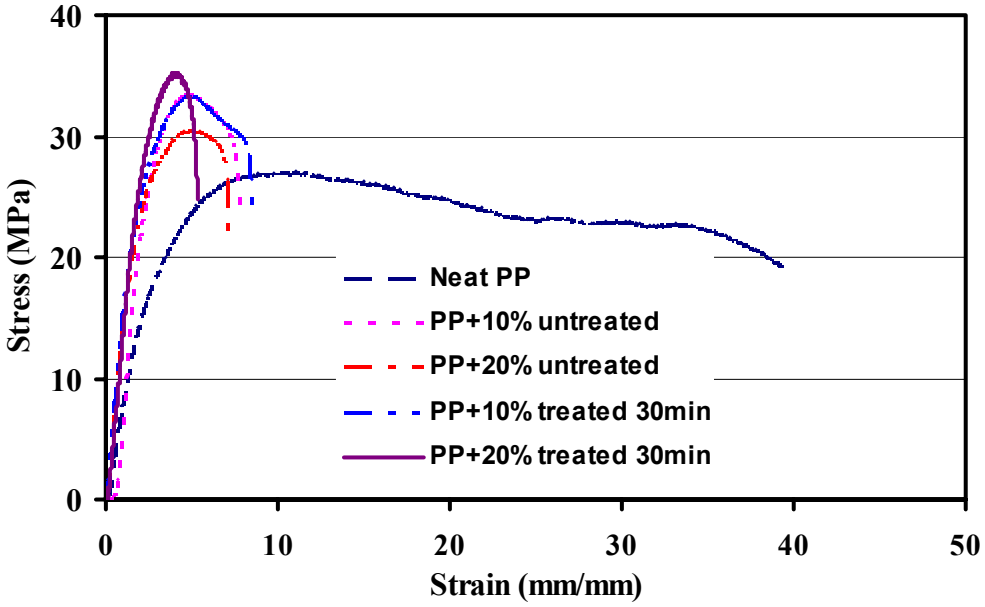

Figure 6.15 Typical stress-strain curves of PP and its composites

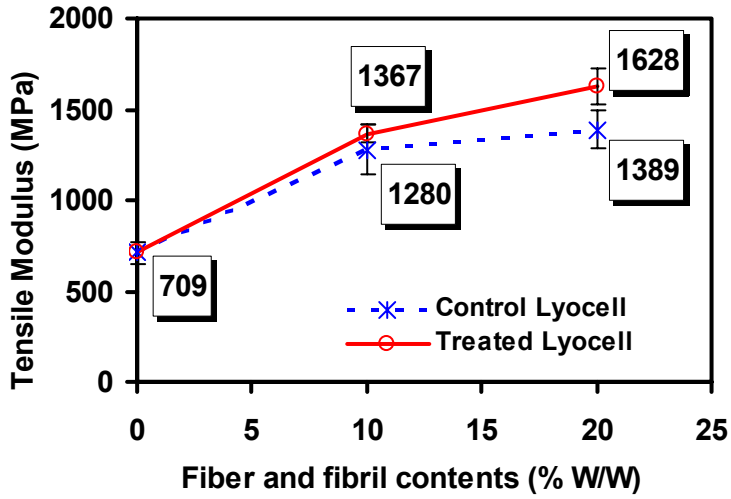

a)

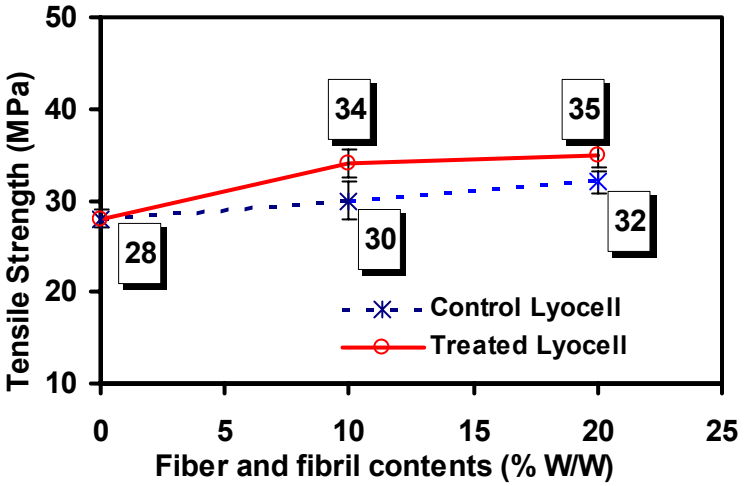

b)

Figure 6.16 Comparison of the mechanical properties of PP and its composites: modulus (a) and strength (b)

10% and 20% reinforcement respectively. Both of the tensile modulus and strength of the composites reinforced with treated fibers were significantly (α=0.05, except MOE of 10% loading) higher than those of the composites reinforced by untreated fibers.

6.4.5. Morphology of the composites

PVA composite by film casting

Using SEM, the fracture surfaces of the composites were studied in order to understand the failure mechanisms and the possible interaction between different components. Figure 6.17 shows an overview (a) and detail profile (b) of PVA/Lyocell composites. Most fibers were sunk to the bottom of the film (Figure 6.17 a) because the untreated fibers would not suspend in water and had higher density than the PVA solution. The detail image shows that the adhesion was poor because of the gaps between fibers and PVA matrix and the smooth surfaces of the untreated fibers by visual inspection of randomly selected features. This was one of the main reasons that the tensile strength was decreased after adding the untreated fiber in PVA matrix (Figure 6.12).

For treated Lyocell fibers, a better distribution of the fibers and fibril aggregates in the composite cross-sections can be seen in Figure 6.18. The top image shows a good dispersion of fibril aggregates in the PVA matrix and the detail micrograph shows the interphase between the fibrils and the matrix. Comparing with untreated fibers (Figure 6.17), the rough fracture cross-sections (Figure 6.18) and the rough surfaces of the treated fibers (Figure 6.6) could help the fibers and fibrils imbed in PVA matrix. Some voids and

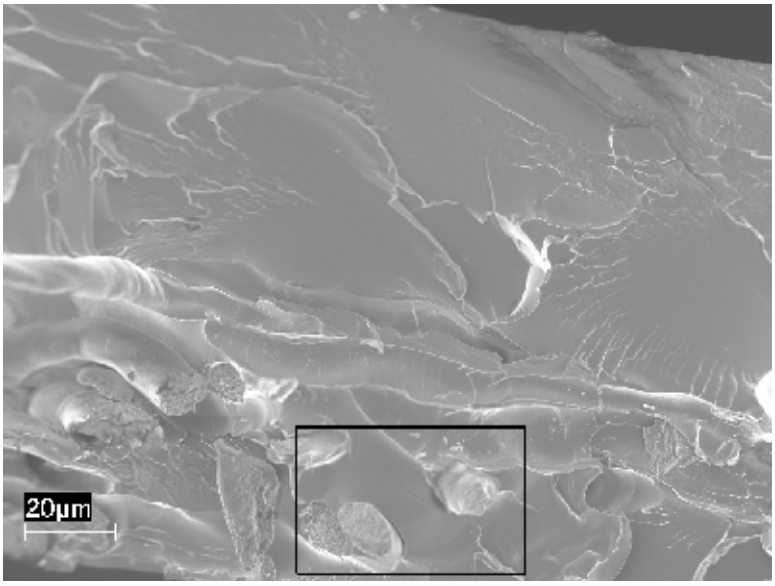

a)

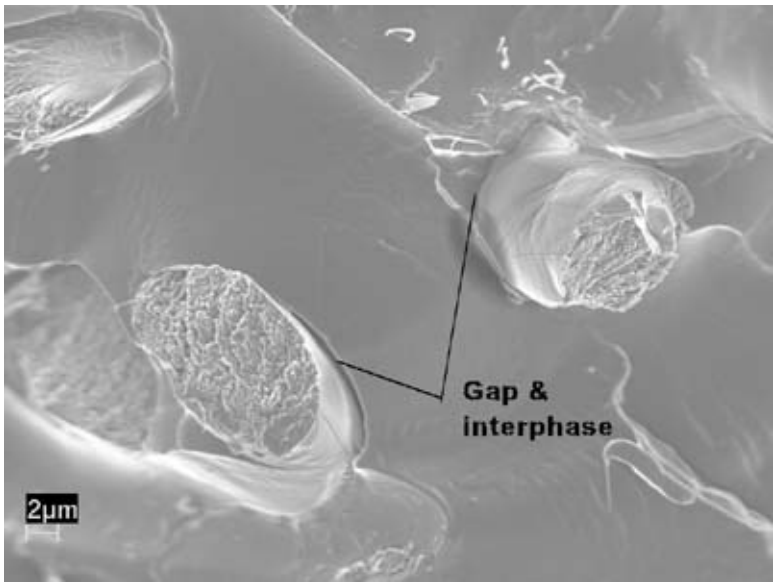

b)

Figure 6.17 SEM fracture cross-sections of PVA composites reinforced with 10% untreated Lyocell fiber: overview (a), detail (b)

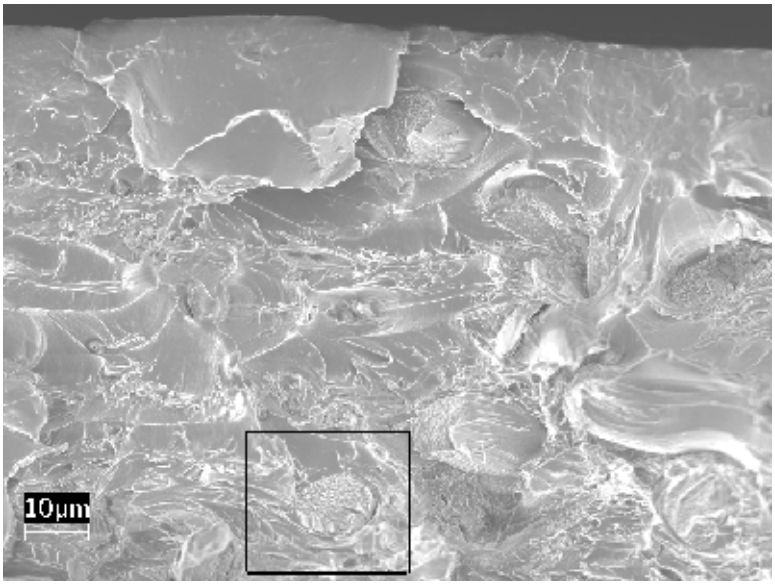

a)

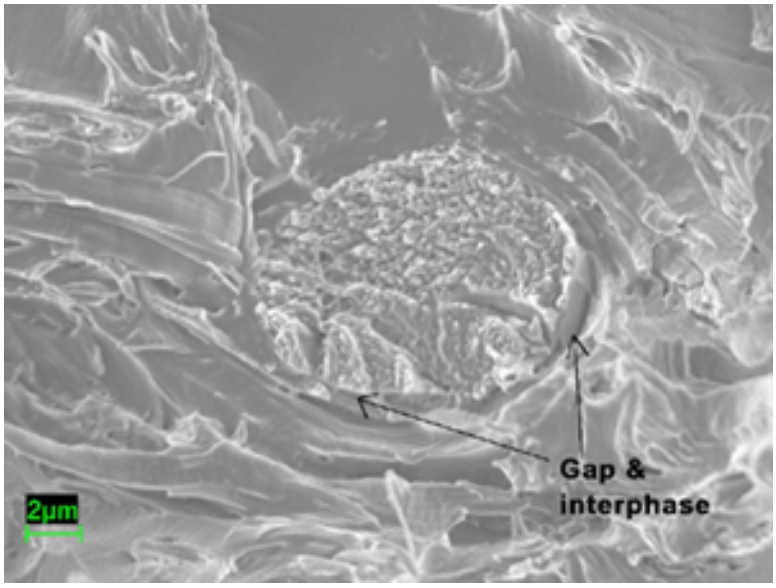

b)

Figure 6.18 SEM fracture cross-sections of PVA composites reinforced with 10% treated Lyocell fiber: overview (a), detail (b)

gaps around the big fibril aggregates still existed as the case in the untreated fiber composites by visual inspection of randomly selected features. These indicate that adhesion between the PVA matrix and the fibril aggregates was not perfect, but better than those of untreated fiber composites.

The PLM images were used to observe the fibers and fibril aggregates distribution in the film from the surfaces. The PLM surface profiles in Figure 6.19 shows the PVA reinforced by untreated and treated Lyocell fibers with 2% by weight. And Figure 6.20 shows the PVA reinforced by MFC with 2%, 6%, and 10%. The results indicate that all the composites had a good dispersion of fibers and fibril aggregates from the surfaces. It is clear that many fibril aggregates can be identified for the treated fibers reinforced composites (Figure 6.19, a) and the similar situation in Figure 6.20 for the commercial MFC. The lengths and aspect ratios of the big MFC were smaller than those of the treated Lyocell fibers as evident from the measurements of randomly selected features (Figures 6.19 and 6.20). This is one reason that MFC reinforced PVA composites decreased the tensile strength of PVA (Figure 6.12).

PLA composite by compression molding

Some holes in the PLA matrix and some gaps around big fibers were observed by SEM (Figure 6.21). This indicates that the adhesion between the PLA and the mixture of fibers and fibrils was not high enough, so that the stress transfer across the interphase was poor. The PLM surface profiles in Figures 6.22 shows the PLA reinforced by untreated and treated Lyocell fibers with 10% by weight. The results indicate that all the composites

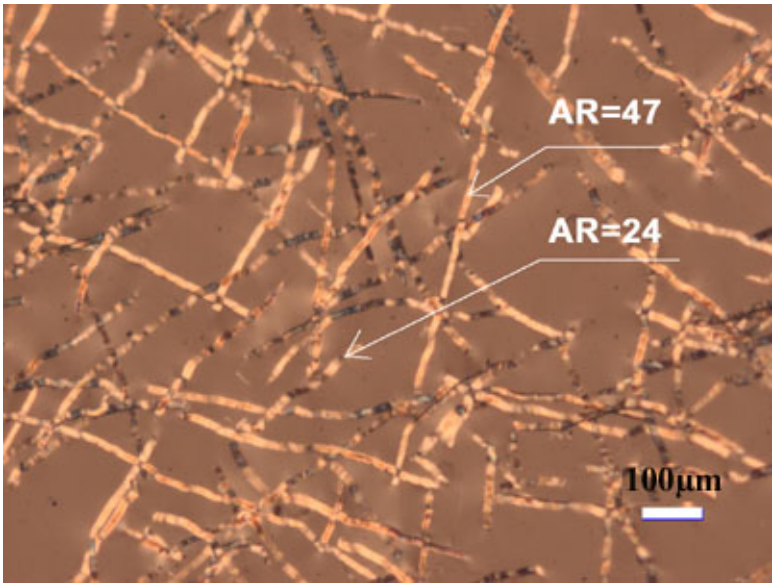

a)

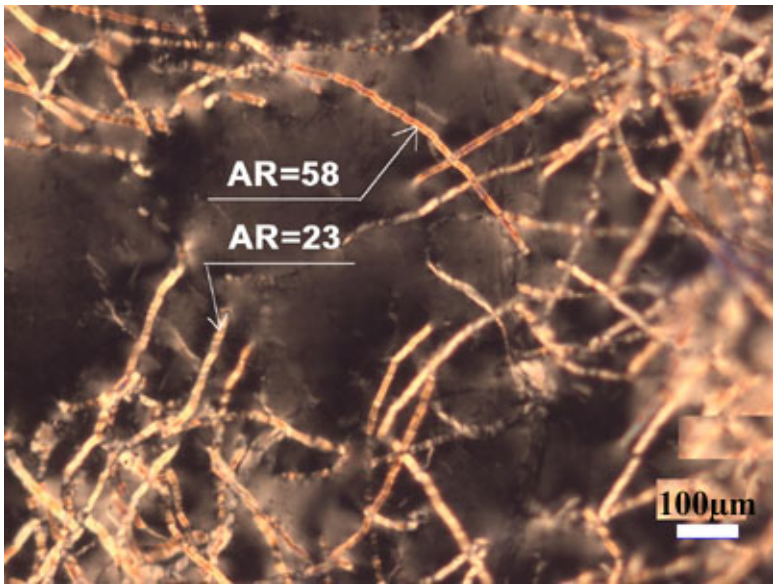

b)

Figure 6.19 PLM surface profiles of PVA composites (AR=Aspect Ratio): untreated Lyocell fiber 2% (a), treated Lyocell fiber 2% (b)

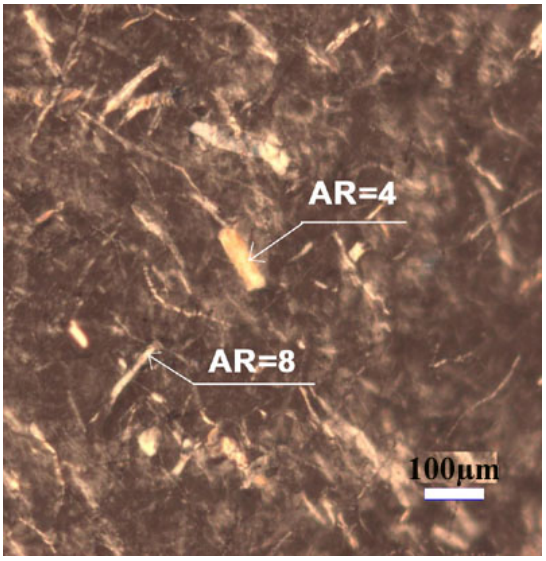

a)
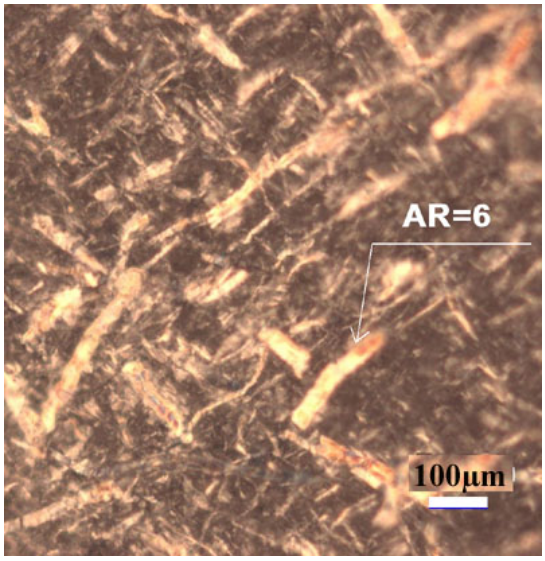

b)
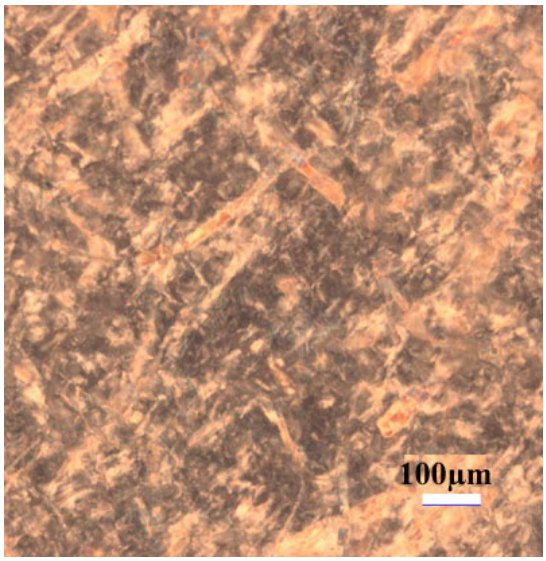

c)

Figure 6.20 PLM surface profiles of PVA/MFC composites (AR=Aspect Ratio): 2% (a), 6% (b), and 10% (c)

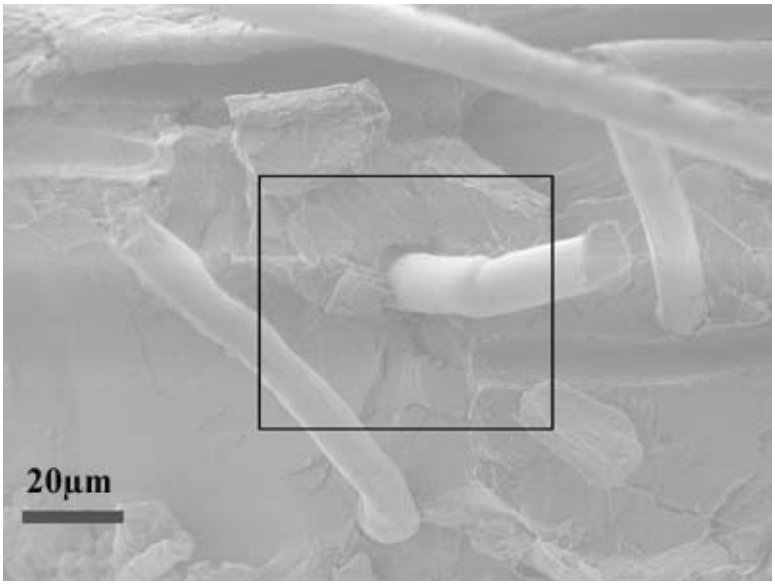

a)

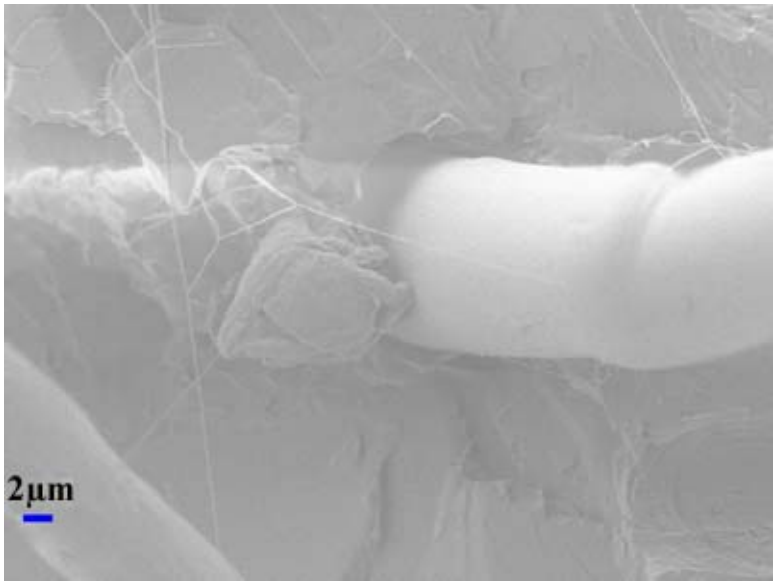

b)

Figure 6.21 The fractured cross-sections of PLA composites by SEM: a) overview, and b) detailed view

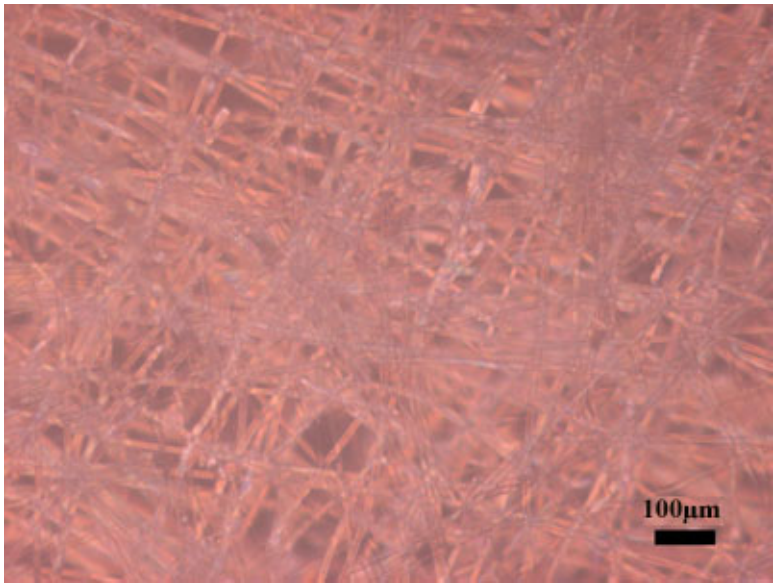

a)

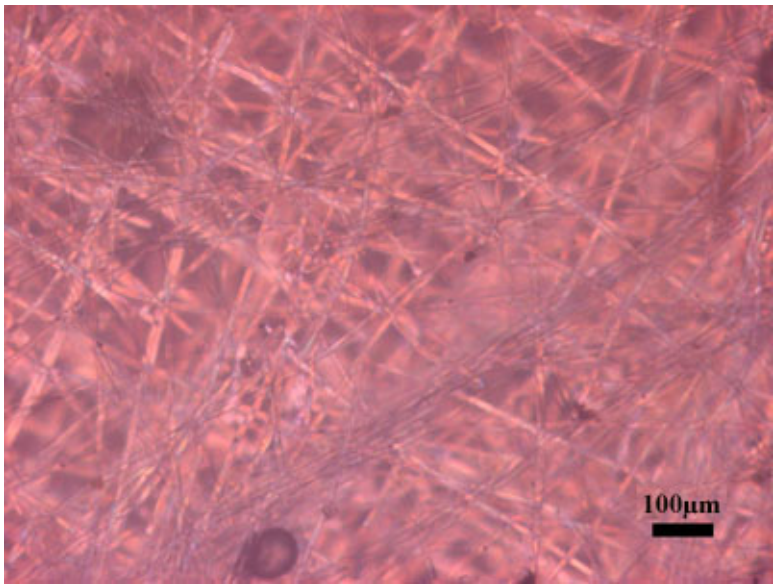

b)

Figure 6.22 PLM surface profiles of PLA/untreated Lyocell fiber 10% (a), PLA/treated Lyocell fiber 10% (b)

had a good dispersion of fibers and fibrils from the surfaces.

PP composite by compression molding

SEM images (Figure 6.23) show the fracture cross-sections of PP composites reinforced with treated Lyocell fibers. The fibril aggregates had a good distribution in the thickness of the composites, but some holes in the PP matrix and some gaps between fibers and PP matrix were observed as evident from the measurements of randomly selected features, which indicate that there was not a good adhesion between the PP matrix and the fibril aggregates. The detail micrograph (Figure 6.23, b) shows some thread-like material in the fracture surfaces and the rough surfaces of the treated fibers. Similar situation as the PVA composites reinforced by treated Lyocell fibers, the treated fibers had higher mechanical reinforcement for PP composites.

Two PLM surface profile images of PP composites reinforced with untreated and treated Lyocell fibers are shown in Figure 6.24. A good dispersion of fibers and fibril aggregates from the surfaces of the composites can be seen from the observations of randomly selected features. The fibers in the composite of untreated Lyocell fibers (a) were much clearer than the fibril aggregates in the composites of treated fibers (b) because of the fibril aggregates isolated and on the surfaces of the big fibers and fibrils. This also explains that the PP composites reinforced with treated Lyocell fibers had higher mechanical properties than those of the composites reinforced with untreated Lyocell fibers.

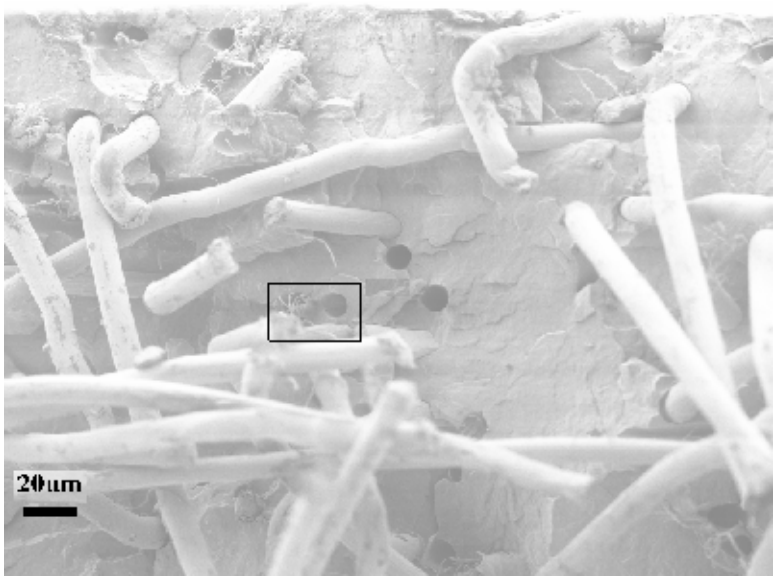

a)

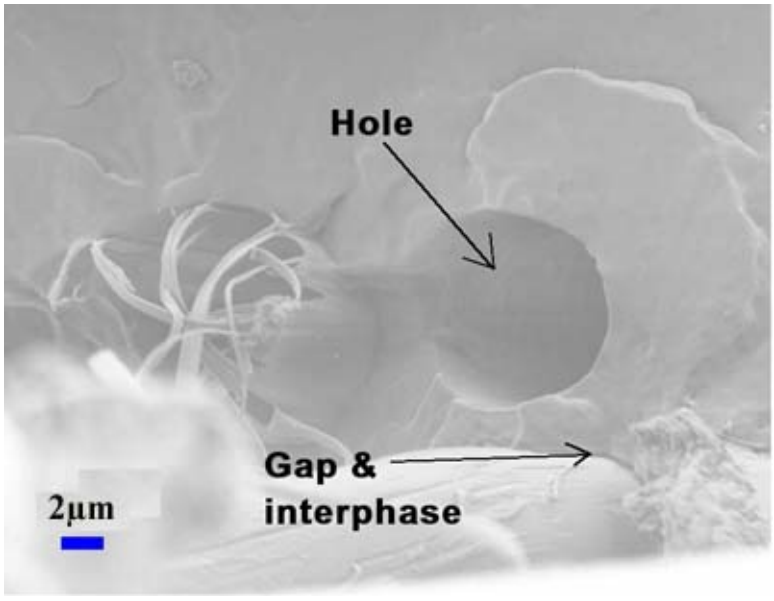

b)

Figure 6.23 SEM fracture cross-sections of PP composites reinforced with 10% treated Lyocell fiber: overview (a), detail (b)

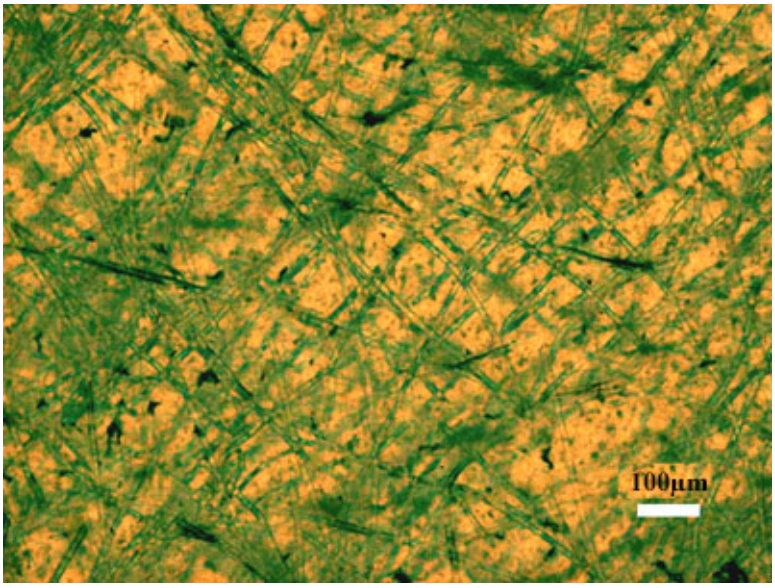

a)

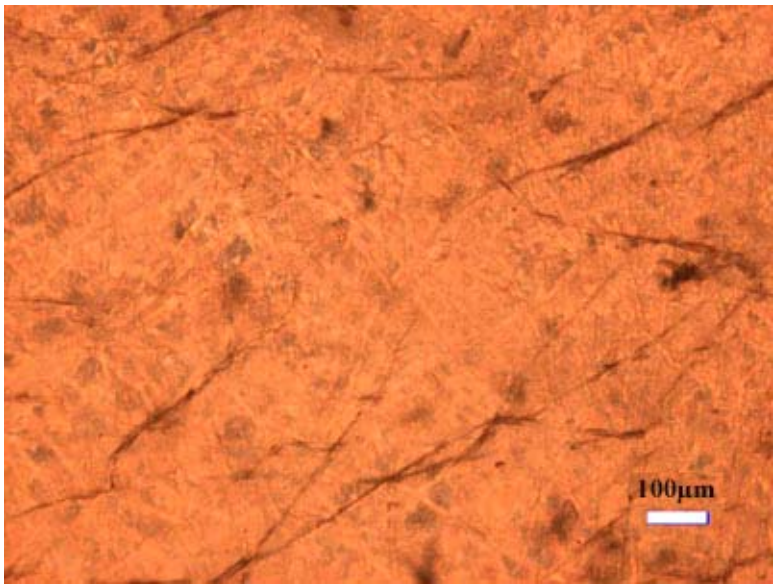

b)

Figure 6.24 PLM surface profiles of PP/untreated Lyocell fiber 10% (a), PP/treated Lyocell fiber 10% (b)

6.5. Conclusions

A mixture of fibril aggregates in micro and nano scales was obtained by ultrasonication treatment from Lyocell fibers. Both of the water retention value and crystallinity were increased as treatment time increasing. The mixture can be used to increase the tensile modulus and strength of PVA, PLA, and PP by fabrication methods of film casting and compression molding, respectively. SEM and PLM observations show that the mixture of treated fibers had better dispersion in the composites. There were not perfect adhesions between the polymers and the fibers and fibril aggregates without further modification. The fibril aggregates on the surfaces of big ones and isolated from the fibers were the main reason that the tensile modulus and strength of the mixture reinforced composites were higher than those of the composites reinforced with untreated fibers.

References

ASTM, D 1708-2002a. Standard Test Method for Tensile Properties of Plastics By Use of Microtensile Specimens.

Beck-Candanedo, S., Roman, M. and Gray, D.G., 2005. Effect of reaction conditions on the properties and behavior of wood cellulose nanocrystal suspensions. Biomacromolecules, 6(2): 1048-1054.

Berglund, L., 2005. Cellulose-based nanocomposites. In: A.K. Mohanty, M. Misra and L. Drzal (Editors), Natural Fibers, Biopolymers, and Biocomposites. Taylor & Francis, pp. 807-832.

Bondeson, D., Mathew, A. and Oksman, K., 2006. Optimization of the isolation of nanocrystals from microcrystalline cellulose by acid hydrolysis. Cellulose, 13(2): 171-180.

Chakraborty, A., Sain, M. and Kortschot, M., 2005. Cellulose microfibrils: A novel method of preparation using high shear refining and cryocrushing. Holzforschung, 59(1): 102-107.

Chakraborty, A., Sain, M. and Kortschot, M., 2006a. Cellulose microfibers as reinforcing agents for structural materials, Cellulose Nanocomposites: Processing, Characterization, and Properties. Acs Symposium Series, pp. 169-186.

Chakraborty, A., Sain, M. and Kortschot, M., 2006b. Reinforcing potential of wood pulp-derived microfibres in a PVA matrix. Holzforschung, 60(1): 53-58.

Cheng, Q., Wang, S., Zhou, D., Zhang Y. and Rials, T.G., 2007a. Lyocell-derived cellulose fibril and its biodegradable nanocomposite. Journal of Nanjing Forestry University, 31(4): 21-26.

Cheng, Q., Wang, S., Rials, G.T. and Lee, S.H., 2007b. Physical and mechanical properties of polyvinyl alcohol and polypropylene composite materials reinforced with fibril aggregates isolated from regenerated cellulose fibers. Cellulose, online first, DOI: 10.1007/s10570-007-9141-0.

Choi, Y.J. and Simonsen, J., 2006. Cellulose nanocrystal-filled carboxymethyl cellulose nanocomposites. Journal of Nanoscience and Nanotechnology, 6(3): 633-639.

Dufresne, A., Cavaille, J.Y. and Vignon, M.R., 1997. Mechanical behavior of sheets prepared from sugar beet cellulose microfibrils. Journal of Applied Polymer Science, 64(6): 1185-1194.

Dufresne, A., Dupeyre, D. and Vignon, M.R., 2000. Cellulose microfibrils from potato tuber cells: Processing and characterization of starch-cellulose microfibril composites. Journal of Applied Polymer Science, 76(14): 2080-2092.

Eichhorn, S.J. and Young, R.J., 2001. The Young's modulus of a microcrystalline cellulose. Cellulose, 8(3): 197-207.

Favier, V., Canova, G.R., Cavaille, J.Y., Chanzy, H., Dufresne, A. and Gauthier, C., 1995. Nanocomposite Materials from Latex and Cellulose Whiskers. Polymers for Advanced Technologies, 6(5): 351-355.

Ganster, J. and Fink, H.P., 2006. Novel cellulose fibre reinforced thermoplastic materials. Cellulose, 13(3): 271-280.

George, J., Sreekala, M.S. and Thomas, S., 2001. A review on interface modification and characterization of natural fiber reinforced plastic composites. Polymer Engineering and Science, 41(9): 1471-1485.

Hajji, P., Cavaille, J.Y., Favier, V., Gauthier, C. and Vigier, G., 1996. Tensile behavior of nanocomposites from latex and cellulose whiskers. Polymer Composites, 17(4): 612-619.

Herrick, F.W., Casebier, R.L., Hamilton, J.K. and Sandberg, K.R., 1983. Microfibrillated cellulose: morphology and accessibility. Journal of Applied Polymer Science: Applied Polymer Symposium, 37: 797-813.

Lima, M.M.D. and Borsali, R., 2004. Rodlike cellulose microcrystals: Structure, properties, and applications. Macromolecular Rapid Communications, 25(7): 771-787.

Mathew, A.P., Oksman, K. and Sain, M., 2005. Mechanical properties of biodegradable composites from poly lactic acid (PLA) and microcrystalline cellulose (MCC). Journal of Applied Polymer Science, 97(5): 2014-2025.

Nakagaito, A.N. and Yano, H., 2005. Novel high-strength biocomposites based on microfibrillated cellulose having nano-order-unit web-like network structure. Applied Physics a-Materials Science & Processing, 80(1): 155-159.

Peng, S.J., Shao, H.L. and Hu, X.C., 2003. Lyocell fibers as the precursor of carbon fibers. Journal of Applied Polymer Science, 90(7): 1941-1947.

Sakurada, I., Nukushina, Y. and Ito, T., 1962. Experimental determination of elastic modulus of crystalline regions in oriented polymers. Journal of Polymer Science, 57(165): 651-660.

Samir, M., Alloin, F., Sanchez, J.Y. and Dufresne, A., 2004. Cross-linked nanocomposite polymer electrolytes reinforced with cellulose whiskers. Macromolecules, 37(13): 4839-4844.

Sturcova, A., Davies, G.R. and Eichhorn, S.J., 2005. Elastic modulus and stress-transfer properties of tunicate cellulose whiskers. Biomacromolecules, 6(2): 1055-1061.

Taniguchi, T., 1996. Microfibrillation of natural fibrous materials. J. Soc. Mat. Sci. Japan, 45(4): 472-473.

Thygesen, A., Oddershede, J., Lilholt, H., Thomsen, A.B. and Stahl, K., 2005. On the determination of crystallinity and cellulose content in plant fibres. Cellulose, 12(6): 563-576.

Turbak, A.F., Snyder, F.W. and Sandberg, K.R., 1983. Microfibrillated cellulose, a new cellulose product: properties, uses, and commercial potential. Journal of Applied Polymer Science: Applied Polymer Symposium, 37: 815-827.

Woodings, C., 2000. Regenerated cellulose fibers. Woodhead Publishing Limited, Cambridge England.

Zimmermann, T., Pohler, E. and Geiger, T., 2004. Cellulose fibrils for polymer reinforcement. Advanced Engineering Materials, 6(9): 754-761.

CHAPTER 7. POLY(VINYL ALCOHOL) NANOCOMPOSITES REINFORCED WITH CELLULOSE FIBRILS ISOLATED BY HIGH INTENSITY ULTRASONICATION

7.1. Abstract

Cellulose fibrils in micro and nano scales are relative new reinforcing materials for polymer composites, which have potential lightweight and high strength and are biodegradable. A mixture of fibrils in micro and nano scales was generated from several cellulose resources by ultrasonic treatment. The geometrical characteristics of the fibrils were investigated using polarized light microscopy (PLM), scanning electron microscopy (SEM) and atomic force microscopy (AFM). The degree of fibrillation of the fibers was indirectly evaluated by water retention value (WRV) and the crystallinities of the treated fibers were evaluated by Fourier transform infrared spectroscopy (FTIR). The treated cellulose and separated fibrils were used to reinforce poly(vinyl alcohol) (PVA) to make biodegradable nanocomposites by film casting. The mechanical properties of the nanocomposites were evaluated by tensile test and the morphological characteristics of the nanocomposites were investigated with PLM, SEM, and AFM. As reference, a commercial microfibrillated cellulose (MFC) was used to reinforce PVA.

Keywords: Cellulose, Fibril, Mechanical property, Micro, Morphology, Nanocomposite, Nano

7.2. Introduction

Cellulose is the most abundant natural biopolymer in the world, which is renewable and biodegradable. Fibrils in nano and micro scales generated from cellulose fibers have much higher mechanical properties than those of single fibers. It was reported

that the cellulose crystal regions had Young's modulus of up to 137 GPa (Sakurada et al., 1962), and elastic modulus of Lyocell fibrils with diameter from 150 nm to 180 nm was evaluated about 98 GPa (Chapters 4 and 5). Isolating cellulose fibrils and reinforcing polymers by them to make nanocomposites are very attractive (Berglund, 2005; Herrick et al., 1983; Turbak et al., 1983; Cheng et al., 2007a and b). Nanocomposite is defined as composite that includes at least one-dimension of one component in the composite at the nanometer scale.

Cellulose fibrils can be generated by chemical or mechanical treatment. The chemical method, such as strong acid hydrolysis, removes the amorphous regions of cellulose fiber and produces nano-size fibrils. Wood fibers (Beck-Candanedo et al., 2005), cotton (Choi and Simonsen, 2006), sea animals (Sturcova et al., 2005) and sugar beet (Dufresne et al., 1997) were used as raw materials to isolate fibrils by chemical method. Mechanical method includes a high pressure refiner treatment (Chakraborty et al., 2005), a grinder treatment (Taniguchi, 1996), a microfluidizer (Zimmermann et al., 2004), and a high-pressure homogenizer treatment (Herrick et al., 1983; Turbak et al., 1983). The fibrils made by these mechanical methods are bundles of microfibrils, which are referred as cellulose microfibril or mcirofibrillated cellulose (MFC). For nanocomposites reinforced by fibrils or fillers, there are two common fabrication methods: one is film casting by vaporizing the solvents (Favier et al., 1995), and the other is freeze drying followed by classical compression or extrusion processes (Hajji et al., 1996). Additional method of filtration mats followed by a compressive molding was used in our previous study (Chapter 6; Cheng et al., 2007a).

Lyocell fiber, a regenerated cellulose derived from wood-pulp, was treated by ultrasonication. An obtained mixture of fibrils in micro and nano scales was used to reinforce poly(vinyl alcohol) (PVA) and polypropylene (Cheng et al., 2007a), and poly(lactic acid) (PLA) (Cheng et al., 2007b) as described in Chapter 6.

To check the reinforcements of separated fibrils obtained from the mixtures of cellulose fibers and fibrils treated by HIUS, and to compare the polymer reinforcements of the mixture mentioned in Chapter 6, the purposes of this Chapter were to characterize the fibrils separated from the mixtures of treated Lyocell fibers, TC180 (pure cellulose fiber), and Avicel (microcrystalline cellulose (MCC)) treated by ultrasonication and to investigate the physical and mechanical properties of PVA composites reinforced with these fibrils. The fibrils were characterized by polarized light microscopy (PLM), scanning electron microscopy (SEM), and atomic force microscopy (AFM). The degree of fibrillation of the fibers was evaluated indirectly by water retention value (WRV) and the crystallinities of treated and untreated cellulose fibers were studied by FTIR. PVA nanocomposites were prepared by film casting. The tensile properties and morphologies of the composites were evaluated and compared by tensile test, and observations of PLM, SEM, and AFM, respectively.

7.3. Experimental

7.3.1. Materials

Regenerated cellulose fiber (Lyocell fiber, Lenzing, Austria), pure cellulose fiber (TC180, by CreaFill Fibers Corp.), and microcrystalline cellulose (MCC, Avicel PH-101,

FMC BioPolymer) were used as raw material. Commercial microfibrillated cellulose (MFC, 10% solid slurry, Daicel Chemical Industries, LTD., Japan) was used as a reference. Biodegradable polymer: poly(vinyl) alcohol (PVA, 99+% hydrolyzed, typical average M_W 85,000-124,000, purchased from Sigma-Aldrich) was used as matrix.

7.3.2. Fibril isolation and composite preparation

The short Lyocell and pulp fibers (cut and passed a screen with holes of 1 mm in diameter by a Willey mill), as well as Avicel PH-101were soaked in distilled water for more than 24 hours and then treated 30 min by high intensity ultrasonication to isolate fibrils (Chapter 3; Wang and Cheng, 2007). Centrifuge was used to separate fibrils from the treated materials with relative centrifugal force of 900 g (g is the earth gravity acceleration) and 5 (Lyocell) or 10 (TC180 and Avicel) minutes. After setting 5 minutes, the top portion was used as small fibrils to reinforce PVA.

PVA water solution (10% W/W) and cellulose fibril water suspension were mixed and stirred manually and then dispersed by ultrasonic treatment (Sonic Newtown, CT, 20 kHz, Model 1500 W) for about one minute with 50% power level. The mixtures were degassed in a desiccator with vacuum and evaporated in room temperature and relative humidity of 30% until films were formed, and then the films were heat treated in an oven at 70 °C for more than 4 hours. The samples were kept in a desiccator, or room conditions (relative humidity (RH): ~30%, temperature (T): ~20°C), or after-treated in humidity control chamber (RH: 65%, T: 20°C) before the mechanical properties were performed.

7.3.3. Fibril characterizations

The appearance and dimensions of the treated and untreated Lyocell fibers and small fibrils were investigated by polarized light microscopy (PLM, Olympus-BX51). The Morphology of the fibrils was examined using a SEM (LEO 1525) and AFM (PASI XE-100) with non-contact mode after a drop of fibril suspension was dried on silicon wafer.

Water retention value (WRV), which can be used to measure the degree of homogenization or microfibrillation of fibers (Herrick et al., 1983), is a percent ratio of the water contained in the sample after centrifuged in certain force (900 g) and time (30 min) to the dry weight of the sample (Chapter 3; Cheng et al., 2007a).

Fourier transform infrared spectroscopy (FTIR) (PerkinElmer Molecular Spectroscopy, Spectrum One) was used to obtain spectra to estimate the crystallinities of the treated and untreated cellulose fibers. Mid infrared spectra were recorded in the wavenumber range of 4000 to 600 cm^{-1}. Spectra were taken at the resolution of 4 cm^{-1} with a total of 16 scans for each sample. The fiber spectra were normalized on the peak at about 1019 cm^{-1} attributed to a CO stretching mode and then modified by ATR (Attenuation Total Reflection) correlation with the contact factor of 0. The cellulose FTIR crystallinity index was evaluated as the intensity ratio between FTIR absorptions at 1419 and 895 cm-1 for Lyocell fiber and 1429 and 898 cm^{-1} for Avicel and TC180, which are assigned to CH_2 bending mode and deformation of anomeric CH respectively (Kataoka and Kondo, 1998). At least three specimens were scanned for each cellulose sample and the samples were used to measure WRV (Chapter 3).

7.3.4. Nanocomposite characterizations

The mechanical tests were performed using an Instron testing machine (model 5567). The crosshead speed was 1 mm/min. The samples were kept in a desiccator, or room conditions (relative humidity (RH): ~30%, temperature (T): ~20°C), or after-treated in humidity control chamber (RH: 65%, T: 20°C) after dried in an oven. The specimens were cut to dogbone shapes with width of 5 mm for the narrow portion and total length of 40 mm (gauge length was 20 mm). According to the ASTM D1708 standard (ASTM, D 1708-2002a), at least five specimens were tested for each composition. Tensile modulus was tangent modulus from the linear portion in the stress-strain curves with ignoring the initially unstable part. Multiple comparisons by the Statistical Analysis System (SAS) (t Tests (LSD)) were used to detect the overall significant differences of the influences on the tensile elastic modulus and strength of composites (α =0.05).

The morphology of the fractured surfaces of the composites after tensile test was investigated using a SEM (LEO 1525). The fractured surfaces were coated with gold on an ion sputter coater, and operating voltages of SEM were 5 to 10 kV. PLM was also used to observe the distributions of the fibrils in the composites from surfaces. To observe the cross-sections by AFM (PSIA, XE-100) with non-contact mode, the Lyocell fibril reinforced films were embedded in epoxy resin and cut to smooth surfaces by Microtome with diamond knifes. A silicon cantilever with nominal spring constant of 42 N/m, resonant frequency of 330 KHz was used (PPP-NCH, Nanosensor).

7.4. Results and Discussions

7.4.1. Morphology of fibers and fibrils

Figures 7.1 and 7.2 show PLM images of untreated cellulose and AFM images of separated fibrils by centrifuge for Avicel (MCC) and TC180, separately. The separated fibrils had a wide range of diameter from microns to tens of nanometers and length in microns. After only 30 minutes ultrasonic treatment, more than 40% in weight of Avicel was separated from particles to needle-like small fibrils (Figure 7.1).

PLM images of treated Lyocell fibers before (left) and after (right) separated by centrifuge are shown in Figure 7.3. A mixture suspension of fiber and fibrils with diameter ranging from microns to tens of nanometers was obtained after 30 minutes ultrasonic treatment. It can be seen that many small fibrils with diameter less than 1 μm were peeled from the fibers. The structure and appearance of the cellulose fibrils on silicon wafers observed by SEM and AFM are shown in Figure 7.4. More details were described in Chapter 3.4.13.

7.4.2. Water retention value (WRV) of untreated and treated cellulose

WRV of treated cellulose was significantly increased after ultrasonication treatment for all the three materials, which means the degree of microfibrillation of the treated fibers increased because WRV is related to fibril and microfibril surface and volumetric phenomena (Herrick et al., 1983). Avicel (MCC) was much easier to break down to smaller fibrils than those of TC80 and Lyocell fibers (Figure 7.5).

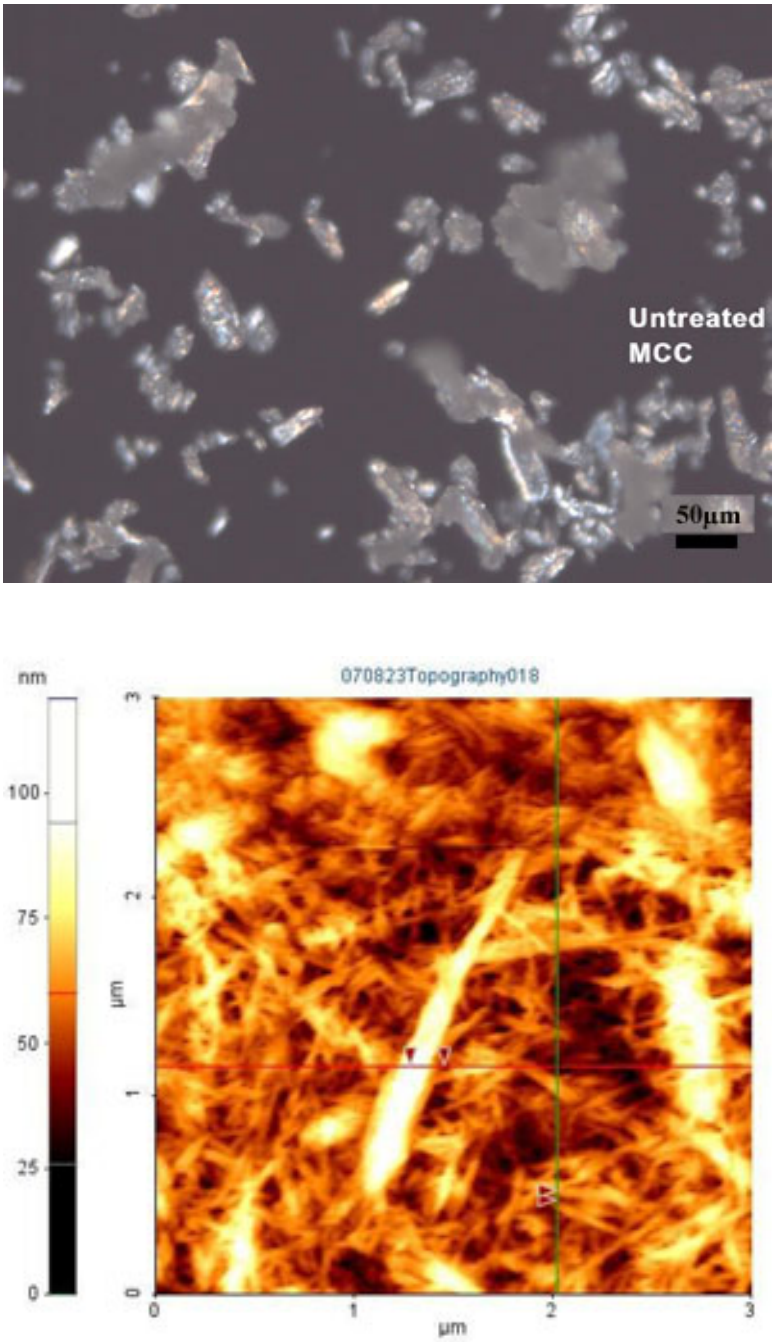

Figure 7.1 Structure and appearance of untreated Avicel (MCC) (top, PLM) and separated Avicel fibrils (bottom, AFM)

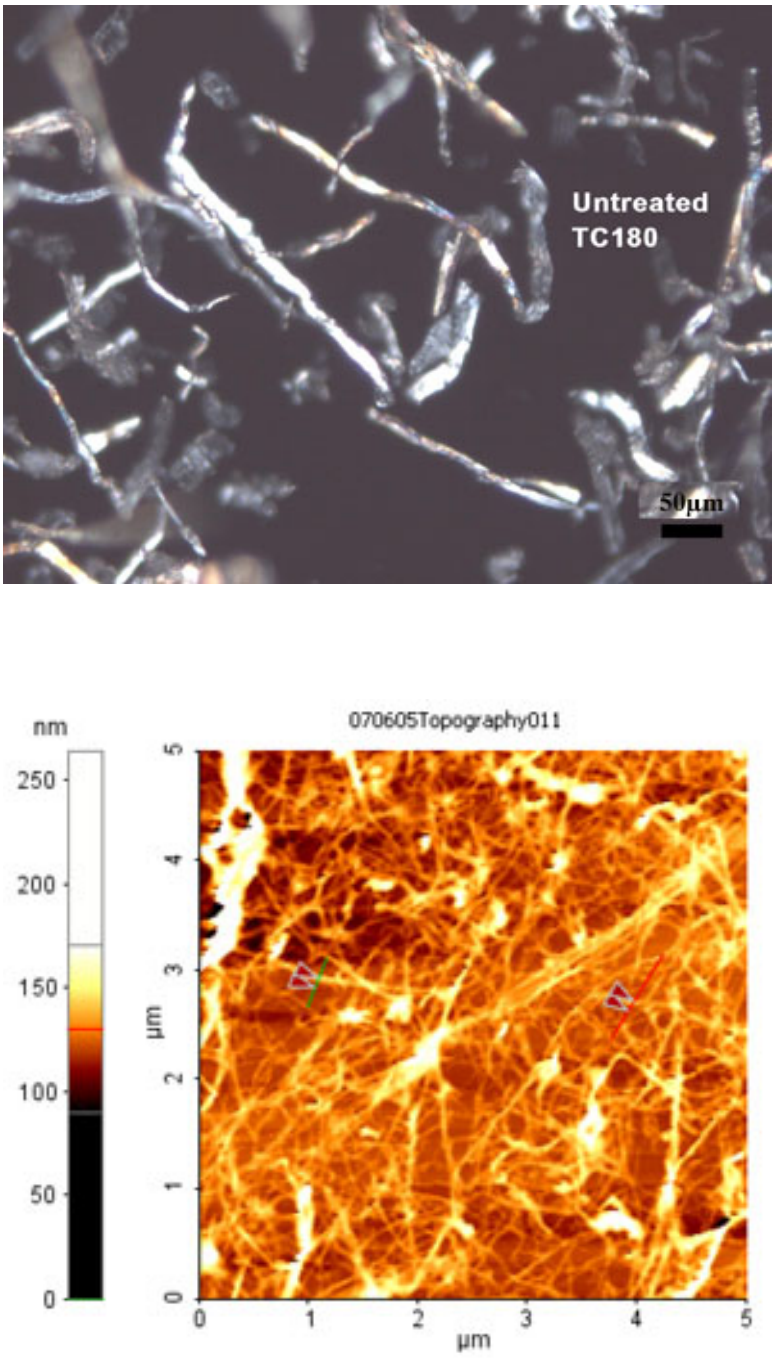

Figure 7.2 Structure and appearance of untreated TC180 (top, PLM) and separated TC180 fibrils (bottom, AFM)

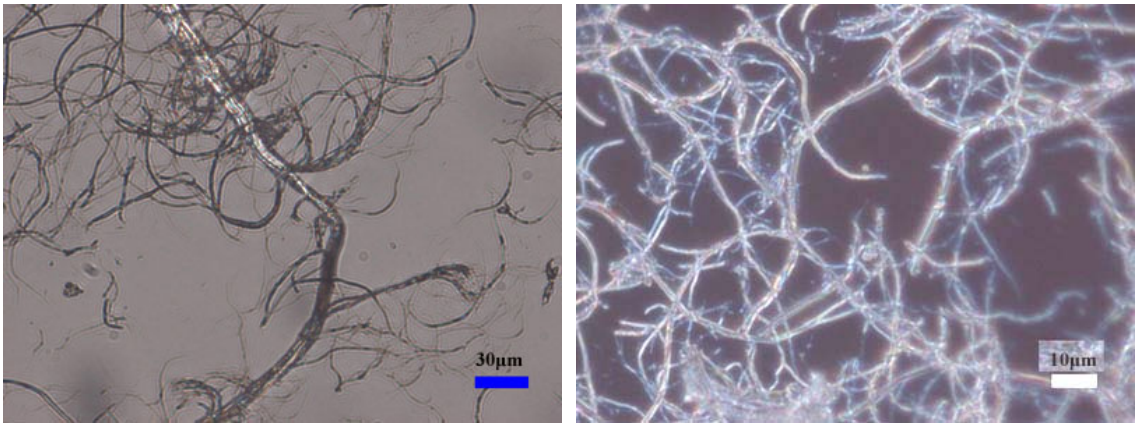

Figure 7.3 PLM images of treated Lyocell fibers before (left) and after (right) separation

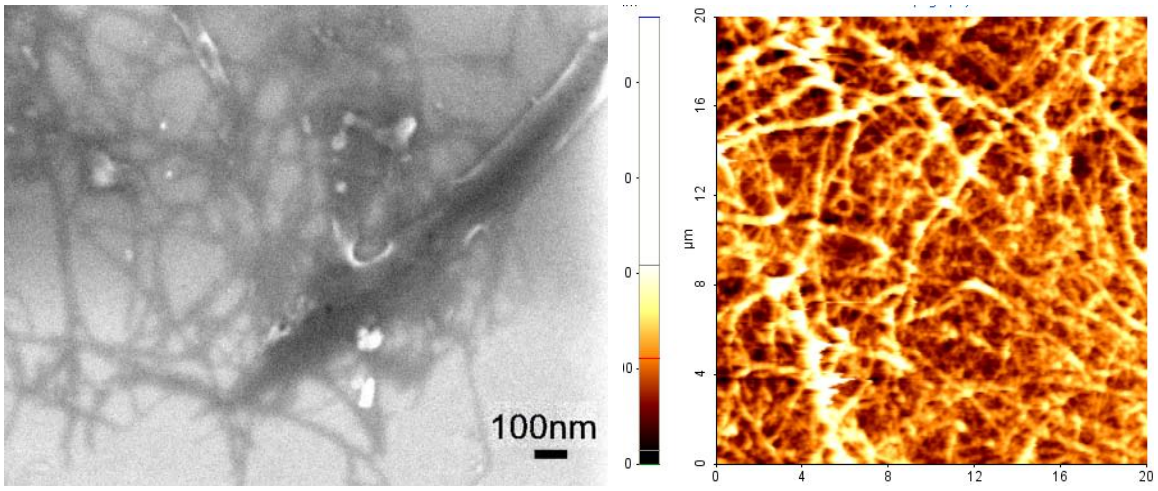

Figure 7.4 SEM (left) and AFM (right) images Lyocell fibrils after separated by centrifuge

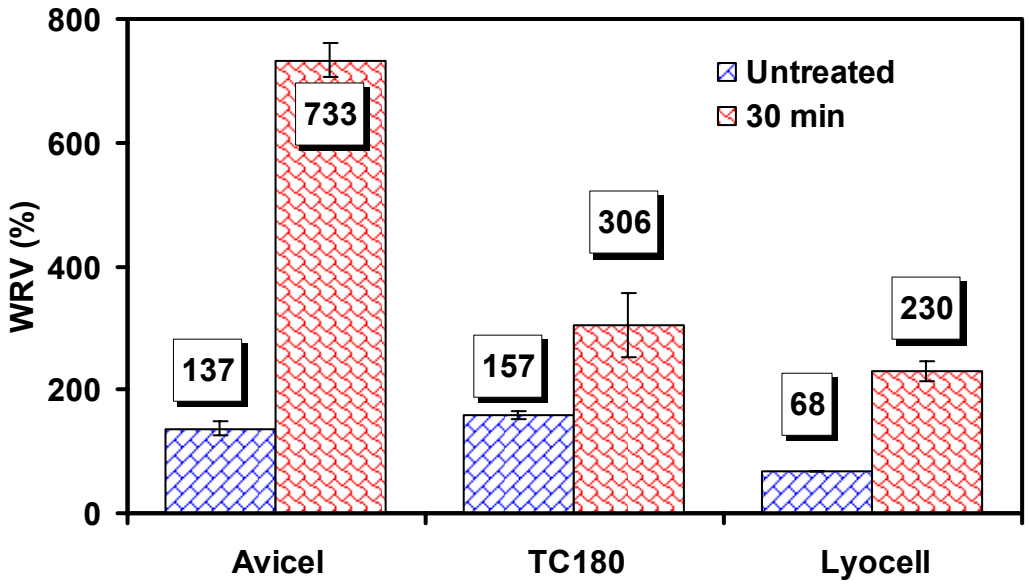

Figure 7.5 WRV of the three materials before and after 30 min treatment by HIUS

7.4.3. Crystallinity of untreated and treated cellulose

The FTIR crystallinity indexes (C_x) of Lyocell, Avicel, and TC180 for different treatment time are shown in Figure 7.6. Unlike WAXD results that the crystallinity of HIUS treated Lyocell fibers were significantly increased, C_x of Lyocell fiber from FTIR was not changed much after treatment (Chapter 3; Cheng et al., 2007a). HIUS treatment significantly decreased the FTIR C_x of Avicel. This may be because Avicel has very high crystallinity and HIUS treatment changed some molecular structure of Avicel cellulose. For pure cellulose fiber (TC180), HIUS treatment did not change FTIR crystallinity index too much. These indicated that different materials had different response to the HIUS treatment.

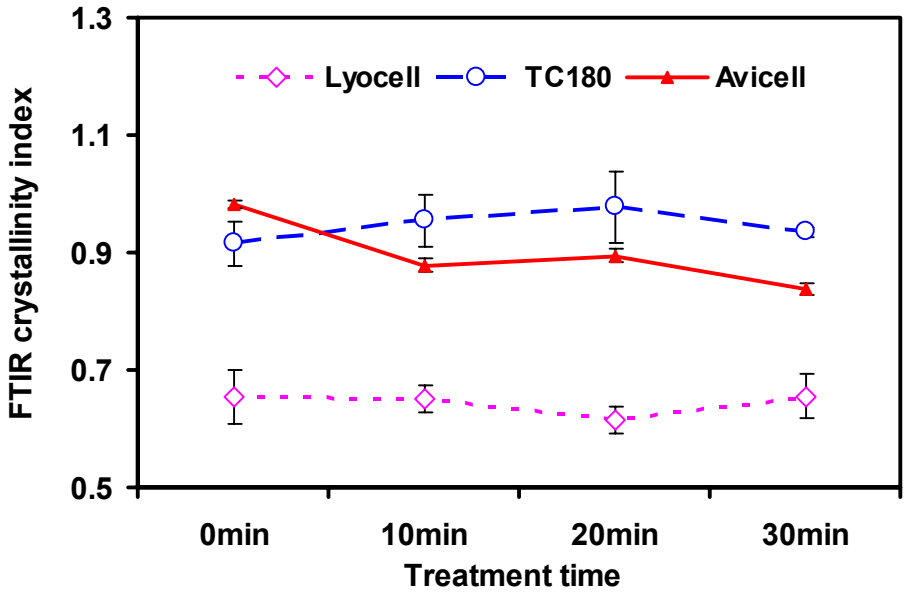

Figure 7.6 FTIR Crystallinity indexes of Lyocell, TC180, and Avicel for different treatment time

7.4.4. Mechanical properties of the composites

Avicel fibril reinforced composites

The tensile modulus and strength of neat PVA and its composites reinforced by untreated and treated (30 min) Avicel, and separated fibril (from 30 min treated Avicel) with 2%, 6%, and 10% by weight (W/W) are shown in Figures 7.7 and 7.8, respectively. The tensile modulus of neat PVA was decreased significantly by untreated and treated (mixture) Avicel, but increased by separated Avicel fibrils. The tensile strength of PVA was decreased significantly by untreated and treated Avicel, but it did not change much by separated Avicel fibrils. The treated Avicel was better than untreated Avicel for both modulus and strength. These demonstrated that Avicel might not be used as PVA reinforcement mainly because of its low aspect ratio; while treated Avicel, especially

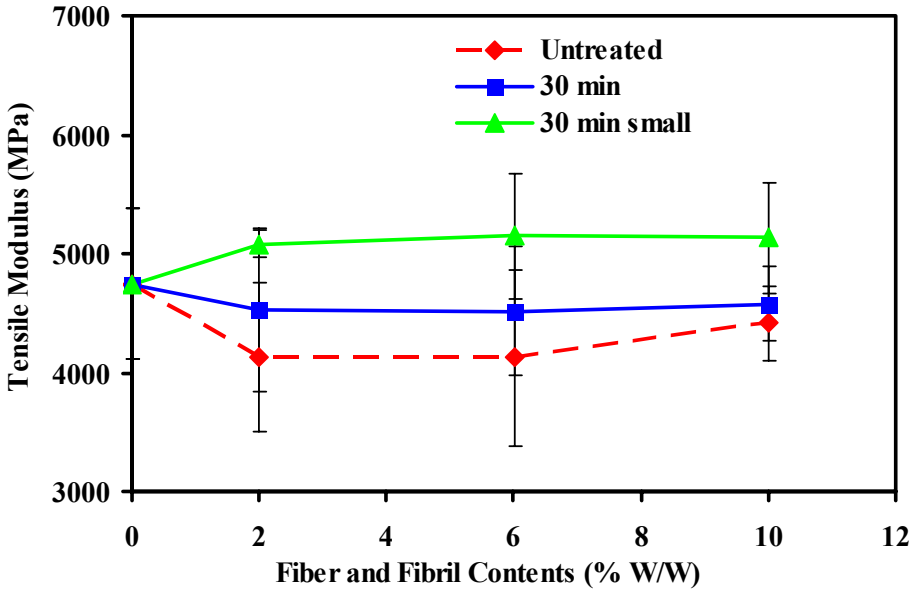

Figure 7.7 Tensile modulus of PVA and its composites reinforced by untreated and treated Avicl, and separated fibrils

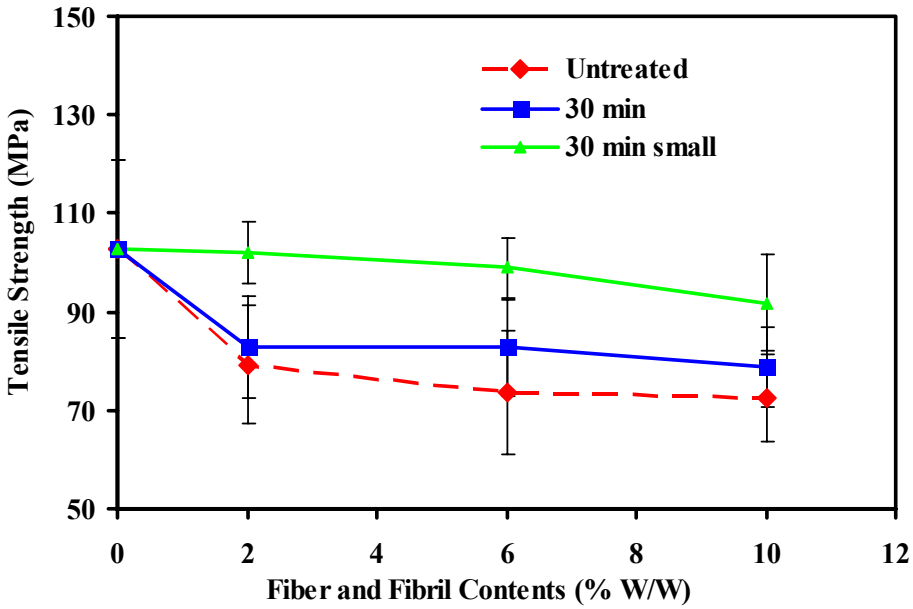

Figure 7.8 Tensile modulus of PVA and its composites reinforced by untreated and treated Avicel, and separated fibrils

separated fibrils with high aspect ratio could reinforce the mechanical properties of PVA, although the Cx of Avicel was decreased by HIUS treatment. Similar results were discussed that MCC does not demonstrate an improvement of the tensile modulus value in the carboxymethyl cellulose (CMC) composite (Choi and Simonsen, 2006).

Figure 7.9 shows the tensile modulus and strength of PVA composites reinforced by 2% (W/W) untreated and treated Avicel (treated 30 min), and separated small (30 min small) and big (30 min big) fibrils from treated Avicel cellulose for 30 min by HIUS. Again, the separated fibrils were much better than those of untreated and treated Avicel for PVA reinforcement. And no significant difference was found between small and big fibrils. To check how much the moisture could affect the mechanical properties of fibril reinforced PVA composites, after-treatment effects on tensile modulus and strength of

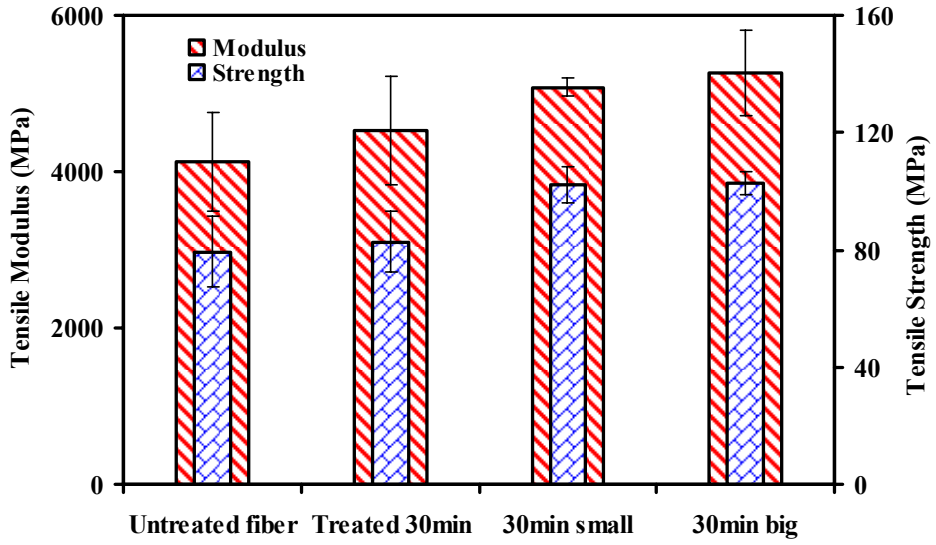

Figure 7.9 Tensile modulus and strength of PVA composites reinforced by 2% untreated and treated Avicel, and separated small and big Avicel fibrils after 30 min treatment

PVA composites reinforced by separated big Avicel fibrils were showing in Figure 7.10. High humidity did dramatically decrease the mechanical properties. This is mainly because that PVA is a water-soluble polymer. This indicates that the after-treatment should be kept the same condition to compare the mechanical properties of PVA composites reinforced by different fibrils.

TC180 fibril reinforced composites

Figure 7.11 shows the tensile modulus and strength of PVA and its composites reinforced by 2% (W/W) untreated and treated TC180, and separated small (30 min small) and big (30 min big) fibrils from treated TC180 for 30 min by HIUS. The separated fibril (small and big) reinforced composites had much higher mechanical properties than those of untreated and treated TC180 reinforced PVA composites, which were lower than those of neat PVA. Unlike Avicel fibrils, small TC180 fibril reinforced composites had higher improvement for both modulus and strength than those of big fibril. This may be because small TC180 fibrils had higher mechanical properties than those of big fibrils, and TC180 fibrils had higher aspect ratio than that of Avicel fibrils.

Lyocell fibril reinforced composites

The tensile modulus and strength of neat PVA and its composites reinforced by untreated and treated Lyocell fibers, fibril, and MFC of 2%, 6%, and 10% by weight (W/W) are shown in Figures 7.12 and 7.13, respectively. The tensile modulus of neat PVA was increased by all the three contents of fibers, fibrils, and MFC, but the modulus

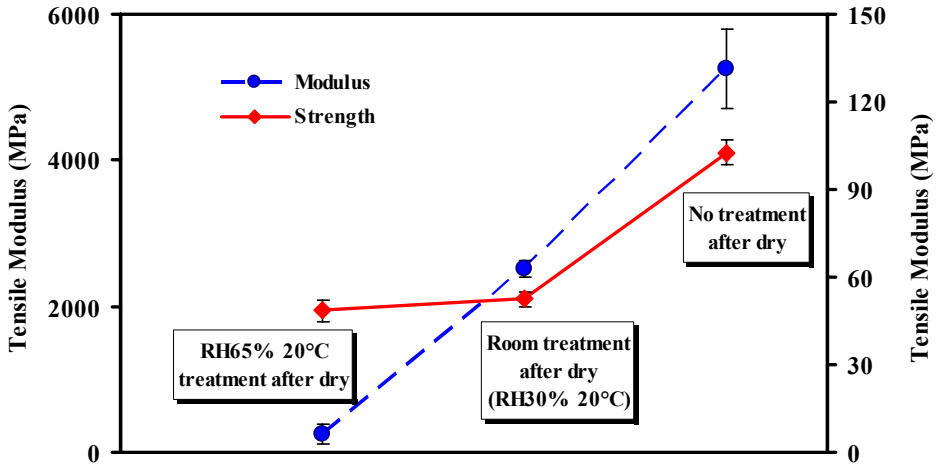

Figure 7.10 After-treatment effects on tensile modulus and strength of PVA composites reinforced by separated big Avicel fibrils (2%)

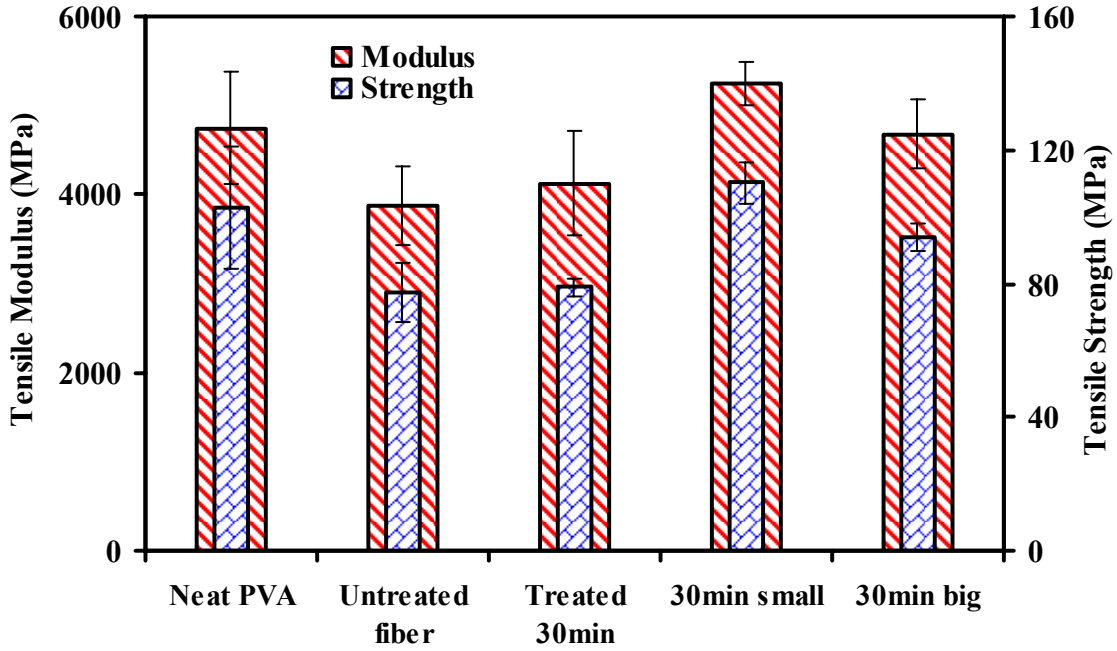

Figure 7.11 Tensile modulus and strength of PVA and its composites reinforced by untreated and treated TC180, and separated small and big TC180 fibrils

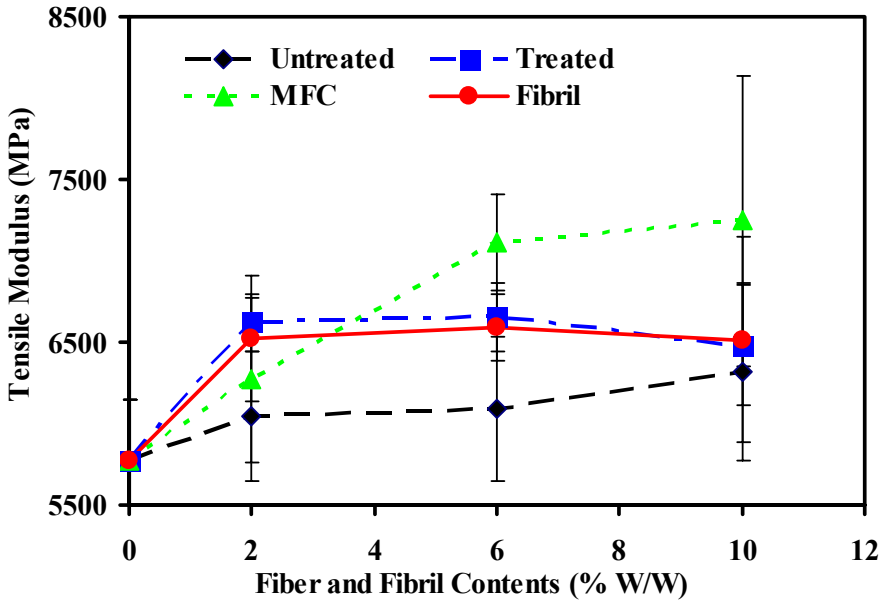

Figure 7.12 Tensile modulus of PVA and its composites reinforced by untreated and treated Lyocell fiber, separated fibril, and MFC

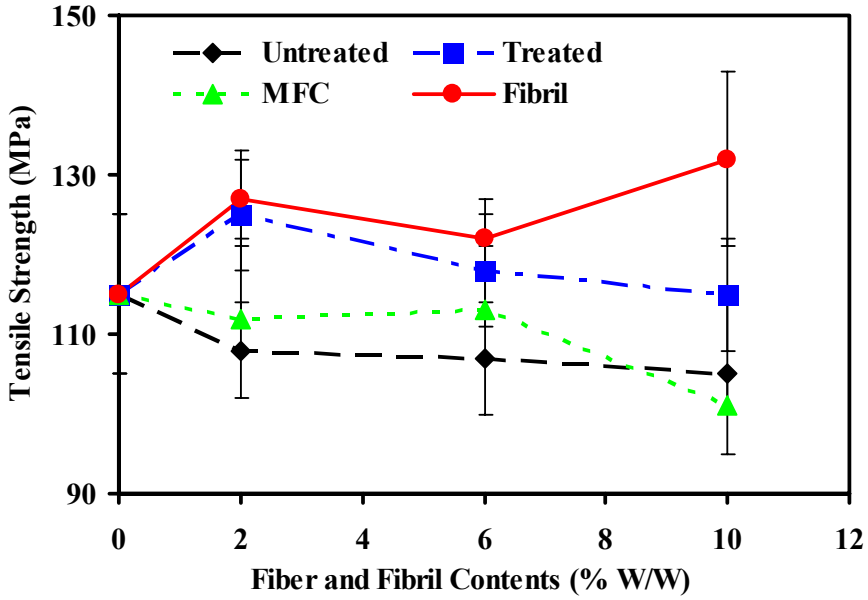

Figure 7.13 Tensile strength of PVA and its composites reinforced by untreated and treated Lyocell fiber, separated fibril, and MFC

changes were not significant (α=0.05) among the loadings of 2%, 6%, and 10% except between the 2% and 6% of MFC. The tensile strength of PVA was decreased by untreated Lyocell fiber and MFC, but it was increased significantly by only 2% of treated Lyocell fibers and separated fibrils, but adding more fiber and fibrils did not increase more strength except 10% of separated fibrils, which was better than the reinforcement of 10% of treated fiber. The results indicated that small fibrils on the surfaces of big ones and isolated from the fibers were the main reason that the tensile modulus and strength of the mixture and separated fibrils reinforced composites were higher than those of the composites reinforced with untreated fibers (Chapter 6; Cheng et al., 2007a). The reinforcement of Lyocell fibrils was much better that that of Avicel and TC180 fibrils. The possible reasons may be the aspect ratio of Lyocell fibrils was higher and the elastic modulus of Lyocell fibrils was higher than that of natural fibers (Chapter 5).

The improvements of PVA were not as high as those of microfibers generated from wood pulp. The tensile strength was doubled (from 42 to 102 MPa), and the stiffness was increased from 2.3 to 5.2 GPa by 5% microfiber loading (Chakraborty et al., 2006). This may be because the resources of neat PVA were different, and film making conditions e.g. drying temperature and time, which may influence the adhesion between the fibers and the polymer matrix, the uniform distribution of the fibril aggregates, aspect ratio and orientation of the fibers, and the degree of crystallinity of the matrix (Mathew et al., 2005). So that the properties of neat PVA were much different (modulus 2.3 vs. our 5.78 GPa, strength 42 vs. our 115 MPa). The results of neat PVA in this study were similar as those of microfiber reinforced composites. The other reason may be that the

fibrils and MFC had bigger fibrils (> 1 μm) may not be even and fine enough, which had more defects and low mechanical property than those of smaller fibrils (Chapter 5).

7.4.5. Morphology of the composites

Avicel fibril reinforced composites

Figure 7.14 shows PLM surface profiles of PVA composites reinforced with untreated Avicel 2% (left) and small Avicel fibrils 2% (right). The dispersion of Avicel and small fibrils from the surface were good, but SEM images of fracture surfaces (Figure 7.15) demonstrated that the dispersion of fibrils from the cross-section was not perfect for both composites. And clear gaps were observed between cellulose and polymer, especially for untreated Avicel. These may be the main reasons that the tensile strength and modulus of the composites were not improved.

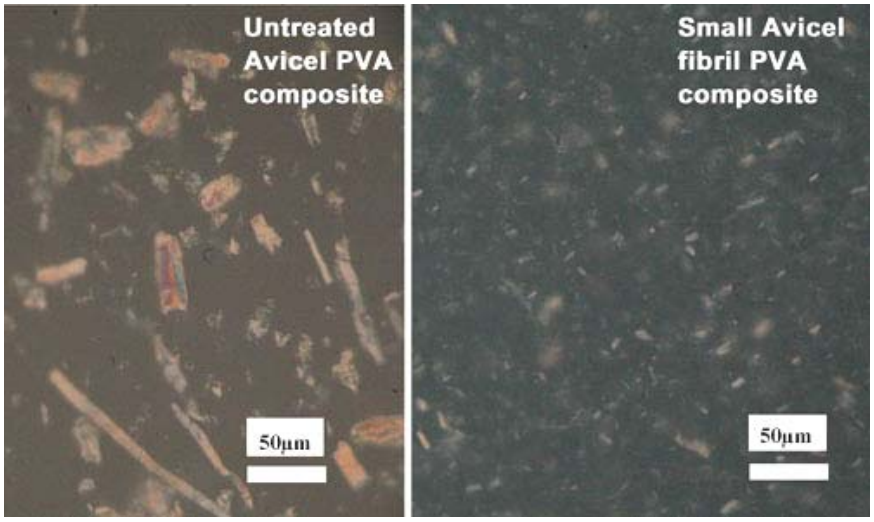

Figure 7.14 PLM surface profiles of PVA composites: untreated Avicel 2% (left), small Avicel fibrils 2% (right)

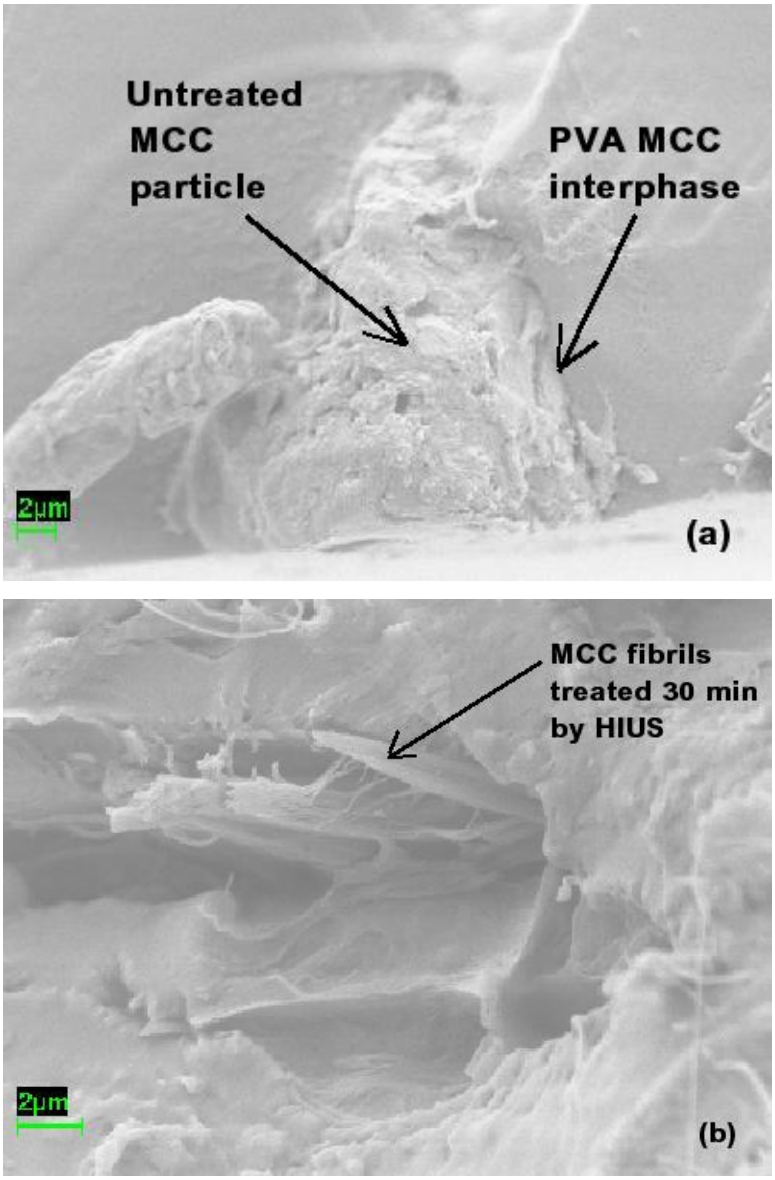

Figure 7.15 SEM images of the fractured cross-sections of PVA composites reinforced with a) untreated Avicel, and b) separated small Avicel fibrils

TC180 fibril reinforced composites

Figure 7.16 shows PLM surface profiles of PVA composites reinforced with 2% of untreated TC180 (left) and treated TC180 (right). The dispersion of cellulose from the surface was good. The similar as Avicel reinforced composites, SEM images of fracture surfaces (Figure 7.17 (a)) of untreated TC180 demonstrated clear gaps between cellulose and polymer. The separated small TC180 fibrils from the cross-section were not clear and may not have perfect dispersion (Figure 7.17 (b)).

Lyocell fibril reinforced composites

Figure 7.18 shows a PLM surface image of PVA composite reinforced by Lyocell fibrils with 10% by weight. And Figure 7.19 shows PLM images of surface and cross-sections of PVA composites reinforced with separated Lyocell fibrils and MFC (as reference). These indicate that the dispersion of fibrils from the surface was good. But SEM images of fracture surface (Figure 7.20) and AFM images of cross-sections after cut by microtome (topography in Figure 7.21 and phase in Figure 7.22) of the PVA composites reinforced by separated Lyocell fibrils demonstrated that the dispersion of fibrils from the cross-section was not perfect. And some fibrils were pulled out after tensile test. These may be the main reasons that the increments of tensile strength and modulus of the composites were not very high, especially after the fibril loadings of more than 2% in weight (Figures 7.12 and 7.13).

7.5. Conclusions

After treated by high intensity ultrasonication, a mixture of fiber and fibril in micro and nano scales was obtained from regenerated cellulose fiber (Lyocell), pure cellulose fiber (TC180), and microcrystalline cellulose (MCC). Both of the mixture and separated fibrils of Lyocell can be used to increase the tensile modulus and strength of PVA. The mixture and separated fibrils of TC180 and MCC had better reinforcement than that of untreated ones. PLM, SEM, and AFM observations show that the size of the fibrils have a wide diameter range from tens of nm to μm, the dispersion of cellulose was not perfect in the matrix, and the adhesions between the polymer and fibrils were not perfect without further modification of the fibrils and/or matrix, so that the increments of tensile strength and modulus of the composites were not as high as expected.

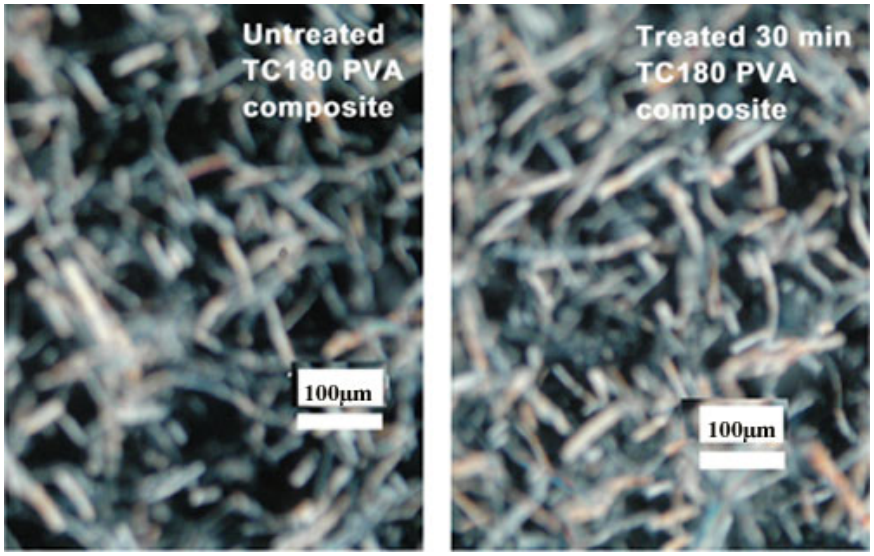

Figure 7.16 PLM surface profiles of PVA composites reinforced with 2% of untreated (left) and treated (right) TC180

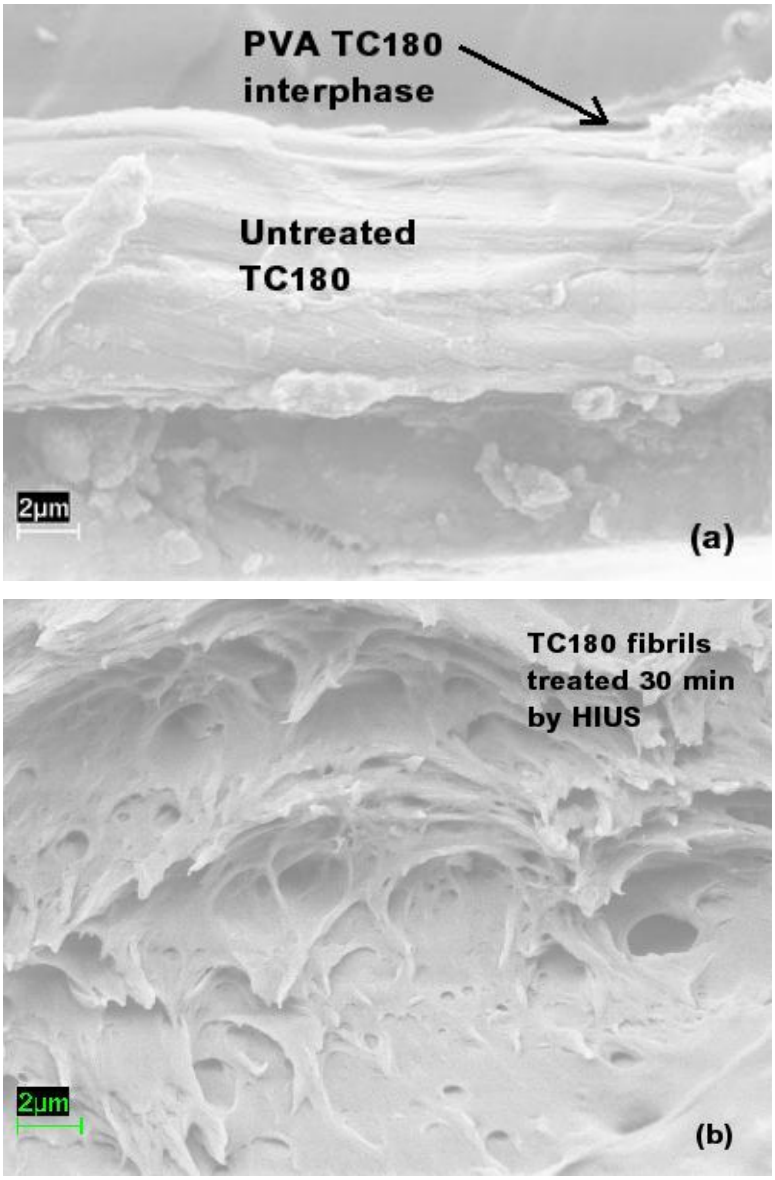

Figure 7.17 SEM images of the fractured cross-sections of PVA composites reinforced with a) untreated TC180, and b) separated small TC180 fibrils

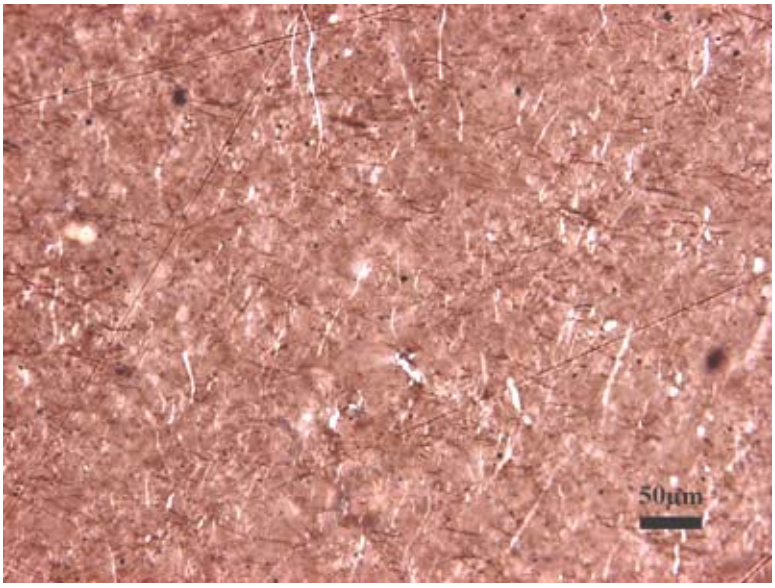

Figure 7.18 PLM surface profiles of PVA composites with separated Lyocell fibrils

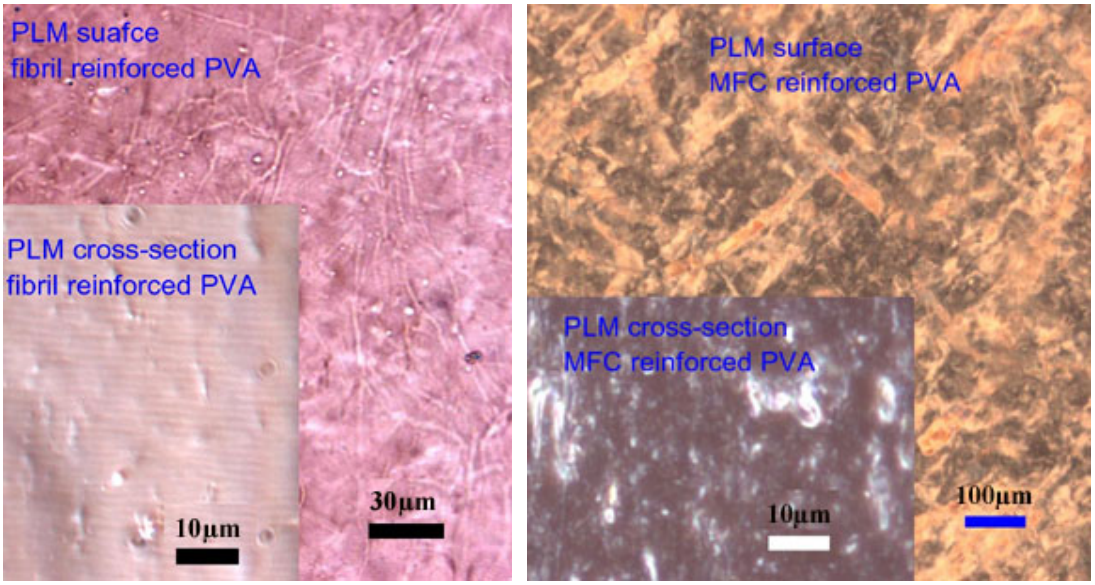

Figure 7.19 PLM images of surface and cross-sections of PVA composites reinforced with Lyocell separated fibrils (left), and MFC (right)

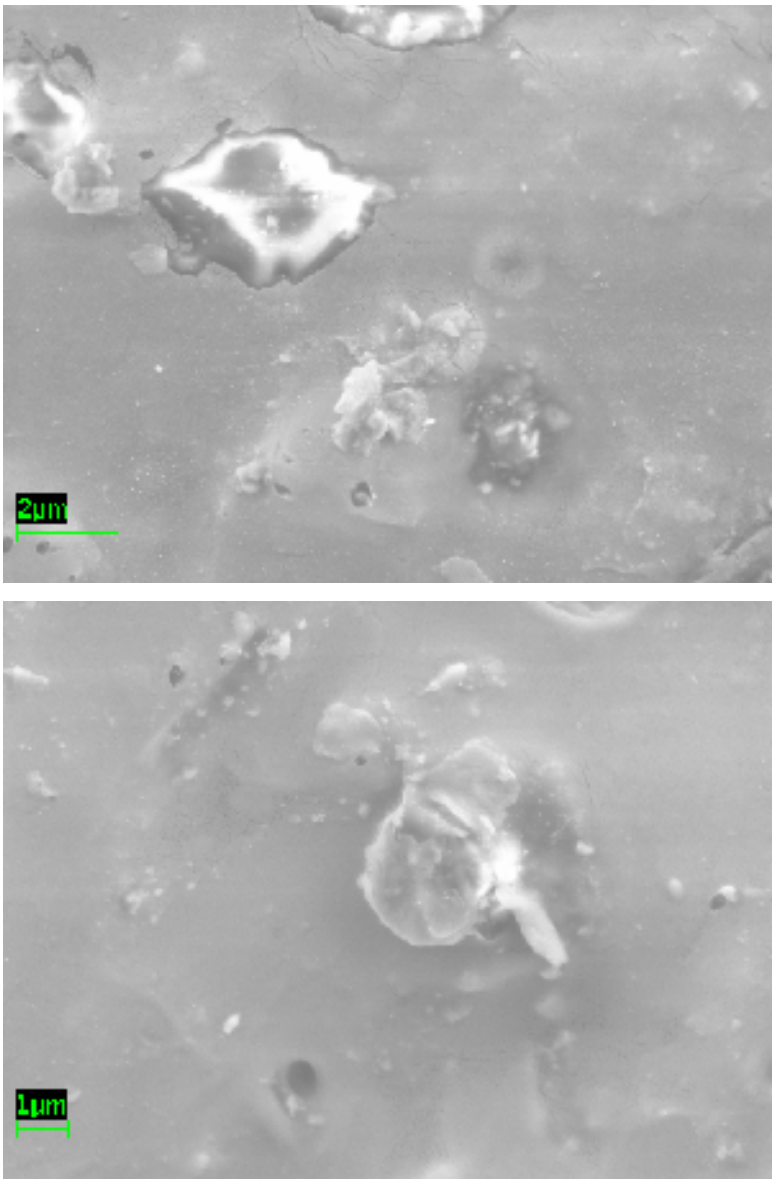

Figure 7.20 SEM images of the fractured cross-sections of PVA composites reinforced with separated Lyocell fibrils

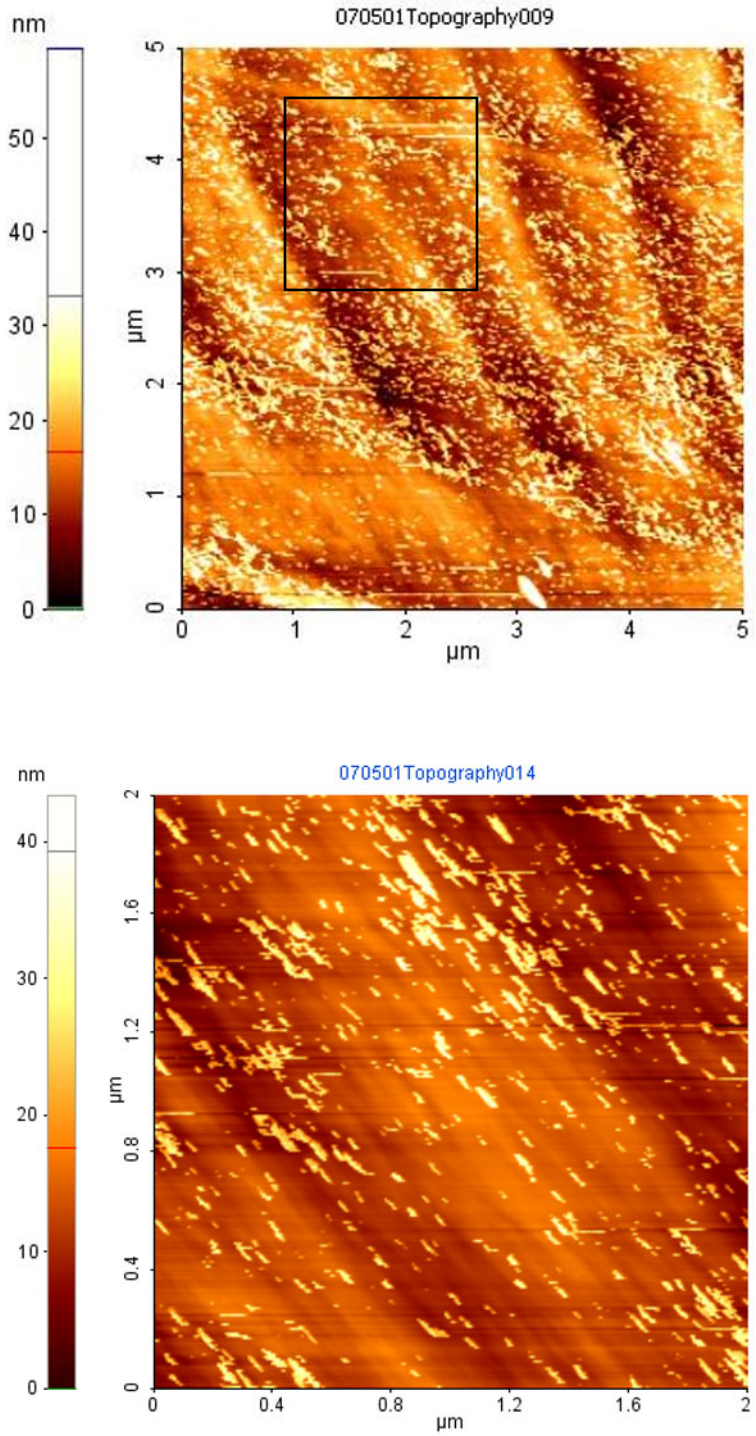

Figure 7.21 AFM topography images of the cross-sections of PVA composites reinforced with separated Lyocell fibrils

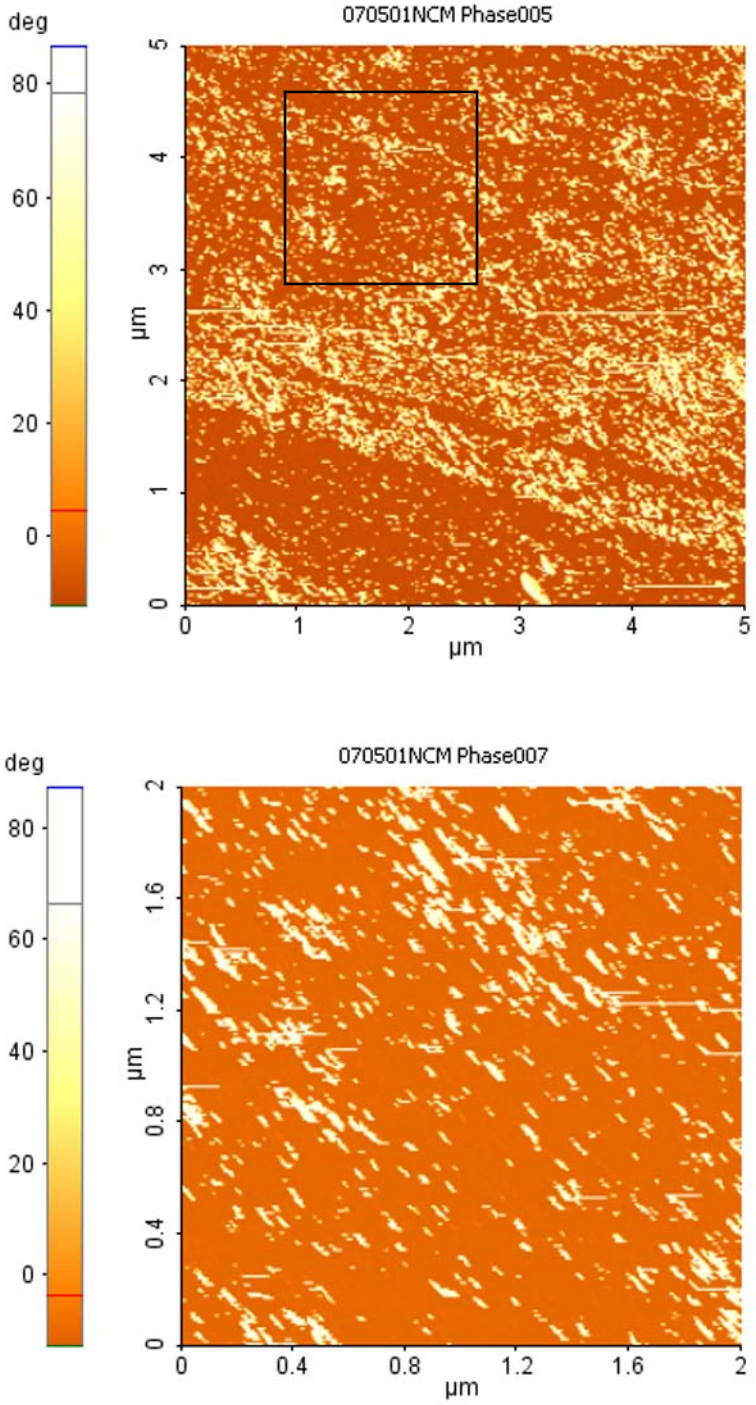

Figure 7.22 AFM phase images of the cross-sections of PVA composites reinforced with separated Lyocell fibrils

References

ASTM, D 1708-2002a. Standard Test Method for Tensile Properties of Plastics By Use of Microtensile Specimens.

Beck-Candanedo, S., Roman, M. and Gray, D.G., 2005. Effect of reaction conditions on the properties and behavior of wood cellulose nanocrystal suspensions. Biomacromolecules, 6(2): 1048-1054.

Berglund, L., 2005. Cellulose-based nanocomposites. In: A.K. Mohanty, M. Misra and L. Drzal (Editors), Natural Fibers, Biopolymers, and Biocomposites. Taylor & Francis, pp. 807-832.

Chakraborty, A., Sain, M. and Kortschot, M., 2005. Cellulose microfibrils: A novel method of preparation using high shear refining and cryocrushing. Holzforschung, 59(1): 102-107.

Chakraborty, A., Sain, M. and Kortschot, M., 2006. Reinforcing potential of wood pulp-derived microfibres in a PVA matrix. Holzforschung, 60(1): 53-58.

Cheng, Q., Wang, S., Rials, G.T. and Lee, S.H., 2007a. Physical and mechanical properties of polyvinyl alcohol and polypropylene composite materials reinforced with fibril aggregates isolated from regenerated cellulose fibers. Cellulose, online first, DOI: 10.1007/s10570-007-9141-0.

Cheng, Q., Wang, S., Zhou, D. and Rials, T.G., 2007b. Lyocell-derived cellulose fibril and its biodegradable nanocomposite. Journal of Nanjing Forestry University, 31(4): 21-26.

Choi, Y.J. and Simonsen, J., 2006. Cellulose nanocrystal-filled carboxymethyl cellulose nanocomposites. Journal of Nanoscience and Nanotechnology, 6(3): 633-639.

Dufresne, A., Cavaille, J.Y. and Vignon, M.R., 1997. Mechanical behavior of sheets prepared from sugar beet cellulose microfibrils. Journal of Applied Polymer Science, 64(6): 1185-1194.

Favier, V., Canova, G.R., Cavaille, J.Y., Chanzy, H., Dufresne, A. and Gauthier, C., 1995. Nanocomposite materials from latex and cellulose whiskers. Polymers for Advanced Technologies, 6(5): 351-355.

Hajji, P., Cavaille, J.Y., Favier, V., Gauthier, C. and Vigier, G., 1996. Tensile behavior of nanocomposites from latex and cellulose whiskers. Polymer Composites, 17(4): 612-619.

Herrick, F.W., Casebier, R.L., Hamilton, J.K. and Sandberg, K.R., 1983. Microfibrillated cellulose: morphology and accessibility. Journal of Applied Polymer Science: Applied Polymer Symposium, 37: 797-813.

Kataoka, Y. and Kondo, T., 1998. FT-IR microscopic analysis of changing cellulose crystalline structure during wood cell wall formation. Macromolecules, 31(3): 760-764.

Mathew, A.P., Oksman, K. and Sain, M., 2005. Mechanical properties of biodegradable composites from poly lactic acid (PLA) and microcrystalline cellulose (MCC). Journal of Applied Polymer Science, 97(5): 2014-2025.

Sakurada, I., Nukushina, Y. and Ito, T., 1962. Experimental determination of elastic modulus of crystalline regions in oriented polymers. Journal of Polymer Science, 57(165): 651-660.

Sturcova, A., Davies, G.R. and Eichhorn, S.J., 2005. Elastic modulus and stress-transfer properties of tunicate cellulose whiskers. Biomacromolecules, 6(2): 1055-1061.

Taniguchi, T., 1996. Microfibrillation of natural fibrous materials. J. Soc. Mat. Sci. Japan, 45(4): 472-473.

Turbak, A.F., Snyder, F.W. and Sandberg, K.R., 1983. Microfibrillated cellulose, a new cellulose product: properties, uses, and commercial potential. Journal of Applied Polymer Science: Applied Polymer Symposium, 37: 815-827.

Wang, S. and Cheng. Q., 2007. A novel method to isolate fibrils from cellulose fibers by high intensity ultrasonication (in preparation).

Zimmermann, T., Pohler, E. and Geiger, T., 2004. Cellulose fibrils for polymer reinforcement. Advanced Engineering Materials, 6(9): 754-761.

CHAPTER 8. CONCLUSIONS AND RECOMMENDATIONS

8.1. Fibrils Isolation by High Intensity Ultrasonication

Single and boundless of cellulose microfibrils may have high strength and possibility to reinforce polymers. It is attractive to study how to generate fibrils and how to combine them with polymers to make nanocomposites. However, the existing processes of fibril isolation have some disadvantage, such as chemical method produces low yields, and is not environmentally friendly and energy efficient, while mechanical method severely degrades cellulose, and is not energy efficient. In this study, a novel process using high-intensity ultrasonication (HIUS) was developed to isolate fibrils from several cellulose resources. HIUS can produce very strong mechanical oscillating power, so the separation of cellulose fibrils from biomass is possible by the action of hydrodynamic forces of ultrasound.

HIUS by batch process has been used to isolate fibrils from several cellulose resources: regenerated cellulose fiber (Lyocell), pure cellulose fiber (TC40, 180, and 2500), microcrystalline cellulose (Avicel), and pulp fiber. The geometrical characteristics of the fibrils were investigated using polarized light microscopy (PLM), scanning electron microscopy (SEM) and atomic force microscopy (AFM). Results demonstrated that small fibrils with diameter ranging from about thirty nm to several μm were peeled from the fibers. Some small fibrils were still on the big ones' surfaces, while some were already separated from the fibers. Water retention value (WRV) was used to evaluate the cellulose fibrillation, which was significantly increased by HIUS treatment for all cellulose resources. The cellulose crystallinities or molecular structures evaluated by wide angle X-ray diffraction (WAXD) and Fourier transform infrared spectroscopy

(FTIR) were changed by ultrasonic treatment for most cellulose resources, and the changes were different for different cellulose resources.

According to the nominal power level, the power consumption of HIUS treatment was low. Higher HIUS power and higher process temperature were benefit for cellulose fibrillation. Cellulose concentration is also important and it depends on the dimensions of origin cellulose, which should be lower if the fiber is longer. Too short or too long distance from tip to beaker bottom may not have benefit to cellulose fibrillation. Pressure and pass time are very important for high-pressure homogenizer (HPH). Several passes using HPH after HIUS treatment are helpful to make good cellulose suspension and more uniform cellulose fibrils than those treated by HIUS or HPH only.

8.2. Elastic Modulus Measurements of Single Fibrils

Understanding the mechanical properties of cellulose fibrils in micro and nano scales is important to evaluate the degradation of isolation processes and reinforcement potentials, especially when the fibrils are used as polymer reinforcement materials. The measurement of mechanical properties of single fibrils is difficult because of the very small forces and dimensions involved. In order to investigate the mechanical property of cellulose fibrils, atomic force microscope (AFM) was used to measure the nano Newton forces and nanometer deflections of fibrils by nanoscale three-point bending, and the elastic moduli of single fibrils were evaluated by a model. This method was modified for this material by considering several factors including data mining, AFM tip selection, and the testing position of the reference to observe and discuss the determination of the fibril

deflections in bending test. The results indicated that it was necessary to consider the penetration of AFM tips to the cellulose fibril surfaces. The AFM cantilever deflection for the tip loaded on the fibril laid on the wafer was better than the cantilever deflection for the tip loaded on the wafer as reference to calculate the deflection of fibrils suspended above wafer grooves.

The elastic moduli of single cellulose fibrils isolated by mechanical treatments were evaluated by this method performed in AFM. Most of the fibrils generated by mechanical methods were bundles of microfibrils and the fibrils had complex surfaces and wide range of diameters. The elastic moduli of cellulose single fibrils with diameters ranging from 150 to 300 nm were measured in this study. In this diameter range, the elastic moduli of Lyocell fibrils did not have significant differences between the HIUS treatment time of 30 min and 60 min. The modulus of Lyocell fibrils with diameters from 150 to 180 nm was evaluated about 98 GPa and it decreased dramatically when the diameter was more than 180 nm. The results also indicated that the elastic moduli of cellulose fibrils were not significantly different between isolation methods of HIUS and high-pressure homogenizer, and between different cellulose sources of pulp fibers treated by homogenizer. The elastic modulus of fibrils from regenerated cellulose fibers was higher than that of natural fibers. AFM nanoindentation test with a diamond-coating tip was also used to estimate the elastic modulus of the same Lyocell fibrils, but results calculated from the unmodified Hertz theory model did not match the results obtained from AFM three-point bending.

8.3. Composites Reinforced with Fibers and Fibrils Treated with Ultrasonication

To investigate the reinforcements of cellulose treated by HIUS and cellulose fibrils separated from the treated cellulose materials, poly(vinyl alcohol) (PVA), poly(lactic acid) (PLA), and polypropylene (PP) were chosen as matrixes to make composites by film casting and compression molding. The mechanical properties of the composites were evaluated by tensile test. The morphological characteristics of the nanocomposites were investigated with PLM, SEM, and AFM. As reference, commercial microfibrillated cellulose (MFC) was also used to reinforce PVA.

The treated Lyocell fibers increased the tensile modulus and strength of PVA, PLA, and PP by fabrication methods of film casting (PVA) and compression molding (PLA, PP). SEM and PLM observations show that the mixture of treated Lyocell fibers had better dispersion in the composites. There were not perfect adhesions between the polymers and the fibers and fibril aggregates without further modification. The Lyocell fibrils on the surfaces of big ones and isolated from the fibers were the main reason that the tensile modulus and strength of the mixture reinforced composites were higher than those of the composites reinforced with untreated Lyocell fibers.

Small fibrils were separated by centrifuge from the mixture of regenerated cellulose fiber (Lyocell), pure cellulose fiber (TC180), and microcrystalline cellulose (MCC) treated by HIUS. Lyocell fibrils significantly increased the tensile modulus and strength of PVA. But the separated fibrils from TC180 and MCC did not reveal good reinforcement for PVA, although the mixture and separated fibrils of TC180 and MCC

had better reinforcement than that of untreated ones. PLM, SEM, and AFM observations showed that the dispersion of cellulose was not perfect in the matrix, and the adhesions between the polymer and fibrils were not perfect without further modification of the fibrils and/or matrix. These were the main reasons that the increments of tensile strength and modulus of the composites were not as high as expected.

8.4. Recommendations for Future Work

8.4.1. Fibrils isolation by HIUS

One problem is the scale up, which limits the application because it is difficult to treat large-scale cellulose in batch process. One way is to use continuous process, but it did not have high efficiency with the commercial system and it needs long time to process large volume cellulose. Modification is needed for this system. The second problem is that Titanium (Ti) tips of HIUS were eroded quickly if the cellulose treated continually more than 30 min or the tip was used many times of less than 30 min. So a replaceable tip material with low ultrasonic erosion may be necessary for this application. The third problem is the fibril yield and uniformity with only the HIUS treatment. Shorter fibers are easier for fibrillation but the isolated fibrils are shorter too and more particles with low aspect ratio can be generated. An after-treatment such as homogenizer or supergrinder may be helpful to make more uniform fibrils.

8.4.2. Mechanical property measurements of single fibrils

The model used for elastic modulus evaluation by nanoscale three-point bending is very sensitive with the fibril diameter, which should be carefully determined. For fibrils with diameter less than 150 nm, small span groove is needed because the fibrils are bended above long span grooves during drying. AFM nanoindentation test with a diamond coating tip may be another good way to estimate the elastic modulus of same cellulose fibrils, but the Hertz theory for nanoindentation test may be not suitable for cellulose fibrils before it is modified using more factors.

8.4.3. Composites reinforced with cellulose fibers and fibrils

The increments of tensile strength and modulus of the composites were not as high as expected. The main reasons may include that the dispersion of fibrils was not perfect in the matrix, and the adhesions between the polymer and fibrils were not perfect without further modification of the fibrils and/or matrix. Other processes, such as freeze dry of the fibrils followed by extrusion, may help the fibril dispersion. Surface modification may be necessary to improve the adhesion between the polymer and fibril. Future work may also include modeling of the mechanical properties of nanocomposites.

APPENDIXES

APPENDIX A. Publications from This Work

A.1. Journal articles

1. **Cheng, Q.,** S. Wang. 2007. A method for testing the elastic modulus of single cellulose fibrils via atomic force microscopy (In preparation).
2. **Cheng, Q.,** S. Wang. 2007. Effects of process and resource on elastic modulus of single cellulose fibrils evaluated by atomic force microscopy (In preparation).
3. Wang, S., **Q. Cheng**. 2007. A novel method to isolate fibrils from cellulose fibers by high intensity ultrasonication (In preparation).
4. **Cheng, Q.,** S. Wang, T. Rials and S.-H. Lee. 2007. Physical and mechanical properties of polyvinyl alcohol and polypropylene composite materials reinforced with fibril aggregates isolated from regenerated cellulose fiber. Cellulose. online first, DOI: 10.1007/s10570-007-9141-0.
5. **Cheng, Q.,** S. Wang, D. Zhou, Y. Zhang and T. Rials. 2007. Lyocell-derived cellulose microfibril/nanofibril and its biodegradable nanocomposites. Journal of Nanjing Forestry University. 31(4): 21-26.
6. **Cheng, Q.,** S. Wang. 2007. Recent research on nanocomposites reinforced by natural cellulosic micro/nanofibrils. China Forest Products Industry. 34(3): 3-7 (In Chinese with English abstract).

A.2. Proceeding articles

1. **Cheng, Q.,** S. Wang. 2007. A testing method of mechanical property of single cellulosic fibrils using AFM. The 9th International Conference on Wood & Biofiber Plastic Composites May 21-23, 2007, Madison, Wisconsin (In press).
2. **Cheng Q.,** S. Wang. 2007. Cellulose fibrils isolated from Lyocell fiber by a novel process and its reinforced PVA nanocomposites. International Symposium on Advanced Biomass Science and Technology for Bio-based Products, May 23-25, 2007, Beijing, China (In press).
3. Wang, S., **Q. Cheng,** T. Rials and S.-H. Lee. 2006. Cellulose microfibril/nanofibril and its nanocomposites. The 8th Pacific Rim Bio-Based Composites Symposium. Kuala Lumpur, Malaysia. P. 301-308.

A.3. Conference presentation and posters

1. **Cheng, Q.,** S. Wang, T. Rials. 2007. Fibrils isolated from cellulose fibers by a novel method and its reinforced nanocomposites. Forest Product Society, 2007 Annual Meeting, June 10-13, Knoxville, TN. p. 15 (Oral presentation).
2. **Cheng, Q.,** S. Wang, T. Rials. 2007. Biodegradable nanocomposites reinforced with cellulose fibrils. Technical Association of Pulp and Paper Industry (TAPPI) & Forest Product Society, 2007 International Conference on Nanotechnology for

the Forest Products Industry, June 13-15, Knoxville, TN. p. 47 (Oral presentation).

3. **Cheng, Q.,** S. Wang, T. Rials. 2007. Fibril isolation and its reinforced nanocomposites from natural biomass. Forest Product Society, 2007 Annual Meeting, June 10-13, Knoxville, TN. p. 34 (Poster).
4. **Cheng, Q.** 2007. A novel method to isolate fibrils from natural cellulose fibers by high intensity ultrasonication. Society of Wood Science and Technology & Forest Product Society, 2007 Annual Meeting, June 10-13, Knoxville, TN. p. 33 (Poster).
5. **Cheng, Q.,** S. Wang, T. Rials. 2007. Biodegradable nanocomposites reinforced with cellulose fibrils. Technical Association of Pulp and Paper Industry (TAPPI) & Forest Product Society, 2007 International Conference on Nanotechnology for the Forest Products Industry, June 13-15, Knoxville, TN. p. 61 (Poster).
6. **Cheng, Q.,** S. Wang, T. Rials. 2007. Mechanical properties of single natural cellulose fibrils. Technical Association of Pulp and Paper Industry (TAPPI) & Forest Product Society, 2007 International Conference on Nanotechnology for the Forest Products Industry, June 13-15, Knoxville, TN. p. 72, and The 9th International Conference on Wood & Biofiber Plastic Composites, May 21-23, 2007, Madison, Wisconsin. p.21 (Poster).
7. **Cheng, Q.,** S. Wang, T. Rials. 2007. A novel method to isolate fibrils from cellulose fibers and its reinforced PVA nanocomposites. The 9th International

Conference on Wood & Biofiber Plastic Composites, May 21-23, 2007, Madison, Wisconsin: p. 21 (Poster).

8. Wang S., **Q. Cheng.** 2007. A novel method to isolate micro/nanofibril from cellulose fiber and its reinforced PVA nanocomposites. International Symposium on Advanced Biomass Science and Technology for Bio-based Products, May 23-25, 2007, Beijing, China. p. 2 (Oral presentation).
9. **Cheng, Q.,** S. Wang, S. Lee, and T. Rials. 2006. Composite Materials from Microfibrils Isolated from Regenerated Cellulose Fiber. 231ST American Chemical Society (ACS) National Meeting. March 26-30, 2006. Atlanta, GA (Oral presentation).

APPENDIX B. Bonus Paper Not Included In This Work: Fiber-Reinforced Polypropylene Composites from Small-Diameter Southern Pine Trees by Wet Process

(The 1st International conference on Energy Conversion and Efficient Utilization of Woody Biomass (CECUWB), May 14-16, 2006, Beijing, China. p. 250-256)

Siqun WANG, Qingzheng CHENG and Tim RIALS
Tennessee Forest Products Center, University of Tennessee, 2506 Jacob Dr. Knoxville, TN 37996-4570
Kevin M. KIT and Marion HANSEN
Department of Materials Science & Engineering, 434 Dougherty Engineering Building, University of Tennessee, Knoxville TN 37996-2200

B.1. Abstract

Wood-plastic composites are being expanded rapidly in these years. To take advantage of the unique characteristics of the wood fiber by combining them with plastic in conventional panel pressing methods, a new wet process was developed to make fiber-reinforced plastic composites using PP and steam-exploded flour from small-diameter loblolly pine. Wet-laid wood fiber/polymer composites were fabricated using a standard TAPPI handsheet method followed by compression molding to consolidate the mixed mats into panels. MAPP was used as a coupling agent to enhance the strength of PP composites. DMA and DSC measurement led some insights into the structure of composites and SEM was used to observe the interfacial adhesion. The variables that may affect the product properties were investigated as well, which include mat layer number, wood fiber content, MAPP content, fiber dimension, and molding temperature.

Keywords: pine, small-diameter, steam-exploded, composite, PP, plastic

B.2. Introduction

Wood plastic composites (WPC) are utilized worldwide, particularly in North America as durable outdoor materials and automotive interior substrates (English and Falk, 1995). Extrusion and injection molding are the typical methods to manufacture WPC using wood flour/small particles or fibers and polymers (Killough, 1995). Many factors of materials used for WPC may affect the end-product properties. First, moisture content is one of the most important factors. Second, wood is sensitive to temperature change. At higher temperature wood can become volatile and partly burn. Third, wood can affect the product properties as the bulk density material. The flexural strength of extruded WPC was increased by different wood flour species. The flexural MOE was increased in a linear relationship with the increasing of wood flour content. The maximum flexural strength was occurred in the range of 30 to 40% percent filler for different wood species (Berger and Stark, 1997). The flexural and tensile modulus and strength were increased with increasing wood particle size (Stark and Berger, 1997). Maleic anhydride polypropylene (MAPP) is a graft copolymer widely used as modifier to improve the properties of lignocellulose-filled polypropylenes. The maleic anhydride content can graft to each polymeric polypropylene chain and increased the strength of WPC (Snijder and Bos, 1999). MAPP dramatically altered the crystal structure around the wood fiber (Yin et al., 1999).

Typically, the wood flour/fibers are from wood wastes or prepared by cutting or chipping wood from logs, chips, and dried before extruded or injection molded. Steam explosion (SE) treatment is an effective method to produce wood flour/fibers. After

pressuring and penetrating saturated steam into wood chips or fiber bundle, they are split by the explosive expansion to a mixture of wood elements of different sizes, which includes small and big particles, single fibers, and fiber fragments. The nonfibrous byproducts are dissolved and remove from this process. Single fibers have higher specific surface than fiber bundles (Kohler and Kessler, 1999). The steam-exploded wood flour can increase the fracture strength and water resistance of the polymer composite board (Okamoto, et al.; 1999; Anglès et al., 1999; Takatani, 2000).

The MOE of SE wood flour and PP composites by dry process were increased remarkably by using 50% flour without compatibilizer. After adding 2.5% of MAPP, the flexural properties of the composites were improved significantly (Yin et al., 2005). In this study, a wet processing was investigated to make WPC using SE wood flour/fibers and PP. Compared with traditional intensive mixing processes, the wet forming process can be used to make in-plane randomly oriented composite mats with little fiber damage and a more uniform fiber distribution in polymer matrix.

B.3. Experimental

B.3.1. Materials

Small-diameter loblolly pine (*Pinus taeda L.*) chips were converted to wood flours by a steam explosion process. It is a mixture of wood elements of different sizes. To make a homogeneous distribution in the plastic matrix, the flour must be sufficiently fine and oversized particles eliminated by screen filtering. The big particles were refined using a mill chipper in order to use the whole materials after steam explosion and #20 and

#16 screens were used to separate the oversized particles. Polypropylene was provided by FiberVisions Inc. (Covington, GA) in the form of fiber bundles. MAPP was provided by Eastman Chemicals.

B.3.2. Wet Process Development and Composite Processing

Generally speaking, the wet-laid wood fiber/polymer composites were fabricated using a standard TAPPI handsheet method followed by a hot compression molding process. The wood flour and polymer fiber were suspended in water, and after sheet formation using a standard 159mm sheet machine and drying, the mats were compression molded into round sheets with a diameter of 159 mm and a thickness of 1, 2 or 3 mm. The target density of the composites was 1 and 0.91 g/cm^3 for neat PP panels. A typical hot press profile was used for compression molding. After the temperature was raised to 175°C, the pressure was then increased gradually to 4 MPa from less than 0.5 MPa in about 5 minutes until the temperature of 195°C or expected levels and held at this pressure for another 4 min to 5 min. Then cold water was used to cool down the mold temperature to around 50°C.

B.3.3. Experimental Design

At least two panels were made for each condition. Neat PP panels were made as control tests. To observe the effects of different forming and molding, single and multiple layers were used to mold the composites. The wood flour was passed through #16 screen. The ratio of PP/wood was 1:1. The top-top in core and bottom-bottom in core

combinations were used to combine two layers into a single mat. To investigate the effects of different factors on the mechanical properties of the composite, seek a better technical procedure and save experiment numbers, an orthogonal test ($L_9(3^4)$) was chosen to design the experiment. Nine samples were made and consolidated using 2 layers and 2 mm in thickness. Four factors and three levels were chosen: (1) wood fiber contents (35%, 50%, and 65%), (2) MAPP contents (0, 2.5%, 5%), (3) fiber sizes (screen size: <16#, 16#-20#, and <20#), and (4) molding temperature (195, 210, 225ºC).

B.3.4. Material Characterization

Flexural properties were chosen to evaluate the composites according to ASTM D 790 by an Instron testing machine. The nominal width of specimens was 12.5mm. The specimens were tested until rupture occurred in the outer surface of the composite specimens or until a maximum load was obtained for neat PP panels. A strain rate of 0.09 mm/min for 2mm panel and 1.27 mm/min for 3mm panel was employed. At least five specimens were tested for each sample.

A Perkin-Elmer Diamond dynamic mechanical analyzer (DMA) was used to determine the storage modulus *E'* and the loss tangent *tan* . The specimens were heated at a rate of 2°C min from -60°C to 130°C in a nitrogen atmosphere and applied oscillating stress at a frequency of 1 Hz. Differential scanning calorimetry (DSC, Perkin-Elmer Diamond) was performed to observe the melting properties of the composites under a nitrogen atmosphere from -50 to 220 ºC with a heating rate of 10 ºC/min. The mass of specimens was 5-6 mg. The morphology of fractured surfaces was examined

using a Hitachi S-800 Scanning electron microscope (SEM). Fresh fractured surfaces were coated with gold on an ion sputter coater. SEM microscope was operated at 10 kV and various magnification levels.

B.4. Results and Discussions

B.4.1. The Effects of Single and Multiple Layers

Although the wood flours distributed quite well in the mats, it was not thick enough for 1mm composite. For 2mm and 3mm panels, the results indicated that there were not significant differences in flexural properties between single and multiple layers. The standard deviations of multiple layers were slightly smaller and this means that they were more uniform. For two layers combinations, there was not a big difference of the flexural properties between top-top and bottom-bottom in core combinations, but the surfaces of bottom-bottom in core combinations appear more homogeneous. So two layers for 2mm panels with bottom-bottom in core combinations were used for further experiments.

B.4.2. Orthogonal Tests

To analyze the effects of the different factors on the mechanical properties, maximum difference was used to compare the properties. The results indicate that the effects of factors for MOE rank as: Wood content > MAPP content > Fiber size > Temperature. There were not too much different among MAPP content, fiber size, and temperature. The MOE increased with the wood flour content and MAPP content

increasing, but not linear increasing. These are the similar results as reported by Stark and Berger (1997). The flexural MOE decreased with the temperature increasing at higher temperatures and longer times could degrade the wood flour. For MOR, the effects of factors rank as: Wood content > MAPP content > Temperature > Fiber size. The best factor group may be Wood (50%) + MAPP (5%) + Fiber size (#16-#20) + Temperature (195ºC) for both of MOR and MOE. The MOR decreased linearly with the wood flour content increasing, increased with MAPP content increasing and decreased with the temperature increasing. The larger particles were a benefit to both of MOR and MOE.

Generally, the modulus of the composites could be increased by adding fillers with higher modulus than that of the matrix, and the strength may be decreased because there is not enough or no adhesion between the filler and the matrix. The results indicated that the flexural MOE of composites made with PP and SE wood flour was much higher than that of neat PP (Figure 1). Apparently, the addition of wood fiber decreased the flexural strength (Figure 2). Addition of MAPP improved the flexural and tensile strength, impact strength and strain at break by increasing the interface adhesion of PP and wood. The results revealed that both flexural MOE and MOR of composites made with PP and SE wood flour had increasing trends by the MAPP contents increasing. The increasing trends were not very clear. This may be because there were some interactions among the factors.

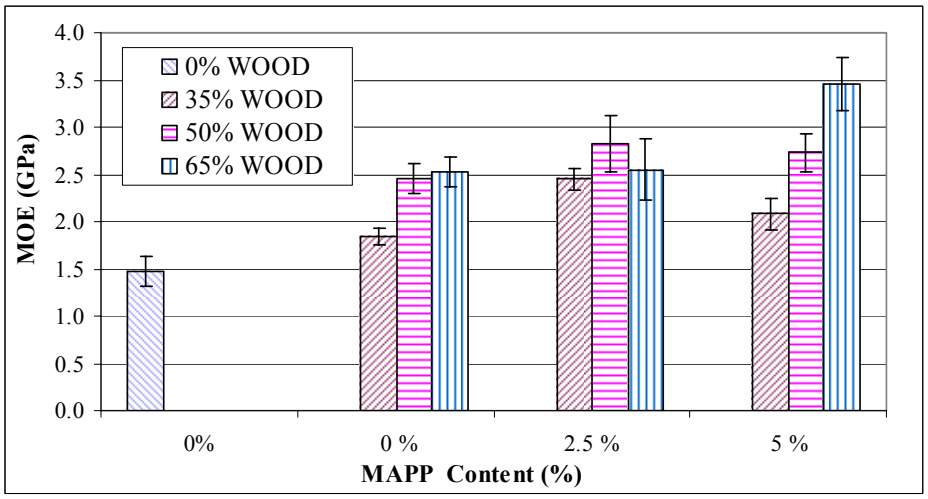

Figure B.1 The effect of wood content on flexural MOE in groups of MAPP contents

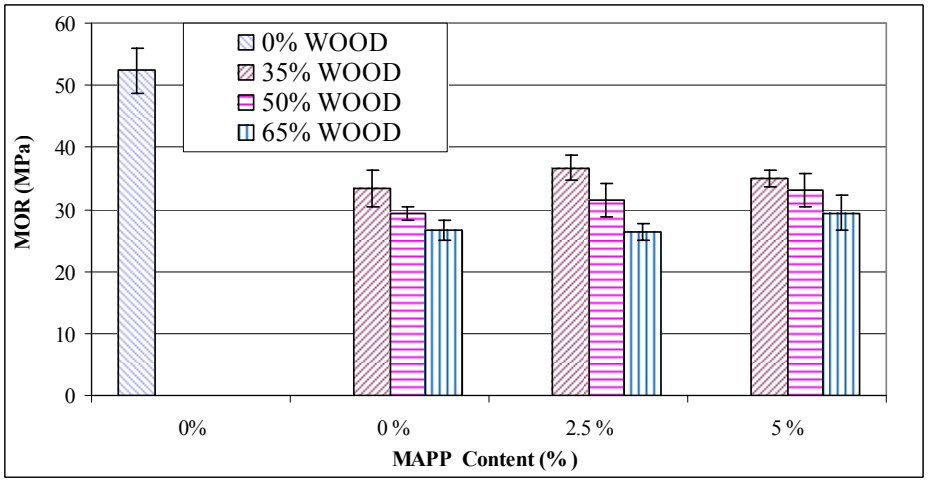

Figure B.2 The effect of wood content on flexural MOR in groups of MAPP contents

B.4.3. Dynamic mechanical analysis (DMA)

For composites, the responses to a dynamic load are very specific to its compositions and the history prior to the test, so specific test conditions are needed. Figure 3 shows the temperature dependence of *tanδ* in the range of -50 to 120°C for PP, PP/DP and PP/MAPP/DP composites, respectively. Neat PP displayed two rubbery transitions in the vicinity of 10°C and 85°C. The low temperature one corresponded to the -transition and the higher peak is -transition. The E' value decreased with the temperature increasing. The composites exhibited a distinct -transition peak with reduced magnitude, but did not have clear -transition peak. The location of the T_g was shifted to lower temperatures by the SE flour loading because of the role of SE flour in the crystallization of PP (Yin et al., 2005).

B.4.4. Differential scanning calorimetry

One typical DSC curves of PP, MAPP, PP/SE and PP/MAPP/SE composites are shown in Figure 4. In the first fusion, all the samples display a peak around 162-165°C, associated with the melting of PP. The apparent melting temperature of neat PP was about 162°C and this temperature was slightly shifted upwards, by incorporation of SE flour and/or MAPP. The results signified that more energy was needed to transform the PP in the composites from a semi-crystalline solid to a molten liquid, reflecting that the interactions among the filler, MAPP and PP have restricted the ability of PP molecules to some extent.

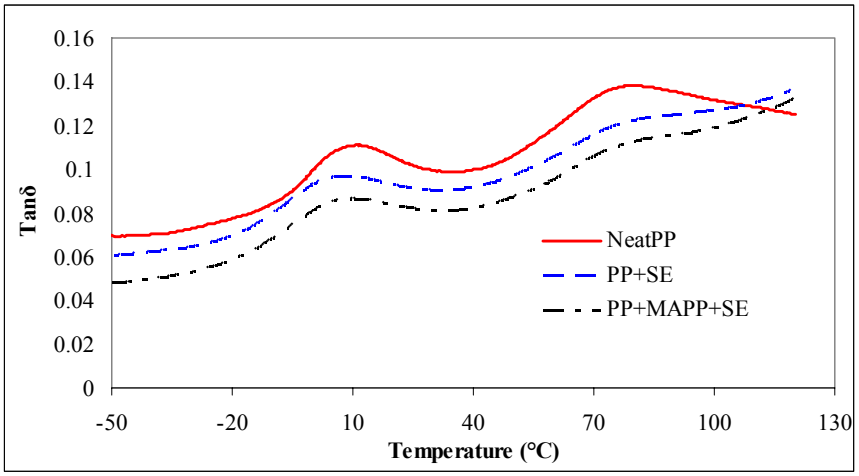

Figure B.3 Tanδ of PP, PP/SE and PP/MAPP/SE composites vs. temperature

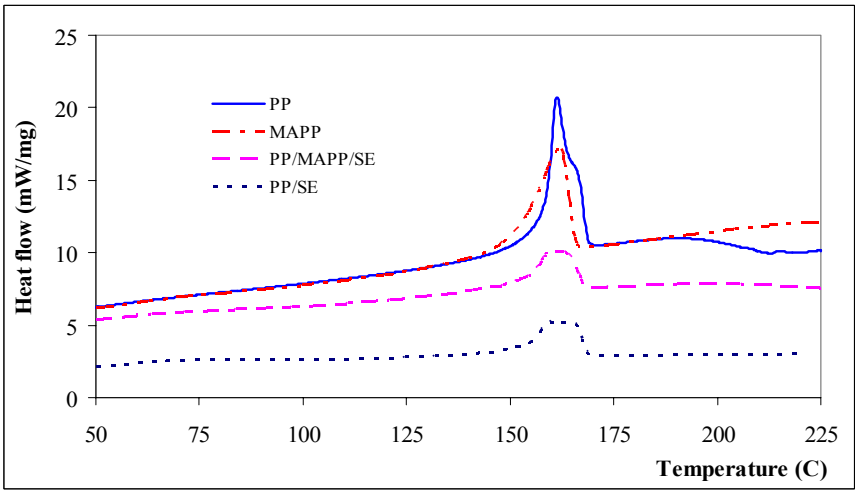

Figure B.4 DSC curves for PP, MAPP, and composites

B.4.5. Morphology of the fractured surfaces of the composites

For the composites without MAPP, some fibers or fiber fragments were pulled out and there were some gaps between fiber and matrix (Figure 5a), indicating that the interfacial failure was the main mechanism causing the rupture. The addition of MAPP produced better compatibility between the SE flour and the PP, and hence stronger interfacial adhesion, as illustrated by the rougher surface, less gaps between fiber and matrix, and the fiber breakage in the longitudinal direction (Figure 5b). These observations imply the interfacial adhesion around some of the fibers was stronger than the individual components so that matrix cracking and fiber breakage after adding MAPP, but the weak interphase regions still existed because the gaps between the PP matrix and some fibers can be observed.

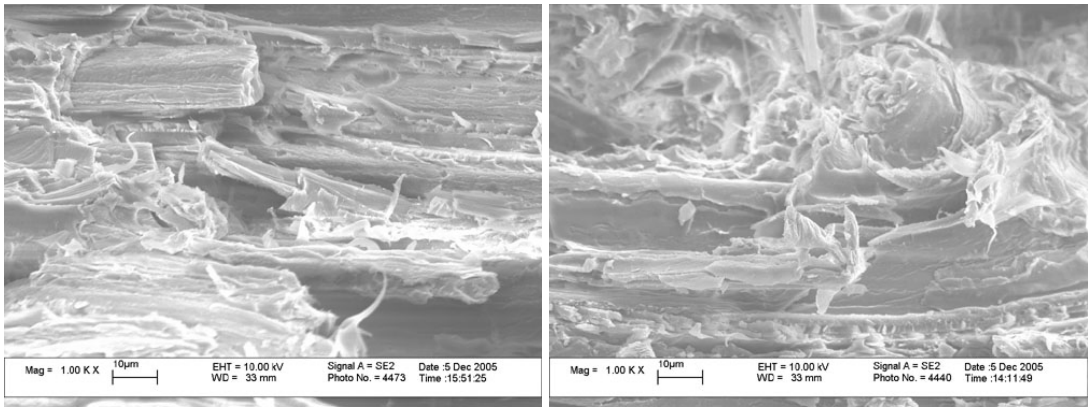

Figure B.5 SEM micrographs of the fractured surface: a) (left): Without MAPP, b) (right): With MAPP

B.5. Conclusion

A wet process was developed to form mats using SE wood flours and PP fibers and followed by a compressive molding process to make wood plastic composite. This method produced less damage to the wood fibers than those by dry process but may have lost some very fine wood flours and water resolvable components during wet forming. The whole materials after SE treatment can be used to manufacture WPC. The MOE increased, while MOR decreased with the SE wood flour content increasing. After MAPP was added, both MOE and MOR of the composites were increased. The larger particles were better for reinforcing the properties and higher temperature could decrease the mechanical properties of the composites. DMA and DSC measurements revealed that the SE wood flours increased the crystallinity of PP. SEM observations also demonstrated the better interfacial adhesion produced by the interactions among the filler, MAPP and PP.

Acknowledge

The authors gratefully acknowledge Bob Wright, Richard Johnson and Wolfgang Glasser of Virginia Tech for their great help in the SE processing; John R. Dunlap of the Division of Biology, University of Tennessee for their valuable assistances in SEM experiments; Richard M Evans of University of Tennessee Forestry Experimental Station for his assistance in log harvest. The authors are indebted to the Cherokee National Forest for financial support, project numbers 03-DG-11083150-930 and 03-DG-11083150-400.

References

Alince, B. and P. Lepoutre. 1983. Retention of dispersed fine particles. Tappi Journal. Vol 66(2):101-102.

Angles, M. Neus, Joan Salvado, Alan Dufresne. 1999. Steam-Exploded Residual Softwood-Filled Polypropylene Composites, Journal of Applied Polymer Science, 74: 1962–1977

ASTM. 2003. Standard Test Method for Flexural Properties of Unreinforced and Reinforced Plastics and Electrical Insulating Materials: ASTM D790-03. American Society for Testing and Materials, West Conshohocken, PA, USA.

Berger, M.J. and N.M. Stark. 1997. Investigations of species effects in an injection-molding-grade, wood-filled polypropylene. The Fourth International Conference on Woodfiber-Plastic Composites. May 12-14, 1997. Madison, Wisconsin.

Kazayawoko, M. and J.J. Balatinecz. 1997. Adhesion mechanisms in woodfiber-polypropylene composites. The Fourth International Conference on Woodfiber-Plastic Composites. May 12-14, 1997. Madison, Wisconsin.

Killouugh,J.M. 1995. The plastic side of equation. Woodfiber-Plastic composites: Virgin and recycled wood fiber and polymers for composites. May 1-3, 1995. Madison, Wisconsin.

Kohler, R. and R. W. Kessler. 1999. Designing natural fiber for advanced materials. The Fifth International Conference on Woodfiber-Plastic Composites. May 26-27, 1999. Madison, Wisconsin.

Machado,A and C.Martin. 1997. Processing wood polymer composites with twin-screw extruders. The Fourth International Conference on Woodfiber-Plastic Composites. May 12-14, 1997. Madison, Wisconsin.

Martin, C. 1999. Using twin-screw extruders to manufacture woodfiber-plastic pellets or parts. The Fifth International Conference on Woodfiber-Plastic Composites. May 26-27, 1999. Madison, Wisconsin.

Okamoto, T., M. Takashi, T. Kitayama, O. Kato, H. Ito, and K. Miwa. 1999. Designing natural fiber for advanced materials. The Fifth International Conference on Woodfiber-Plastic Composites. May 26-27, 1999. Madison, Wisconsin.

Osswald, T.A. 1999. Fundamental principles of polymer composites: processing and design. The Fifth International Conference on Woodfiber-Plastic Composites. May 26-27, 1999. Madison, Wisconsin.

Snijder, M.H.B. and H.L. Bos. 1999. Reinforcement of commodity plastics by annual plant fibers: optimization of the coupling agent efficiency. The Fifth International Conference on Woodfiber-Plastic Composites. May 26-27, 1999. Madison, Wisconsin.

Stark N.M. and M.J. Berger. 1997. Effect of particle size on properties of wood-flour reinforced polypropylene composites. The Fourth International Conference on Woodfiber-Plastic Composites. May 12-14, 1997. Madison, Wisconsin.

Takatani, M, H. Ito, S. Ohsugi, T. Kitayama, M. Saegusa, S. Kawai, T. Okamoto. 2000. Effect of lignocellulosic material on the properties of thermoplastic polymer/wood composite. Holzforschung. 54(2): 197-200.

Yin, S., S. Wang, T. G. Rials, K. Kit and M. Hansen. 2007. Polypropylene composites filled with steam-exploded wood flour from insect-killed loblolly pine by compression-molding. Wood Fiber Science. 39 (1): 95-108.

Yin, S., T.G. Rials and M.P. Wolcott. 1999. Crystallization behavior of polypropylene and it effect on woodfiber composite properties. The Fifth International Conference on Woodfiber-Plastic Composites. May 26-27, 1999. Madison, Wisconsin.

VITA

Qingzheng Cheng was born in Shangdong province, People's Republic of China. After graduating from Yishi First High School in 1988, he went on to attend Northeast Forestry University in Harbin and graduated with a Bachelor of Engineering degree in Wood Processing in 1992. Then he worked in a furniture factory as a Technician for one year. He continued to study at Northeast Forestry University and got his Master of Engineering degree in Wood Processing and Composite Technology in 1996. After that, he joined the Research Institute of Wood Industry, Chinese Academy of Forestry (CAF) as a Research Assistant and then an Assistant Professor for about six years. He received his second M.S. degree in Forestry at the Advanced Engineered Wood Composites Center and the Department of Forest Management, the University of Maine, Orono, Maine in 2004. He came to the Tennessee Forest Products Center, the University of Tennessee at Knoxville to pursue his PhD degree. He currently is a PhD Candidate and Research Assistant working under the advising of Dr. Siqun Wang and Dr. Tim Rials majoring in Natural Resources in the College of Agricultural Sciences and Natural Resources. He graduated from the University of Tennessee with a Ph.D. in Natural Resources in December of 2007.